THE UNIVERSITY
of EDINBURGH

MACHINE LEARNING-BASED DEXTEROUS CONTROL OF HAND PROSTHESES

AGAMEMNON KRASOULIS

Doctor of Philosophy
School of Informatics
University of Edinburgh

2017

Agamemnon Krasoulis:
Machine learning-based dexterous control of hand prostheses
Doctor of Philosophy, 2017

SUPERVISORS:
Prof. Sethu Vijayakumar, Ph.D., FRSE
Kianoush Nazarpour, Ph.D.

EXAMINERS:
Prof. Dario Farina, Ph.D.
Subramanian Ramamoorthy, Ph.D.

ABSTRACT

Upper-limb myoelectric prostheses are controlled by muscle activity information recorded on the skin surface using *electromyography* (EMG). Intuitive prosthetic control can be achieved by deploying statistical and *machine learning* (ML) tools to decipher the user's movement intent from EMG signals. This thesis proposes various means of advancing the capabilities of non-invasive, ML-based control of myoelectric hand prostheses. Two main directions are explored, namely classification-based hand grip selection and proportional finger position control using regression methods. Several practical aspects are considered with the aim of maximising the clinical impact of the proposed methodologies, which are evaluated with offline analyses as well as real-time experiments involving both able-bodied and transradial amputee participants.

It has been generally accepted that the EMG signal may not always be a reliable source of control information for prostheses, mainly due to its stochastic and non-stationary properties. One particular issue associated with the use of surface EMG signals for upper-extremity myoelectric control is the limb position effect, which is related to the lack of decoding generalisation under novel arm postures. To address this challenge, it is proposed to make concurrent use of EMG sensors and *inertial measurement unit*s (IMUs). It is demonstrated this can lead to a significant improvement in both *classification accuracy* (CA) and real-time prosthetic control performance. Additionally, the relationship between surface EMG and inertial measurements is investigated and it is found that these modalities are partially related due to reflecting different manifestations of the same underlying phenomenon, that is, the muscular activity.

In the field of upper-limb myoelectric control, the *linear discriminant analysis* (LDA) classifier has arguably been the most popular choice for movement intent decoding. This is mainly attributable to its ease of implementation, low computational requirements, and acceptable decoding performance. Nevertheless, this particular method makes a strong fundamental assumption, that is, data observations from different classes share a common covariance structure. Although this assumption may often be violated in practice, it has been found that the performance of the method is comparable to that of more sophisticated algorithms. In this thesis, it is proposed to remove this assumption by making use of general class-conditional Gaussian models and appropriate regularisation to avoid overfitting issues. By performing an exhaus-

tive analysis on benchmark datasets, it is demonstrated that the proposed approach based on *regularised discriminant analysis* (RDA) can offer an impressive increase in decoding accuracy. By combining the use of RDA classification with a novel confidence-based rejection policy that intends to minimise the rate of unintended hand motions, it is shown that it is feasible to attain robust myoelectric grip control of a prosthetic hand by making use of a single pair of surface EMG-IMU sensors.

Most present-day commercial prosthetic hands offer the mechanical abilities to support individual digit control; however, classification-based methods can only produce pre-defined grip patterns, a feature which results in prosthesis under-actuation. Although classification-based grip control can provide a great advantage over conventional strategies, it is far from being intuitive and natural to the user. A potential way of approaching the level of dexterity enjoyed by the human hand is via continuous and individual control of multiple joints. To this end, an exhaustive analysis is performed on the feasibility of reconstructing multidimensional hand joint angles from surface EMG signals. A supervised method based on the eigenvalue formulation of *multiple linear regression* (MLR) is then proposed to simultaneously reduce the dimensionality of input and output variables and its performance is compared to that of typically used unsupervised methods, which may produce suboptimal results in this context. An experimental paradigm is finally designed to evaluate the efficacy of the proposed finger position control scheme during real-time prosthesis use.

This thesis provides insight into the capacity of deploying a range of computational methods for non-invasive myoelectric control. It contributes towards developing intuitive interfaces for dexterous control of multi-articulated prosthetic hands by transradial amputees.

LAY SUMMARY

Upper-extremity myoelectric prostheses are electromechanical devices that aim to partially restore the appearance and functionality of a missing limb. They are typically controlled by processing the user's muscular activity information recorded non-invasively on the skin surface using electrodes. Although sophisticated multi-articulated hands are nowadays commercially available, their potential is not fully exploited. Furthermore, they often exhibit control strategies that are non-intuitive and can thus prove cumbersome for the user. A large body of work has been undertaken to achieve naturalistic prosthetic control by deploying algorithms and tools from the fields of statistics and artificial intelligence.

This thesis proposes ways of improving the dexterity and ease of control of myoelectric hands. Two main directions are explored. In the first paradigm, the user's muscular activity is used to decipher the intended hand grip in order to drive the prosthesis into the desired posture in an automated fashion. For the end-user, the ability to intuitively select and utilise 4-5 hand grips to grasp objects can offer a tremendous benefit in performing activities of daily living. In the second paradigm, it is proposed to provide the user with the ability to control each digit of the prosthesis individually, as they would naturally do with an intact limb. The latter scheme has the potential to significantly improve the dexterity of prosthetic control.

The advancements proposed in this thesis are evaluated with laboratory experiments including able-bodied and transradial amputee participants. Special attention is given to relevant practical aspects in order to maximise the clinical impact of the work. This thesis contributes to the long-term objective of developing dexterous and intuitive interfaces for prosthetic hand control with the aim of improving the quality of life of upper-extremity amputees.

ACKNOWLEDGEMENTS

The success and completion of any research project largely depend on the collective effort and contribution of many individuals. I would like to express my sincere gratitude to all those who made this dissertation possible.

First and foremost, I would like to wholeheartedly thank my supervisors Sethu Vijayakumar and Kianoush Nazarpour for giving me complete freedom to pursue my research interests and providing me with excellent guidance and support along the way. Sethu and Kia contributed to this work from different scientific perspectives and also taught me important lessons about aspects of academic/research life which I was completely unaware of four years ago. I am also grateful to Barbara Webb for providing me with insightful feedback and advice during my annual review meetings. John Mourjopoulos was the first person to encourage me to pursue doctoral studies a few years ago and for that I am truly grateful. I also thank my thesis examiners, Dario Farina and Subramanian Ramamoorthy, for providing me with valuable feedback and comments which helped improve the quality of the dissertation.

I would also like to express my sincere thanks to the Ninapro team for publicly releasing their myoelectric datasets that were heavily used throughout the thesis and additionally sharing with me their code and protocol. Special thanks to Manfredo Atzori for hosting my visit in Sierre, Switzerland and training me in data collection. I wish also to thank Iris Kyranou for her contribution in Chapter 3 of the thesis as part of her MRes dissertation, which included software development and data collection for the real-time control experiment described in the second half of the chapter.

I would also like to express my gratitude to everyone who took part in my trials and, in particular, the two amputees who generously volunteered their time on numerous occasions to make this work possible. Their patience during the long experimental sessions and excitement about contributing to research have both inspired me and also been a source of motivation during the tough times of the thesis.

The DTC Neuroinformatics has been a stimulating working environment and I feel privileged to have been part of it. Special thanks to the DTC '12 cohort for fruitful discussions, occasional technical assistance and, more importantly, for creating a brilliant atmosphere in 5.08 and serving me many cups of tea. I would also like to thank the members of the SLMC lab and PIGS reading group for discussions and feedback on various aspects of the work. I am also thankful to the School of Informatics electronics workshop technicians, and particularly Gilbert Inkster, for their constant

willingness to solder wires for me and fix any hardware issues I had from time to time.

On a personal note, I am indebted to all my friends, old and new (you know who you are), for all their love and support and for making my life in Edinburgh so enjoyable. Among them Iain and Tom worth special mention for carefully proofreading parts of this thesis, as well as does Myrto for being brave enough to proofread the document in its entirety and offering me great advice.

Finally, I am grateful to my family, Konstantinos, Mirella, and Karolina, as well as my partner Ersi, more than words can describe; without you none of this would have been possible. Thank you. This thesis is dedicated to the memory of the most wonderful grandmother I was lucky enough to have, but lost during the course of the Ph.D., and whose love, strength, and wisdom I will carry with me for the rest of my life.

My doctoral studies were funded by a scholarship from the EPSRC, BBSRC, and MRC. The work presented in this thesis made use of the following free and/or open-source projects: the Scientific Linux distribution; the Python 2.7 programming language under an Anaconda distribution; Python libraries NumPy, SciPy, matplotlib, seaborn, scikit-learn, pandas, python-can, pyserial, and Jupyter Notebook. This thesis was written in LaTeX using the TeXstudio environment and the classicthesis template.

PUBLICATIONS

Some of the research leading to this thesis has previously appeared in the following list of peer-reviewed publications. Some passages have been quoted verbatim from the respective sources.

JOURNAL ARTICLES

- A. Krasoulis, I. Kyranou, M. S. Erden, K. Nazarpour, and S. Vijayakumar (2017). "Improved prosthetic hand control with concurrent use of myoelectric and inertial measurements." In: *Journal of NeuroEngineering and Rehabilitation* 14.1, p. 71 (Chapter 3).

CONFERENCE ARTICLES

- A. Krasoulis, K. Nazarpour, and S. Vijayakumar (2017b). "Use of regularized discriminant analysis improves myoelectric hand movement classification." In: *2017 8th International IEEE/EMBS Conference on Neural Engineering (NER)*, pp. 395–398 (Chapter 4).
- I. Kyranou, A. Krasoulis, M. S. Erden, K. Nazarpour, and S. Vijayakumar (2016). "Real-time classification of multi-modal sensory data for prosthetic hand control." In: *2016 6th IEEE International Conference on Biomedical Robotics and Biomechatronics (BioRob)*. IEEE, pp. 536–541 (Chapter 3).
- A. Krasoulis, K. Nazarpour, and S. Vijayakumar (2015). "Towards low-dimensionsal proportional myoelectric control." In: *2015 37th Annual International Conference of the IEEE Engineering in Medicine and Biology Society (EMBC)*. IEEE, pp. 7155–7158 (Chapter 7).
- A. Krasoulis, S. Vijayakumar, and K. Nazarpour (2015). "Evaluation of regression methods for the continuous decoding of finger movement from surface EMG and accelerometry." In: *2015 7th International IEEE/EMBS Conference on Neural Engineering (NER)*. IEEE, pp. 631–634 (Chapter 6).

- A. Krasoulis, K. Nazarpour, and S. Vijayakumar (2017a). "Real-time classification of five grip patterns with only two sensors." In: *Proceedings of the 2017 Myoelectric Controls Symposium (MEC)*, pp. 142–142 (Chapter 5; awarded the 3rd best student poster presentation prize).
- A. Krasoulis, S. Vijayakumar, and K. Nazarpour (2017). "Real-time proportional myoelectric control of digits." In: *Proceedings of the 2017 Myoelectric Controls Symposium (MEC)*, pp. 141–141 (Chapter 8).

DECLARATION

I declare that this thesis was composed by myself, that the work contained herein is my own except where explicitly stated otherwise in the text, and that this work has not been submitted for any other degree or professional qualification except as specified.

Edinburgh, 2017

Agamemnon Krasoulis,
December 22, 2017

Dedicated to the loving memory of
Καίτη Αϊβατίδου - Κυριακού
(1931 – 2014)

CONTENTS

LIST OF FIGURES

LIST OF TABLES

LIST OF ALGORITHMS

LIST OF ACRONYMS

2D two-dimensional

3D three-dimensional

CA classification accuracy

CCA canonical correlation analysis

CEL cross-entropy loss

CR completion rate

CT completion time

CV cross-validation

DA discriminant analysis

DIP distal interphalangeal

DLDA diagonal linear discriminant analysis

DOA degree of actuation

DOF degree of freedom

DQDA diagonal quadratic discriminant analysis

EMG electromyography/electromyographic

FPR false positive rate

FRR full rank regression

GNB Gaussian naive Bayes

ICA independent component analysis

IMU inertial measurement unit

κ-NN K-nearest neighbours

KRR kernel ridge regression

LDA linear discriminant analysis

LR linear regression

MCP metacarpophalangeal

ML machine learning

MLP multi-layer perceptron

MLR multiple linear regression

NMF non-negative matrix factorisation

PC principal component

PCA principal component analysis

PIP proximal interphalangeal

PLS partial least squares

QDA quadratic discriminant analysis

R^2 coefficient of determination

RDA regularised discriminant analysis

ROC receiving operating characteristic

RRR reduced rank regression

SFFS sequential forward feature selection

SFSS sequential forward sensor selection

TPR true positive rate

1

INTRODUCTION

The loss or congenital absence of an upper extremity can dramatically impair an individual's ability to perform functional movements and activities of daily living. Moreover, they can cause a significant psychological, professional, and socio-economical distress on the affected person's life.

Upper-extremity prostheses are electromechanical devices that aim to partially restore the appearance and/or functionality of a missing upper-limb. They typically fall into one of the following three main categories: 1) passive/cosmetic; 2) body-powered; and 3) externally-powered myoelectric. Passive, or cosmetic prostheses, are only intended to substitute the physical appearance of the missing body part and, thus, do not provide any practical functionality to the user. Body-powered prostheses work by linking the user's body movements (e.g. shoulder shrugging) to a terminal device, such as a prosthetic hand or hook. Finally, myoelectric prostheses are controlled by the user's muscular activity, typically recorded non-invasively on the skin surface using a specialised technique called *electromyography* (EMG).

The following four main strategies have been proposed for upper-limb myoelectric control: 1) mode switching; 2) *machine learning* (ML) (or pattern recognition); 3) user learning (or motor learning); and 4) musculoskeletal modelling. The mode switching strategy allows the user to control a single *degree of actuation* (DOA) of the prosthesis at a time (e.g. hand opening/closing or wrist pronation/supination) through agonist/antagonist muscle contraction. To switch to a different control mode (e.g. from hand to wrist control), the user has to produce a required biosignal, typically through muscle co-contraction. This scheme has been proven robust, but lacks intuitiveness and can also be cumbersome for the user. On the other hand, ML-based approaches allow for simultaneous access to multiple functions by creating a mapping between the user's muscular co-activation patterns and prosthesis control actions. One such example is when the user can access different hand grips by activating their muscles in a natural way, in the same way that they would do with an intact limb. The automatic grip selection is in this case achieved by means of myoelectric signal classification. One limitation of this strategy is that it may lead to prosthesis under-actuation, as a result of exploring only a fraction of the multidimensional joint activation space of the robotic device. Proportional control schemes based on regression methods offer a promising alternative, whereby the user can control the prosthesis in the full

joint kinematic space. The motor learning approach is similar to ML-based control, except that the association between the user's muscle activation signals and control of prosthesis DOAs is not intuitive (i.e. natural); therefore, the user has to learn the mapping from experience. Finally, the musculoskeletal modelling strategy defines a full biomechanical model which is then employed to compute prosthesis activation commands from muscle activations through forward-dynamical model simulation.

1.1 AIM AND OBJECTIVES

The *aim* of this thesis is to advance the state-of-the-art in non-invasive, ML-based, dexterous control of myoelectric hand prostheses targeted for use by transradial amputees. To achieve this goal, the following two *objectives* are established:

1. Improve the performance of classification-based myoelectric grip control.
2. Develop and evaluate a framework for continuous finger position control of multiple joints.

Throughout this thesis, special focus is given to clinical and practical aspects of myoelectric control, with the hope of making the research outcomes beneficial for the end users, that is, the transradial amputee community. The advances proposed in the thesis are evaluated by performing exhaustive offline analyses, as well as by designing experimental protocols used to assess the efficacy of the proposed schemes during real-time, closed-loop control of commercial and research prosthetic/robotic hands.

1.2 THESIS OUTLINE

The remainder of this thesis is organised as follows:

- **Chapter 2** introduces the relevant to the thesis background information on upper-extremity amputation, the history of development and use of upper-limb prostheses, fundamentals of EMG and *inertial measurement unit*s (IMUs), and the current academic and clinical state-of-the-art in myoelectric control.
- **Chapter 3** proposes the concurrent use of surface EMG and IMUs for improving the performance of classification-based, myoelectric grip control.
- **Chapter 4** offers a thorough investigation on the performance of a broad family of *discriminant analysis* (DA) models on the task of classifying myoelectric data into hand motions and gestures.

- **Chapter 5** proposes a full framework for efficient, classification-based, real-time hand grip control by using only two sensors. Several advancements are introduced with regards to the deployed classification algorithm, hyper-parameter tuning, and confidence-based prediction rejection.
- **Chapter 6** features a systematic offline analysis on decoding finger joint angles from surface EMG signals using regression methods.
- **Chapter 7** proposes a supervised method for simultaneous input-output linear dimensionality reduction for joint angle reconstruction from EMG measurements.
- **Chapter 8** evaluates a continuous finger position control scheme for multi-articulated hand prostheses.
- **Chapter 9** summarises the work, considers its limitations, outlines proposals for future work, and concludes the thesis.

The schematic diagram of Figure 1.1 illustrates the challenges addressed in this thesis within the general context of upper-limb myoelectric control.

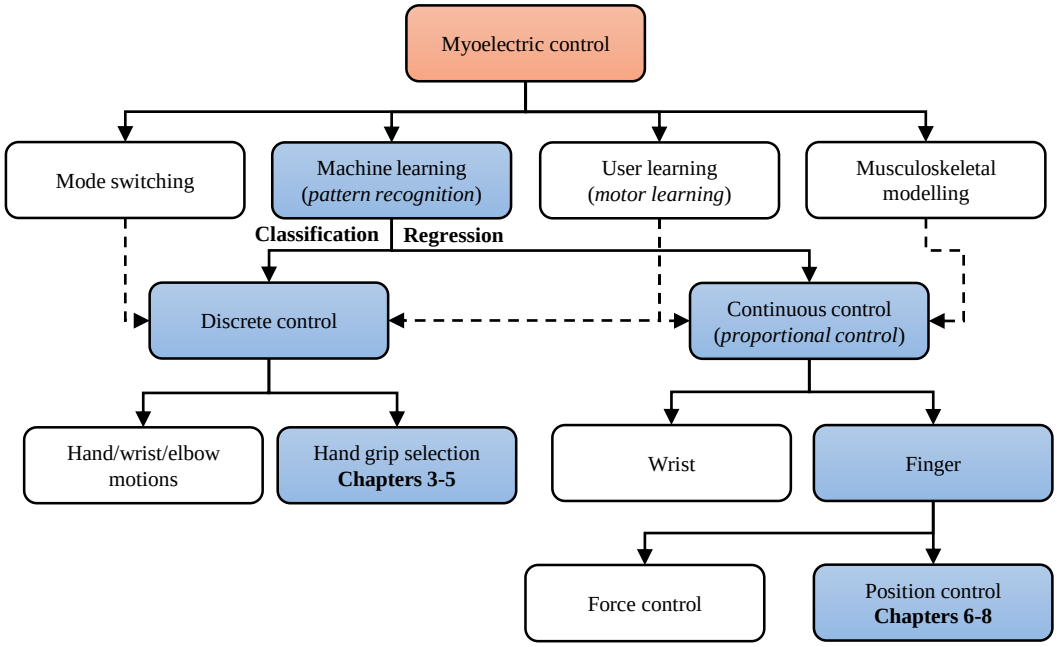

Figure 1.1: Myoelectric control strategies. The highlighted boxes are discussed in this thesis.

2

BACKGROUND

This chapter introduces the relevant to the thesis background information. Rather than presenting an exhaustive review, it aims at providing only a general overview of the field of myoelectric control. In contrast, the introductory sections of subsequent chapters provide extensive reviews of research aspects relevant to their content.

The current chapter is organised as follows: Section 2.1 provides an introduction to upper-extremity amputation, briefly describes the history of upper-limb prostheses, and discusses reasons for myoelectric prosthesis use abandonment; Section 2.2 introduces the fundamentals of recording and processing *electromyographic* (EMG) signals; Section 2.3 provides a brief introduction to *inertial measurement unit*s (IMUs); Section 2.4 presents the current industrial and academic research state-of-the-art in myoelectric control; finally, Section 2.5 introduces a range of standardised procedures and tests used for assessing the performance of myoelectric control systems.

2.1 UPPER-LIMB PROSTHESES

2.1.1 *Upper-limb loss*

In Scotland alone, an estimated average of 458.7 ± 9.9 (mean $\pm$ standard error) upper-limb amputations are reported every year (NHS Scotland, 2014). In the USA, the total number of upper-limb amputees in 2005 was 541,000 and this figure is expected to increase by 131% by 2050 (Ziegler-Graham et al., 2008). The most common causes of upper-limb loss are trauma, neoplasia (i.e. tumours), infection, dysvascularity, neurological disorders (e.g. diabetic neuropathies), and birth defects.

Upper-limb loss can be classified according to the shape and length of the residual limb, and can vary from partial removal of a digit to loss of an entire arm. Some of the most common upper-limb amputation types are: forequarter amputation, that is, loss of entire shoulder and arm structure; shoulder disarticulation; transhumeral or above-elbow amputation; elbow disarticulation; transradial or below-elbow amputation; wrist disarticulation; partial hand amputation; and upper digit amputation. Demographic data for upper-extremity amputations in the United Kingdom are presented in Figure 2.1. Amputation breakdowns by cause and type are shown in the top and bottom panels of the figure, respectively. The demographic data correspond

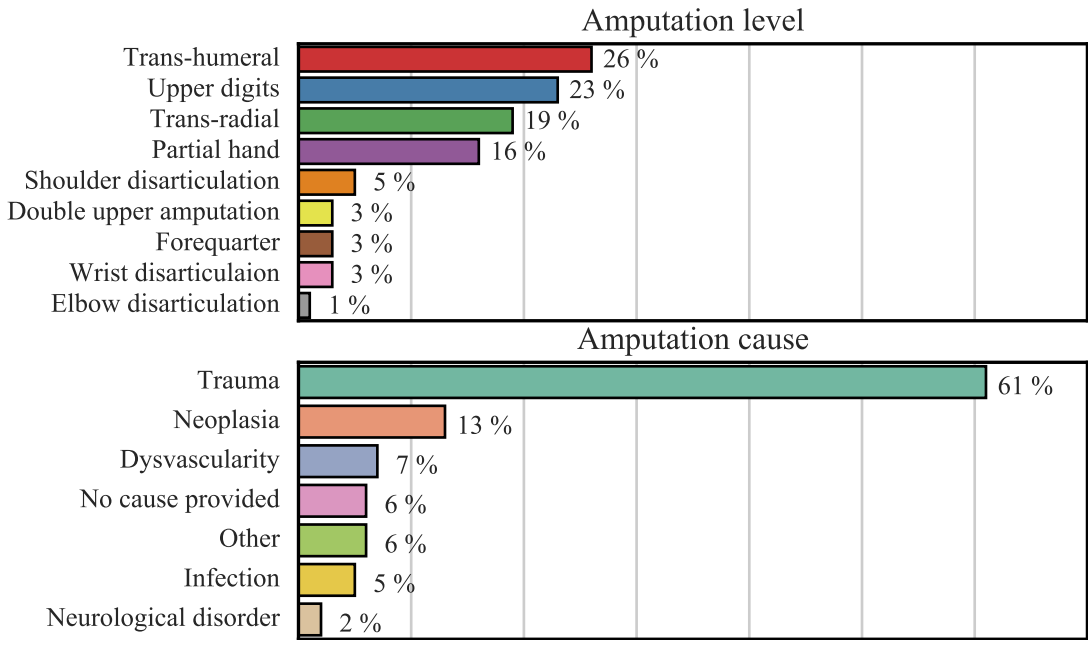

Figure 2.1: Upper-limb amputation demographics in the United Kingdom. Data are acquired from Luff, Forrest, and Huntley (2009) and correspond to the period 2004-2005.

to the chronological period from 2004 to 2005 and have been acquired from a survey by Luff, Forrest, and Huntley (2009).

2.1.2 *A brief history of upper-limb prostheses*

Although the oldest surviving prosthetic device is an ancient Egyptian artificial toe (Finch, 2011), the first documented user of a prosthetic hand is Marcus Sergius, a Roman general during the Second Punic War (218-201 BC) (Romm, 1989). Significant advancements in the development of artificial hands were made in the 16th century AD. One notable example is a mechanical prosthetic hand operated with catches and springs designed by Ambroise Paré, a French barber surgeon (Thurston, 2007). Iron-made prosthetic arms were also developed in the same period, some of which have survived until today (see Figure 2.2).

The scientific and technological advancements achieved during the current and previous centuries heavily transformed the field of prosthetics. The first myoelectric hand was developed in the 1950s by Reiter (1948) and since then, the design and functionality of this type of devices have undergone great improvement. Present-day commercial myoelectric hands are anthropomorphic, lightweight, and can offer a high level of dexterity, as a result of comprising multiple *degrees of freedom* (DOFs). Representative examples of modern hand prostheses are shown in Figure 2.3.

Figure 2.2: Historical prosthetic hands. (a) Mechanical hand designed by Ambroise Paré, 1564 (photograph by Wellcome Library, London); (b) iron prosthetic arm, 1560-1600 (photograph by Science Museum, London); (c) iron prosthetic hand believed to be owned by German knight, circa 1504 (photograph by Wilhelm Kratt). All photographs are distributed under a CC BY 4.0 International license (https://creativecommons.org/licenses/by/4.0/).

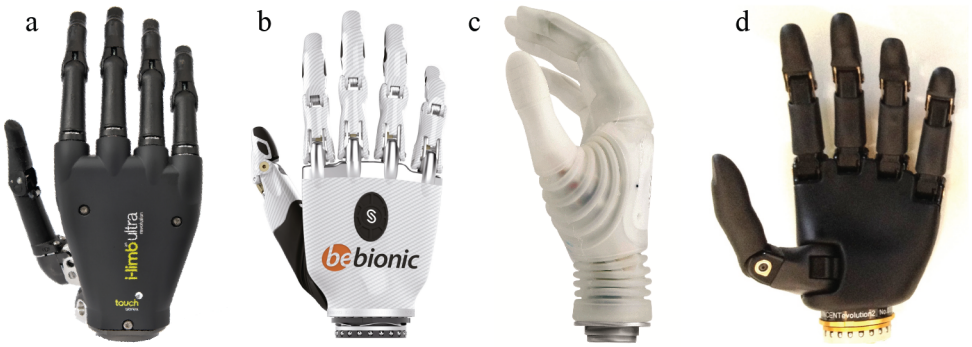

Figure 2.3: Modern commercial prosthetic hands. (a) Touch Bionics i-limb™ (Touch Bionics, Inc., 2003); (b) Ottobock bebionic (Ottobock, Inc., 1919); (c) Ottobock Michelangelo (Ottobock, Inc., 1919); (d) Vincent Evolution 2 (Vincent Systems, GmbH, 2013). All photographs have been provided and are used with permission from the respective manufacturers.

2.1.3 *Prosthesis rejection*

Biddiss and Chau (2007) carried out a thorough literature review and reported an average rejection rate of myoelectric prostheses of 23% and 32% in adults and children, respectively. The same figures for passive and body-powered prostheses were

39% and 26% (adults), and 38% and 45% (children), respectively. A follow-up survey revealed that 74% of non-prosthesis users would be willing to reconsider adopting a prosthetic solution, should improvements in functionality occur at a reasonable cost (Biddiss, Beaton, and Chau, 2007). Amongst the most commonly provided justifications for myoelectric prosthesis rejection are increased weight, excessive wear temperature, and lack of comfort, functionality and durability (Glynn et al., 1986; Datta, Kingston, and Ronald, 1989; Routhier et al., 2001). Myoelectric prostheses users have indicated the following suggestions and preferences for improving their functionality: individual digit movement, thumb abduction and adduction, wrist movement, simultaneous control of multiple joints, greater intuitiveness and naturalness of prosthesis control, grip strength adaptability, and sensory feedback (Atkins, Heard, and Donovan, 1996; Biddiss, Beaton, and Chau, 2007).

2.2 ELECTROMYOGRAPHY

Myoelectric prostheses are controlled by processing the user's muscular activity information recorded on the skin surface with EMG. The following sections offer an introduction to the physiology of EMG recordings and related signal processing techniques for myoelectric control.

2.2.1 *Neurophysiology of movement*

Motor control is a complex process by which living organisms activate and coordinate their limbs and muscles to perform actions. It is achieved through the interaction of a large number of subsystems, which includes motor cortical areas (predominantly the primary motor and premotor cortex), the brainstem, basal ganglia, cerebullum, and spinal cord circuits (Purves, 2012).

The British neurophysiologist Charles Sherrington used the term *motor unit* to describe the relationship between a motor neuron located in the ventral horn of the spinal cord grey matter, or in the motor nuclei of cranial nerves in the brainstem, and the skeletal muscle fibres innervated by the neuron's axon terminals. When an action potential is generated by a motor neuron, all of the muscle fibres it contacts contract. Muscle fibre contraction generates force that is applied to the skeleton, which in the case of an isotonic contraction results in body movement. The amount of force produced by a muscle is directly related to the number of active motor units and their corresponding firing rates. In general, the number of muscle fibres per motor unit can vary within and more widely across muscles (Buchthal and Schmalbruch, 1980). The number of motor neurons and fibres per muscle can also vary greatly, and

are typically in the range of hundreds and tens/hundreds of thousands, respectively (Feinstein et al., 1955). The total number of motor neurons innervating the human upper-limb is approximately 22150 (Gesslbauer et al., 2017).

2.2.2 *Neural information in electromyographic signals*

The electromyogram is an electrical muscle signal recorded either non-invasively on the surface of the skin or invasively (i.e. directly from the muscle tissue) using electrodes. EMG signals convey information about the fibre neural activity of the targeted muscle. Since an action potential generated by a motor neuron brings to threshold all of the muscle fibres it contacts, there is a one-to-one correspondence between the action potential activity of a motor neuron and that of its associated muscle fibres; therefore, EMG signals convey information about the neural drive sent from the spinal cord to the muscles (Farina et al., 2014).

The recorded EMG signal can be modelled as a superposition of the action potentials of multiple motor units (De Luca, 1979). Using this model, it can be shown that the power of the EMG signal is an approximation of the sum of individual motor unit action potentials, each weighted by the corresponding firing rate; therefore, there is a monotonic relationship between the power of the EMG signal and the neural drive. Furthermore, the EMG power is related to the force exerted by the targeted muscle. However, it is hard to establish a quantitative description of this relationship, as the surface EMG signal is affected by various factors, including among others: anatomical characteristics; changes in electrode positioning and electrode-skin impedance, for example, due to sweating; and relative movement of the muscle with respect to electrode due to fibre shortening and lengthening (known as *movement artefact*) (De Luca, 1997; Farina et al., 2014).

2.2.3 *EMG signal processing for prosthesis control*

The monotonic relationship between EMG signal power and force exerted by the targeted muscle has been exploited since the early days of myoelectric control in the 1950s, when the EMG power was proposed as a potential control signal for prosthetic devices (Battye, Nightingale, and Whillis, 1955). Another closely related and commonly used approximation of the force exerted by a muscle can be obtained via extracting the *linear envelope* of the EMG signal. This transformation involves full-wave rectification of the signal followed by low-pass filtering (i.e. smoothing) using a cut-off frequency in the range of 5 Hz to 20 Hz. An example of EMG linear en-

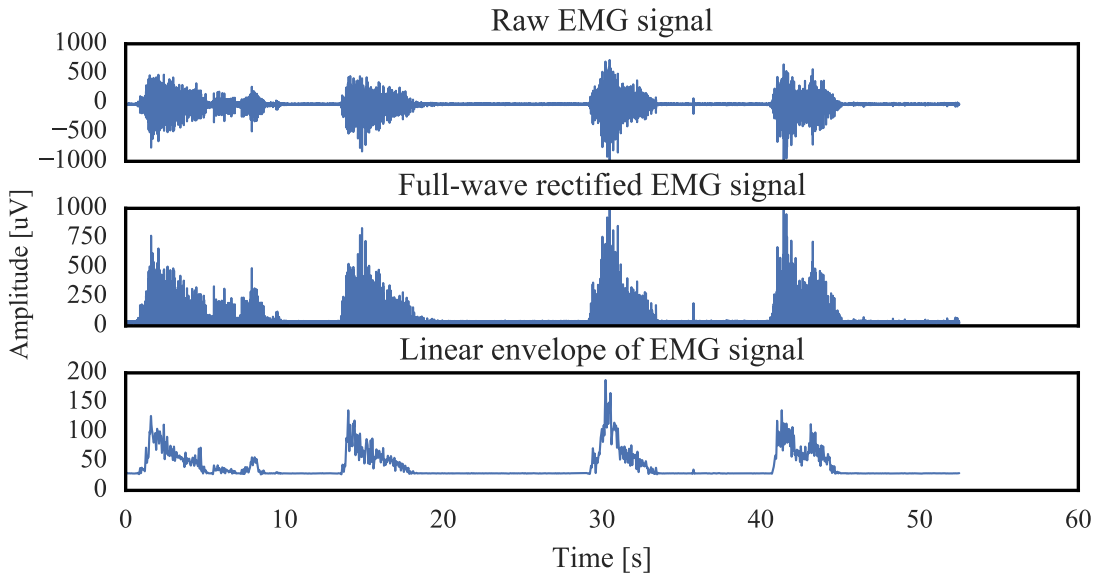

Figure 2.4: An example of EMG signal linear envelope extraction. The raw EMG signal (top panel) is firstly full-wave rectified (middle panel) and subsequently smoothed via low-pass filtering (bottom panel).

velope extraction is illustrated in Figure 2.4. For this example, a 4^{th}-order low-pass Butteworth filter was used and the cut-off frequency was set to 10 Hz.

For prosthesis control, muscular activity recorded with EMG has to be analysed in real-time. Since the EMG signal is stochastic (De Luca, 1979), instantaneous (i.e. sample-by-sample) processing is not useful, as it cannot provide information about the power in the signal. For that reason, a block processing approach is required; in other words, a *sliding window* is used to analyse the EMG signal in batches of consecutive samples. Analysis windows can be either disjoint, that is, the starting point of each window follows the end point of its predecessor, or overlapping, whereby the signal samples are included in multiple consecutive window(s).

Surface EMG signals are inevitably contaminated by many sources of noise including, but not limited to, power line interference, baseline noise, and movement artefact. Typically, a combination of low-pass and notch filtering is required to remove noise components from the EMG signal while preserving at the same time the desired information. In commercial EMG sensors, this type of filtering is nowadays often implemented in hardware (De Luca et al., 2010).

2.2.3.1 *EMG feature extraction*

One important aspect affecting the performance of *machine learning* (ML)-based myoelectric systems is the choice of EMG feature representation. Therefore, it should come as no surprise that a large body of work has studied this relationship by carrying out exhaustive EMG feature performance comparisons (e.g. Zardoshti-Kermani

et al., 1995; Englehart et al., 1999; Boostani and Moradi, 2003; Phinyomark, Phukpattaranont, and Limsakul, 2012; Phinyomark et al., 2013). In general, EMG features can be classified in three main categories: time-domain, frequency domain, and time-frequency domain.

The current section introduces some of the most commonly used time-domain EMG features in the myoelectric control literature. Let $\mathbf{x} = x_1, x_2, \ldots, x_N$ denote the raw EMG signal within a processing window of length N, and

$$\bar{x} = \frac{1}{N} \sum_{n=1}^{N} x_n \tag{2.1}$$

be the empirical mean of the vector $\mathbf{x}$, which is typically close to zero. The following EMG features are defined:

- Mean absolute value:

$$MAV = \frac{1}{N} \sum_{n=1}^{N} |x_n| . \tag{2.2}$$

- Variance:

$$VAR = \frac{1}{N-1} \sum_{n=1}^{N} (x_n - \bar{x})^2 . \tag{2.3}$$

- Log-variance:

$$LogVar = \log \left(\frac{1}{N-1} \sum_{n=1}^{N} (x_n - \bar{x})^2 \right) . \tag{2.4}$$

- Root mean square:

$$RMS = \sqrt{\left(\frac{1}{N} \sum_{n=1}^{N} x_n^2 \right)} . \tag{2.5}$$

- Waveform length:

$$WL = \sum_{n=1}^{N-1} |x_{n+1} - x_n| . \tag{2.6}$$

- Wilson amplitude:

$$WAMP = \sum_{n=1}^{N-1} f\left(|x_{n+1} - x_n|\right), \tag{2.7}$$

where

$$f(x) = \begin{cases} 1, \text{if } x \geqslant \text{threshold}, \\ 0, \text{ otherwise.} \end{cases}$$

- Slope sign change:

$$SSC = \sum_{n=2}^{N-1} f\left[(x_n - x_{n-1})\,(x_n - x_{n+1})\right], \tag{2.8}$$

where

$$f(x) = \begin{cases} 1, \text{if } x \geqslant \text{threshold}, \\ 0, \text{ otherwise.} \end{cases}$$

- Zero-crossing:

$$ZC = \sum_{n=1}^{N-1} \left[sgn\left(-x_n x_{n+1}\right) \cap |x_n - x_{n+1}| \geqslant \text{threshold}\right] \tag{2.9}$$

where

$$sgn(x) = \begin{cases} 1, \text{if } x \geqslant 0, \\ 0, \text{ otherwise.} \end{cases}$$

- Kurtosis:

$$Kur = \frac{\frac{1}{N}\sum_{n=1}^{N}(x_n - \bar{x})^4}{\left(\frac{1}{N}\sum_{n=1}^{N}(x_n - \bar{x})^2\right)^2}. \tag{2.10}$$

- Histogram with k bins: number of signal samples in equally spaced amplitude segments determined by the number of bins (k).

- Auto-regressive coefficients (order p): the EMG signal within the processing window can be modelled as an auto-regressive time-series model

$$x_n = c + \sum_{i=1}^{p} \alpha_i x_{n-1} + e_n, \tag{2.11}$$

where c is a constant, p is the order of the model, α_i for $i = 1, \ldots, p$ are the parameters of the model (auto-regressive coefficients), and e_n is white noise. The model parameters are estimated by means of ordinary least squares via solving the Yule-Walker equations.

Frequency domain features include the mean frequency, median frequency, peak frequency, mean power, total power, and spectral moments within the processing window (Phinyomark, Phukpattaranont, and Limsakul, 2012). It is worth noting that some time-domain features, such as zero-crossing, Wilson amplitude, waveform length, slope sign change, and histogram also measure frequency-related information of the EMG signal. Time-frequency domain features involve using frequency representations of the signal within the processing window, such as the short-time Fourier transform, the Wavelet transform, and the Wavelet packet transform (Englehart et al., 1999).

2.2.4 *Myoelectric classification*

Classification-based myoelectric control is based on the principle that features extracted from multiple EMG electrodes (see Section 2.2.3.1) form motion-specific clusters in high-dimensional space, which can be therefore used to discriminate different classes of movement in order to control a prosthesis. A qualitative illustration of this principle is depicted in the right column of Figure 2.5 and contrasted to the classical method of mode switching control introduced in Section 2.4.1.1.

A plethora of classification algorithms have been proposed for myoelectric control including, but not limited to, *linear discriminant analysis* (LDA) (e.g. Hargrove, Englehart, and Hudgins, 2008; Young et al., 2013); *quadratic discriminant analysis* (QDA) (Scheme and Englehart, 2011; Phinyomark et al., 2013); *K-nearest neighbours* (k-NN) (Nazarpour, Sharafat, and Firoozabadi, 2007); *multi-layer perceptron*s (MLPs) (e.g. Englehart et al., 1999; Castellini and Smagt, 2009; Ortiz-Catalan, Håkansson, and Brånemark, 2014b); Gaussian mixture models (Huang et al., 2005; Ju et al., 2013); support vector machine classification (e.g. McCool et al., 2014; Gailey, Artemiadis, and Santello, 2017); random forests (Li et al., 2013); and more recently, convolutional neural networks (Atzori, Cognolato, and Müller, 2016; Geng et al., 2016; Du et al., 2017).

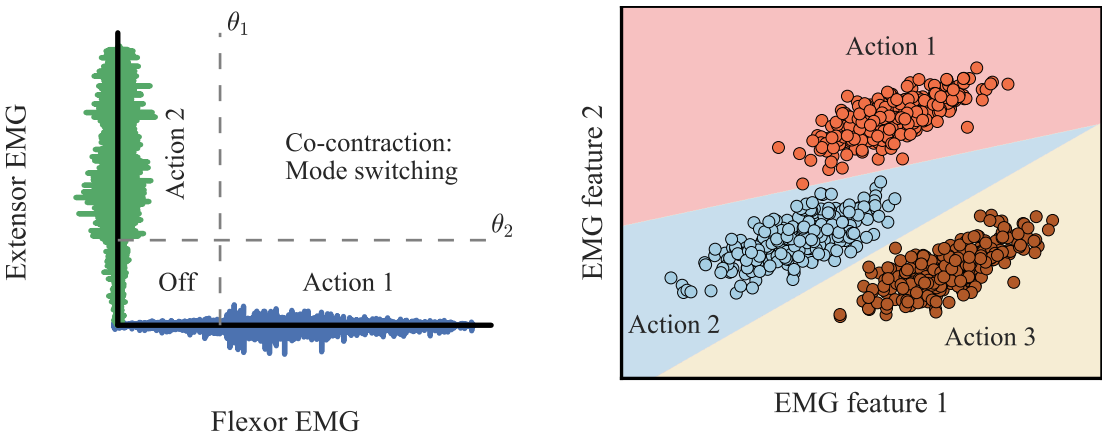

Figure 2.5: Mode switching vs. classification-based myoelectric control. (Left column) an example of amplitude-based mode switching myoelectric control paradigm. Based on a figure by Parker, Englehart, and Hudgins (2006). (Right column) a qualitative illustration of a three-class myoelectric control scheme using a linear classifier (LDA) and two EMG features.

Among these algorithms, the two most commonly used have been the LDA and MLP classifiers (Peerdeman et al., 2011). These are briefly introduced in the following sections. A detailed description of the family of *discriminant analysis* (DA) classifiers, which includes LDA as a special case, is given in Section 4.2.

2.2.4.1 *Linear discriminant analysis*

LDA is a statistical method for linear dimensionality reduction and classification. Given a set of training instances $\{\mathbf{x}^{(n)}, y^{(n)}\}_{n=1,\ldots,N}$, where $\mathbf{x}^{(n)} \in \mathbb{R}^D$ denotes the n^{th} input vector and $y^{(n)}$ the associated class label, LDA seeks to find linear input projections that maximise class separability.

As a probabilistic classifier, LDA assumes class-conditional normal densities sharing a common covariance matrix, called the pooled covariance or within-class scatter matrix. This assumption leads to linear decision boundaries, as illustrated in the example shown in the right column of Figure 2.5.

2.2.4.2 *Multilayer perceptron*

The MLP is a class of feed-forward artificial neural networks. An MLP consists of an input, an output, and at least one hidden layer of nodes. Each node in the network, except for the nodes in the input layer, receives as input a weighted sum of the activity of all the nodes in the previous layer and outputs a non-linear transformation of this sum. The non-linear transformation applied at each layer is called the activation function and typically belongs to the sigmoid family (i.e. logistic or hyperbolic tan-

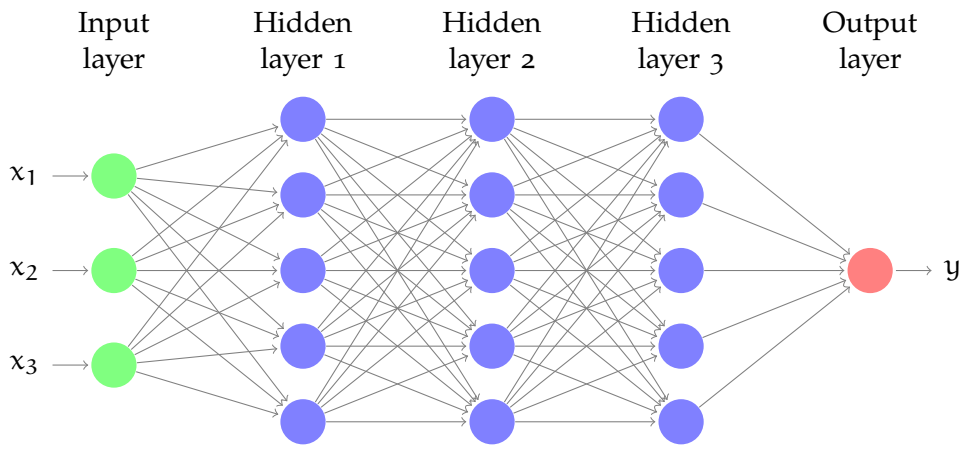

Figure 2.6: An example of an MLP architecture with three input units, three hidden layers consisting of five hidden units each, and one output unit. Based on a figure by Kjell Magne Fauske, distributed under a CC BY 2.5 Generic license (https://creativecommons.org/licenses/by/2.5/).

gent), although other activation functions are also possible. An example of an MLP with three hidden layers is shown in Figure 2.6

MLP classifiers are capable of performing highly non-linear function approximations and can thus be used for supervised learning problems, including both classification and regression. Model training concerns selecting the weights of the network with the aim of optimising a specified cost function. This can be achieved by using the backpropagation method and an optimisation algorithm, typically gradient descent, which iteratively updates the weights of the network until a convergence criterion is met.

2.2.4.3 *Myoelectric controller delay*

In classification-based myoelectric control, class decisions cannot be generated instantaneously due to processing EMG signals in time windows (see Section 2.2.3). Many studies have shown that an increase in the length of the window is associated with improved classification performance (e.g. Englehart and Hudgins, 2003). However, Farrell (2011) demonstrated that the response delay of the system is also directly related to the processing window length in a proportional manner. Other factors influencing the response delay are the computational complexities associated to feature extraction and classification, the length of sliding window increment in the case of overlapping windows, and the number of votes required to trigger a control action when a majority-voting scheme is used to smooth the class prediction time-series (Englehart and Hudgins, 2003). Farrell and Weir (2007) have shown that the optimal delay for myoelectric control is in the range of 100 ms to 175 ms. Moreover, Smith

et al. (2011) demonstrated that a window length in the range of 150 ms to 250 ms offers a good compromise between classification performance and controller delay.

2.3 INERTIAL MEASUREMENT UNITS

An IMU is an electronic device that measures acceleration, angular velocity, and magnetic field using, respectively, accelerometers, gyroscopes, and magnetometers (Woodman, 2007). IMUs are commonly used as navigation sensors for aircraft, spacecraft, satellites, and aerial robots.

IMUs are embedded in many commercial prostheses to provide information about the orientation of the device. Additionally, they have been recently used to allow the user to select a desired grip through arm movement trigger signals (Touch Bionics, Inc., 2003, see Section 2.4.1.2). The use of inertial measurements for myoelectric control is thoroughly investigated in this thesis (see Chapter 3). The following section provides a brief introduction to the basic components of IMUs and their operational principles.

2.3.1 *IMU components and operational principles*

An IMU typically comprises a combination of accelerometers, gyroscopes, and magnetometers. An accelerometer is an electromechanical device measuring static and dynamic forces of acceleration, due to gravity and vibrations/movement, respectively. It measures proper acceleration, that is, acceleration relative to free fall, in one, two, or three axes. Accelerometers have a wide range of applications in engineering, navigation, and industry.

A gyroscope is conceptually a spinning wheel in which the rotation axes are free to assume any orientation. During rotation, the spinning wheel resists changes in orientation due to the law of conservation of angular momentum; therefore, a gyroscope can measure orientation and its rate of change (i.e. angular velocity).

A magnetometer is a sensor measuring the strength and direction of the local magnetic field. The measured signal is a combination of the earth's magnetic field and that of any nearby objects. The simplest example of a magnetometer is the compass, which measures the direction of an ambient magnetic field.

2.3.2 *Inertial navigation and bias effects*

In navigation systems, the raw data recorded with the different types of inertial sensors, that is, accelerometers, gyroscopes, and magnetometers, are fused and transformed into measurements of orientation, velocity, and displacement with respect to a global reference frame. This is achieved by using a combination of integration operations and filtering techniques, such as Kalman and particle filters (e.g. Mourikis and Roumeliotis, 2007).

One major disadvantage of inertial sensors, especially accelerometers and gyroscopes, is that they suffer from constant bias errors. Such biases when integrated cause "drifts" in velocity and position which grow over time. Several methods have been proposed for drift correction and are typically based on sensor fusion algorithms or domain specific assumptions (Woodman, 2007).

2.4 STATE-OF-THE-ART IN UPPER-LIMB MYOELECTRIC CONTROL

2.4.1 *Industry*

2.4.1.1 *Mode switching*

The most commonly deployed control strategy in commercial myoelectric hands is *mode switching* (Atzori and Müller, 2015). In this scheme, two (or more rarely three) EMG sensors are placed on the residual limb surface of the user targeting the remnant flexor and extensor muscle groups. In this way, the amplitude of each EMG signal can be used to control a specific function, for example, hand opening and closing. This can be achieved in either of the following two ways: by defining user-specific amplitude thresholds and using an *on-off* (or *bang-bang*) controller; or in a *proportional* way (see Section 2.4.2.2), whereby the degree of performed action is related to the amplitude of the associated control signal. One main disadvantage of this regime is that it can only allow the user to control a single function at a time. Other functions can be accessed by mode switching, which is typically achieved through muscle co-contraction. Additionally, the control of the hand is not natural; in other words, it relies on the user learning the underlying control principle of the device through training. The working principle of this scheme is illustrated in the left column of Figure 2.5.

2.4.1.2 *Trigger signals*

A different strategy for myoelectric prosthesis control is based on non-intuitive *trigger signals* that can be activated by the user to access multiple functions. One example of this approach is a system recently made available for the i-limb™ Quantum hand (Touch Bionics, Inc., 2003). In this paradigm, a set of pre-defined hand grips are associated with specified arm movement triggers. The latter are recognised by the controller via an IMU (see Section 2.3) embedded in the hand. Alternatively, the wearer may use muscle activation triggers, such as a double/triple impulse or co-contraction. It is worth noting that although this strategy can enable the user to get quicker access to a desired grip than with mode switching, the control of the prosthesis is still far from natural.

2.4.1.3 *Machine learning*

Natural and intuitive prosthetic control can be achieved by making use of ML and pattern recognition methods, such as classification and regression. Recently, the first myoelectric system using ML has appeared on the market (Coapt Engineering, LLC, 2013). The Coapt Complete Control™ is a classification-based myoelectric interface (see Section 2.2.4), which is compatible with a range of upper-extremity prostheses. The system comprises eight EMG electrodes and a micro-processor. It can be used to discriminate classes involving movement of the hand, wrist, and elbow. A typical configuration includes six classes of movement, that is, elbow flexion/extension, wrist pronation/supination, and hand opening/closing.

Moreover, some prostheses manufacturers, for example, Ottobock, Inc. (1919) and Touch Bionics, Inc. (2003), have announced plans of incorporating ML in the control of their devices in the future; however, at the time of writing, such interfaces have not yet been made commercially available.

2.4.2 *Academic research*

2.4.2.1 *Myoelectric classification*

The use of classification methods for myoelectric control was first proposed in the early 1990s (Kelly, Parker, and Scott, 1990; Hudgins, Parker, and Scott, 1993). These two seminal studies demonstrated the feasibility of using artificial neural networks to classify surface EMG signals from a single electrode into multiple limb movements. Since then, a great amount of work has investigated ways of improving classification performance by increasing the number of EMG sensors (e.g. Englehart and Hudgins, 2003); using a variety of classifiers (e.g. Chan et al., 2000; Englehart and Hudgins,

2003; Chan and Englehart, 2005; Huang et al., 2005; Oskoei and Hu, 2008; Ju et al., 2013; Atzori, Cognolato, and Müller, 2016; Geng et al., 2016); suggesting novel EMG features (e.g. Zardoshti-Kermani et al., 1995; Englehart et al., 1999; Englehart, Hudgins, and Parker, 2001; Boostani and Moradi, 2003; Phinyomark, Limsakul, and Phukpattaranont, 2009; Phinyomark, Phukpattaranont, and Limsakul, 2012; Phinyomark et al., 2013); and using pre-processing (e.g. Hargrove et al., 2009; Liu et al., 2013) as well as post-processing techniques (e.g. Englehart and Hudgins, 2003; Hargrove et al., 2010; Scheme, Hudgins, and Englehart, 2013; Scheme and Englehart, 2013b; Amsüss et al., 2014).

Classification-based myoelectric control has been applied to a variety of decoding tasks, including classification of coarse hand, wrist, and elbow movements (e.g. Englehart and Hudgins, 2003; Chan and Englehart, 2005; Fougner et al., 2011); grasp types and gestures (e.g. Fligge, Urbanek, and Smagt, 2013; Liu et al., 2014; Batzianoulis et al., 2017); individuated-finger movements (e.g. Tenore et al., 2009; Al-Timemy et al., 2013); and various combinations thereof (e.g. Hargrove et al., 2009; Atzori et al., 2014). Most of these studies, however, have been concerned with sequential classification; that is, one function (i.e. class of movement) can be active at a time. To address this issue, a few research groups have recently demonstrated the feasibility of simultaneously classifying hand and wrist movement independently, thus resulting in greater flexibility and dexterity (e.g. Young et al., 2013; Fougner, Stavdahl, and Kyberd, 2014; Wurth and Hargrove, 2014; Ortiz-Catalan, Håkansson, and Brånemark, 2014b).

2.4.2.2 *Proportional myoelectric control*

While the use of classification methods can increase the intuitiveness of myoelectric control as compared to mode switching, this approach can only offer a discrete control scheme which is fundamentally different to the natural continuous movement exhibited by living mechanisms.

Fougner et al. (2012) defined *proportional* control as the paradigm where "*the user can control at least one mechanical output (of the prosthesis) within a finite, useful, and essentially continuous interval by varying his/her control input within a corresponding continuous interval*". The authors commented that the term "proportional" in this definition is not used in the strict mathematical sense; it essentially means continuous. In computational terms, this translates into making use of regression rather than classification algorithms with the aim of estimating a scalar or multidimensional continuous target variable, such as kinematics (e.g. position, velocity) or kinetics (e.g. force). Arguably, transitioning from classification-based discrete control schemes to proportional myoelectric control is challenging, due to the finer (i.e. continuous) nature of the target signals and the greater bandwidth of prosthesis control commands.

Proportional myoelectric control has been mainly investigated with regards to the following three applications: 1) wrist position control (e.g. Muceli and Farina, 2012; Jiang et al., 2014a; Ameri et al., 2014b; Smith, Kuiken, and Hargrove, 2016); 2) finger position control (e.g. Smith et al., 2008; Ngeo, Tamei, and Shibata, 2012; Cipriani et al., 2011; Pistohl et al., 2013); and 3) finger force control (e.g. Castellini et al., 2009; Castellini and Koiva, 2012; Gijsberts et al., 2014b; Gailey, Artemiadis, and Santello, 2017). An extensive review of this topic is given in Chapters 6 and 8.

A different approach to proportional (i.e. continuous) control is via using an upper-limb musculoskeletal model and directly mapping muscle activations into control signals for the prosthesis *degrees of actuation* (DOAs) through forward-dynamic simulation of the system (e.g. Blana et al., 2017). A significant challenge of this approach is that musculoskeletal function is largely dependent on the executed motor task, pathology, and training of an individual. Additionally, it typically varies widely across subjects (Sartori, Llyod, and Farina, 2016).

Alternatively, proportional control can be achieved by using a non-intuitive (i.e. abstract) mapping between muscle activations/co-activations and prosthesis DOAs. Since the association between the two domains is in this case not intuitive, this strategy relies on user adaptation (i.e. motor learning) mechanisms taking place during closed-loop myoelectric control. It has been demonstrated that humans can learn such non-intuitive mappings in order to control cursors (Nazarpour, Barnard, and Jackson, 2012; Barnes, Dyson, and Nazarpour, 2016; Dyson, Barnes, and Nazarpour, 2017), prosthetic hand digits (Pistohl et al., 2013), virtual helicopters (Ison and Artemiadis, 2015), and multi-DOF robotic arms (Ison et al., 2016).

2.4.2.3 *Intramuscular EMG recordings*

Many factors influence the surface EMG signal, including, but not limited to, electrode shift (Hargrove, Englehart, and Hudgins, 2008; Young, Hargrove, and Kuiken, 2011), differences in contraction levels (Scheme and Englehart, 2013a), muscle fatigue (Kumar, Pah, and Bradley, 2003), and *crosstalk* among muscles. Crosstalk refers to the phenomenon where a surface EMG electrode targeting a specific muscle also records the activity of muscles in its vicinity. Although crosstalk needs not necessarily be detrimental for myoelectric control, on several occasions it might be desirable to isolate the activity of specific muscles (Farina et al., 2014). One such example is direct control schemes, whereby the activity of each muscle is associated with the control of a specified DOA of the prosthesis (e.g. Cipriani et al., 2014a). For this reason, several studies have investigated the performance of myoelectric controllers receiving input from intramuscular fine-wire electrode recordings. The use of intramuscular EMG electrodes has been proposed both in the context of classification-based (e.g. Har-

grove, Englehart, and Hudgins, 2007; Kamavuako et al., 2013; Kamavuako, Scheme, and Englehart, 2014b; Kamavuako, Scheme, and Englehart, 2014a), as well as proportional control (e.g. Cipriani et al., 2014a; Smith, Kuiken, and Hargrove, 2014; Smith, Kuiken, and Hargrove, 2016).

2.4.2.4 *Multi-modal prosthetic control*

A wide range of sensing technologies have been proposed for movement intent decoding and prosthetic control beyond EMG electrodes. Some examples include accelerometers (e.g. Fougner et al., 2011; Geng, Zhou, and Li, 2012; Radmand, Scheme, and Englehart, 2014; Khushaba et al., 2016, see Section 3.1 for a detailed discussion); mechanomyography (Silva, Heim, and Chau, 2005); near-infrared spectroscopy (Chianura and Giardini, 2010); and force myography (Radmand, Scheme, and Englehart, 2016; Cho et al., 2016). A detailed review of this topic is given by Lobo-Prat et al. (2014). Computer vision-based systems have also been recently used for automatic grasp pre-shaping with promising results (Dosen et al., 2010; Markovic et al., 2014; Ghazaei et al., 2017).

2.4.2.5 *Targeted muscle reinnervation*

Targeted muscle reinnervation is a surgical procedure invented by Kuiken et al. (2004), by which residual nerves originally innervating a muscle of an amputated limb are redirected to spare muscle regions, usually on the stump or chest of the patient. In this way, the target muscle can act as a biological amplifier of afferent neural signals originally controlling the activation of the muscles, and consequently, the movement of the missing limb. The activity of target muscles can then be recorded using surface electrodes and used as a control signal for myoelectric prostheses. Originally invented in 2004, this technique has demonstrated proof-of-principle for dexterous prosthetic control by amputees of all levels, including shoulder disarticulation (e.g. Huang et al., 2008; Kuiken et al., 2009; Tkach et al., 2014; Young, Kuiken, and Hargrove, 2014).

2.4.3 *Discrepancy between academic research and industrial adoption*

Despite recent scientific and technological advancements in the field of myoelectric control, the rejection rate of upper-extremity prostheses remains relatively high (see Section 2.1.3). Moreover, a remarkable gap between academic achievements and clinical adoption can be observed in the recent years (Jiang et al., 2012b); while many research studies have demonstrated the feasibility of deploying ML methods to decode movement intent for prosthesis control (see Section 2.4.2), conventional mode switch-

ing schemes are almost exclusively used in commercial systems (see Section 2.4.1.1). The main advantage of ML-based myoelectric systems over conventional schemes is the greater intuitiveness and naturalness of prosthesis control. However, their commercial adoption has been rather limited due to insufficient control reliability and robustness under realistic conditions, as opposed to the controlled nature of laboratory experiments and purely offline analyses (Ortiz-Catalan et al., 2015; Vujaklija et al., 2017). Nonetheless, the first commercial system employing ML for prosthesis control has recently appeared on the market and is currently being clinically tested with amputees (see Section 2.4.1.3).

2.5 ASSESSMENT PROTOCOLS FOR MYOELECTRIC CONTROL

A plethora of assessment tools have been proposed for evaluating the control performance and dexterity of prosthetic hands. The following sections briefly introduce some of the most commonly used protocols in the myoelectric control literature.

2.5.1 *Southampton hand assessment procedure*

The Southampton hand assessment procedure (or simply SHAP) is a test designed to assess the function of natural and prosthetic hands (Light, Chappell, and Kyberd, 2002). It comprises grasping and relocating six abstract objects of various shapes and weights, and additionally performing 14 activities of daily living, such as coin picking, simulated food cutting, object lifting, zip opening/closing, jug pouring, etc. To complete the test, the participant is required to perform the following six grip patterns: lateral, cylindrical, tripod, pinch, spherical, and extension.

Each task is timed by the participant by pressing a button at the start and end of the trial. Timings from all tasks are then taken into account to compute a single performance score. A complete assessment lasts approximately 20 min.

2.5.2 *Clothespin relocation test*

The clothespin relocation test (Lipschutz et al., 2006) requires the prosthesis user to move clothes pegs from a horizontal bar to a higher vertical bar, or vice versa. The time taken to relocate a fixed number of pegs can then be used as a measure of prosthesis control performance.

2.5.3 *Box and Block test*

The Box and Block test (Cromwell, 1960; Mathiowetz et al., 1985; Radomski and Latham, 2008) is an assessment tool used by occupational therapists to evaluate motor function and manual dexterity. The test comprises a board (i.e. the "Box") split into two compartments of equal size which are divided by a partition and 150 small wooden cubes (i.e. the "Blocks") initially lying in one of the two sides. The participant is given 60 s to transport as many blocks as they can to the initially empty compartment. The count of transported blocks within the given time frame is then used as a measure of manual dexterity.

2.5.4 *Fitts' law test*

In a seminal study, Fitts (1954) quantified human motor performance in terms of information theoretic principles (Shannon, 1948). Fitts' law predicts that the time taken to rapidly point to a target area is a function of the ratio between the target distance D and the target width W. Fitts defined the index of difficulty (in bits) as follows:

$$\mathrm{ID} = \log_2\left(\frac{2\mathrm{D}}{W}\right). \tag{2.12}$$

Using the above definition, Fitts also defined an index of performance, also called throughput (bits/sec):

$$\mathrm{IP} = \left(\frac{\mathrm{ID}}{\mathrm{MT}}\right), \tag{2.13}$$

where MT denotes the time taken to reach the target.

In myoelectric control, the Fitts' law test has been used as a measure of user performance in virtual target reaching tasks. The throughput metric has been used to evaluate target control performance in one (e.g. Scheme et al., 2014), two (e.g. Kamavuako, Scheme, and Englehart, 2014b; Wurth and Hargrove, 2014), and three dimensions (e.g. Scheme, Hudgins, and Englehart, 2013; Ameri et al., 2014b; Smith, Kuiken, and Hargrove, 2016). In the latter case, the first two dimensions correspond to the Cartesian co-ordinates of the target cursor, whereas the third dimension is visualised by

varying the cursor diameter. In the myoelectric control literature, a modified model is often used for the index of difficulty, defined by MacKenzie (1992) as follows:

$$\mathrm{ID} = \log_2\left(\frac{\mathrm{D}}{W} + 1\right). \tag{2.14}$$

2.5.5 *The motion and target achievement control tests*

The motion test was introduced by Kuiken et al. (2009) to quantify the performance of real-time classification-based myoelectric control. In this test, the participant is presented with a target motion for a virtual limb and is required to select the desired movement and maintain it until it has been executed by the virtual prosthesis.

The following three performance measures are defined for the motion test: selection time, that is, is the time taken to select the correct target motion; *completion time* (CT), which is defined as the time from movement onset to the 10^{th} correct classification of the target motion; and *completion rate* (CR), which is the percentage of successfully completed motions.

The motion test lacks two important features: firstly, it does not consider proportional control, as it assumes a fixed speed of movement for the virtual prosthesis, and more importantly, it does not take into account incorrect classifications.

To address these two issues (Simon et al., 2011) introduced the target achievement control test. In this paradigm, the participant is required to select the desired motion of each controllable DOF, as well as the correct level of activation. That is, if the subject overshoots the desired posture, they have to correct that motion to successfully accomplish the trial. In addition to CR and CT, the target achievement control test uses the path efficiency metric to quantify performance, which is defined as the ratio between the distance of the shortest path to the target and the total distance travelled by the virtual limb. It is worth noting that the target achievement control and Fitts' law tests are closely related (Scheme, Hudgins, and Englehart, 2013; Wurth and Hargrove, 2014).

3

CONCURRENT USE OF SURFACE ELECTROMYOGRAPHY AND INERTIAL MEASUREMENTS FOR PROSTHETIC CONTROL

Despite recent advances in the research community, *machine learning* (ML)-based prosthetic control is currently not adopted in the majority of clinical/commercial systems (see Section 2.4.1). The main reason behind this discrepancy is believed to be the lack of robustness of pattern recognition systems under realistic conditions (Vujaklija et al., 2017), which is mainly due to the non-stationary nature of the surface *electromyographic* (EMG) signal (Amsüss, 2014).

The surface EMG signal is inherently noisy (Reaz, Hussain, and Mohd-Yasin, 2006) and, thus, not always a robust source of input information for prosthetic systems. This is especially true for altered conditions such as sweat (Jiang et al., 2012b), fatigue (Kumar, Pah, and Bradley, 2003), and electrode displacement (Hargrove, Englehart, and Hudgins, 2008; Young, Hargrove, and Kuiken, 2011). One of the main issues associated with the use of surface EMG signals is the *limb position effect* (Fougner et al., 2011; Geng, Zhou, and Li, 2012; Jiang et al., 2013), which states that a system trained on a single arm position is likely to fail to generalise to novel arm postures.

In order to achieve reliable and robust pattern recognition-based prosthetic control under realistic conditions, there is an increasing need to move towards multi-modal solutions (Jiang et al., 2012b). The study presented in this chapter investigates the concurrent use of surface EMG and inertial measurements for movement intent decoding and prosthetic hand control. The benefit of including inertial measurements in myoelectric control is initially demonstrated by performing an exhaustive analysis on benchmark datasets, and subsequently validated with a real-time prosthetic control experiment.

3.1 INTRODUCTION

3.1.1 *The limb position effect*

The term *limb position effect* was first introduced by Fougner et al. (2011) and refers to the performance decrease experienced by myoelectric decoders due to variations in limb positions. The authors recorded EMG data from 17 able-bodied subjects whilst they performed 8 wrist and grasp movements under five different limb positions:

straight arm hanging at side; straight arm reaching forward; straight arm reaching up; humerus hanging at side, forearm horizontal; and humerus hanging at side, forearm reaching up. The authors observed that although the average classification error when decoders were trained and tested under the same limb posture was 3.8%, the same figure increased to 18% when they tested the generalisation of the classifiers to novel postures.

Geng, Zhou, and Li (2012) performed a similar analysis on five transradial amputees and replicated the findings of Fougner et al. (2011); 7.3% and 29.9% average errors were reported for intra- and inter-position classification, respectively.

Cipriani et al. (2012) investigated the effect of weight and inertia on the performance of a decoder that classified individual finger movements. Eight able-bodied subjects performed a series of finger motions under different limb and payload conditions. The reported decrease in performance was dramatic, with average classification errors increasing from 2% for ideal, static conditions, to 43% when subjects combined finger with shoulder/elbow movements.

Jiang et al. (2013) demonstrated that the limb position effect also affected the task of using EMG measurements to reconstruct *three-dimensional* (3D) kinematics of wrist movement. The prediction accuracy decreased from 62.9% to 34.0% for able-bodied subjects, and from 61.3% to 46.1% for amputees. The authors concluded that *"changing arm position adversely influences the performance of the algorithm for both subject groups, but that this influence is less pronounced in amputee subjects with respect to able-bodied subjects"*, and this observation was attributed to differences in anatomical structure between amputees and normally-limbed subjects.

Finally, Yang et al. (2017) tested the generalisation of support vector machine classifiers when training data were collected under the following four conditions: static posture, steady muscular contraction level; dynamic posture, steady muscular contraction level; dynamic posture, dynamic muscular contraction level; and dynamic posture, dynamic muscular contraction level with force disturbance. The authors reported that the highest generalisation was achieved when training data were collected with dynamic postures and various levels of muscle contraction and proposed this training data collection paradigm as the most appropriate for real-life applications.

3.1.2 *Use of accelerometers and other means of resolving the limb position effect in prosthetic control*

Fougner et al. (2011) proposed the following two means of addressing the limb position effect: 1) collect EMG data and train classifiers under multiple limb positions, and 2) use accelerometers to disambiguate limb position. These two approaches re-

sulted in a decrease in inter-position classification error from 18% to 5.7% and 5.0%, respectively. Two different strategies were investigated for combining the two input data sources: two-stage position-aware classification, where the accelerometer data were firstly used to classify limb position and the EMG data were subsequently used to classify motion class; and single-stage position-aware classification, where the two sources of data were concatenated and fed as inputs to a single classifier. Fougner et al. reported that the performance of these two strategies was comparable.

In a similar fashion, Geng, Zhou, and Li (2012) collected data under multiple limb positions and employed a two-stage position/motion classifier. The authors reported a decrease in average inter-position classification error from 29.9% to 9.0%.

Boschmann and Platzner (2013) used a slightly different approach and proposed resolving the limb position effect by using high-density EMG recordings and collecting training data under various limb postures. The authors reported an increase in *classification accuracy* (CA) of approximately 16% when 96 EMG channels were included in decoding, as compared to the case where only 4 channels were selected.

Gijsberts et al. (2014a) classified 40 hand, wrist and functional movements and demonstrated that by using solely accelerometry information a higher classification performance was achieved than with surface EMG data. Nevertheless, the highest decoding performance was achieved when the two sources of information were combined. It is worth noting, however, that this study included only static motions, that is, the participants' forearm was kept fixed throughout the course of the experiments.

Khushaba et al. (2016) investigated the combined effect of forearm orientation and muscle contraction level on the decoding accuracy of six motion classes. They demonstrated that the use of time-domain power spectral descriptors (Al-Timemy et al., 2016) yielded the highest decoding performance across different forearm orientations and contraction levels. They also demonstrated that the inclusion of an accelerometer measuring wrist orientation improved EMG decoding performance.

While many studies have proposed the use of accelerometers for resolving the limb position effect, Radmand, Scheme, and Englehart (2014) have been somewhat critical of this approach. They demonstrated that integrating accelerometry data into myoelectric decoders can potentially decrease decoding performance, unless training data are collected under most of the possible configurations in 3D space. They also showed that classifiers trained with static motions generalise poorly when used to decode hand gestures during dynamic movement. To overcome this limitation, and since collection of static training data in all possible positions would be practically impossible, they proposed a method for collecting training data with dynamic motions covering the regions of interest. By using this approach, they reported an im-

provement in CA as compared to static training in multiple positions, as it had been suggested by earlier studies (e.g. Fougner et al., 2011; Geng, Zhou, and Li, 2012).

Betthauser et al. (2017) recently proposed a different approach to address the limb position effect by using solely EMG data and an extreme learning version of adaptive sparse representation. Instead of estimating class decision boundaries, this method tries to reconstruct a test input vector as a linear combination of training data stored in class-specific dictionaries. Test inputs are then assigned to the class whose dictionary yields the smallest reconstruction error. The performance of this method was compared to standard *linear discriminant analysis* (LDA) classification during offline and real-time experiments with both able-bodied and amputees, and it was found that it achieved higher accuracy when tested on novel limb postures.

Finally, it is worth noting that accelerometers have been also used in the context of lower-limb prosthetic control (e.g. Antonelli, Beomonte Zobel, and Giacomin, 2009; Spanias et al., 2015).

3.1.3 *Motivation*

Despite that many studies have proposed the use of accelerometers as a potential means of resolving the limb position effect and improving CA (Fougner et al., 2011; Geng, Zhou, and Li, 2012; Gijsberts et al., 2014a; Radmand, Scheme, and Englehart, 2014; Khushaba et al., 2016), they have all been limited to purely offline analyses. Yet, there has been increasing evidence that an observed boost in offline CA is not necessarily associated with a performance improvement during real-time, task-oriented myoelectric control (Jiang et al., 2014b; Ortiz-Catalan et al., 2015). These observations make imperative the validation of any proposed advancements in the field with real-time prosthetic control experiments. Moreover, most commercial *inertial measurement unit*s (IMUs) nowadays incorporate additional sensors, such as gyroscopes and magnetometers. The potential benefit of using these additional modalities for prosthetic control has not been previously investigated.

The goal of the work presented in this chapter is threefold: 1) investigate whether classification performance can further benefit from the use of additional inertial sensors, such as gyroscopes and magnetometers; 2) assess whether an increase in offline CA can be translated into a performance improvement during real-time prosthetic control; 3) investigate whether the inclusion of inertial measurements can help reduce the number of sensors required to achieve robust classification performance. This last aspect is particularly important for real-life applications, where it is desirable to minimise the number of sensors used by the prosthesis.

3.2 OFFLINE EXPERIMENT

In the first part of this study, a large dataset was collected with 20 able-bodied and two transradial amputee subjects. For data collection, a standardised procedure for recording EMG data was adopted, namely the Ninapro protocol (Atzori et al., 2012; Atzori et al., 2014; Gijsberts et al., 2014a; Atzori et al., 2015). The following sections provide information on the behavioural task and signal acquisition protocol followed for data collection.

3.2.1 *Behavioural task*

Twenty able-bodied (17 male, 3 female; 16 right-hand, 4 left-hand dominant; median age 25.5 years) and two transradial amputee subjects were recruited. Both impaired subjects were right-hand amputees and right-hand dominant prior to amputation. The medical records of the amputee participants are presented in Table 3.1 and photographs of their stumps are shown in Figure 3.2.

The participants sat comfortably on an office chair and were asked to reproduce a series of 40 motions, including various individuated-finger, hand, wrist, grasping and functional movements instructed to them on a computer screen. The movements corresponded to exercises B and C in Atzori et al. (2014), and are shown in Figure 3.1. Each movement was repeated six times and trials were interleaved with 5 s resting periods. The two amputee participants were instructed to perform bilateral imaginary mirrored movements. Data collection with one of the amputee subjects was interrupted early due to a power supply failure; as a result, the participant did not perform the final two movements (i.e. 22 and 23 in exercise C).

3.2.2 *Signal acquisition*

Myoelectric and inertial data were collected by using the Delsys® Trigno™ IM Wireless EMG System (see Section A.1.1). The sampling frequency was set to 2 kHz for myoelectric signals and 128 Hz for inertial data. Readings from IMUs were used in their raw format; therefore, no calibration was required. Typical raw EMG and inertial data recorded from a single sensor are shown in Figure 3.3 and correspond to an able-bodied participant. The number of signals recorded with each sensor was 10 (each column in Figure 3.3, see Section A.1.1).

For sensor placement, the NinaPro protocol (Atzori et al., 2014) was followed, which uses 12 sensors. Eight sensors were equally spaced around the forearm (placed

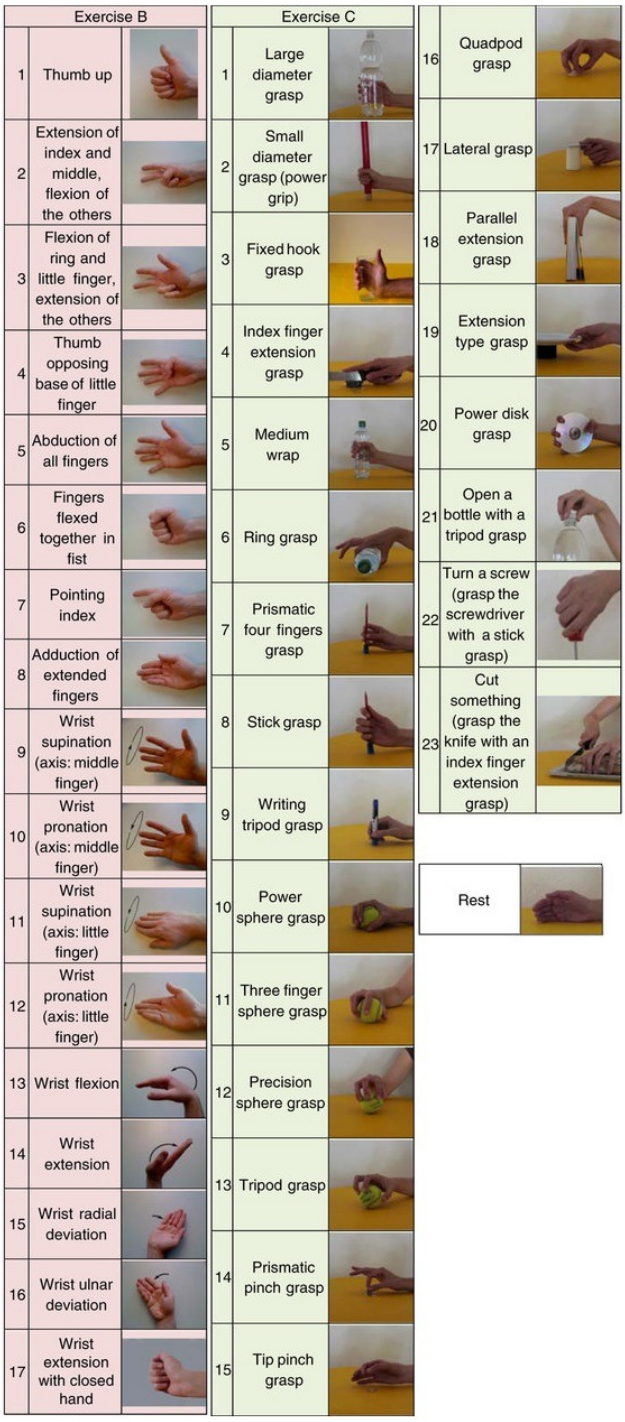

Figure 3.1: Ninapro protocol exercises. Two exercises were included comprising a total of 40 movements. (Left column) exercise B, finger and wrist movements; (middle-right columns) exercise C, grasp and functional movements. The rest position is also shown at the bottom of the right column. Figure has been adapted from Atzori et al. (2014) and is distributed under a CC BY 4.0 International License (https://creativecommons.org/licenses/by/4.0/).

3cm below the elbow), two targeted the extrinsic hand muscles extensor digitorum communis and flexor digitorum superficialis, and the remaining two were placed on

Table 3.1: Amputee participant medical records

Age	Cause of amputation	Years since amputation	Prosthesis use
28	Car accident	6	Split hook
54	Cancer (epithelioid sarcoma)	18	Split hook

Figure 3.2: Amputee participant stumps.

Table 3.2: EMG-IMU sensor placement

Sensor	Location
1-8	Equally spaced around forearm (3 cm below elbow)
9	Targeting extensor digitorum communis
10	Targeting flexor digitorum superficialis
11	Biceps brachii
12	Triceps brachii

the biceps and triceps brachii muscles (see Table 3.2). Prior to electrode placement, participants' skin was cleansed using 70% isopropyl alcohol. Adhesive latex-free elastic bandage was used the keep the sensor positions fixed throughout the experimental sessions. Representative pictures showing electrode placement for two participants (one able-bodied and one amputee) are shown in Figure 3.4.

3.2.3 *Signal pre-processing*

Following Gijsberts et al. (2014a), power line interference was suppressed from the myoelectric signals by applying a Hampel filter (Allen, 2009). The post-hoc relabelling procedure introduced by Kuzborskij, Gijsberts, and Caputo (2012) was used to identify and refine the exact motion timings for each subject and trial. This was done to avoid introducing label-related "noise" in the classifiers due to discrepancies between stimulus presentation and movement execution timings. Such discrepancies

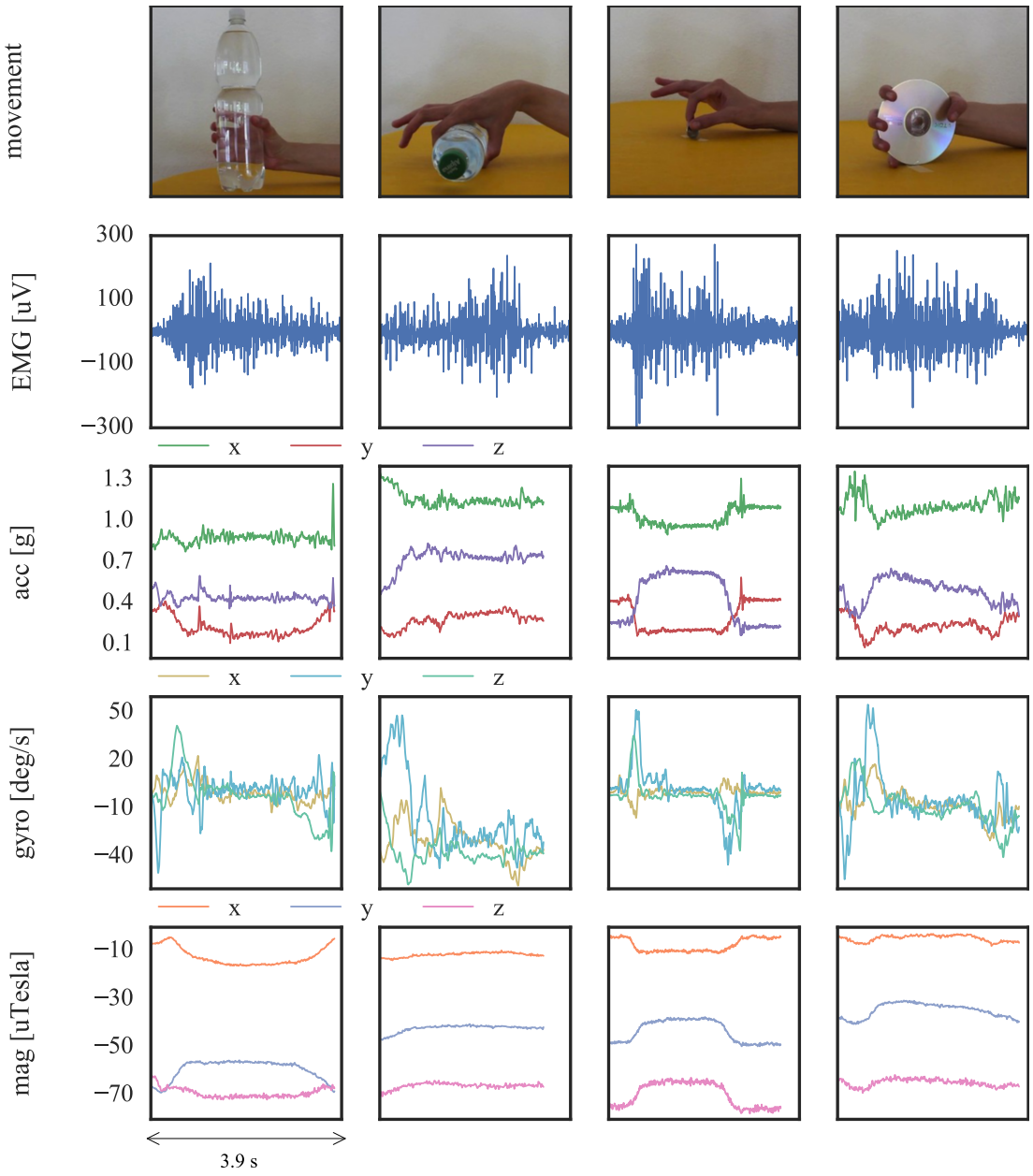

Figure 3.3: Raw EMG and inertial data. Traces of raw signals associated with a single EMG-IMU sensor are shown for four movements (top panel). Raw EMG, 3D accelerometer (acc), gyroscope (gyro), and magnetometer (mag) readings are shown in the four bottom panels. Photographs showing movements (top panel) have been reproduced from Atzori et al., 2014 and are distributed under a CC BY 4.0 International license (https://creativecommons.org/licenses/by/4.0/).

arise from the natural variability introduced when subjects replicate movements instructed to them on a screen (i.e. reaction times, variability in trial lengths, etc.). The relabelling method uses the recorded EMG data and an onset detection algorithm (Staude and Wolf, 1999) to extract the precise timings of movement execution. This is achieved via using a generalised likelihood ratio algorithm that maximises the likeli-

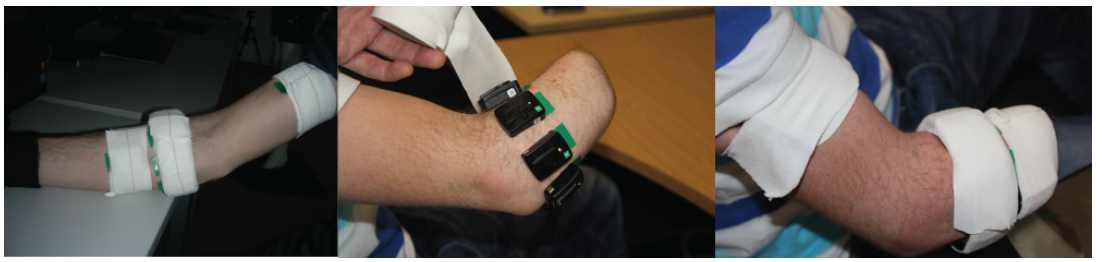

Figure 3.4: Sensor placement. Eight EMG-IMU sensors were equally spaced around the participants' forearm (3 cm below the elbow), two targeted the extensor digitorum communis and flexor digitorum superficialis muscles, and two were placed on the biceps and triceps muscles. Elastic bandage was used to keep the sensor positions fixed. Sensor placement shown for an able-bodied (left) and an amputee subject (centre, right).

hood of a rest-movement-rest sequence. It was verified during preliminary analyses that making using of the relabelling transformation leads to substantially improved classification performance. An illustration of the outcome of this procedure is provided in Figure 3.5.

Myoelectric and inertial signals were synchronised via linear interpolation. By using a sliding window approach (see Section 2.2.3), four EMG features were extracted from each channel; namely, the mean absolute value, waveform length, 4^{th}-order autoregressive coefficients, and log-variance (see Section 2.2.3.1). The selection of these features was based on previous studies demonstrating their efficacy in decoding hand motion intention (Hargrove, Englehart, and Hudgins, 2007; Hahne et al., 2014). Bearing in mind the need for low computational requirements during real-time control, only time-domain EMG features were considered (Boostani and Moradi, 2003). The length of the sliding window was set to 256 ms and the increment to 50 ms (80% overlap). It has been previously shown that this selection offers a good compromise between classification performance and controller delay (Smith et al., 2011). In order to match EMG features, inertial data were also binned in 256 ms windows by extracting the mean value of the signals within the processing window. The total number of features contributed by each sensor was thus 16 (7 EMG, 9 inertial features.)

The columns of the design matrix (i.e. input features) were standardised by subtracting the mean and dividing by standard deviation. Mean subtraction and feature scaling followed *cross-validation* (CV) splitting (see Section 3.2.5), which ensured that there was no information leakage from the test set to the training set. Datasets collected for both types of experiments were included unchanged in the subsequent analyses steps; that is, no segments of activity were manually removed.

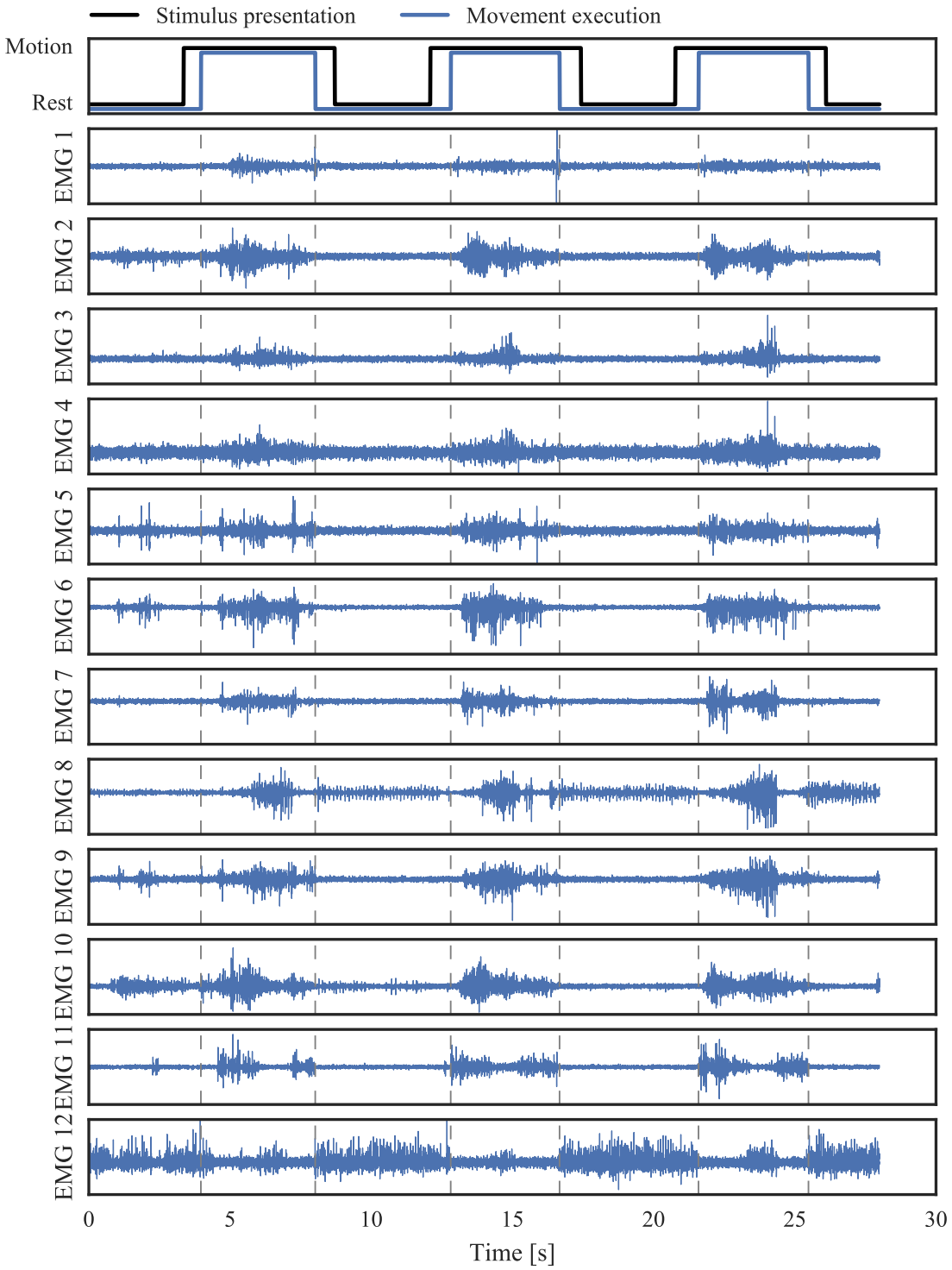

Figure 3.5: Post-hoc relabelling procedure proposed by Kuzborskij, Gijsberts, and Caputo (2012). (Top panel) stimulus presentation and movement execution time-series; (second top-bottom panels) EMG signals used to identify the exact timings of movement execution. Dashed lines indicate refined starting and ending timestamps of movement. The reader is referred to Table 3.2 for EMG sensor placement details.

3.2.4 *Classification algorithm*

To decode movement intent from myoelectric and inertial data, LDA classification was used. The LDA classifier has arguably been the most popular choice in the myoelectric control literature (e.g Al-Timemy et al., 2013; Scheme, Hudgins, and Englehart, 2013; Young et al., 2013). Details about the working principle of the classifier are presented in a following chapter (see Section 4.2.1). The purpose of the current study was to investigate and compare the performance of different sensing modalities; hence, algorithmic comparisons were not performed at this stage. A detailed investigation of the decoding performance of various classifiers is carried out in Chapter 4.

The extracted EMG and/or inertial features were fed as input(s) to the classifiers and the vectors containing the stimulus time-series (i.e. grip performed) were used as the target signals. All types of classifiers were trained and tested by using data from individual subjects.

3.2.5 *Cross-validation and decoding performance assessment*

Participants performed six repetitions of each movement out of which five were used to train the decoders and the left-out repetition was used to assess decoding performance. The procedure was iterated six times by using a different evaluation fold in each iteration, hence resulting in 6-fold CV (see Figure 3.6).

Following classification, the class distribution of the test folds was balanced by removing a large proportion of the instances corresponding to the "rest" class. This step was necessary to prevent performance scores from being biased by the large number of samples in that class. The identity of test samples to be removed was determined by their temporal distance from the nearest segment of muscle activity; that is, samples located nearest movement execution were retained, whereas the majority of intermediate samples were discarded. The class balancing procedure is illustrated in Figure 3.7. Using such a deterministic approach ensured that the repeatability of the analysis was not affected and was thus preferred over randomly sub-sampling the "rest" class. Finally, to evaluate decoding performance, the standard CA metric (see Section B.2) was applied on the balanced dataset.

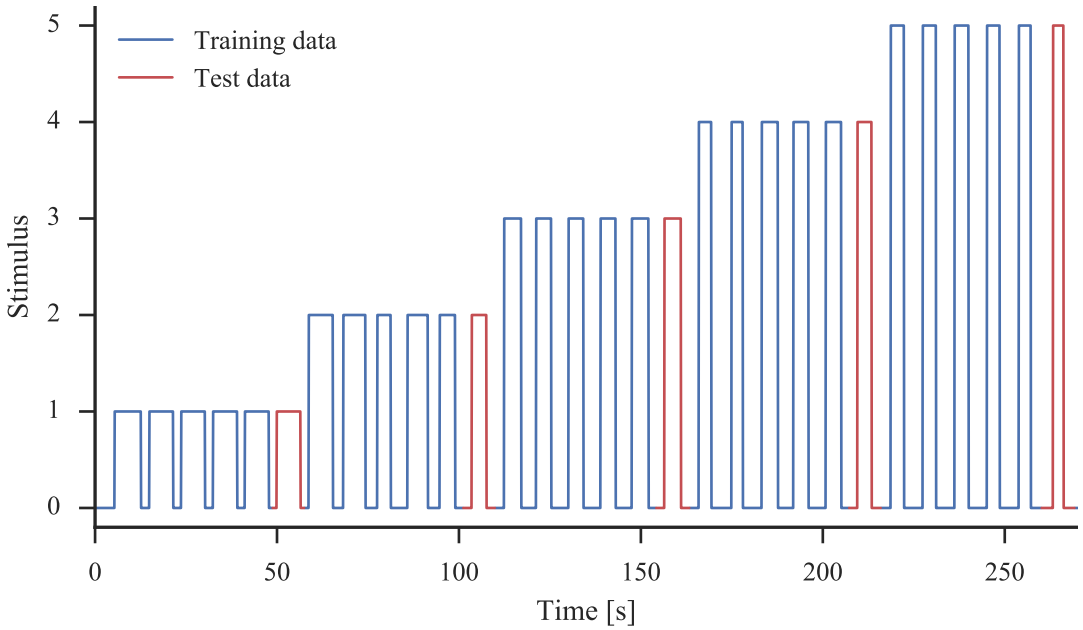

Figure 3.6: Cross-validation for evaluation of movement intention decoding. Five repetitions of each movement (blue) were used to train decoders and the left-out repetition (red) was used to evaluate classification performance. The procedure was iterated six times, hence resulting in 6-fold CV.

3.2.6 *Sequential forward sensor selection*

One of the aims of this study was to assess whether the use of inertial data measured with the same sensor packs that record EMG signals could help reduce the number of channels required to achieve high-level myoelectric control. In this direction, it was investigated whether the use of an optimally selected subset of EMG-IMU sensors could achieve the same level of decoding performance attained by the decoders when all available sensors were used.

A sensor selection method was developed which was based on the classical *sequential forward feature selection* (SFFS) algorithm (e.g. Nazarpour, Sharafat, and Firoozabadi, 2007; Li, Schultz, and Kuiken, 2010; Adewuyi, Hargrove, and Kuiken, 2016). The adapted algorithm was initialised with an empty sensor set. In each iteration, the sensor that yielded the highest performance improvement was added to the pool. Decoding performance was assessed by including all input signals from the associated sensor, that is, 7 EMG and 9 inertial features. To increase the robustness of the method, CV was used in each iteration and the sensor selection decision was based upon a majority vote across the CV folds. For consistency, the CA metric was used for assessing decoding performance at each iteration. The algorithm terminated execution once all sensors were included in the set. Finally, the sensors the addition of which yielded an improvement in CA larger than 1% were selected. The sensor

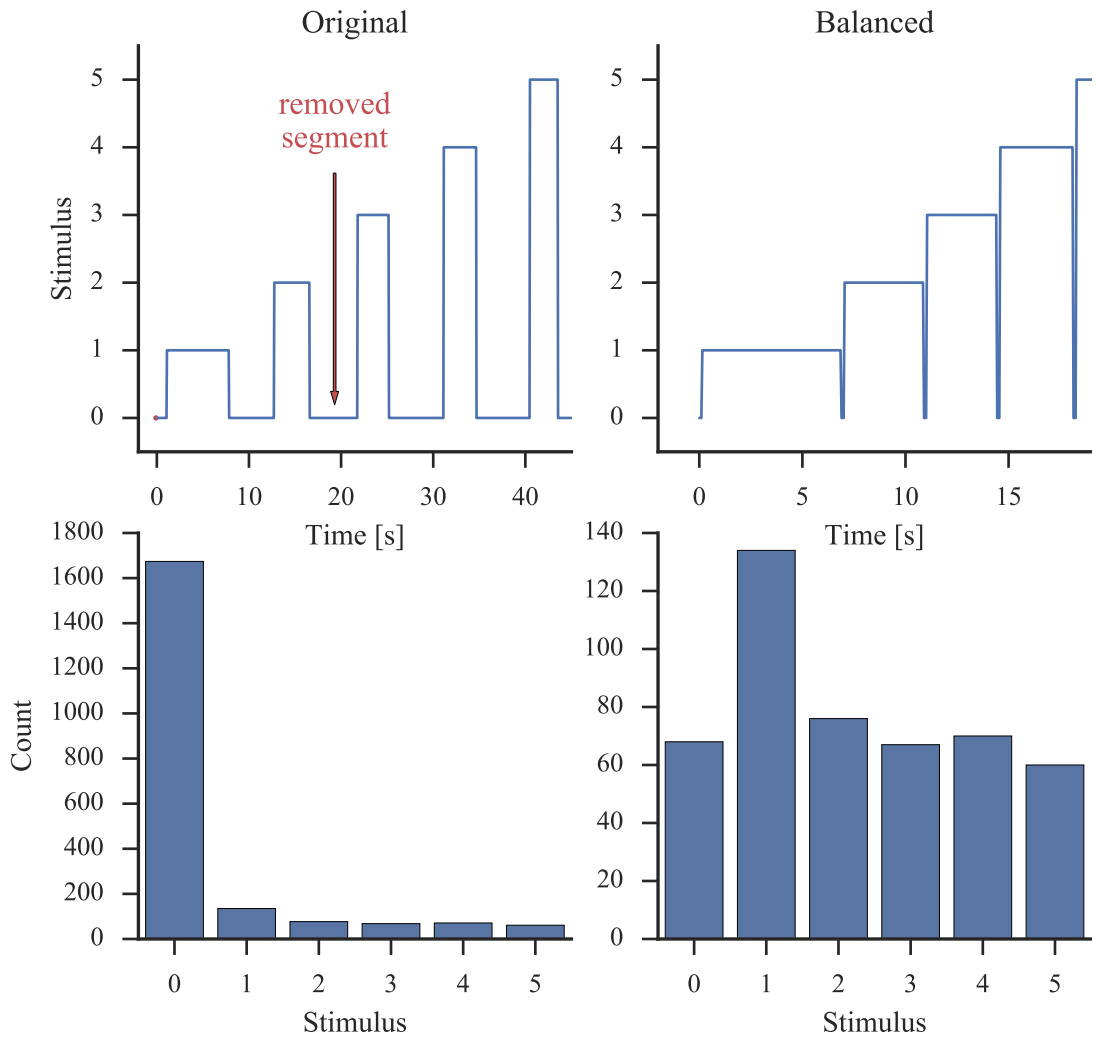

Figure 3.7: Post-hoc class balancing procedure. (Top panel) target signal time series before (left) and after (right) removing a large proportion of the samples corresponding to the "rest" class; (bottom panel) the target signal class distribution before (left) and after (right) class balancing. Note different scale on y-axis.

rankings varied across subjects; thus, the selected subsets were subject-specific. The size of the subsets also varied across participants.

3.2.7 *Statistical tests*

No prior assumptions were made about the distribution of CA scores; therefore, the non-parametric Friedman test (Friedman, 1937) was used to compare the classification performance of the different sensing modalities. Post-hoc pair-wise comparisons were performed using the Wilcoxon signed-rank test (Wilcoxon, 1945) with Šidák correction for multiple comparisons (Šidák, 1967).

3.2.8 *Results*

The aim of this study was to assess the predictive performance of different modalities, that is, surface EMG, accelerometer, gyroscope, and magnetometer measurements, as well as various combinations of these data sources. A systematic comparison was performed on the balanced CA achieved by various decoders on a large pool of gestures and hand movements (40 classes). The case of including both EMG and inertial information from an optimally selected subset of sensors was also examined as a special case. The results of this analysis are presented in Figure 3.8, separately for the able-bodied and amputee populations.

For both populations, the performance of the EMG-IMU classifier was significantly higher than that of any other decoder (median CA for this condition was 82.7% for able-bodied and 77.8% for amputee subjects). The second best performance was achieved by the IMU decoder (81.7% able-bodied, 77.7% amputees), followed by the EMG-IMU subset condition (81.2% able-bodied, 76% amputees). All pairwise differences were significant except for the comparison between the EMG-Acc and Mag classifiers.

One of the motivations of this study was to identify whether the additional inclusion of gyroscope and magnetometer data beyond accelerometry would be beneficial for hand movement decoding. The offline analysis provided evidence supporting this hypothesis, since it was found the EMG-IMU decoder performed significantly better than EMG-Acc (median CA 76.4% able-bodied, 63.9% amputees). That was also the case when myoelectric data were completely discarded; that is, the IMU decoder significantly outperformed the Acc classifier (median CA 73.4% able-bodied, 58.5% amputees). All comparisons were consistent across the able-bodied and amputee populations.

Average confusion matrices are shown in Figure 3.9 for four out of eight decoding conditions, separately for the able-bodied and amputee groups. To estimate confusion matrices, results were averaged across CV folds and participants in the respective groups.

3.3 REAL-TIME PROSTHETIC CONTROL EXPERIMENT

In the previous section, an exhaustive offline analysis on decoding hand movement intention from surface EMG and inertial data was presented. This section aims to investigate the benefits of incorporating inertial measurements for prosthetic hand control. For this purpose, an experiment was designed in which participants modulated their muscular activity to control a commercial prosthetic hand in real-time.

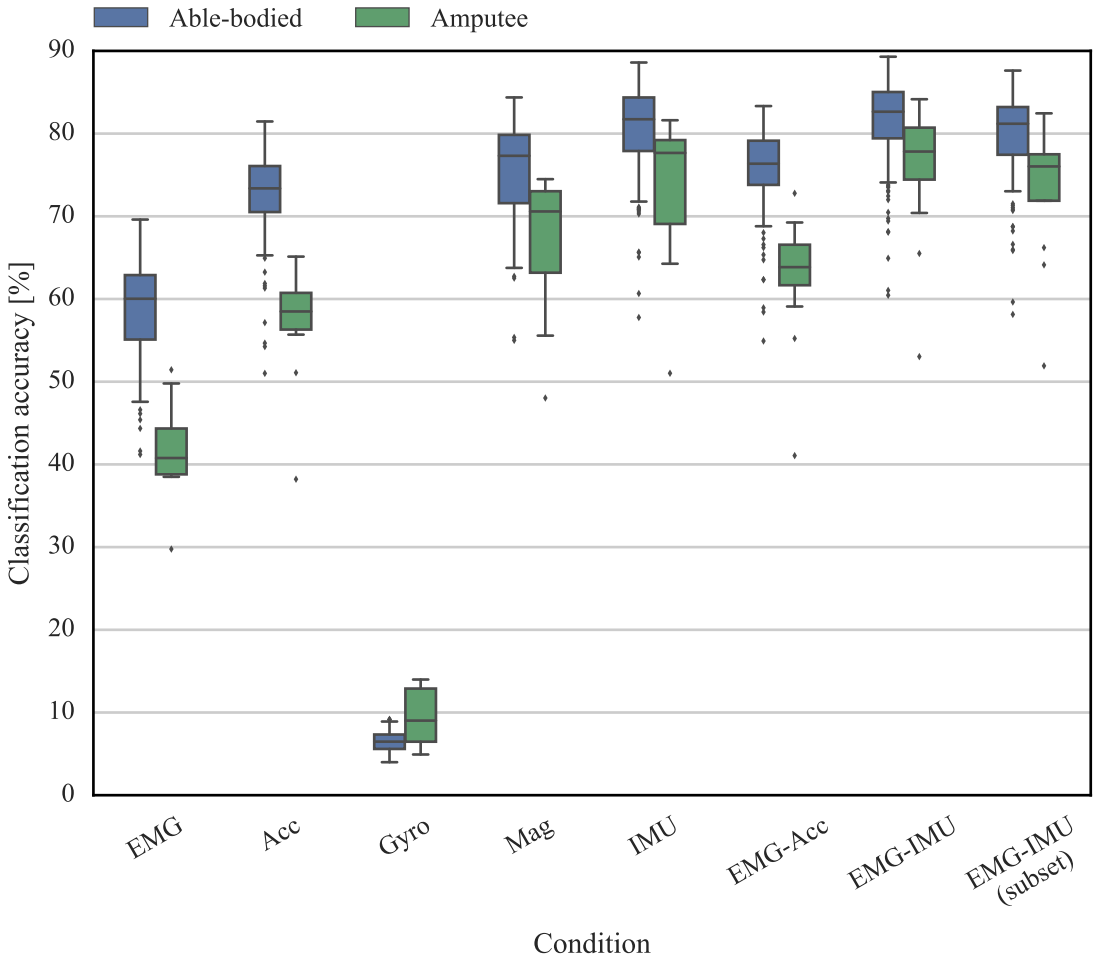

Figure 3.8: Offline decoding performance comparison. Balanced CA scores shown for the able-bodied and amputee populations. Data shown for all subjects (20 able-bodied, two amputees) and CV folds ($k = 6$). Straight lines, medians; solid boxes, interquartile ranges; whiskers, overall ranges of non-outlier data (1.5 IQR); diamonds, outliers. EMG, electromyography; Acc, accelerometer; Gyro, gyroscope; Mag, magnetometer; IMU, inertial measurement unit (accelerometer, gyroscope, magnetometer).

3.3.1 *Experimental setup*

Eleven able-bodied male subjects (8 right-hand, 3 left-hand dominant; median age 26.5 years) and one male amputee (first row in Table 3.1) were recruited. For sensor placement, the procedure described in Section 3.2.2 was followed (see also Figure 3.4). Participants were fitted the Touch Bionics® robo-limb™ prosthetic hand (see Section A.2.1) on their right arm by using a custom-made socket. For able-bodied participants, a splint was fabricated which accommodated the prosthesis on the distal side, such that its movement was not obstructed by the native limb. The fingers of the participants' right hand were constrained in a fist formation by using elastic bandage in an effort to mimic the amputee case as closely as possible. For the amputee participant,

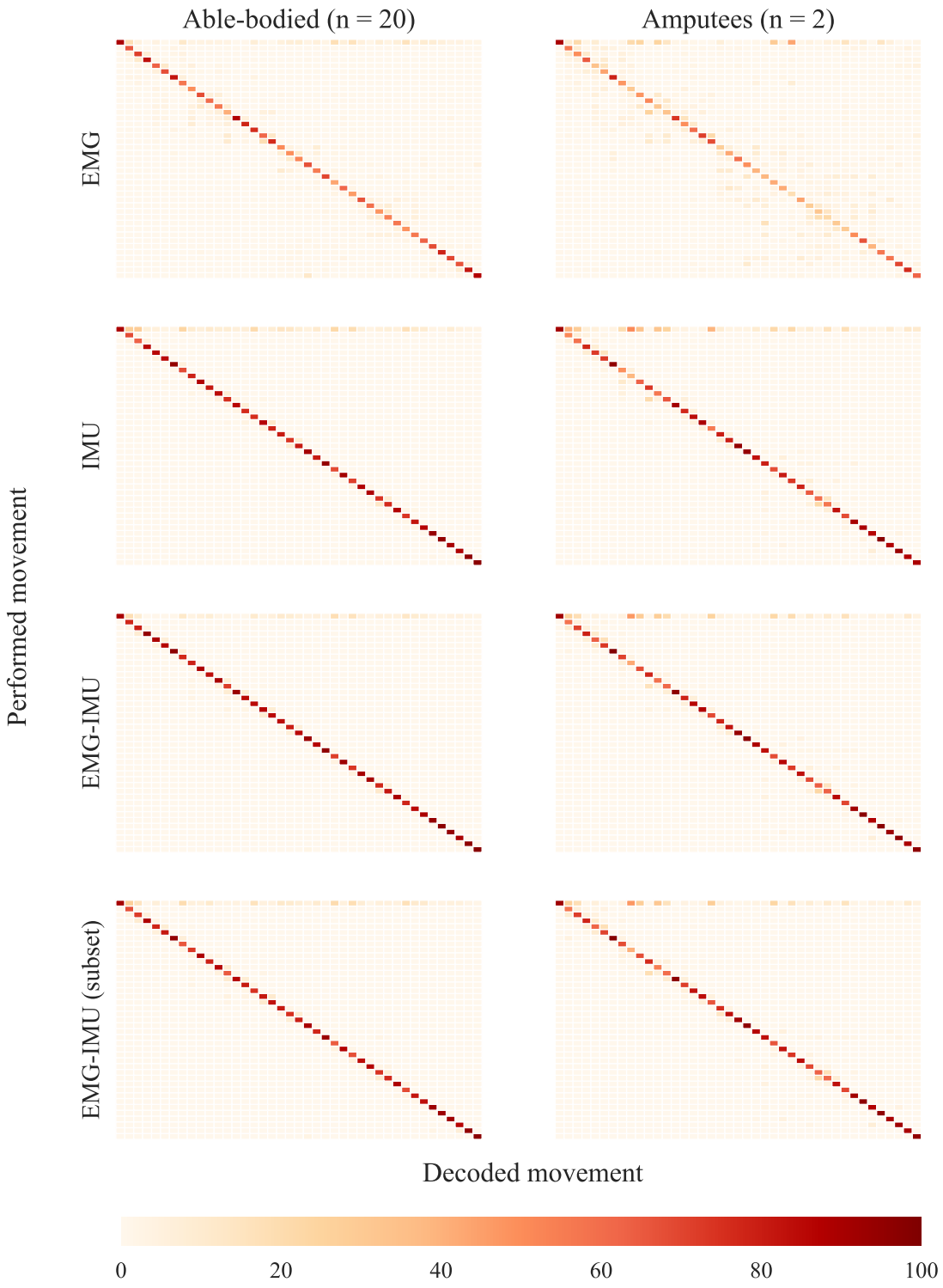

Figure 3.9: Offline classification. Confusion matrices shown for the able-bodied (left) and amputee (right) populations for four types of decoders. Results were averaged across participants (20 able-bodied, 2 amputees) and CV folds ($k = 6$). Colour intensities indicate normalised prediction scores for each class.

a specific socket was designed which fitted exactly the stump of the subject. The two arrangements are shown in Figure 3.10.

Figure 3.10: Socket fitting for real-time experiment. Customised sockets were built for able-bodied subjects (left) and the amputee participant (right).

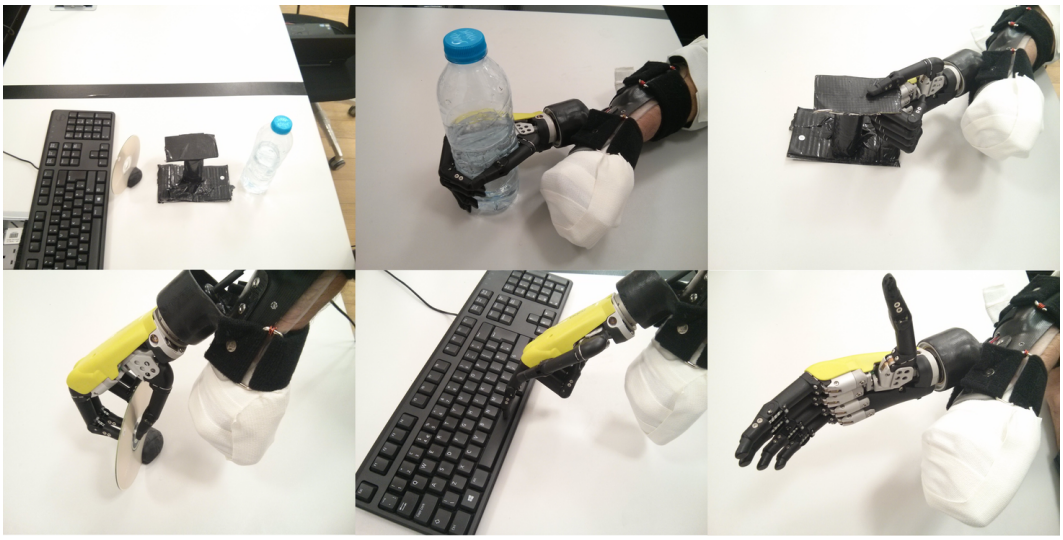

Figure 3.11: Real-time control pick and place experiment. Participants were instructed to use a prosthetic hand to grasp, relocate, and release three objects and finally press the "space" key on a computer keyboard. Five grip types were used: power/ cylindrical (water bottle), lateral (credit card simulator), tripod (CD), index finger pointer (computer keyboard), and hand opening.

Table 3.3: Real-time experiment objects used and associated grip types

Class	Object	Grip
0	-	rest pose
1	bottle	power grip
2	credit card simulator	lateral grip
3	compact disc (CD)	tripod grip
4	keyboard key	index pointer
5	-	hand opening

Participants were instructed to use the hand to grasp, relocate, and release a series of objects and finally press the "space" button on a computer keyboard. Three objects

were used and participants were required to lift each object with an associated grip type which was instructed to them. In total there were six classes, including the hand opening and rest (i.e. no action taken) poses. The objects used and associated hand grips are presented in Table 3.3. The experimental task is illustrated in Figure 3.11.

Each session comprised a *training* and a *testing* phase separated by a short interval. During the training phase, participants were required to perform five reach-to-grasp repetitions of each of the five poses/grips (classes 1-5 in Table 3.3). Throughout this stage, participants were instructed to move their arm at a steady pace and activate their muscles in a natural way without exerting excessive tension. The objects corresponding to the different poses were placed on a computer desk, however participants were not able to physically grasp them due to their fingers being constrained by the elastic bandage. During this phase, which was required to collect training data, the prosthetic hand was kept inactive. To indicate the motion being performed, participants were asked to press down with their contralateral hand a corresponding key on a computer keyboard, with each key (i.e. 1-5) corresponding to a different pose. The amputee participant performed ten repetitions of each movement.

During the testing phase, each trial consisted of picking and placing the three objects approximately 50 cm away from their initial position. A trial ended by pressing the "space" button on the computer keyboard using the index pointer grip. Able-bodied subjects were given 60 s to accomplish the trials with the prosthetic hand and the amputee participant was given 75 s. The objects were presented to the subjects in a pseudo-randomised order, so that the sequence of required grasping motions varied across trials. Able-bodied subjects performed four trials for each decoding condition (see Section 3.3.2) and the amputee participant performed six. When the prosthetic hand performed a different movement than the one intended by the user, for example due to a motion misclassification, participants were asked to open the hand and try performing the intended movement again. The total duration of each experimental session was approximately 90 min, which included skin preparation, sensor placement, training data collection, and testing.

3.3.2 *Classification and prosthesis control*

In the interval between the training and testing phases participants were given a 5 min rest. During this break, four different LDA classifiers were trained. The classification schemes corresponded to the following four conditions, according to the source(s) of input data that were used for decoding:

I. EMG data from all sensors;

Table 3.4: Real-time experiment decoding conditions

Condition	Input	Number of sensors	Input feature dimensionality
I	EMG	12	84
II	IMU	12	108
III	EMG-IMU	12	192
IV	EMG-IMU (subset)	3-7	48-112

II. IMU data from all sensors;

III. EMG and IMU data from all sensors; and

IV. EMG and IMU data from a selected subset of sensors.

The presentation order of the four decoders was counterbalanced across the able-bodied population to avoid favouring certain conditions over others, given the learning mechanisms taking place during prosthetic control (Pistohl et al., 2013; Jiang et al., 2014b; He et al., 2015). For condition IV, sensor selection was performed by using the training data only and the sensor subset for each participant was kept fixed throughout the testing phase. The four decoding conditions are summarised in Table 3.4.

A finite-state machine implementation was used for the real-time control of the prosthetic hand. A movement predicted by the classifier was triggered only if the most recently performed movement had terminated execution. An alternative would have been to provide participants with an "escape" function used to abort the execution of an initiated non-desired grip, however this feature was not included to avoid increasing the cognitive load for participants. Furthermore, a control command was triggered only when it was predicted with high confidence, that is, when the posterior probability of the corresponding class exceeded a cut-off threshold. For this experiment, the threshold was set empirically during pilot trials to $\theta = 0.995$. A data-driven approach for selecting class-specific thresholds in a principled way is later investigated in Chapter 5.

Signal acquisition, pre-processing, and control of the prosthetic hand were implemented in C++ and integrated into the Robot Operating System (Quigley et al., 2009). The average controller delay was 170 ms (Farrell, 2011), which falls within the acceptable range for the purposes of upper-limb myoelectric control (see Section 2.2.4.3).

3.3.3 *Performance assessment*

To evaluate prosthetic control performance in the real-time experiment, two task-related metrics that are commonly used in the literature (e.g. Ortiz-Catalan, Håkansson, and Brånemark, 2014b; Rasool et al., 2016) were adopted; namely, the *completion rate* (CR), which is defined as the ratio of successful to total number of trials; and *completion time* (CT), which is defined as the time taken to accomplish a successful trial (see Section 2.5.5). A trial was considered successful only if it was completed within the given time frame (60 s for the able-bodied subjects or 75 s for the amputee participant).

3.3.4 *Statistical tests*

Experimental trials could only take two possible outcomes: success or failure; therefore, the Cochran's Q test (Cochran, 1950) was used to compare CR scores achieved with the different decoding conditions. For post-hoc pair-wise comparisons, the same test was used together with the Bonferroni correction to account for multiple comparisons (Dunnett, 1955). The non-parametric Kruskal-Wallis test (Kruskal and Wallis, 1952) was used to compare CTs, as these cannot follow normal distributions due to the upper-bound at 60 s (or 75 s for the amputee participant).

3.3.5 *Results*

The working principle of the real-time classification system is illustrated in Figure 3.12. The time series of the real and predicted classes with each of the tested classifiers (see Table 3.4) are shown in the left column of the graph. The temporal evolution of the posterior probability distribution for each classifier is also shown in the same figure (right column). Evidently, for this segment of activity, the inclusion of inertial data increased the robustness of the classifier. For the subject used in this example, six sensors were used in condition IV (EMG-IMU subset).

Performance results for the real-time control experiment are summarised in Figure 3.13. Analogous to the precedent offline analysis (see Section 3.2.8), the highest average CR for the able-bodied group was achieved with condition III (EMG-IMU classifier). The average CR in this case was significantly higher than that of condition I, that is, when solely EMG information was used ($p < 0.01$). The observed pattern was consistent across 10 out of the 11 able-bodied participants (see Figure 3.14) No significant differences were identified among conditions I, II, and IV, although CRs

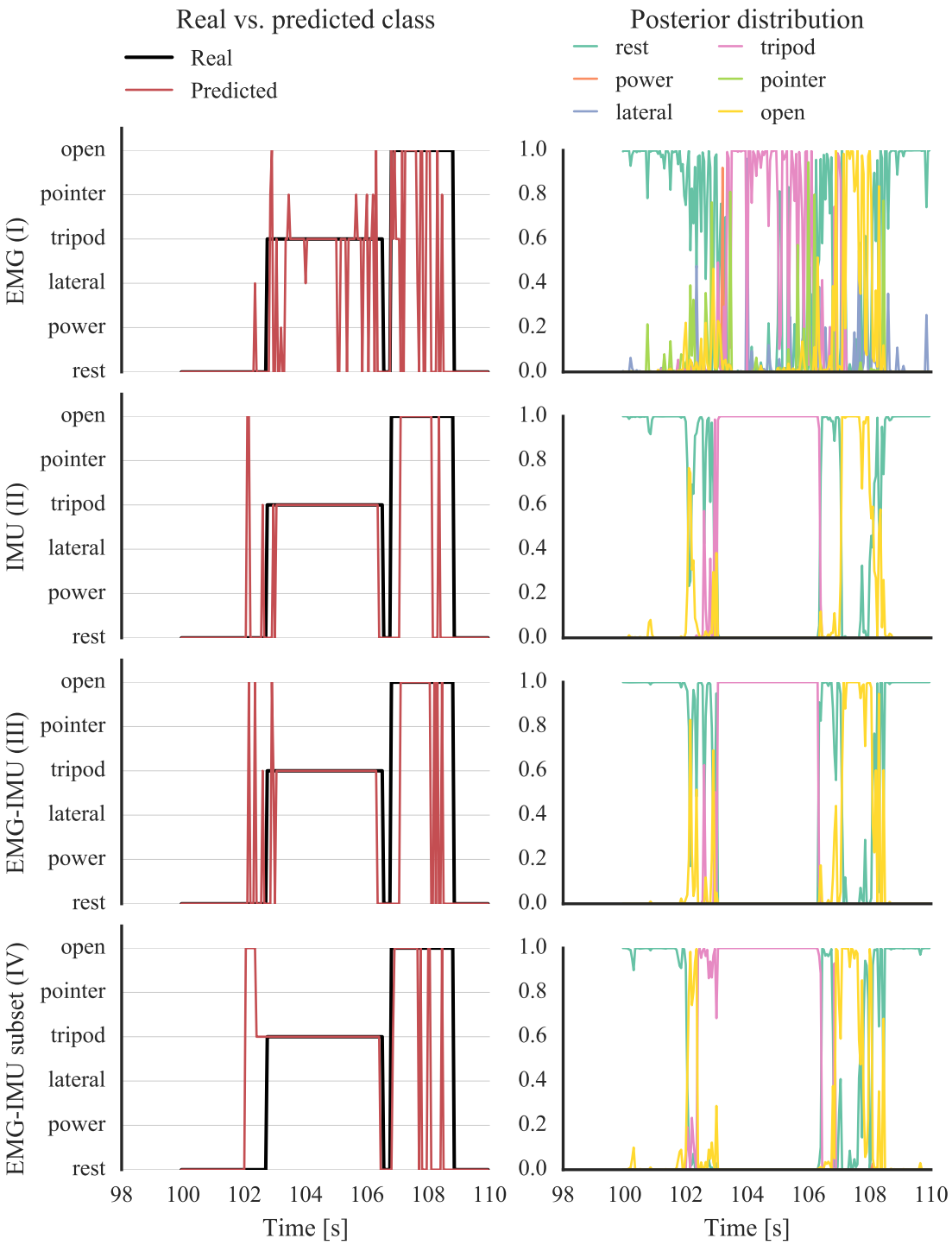

Figure 3.12: Real-time classification. (Left column) the real and predicted classes with the four different decoders; (right column) the evolution of the posterior probability distribution for each classifier. Representative traces shown for one subject using training data and 3-fold CV.

for II and IV were on average 13-14% higher than for condition I. In terms of CTs, the performance of the four conditions was comparable ($p > 0.05$). Nevertheless, con-

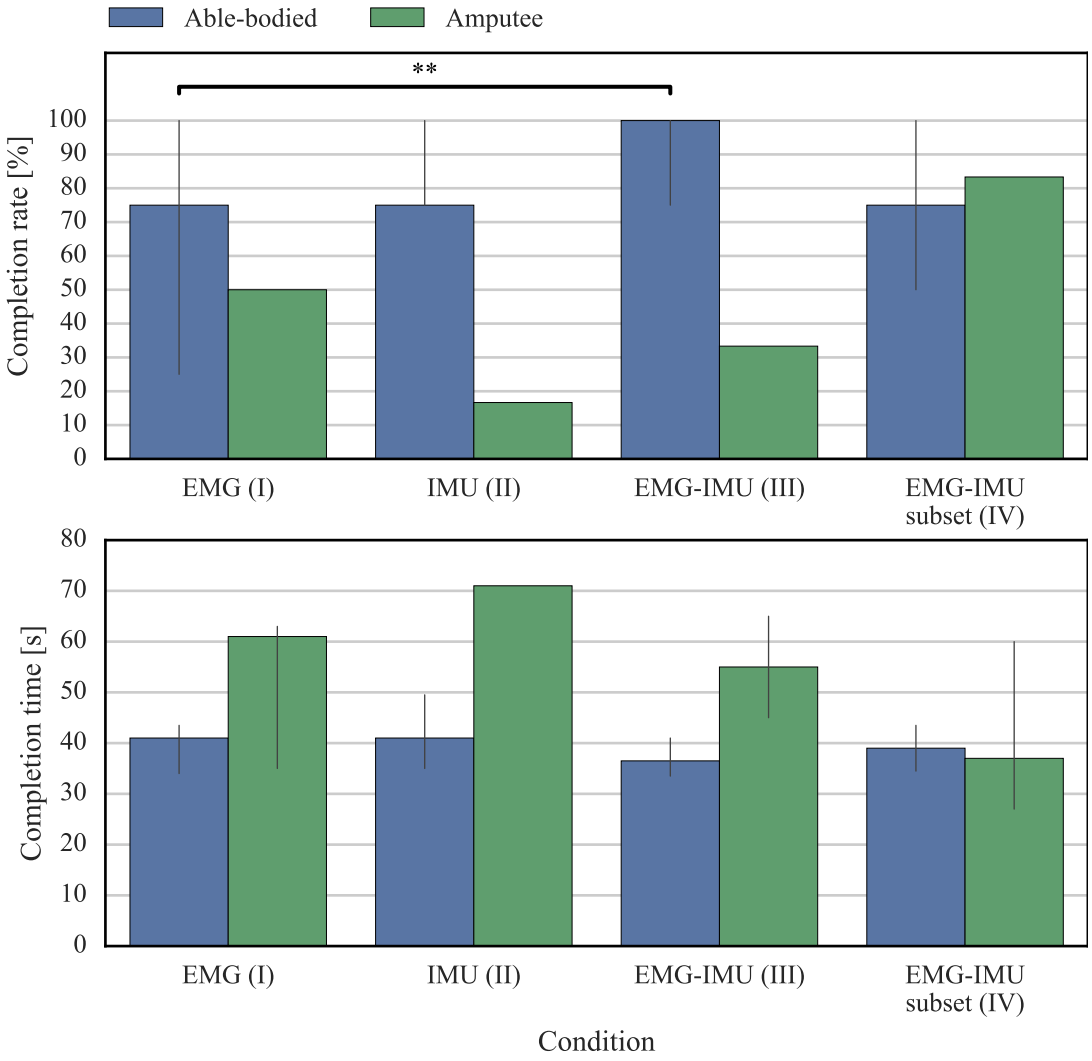

Figure 3.13: Real-time experiment decoding performance comparison. Average CRs and CTs presented for four decoding conditions. Data shown for all subjects (11 able-bodied, one amputee) and trials. Bars, medians; error bars, 95% confidence intervals estimated via bootstrapping (1000 iterations); double asterisk, $p < 0.01$.

dition III achieved marginally better results (i.e. lower average CT) than the other three.

For the amputee participant, a slightly different pattern was observed. The best decoding performance both in terms of CR and average CT was achieved with condition IV, that is, when EMG and inertial data were used from a subset of sensors. Three sensors were used in this condition, one of which targeted the flexor digitorum superficialis muscle, whilst the other two captured the activity of the extensor muscle group (sensors 1, 2 and 10 in Table 3.2). Error bars in Figure 3.13 represent 95% confidence intervals estimated via bootstrapping (1000 iterations). Since there was only one amputee participant in this experiment, there was a single sample for CR (defined as the fraction of successful to total number of trials); therefore, no con-

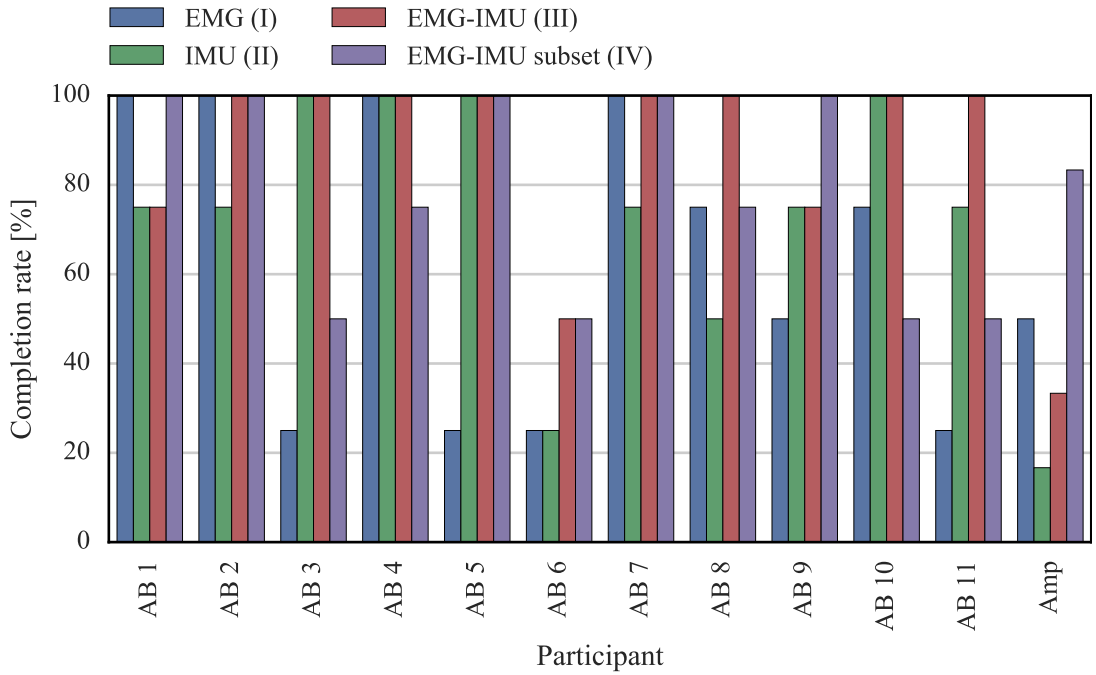

Figure 3.14: Real-time experiment individual subject results. The average CRs achieved with the four types of decoders are presented for each subject. AB, able-bodied; Amp, amputee.

fidence interval was estimated for this measure. Similarly, for condition II there was only one successful trial, hence no confidence interval was estimated for the associated CT. Two video recordings from the experiment with the amputee participant (SV1 and SV2, corresponding to conditions I and IV, respectively) are provided in the supplementary material (see Appendix E).

Average confusion matrices for the real-time experiment are shown in Figure 3.15. These correspond to all subjects and four decoding conditions. Inspection of the confusion matrices suggests that inclusion of inertial data helped disambiguating the "lateral" from "tripod" classes. The average CA of condition III (EMG-IMU classifier) was 8.41% higher than that of condition I (EMG classifier). To estimate the confusion matrices, training data were used by applying 3-fold CV. Estimating confusion matrices during the testing phase of the real-time experiment is not possible, since the ground truth, in other words the participant's intention is not known. This is due to the sequential nature of the trials; within a single trial subjects were required to produce a series of motions (see Figure 3.11), the exact timings of which are neither known, nor can be inferred.

A typical example of the SFSS procedure for selecting the subset used in condition IV is shown in Figure 3.16. The selection of EMG-IMU sensors for all participants is presented in Figure 3.17. The number of selected sensors varied from 3 to 7, but was

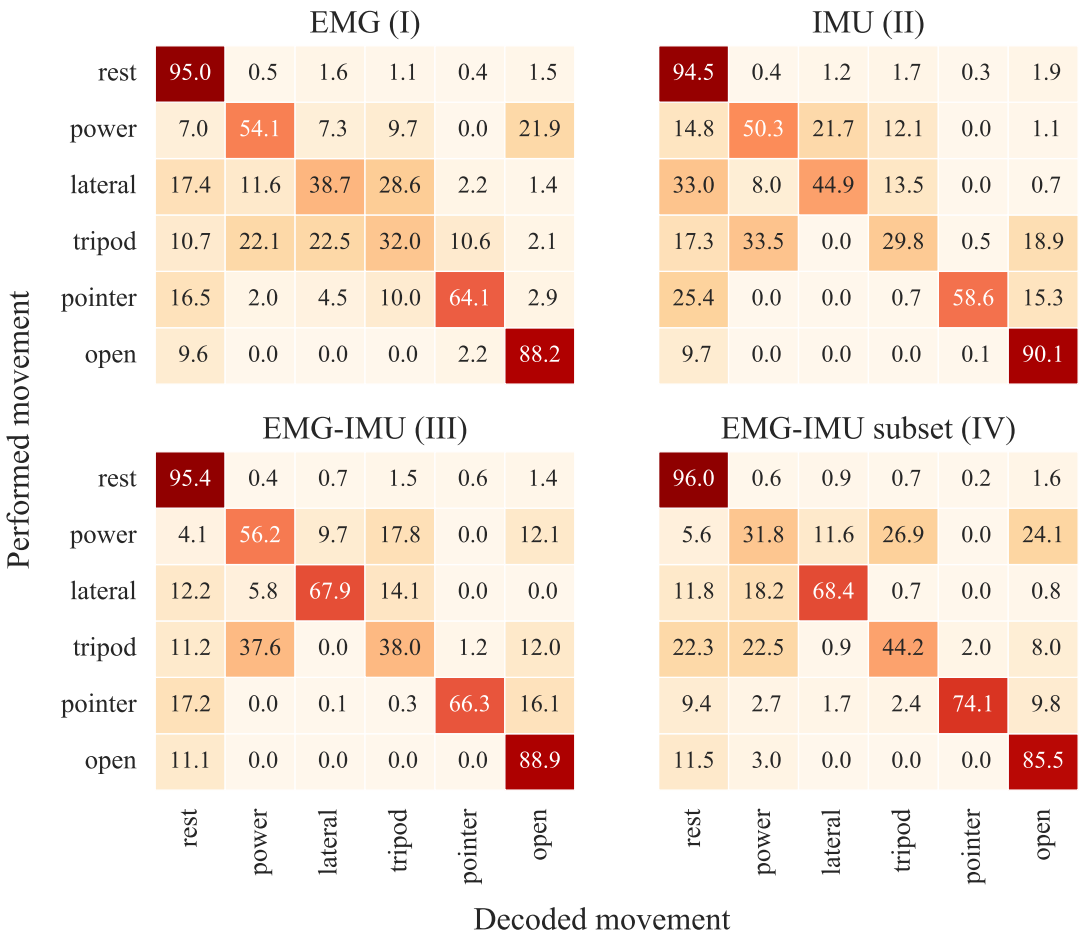

Figure 3.15: Real-time experiment confusion matrices. Predictions shown for all subjects (11 able-bodied, one amputee). Annotated scores represent normalised CA. Confusion matrices have been computed by using training data and 3-fold CV.

typically in the range of four to six (for 10 out of 12 subjects). The average selection frequency of individual sensors is also shown in the same graph (rightmost column).

3.4 DISCUSSION

3.4.1 *Impact*

The study presented in this chapter has investigated whether the performance of myoelectric decoders can benefit from the inclusion of additional information as measured by IMUs integrated within the EMG sensors. For this purpose, a large dataset comprising surface EMG and inertial recordings from 22 subjects performing a variety of movements was collected. Furthermore, a pick and place experiment was conducted to validate the findings during real-time prosthetic control.

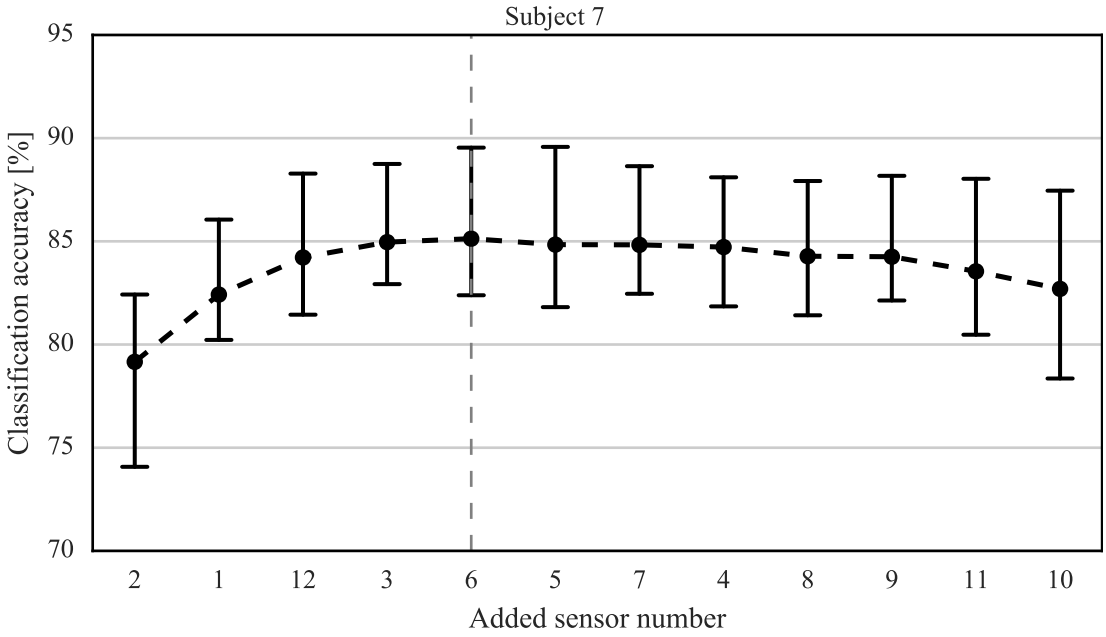

Figure 3.16: SFSS example for one able-bodied subject (real-time experiment). The cross-validated CA is shown as sensors are added to the pool. The dashed line represents the termination of the sensor selection process as further inclusion does not yield an improvement in classification performance. Points, means; error bars, 95% confidence intervals estimated via bootstrapping (1000 iterations).

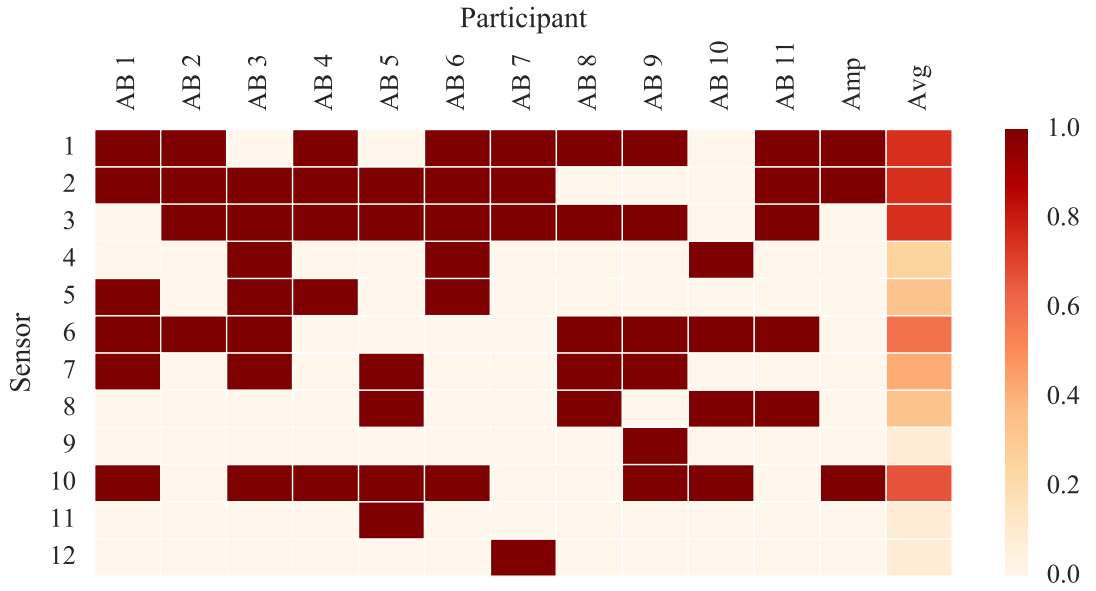

Figure 3.17: Sensor selection for individual subjects (real-time experiment). The selected EMG-IMU sensors are shown column-wise as red boxes for 11 able-bodied subjects and the amputee participant. The rightmost column represents the average selection frequency of individual sensors. The reader is referred to Table 3.2 and Figure 3.4 for details on sensor placement.

The experimental results suggest that both offline CA as well as real-time performance can be improved when inertial measurements are integrated in the decoding process. The main contribution of this work has been threefold; firstly, it has shown

that including information from additional inertial sensors beyond accelerometers can further increase CA; secondly, it has confirmed that such increase in offline CA can lead to improved real-time prosthetic control; thirdly, it has demonstrated that by combining multiple sensing modalities within a single sensor pack, it is possible to reduce the amount of sensors required for movement intent decoding. This last aspect is of significant relevance for clinical applications, where it is desirable to keep the number of used sensors at a bare minimum. For this reason, it is further investigated in Chapter 5.

3.4.2 *Offline decoding of hand gestures with surface EMG and inertial data*

In the offline experiment (Section 3.2), the large number of classes makes gesture recognition a challenging task. It was found that by including inertial data the CA increased by a significant factor. For the able-bodied group, the median CA was 82.7%, which was increased by 22.6% as compared to the EMG-only case. For the amputee group, the same measure was 77.8% and the observed increase in performance was 37.1%. Remarkably, CA for the amputee group almost doubled when inertial measurements were included in the decoders. This score is higher than previously reported for amputee subjects, given the large number of motions in the dataset (i.e. 40 classes). For comparison, Atzori et al. (2014) reported an average CA of 48% for the same set of movements.

3.4.3 *Real-time prosthetic control experiment*

Many studies have suggested that an observed increase in CA attained with purely offline analysis does not necessarily translate into performance improvement during real-time myoelectric control (Jiang et al., 2014b; Ortiz-Catalan et al., 2015). In order to validate findings from the offline analysis, a real-time experiment was conducted in which participants modulated their muscular activity to control a state-of-the-art commercial prosthetic hand. Comparing the real-time performance of all decoding schemes explored in the offline analysis would have been impossible due to time constraints. By taking into account the results from the offline analysis, it was decided to test the real-time performance of the four conditions presented in Table 3.4. Moreover, it is not practical to include 40 classes in a real-time experiment, and perhaps not necessary from a clinical point of view. Thus, only six classes were included (see Table 3.3 and Figure 3.11), which have been previously identified as being the most useful from a user's perspective (Peerdeman et al., 2011). It is worth noting that the proposed experimental protocol bears strong similarities to the "object task"

of the SHAP test that is commonly used in clinical environments (see Section 2.5.1). Although six classes were only included in the real-time experiment, comparisons with all 40 classes were reported in the precedent offline analysis in order to compare the results of the current work to those previously reported by other researchers (see Section 3.4.2).

In comparison with similar studies which previously employed the target achievement control test (e.g. Simon et al., 2011; Ortiz-Catalan, Håkansson, and Brånemark, 2014b; Young et al., 2014; Rasool et al., 2016), the designed experimental task was more challenging. Participants were required to trigger a sequence of control signals (seven in total including the required intermediate hand opening commands), rather than performing a single grasp motion. Additionally, participants were given a rather short time to accomplish trials: 60 s for the able-bodied group and 75 s for the amputee subject. This paradigm was chosen because it was considered as a more realistic experiment that closely matches real-life applications.

Results from the real-time experiment were mostly in accordance with observations from the precedent offline analysis. It was found that the inclusion of inertial information resulted in significant improvement in CRs for the able-bodied group (median increase of 25%). One notable difference was that while offline analysis suggested that the use of inertial data alone could achieve comparable CA to EMG-IMU classifiers (0.9% median difference), in the real-time experiment the hybrid decoders outperformed, although not significantly, IMU classifiers (75.0% and 100.0% median CRs; 48.0 and 37.5 s median CTs for conditions (II) and (III), respectively). Such discrepancies between offline CA scores and task-related metrics have been previously reported (e.g Jiang et al., 2014b; Ortiz-Catalan et al., 2015). It has been commonly accepted that the latter should be regarded as more important than the former, since task-related metrics measuring the performance of real-time prosthetic systems are of greater clinical relevance than offline accuracy (Vujaklija et al., 2017).

The best performance for the amputee participant both in terms of CR and CTs was achieved when EMG and inertial measurements were combined but a smaller subset of the available sensors was used. The performance was inferior when the whole set of sensors was used. One possible explanation for this observation is that the participant was able to develop a more efficient control strategy in the former case due to the lower dimensionality of the input space (Nazarpour, Barnard, and Jackson, 2012). Nevertheless, the chance of observing a statistical error due to the small sample size cannot be neglected.

3.4.4 *Dynamic training data collection*

Radmand, Scheme, and Englehart (2014) demonstrated that integrating accelerometry data into myoelectric decoders can potentially decrease decoding performance unless training data are collected under most of the possible configurations in 3D space. They also showed that classifiers trained with static motions generalise poorly when used to decode hand gestures during dynamic movement. To overcome this limitation, and since collecting static training data in all possible positions would be practically impossible, they proposed a method for training classifiers with dynamic movements covering the regions of interest.

Since the offline experiment involved static hand motions, it was considered imperative to further validate any findings during real-time prosthetic control. During the training phase of the real-time experiment, participants were instructed to move their arms within a constrained workspace (60 cm $\times$ 50 cm $\times$ 30 cm) whilst performing the different grips. This was inspired by the work of Radmand, Scheme, and Englehart (2014). Although this approach helped disambiguate muscle activity patterns under different postures, its potential to generalise to postures not present in the training set remains to be investigated. In practice, acquisition of large and versatile datasets may be required to capture arm posture-related variability, and thereby ensure classification robustness.

3.4.5 *On the relationship between surface EMG and inertial data*

A previous study reported high offline CA by discarding the EMG signal and using solely acceleration signals (Gijsberts et al., 2014a). This finding was replicated in the offline analysis (see Figure 3.8), and it was additionally found that a high CA can be also achieved by using magnetometer data only. Importantly, it was further demonstrated that efficient real-time control is feasible by using exclusively inertial measurements (see Figure 3.13). It is worth noting, however, that the achieved CTs were slightly worse (i.e. increased) for this condition. The first commercial system using inertial data as sensory input has recently appeared on the market (see Section 2.4.1.2), although its working principle is fundamentally different to the one proposed here. To the best of the author's knowledge, this is the first study to demonstrate that real-time prosthetic control can be achieved using exclusively inertial measurements and a biomimetic approach. This finding cannot be solely attributed to a potential association of arm postures to grips, since in the real-time experiments, participants mainly employed two arm postures each of them associated with two different grips; for the "cylindrical" and "lateral" classes the palm of the prosthesis was required to

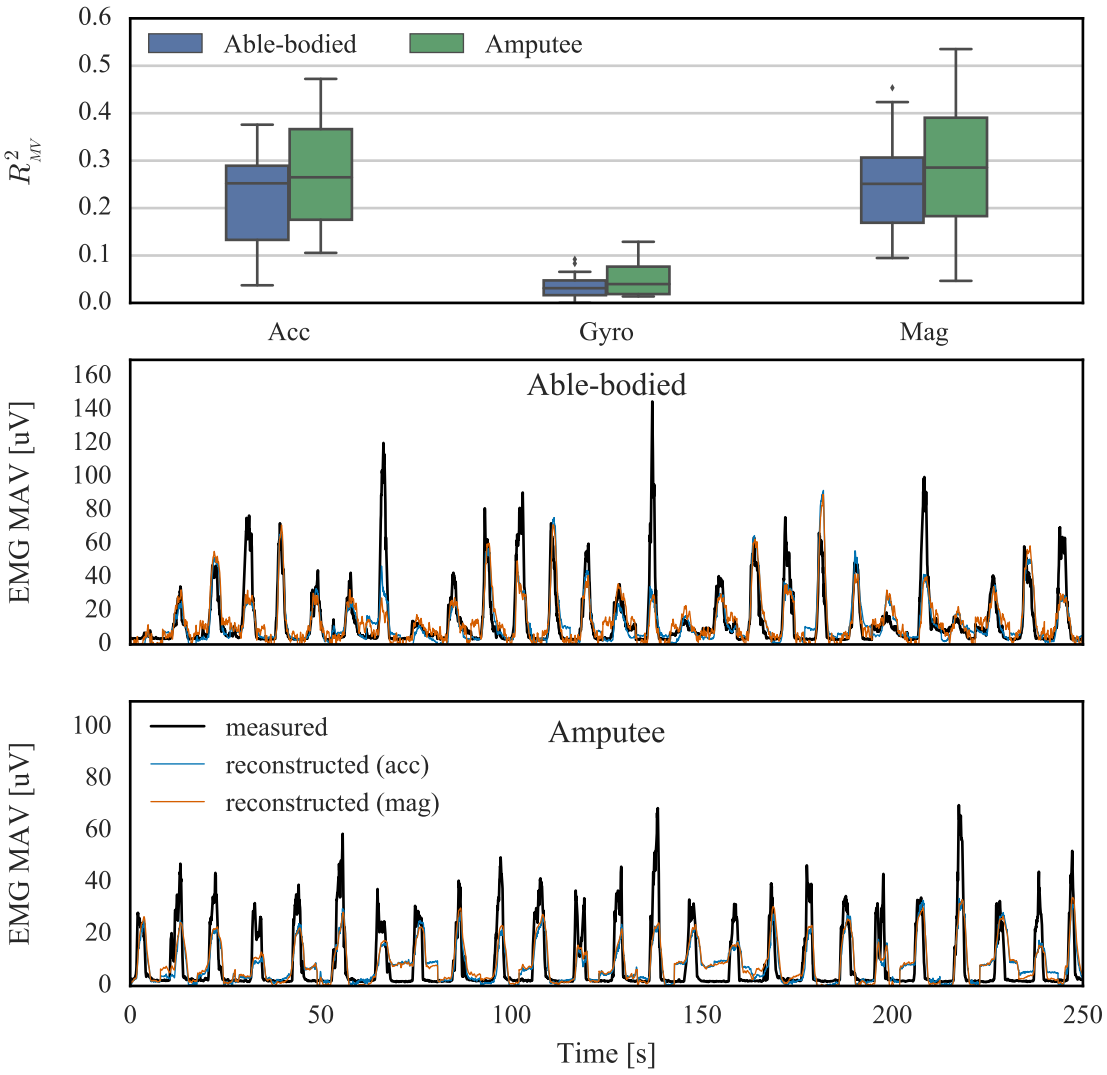

Figure 3.18: Surface EMG envelope reconstruction from inertial measurements. (Top panel) EMG envelope reconstruction accuracy with accelerometer, gyroscope, and magnetometer data using LR models; (middle-bottom panels) EMG envelope reconstruction examples from accelerometer and magnetometer data for an able-bodied subject and an amputee.

be perpendicular to the surface, whereas for the "tripod" and "index pointer" classes it was required to be parallel to the surface. Furthermore, following each object relocation, the hand opening motion was required to be triggered in either postures, depending upon the object being relocated (see Figure 3.11).

A different explanation is proposed for this rather surprising finding; since acceleration is recorded on the skin surface, the associated measurement could be an alternative manifestation of the underlying muscular activity process that also gives rise to the electric field measured over the skin with EMG sensors. This may also be true for magnetometer data, which by measuring the magnetic field around the muscle area could indirectly provide an alternative measurement of muscular activ-

ity. The relationship between the two fields stems directly from the Maxwell–Ampère law that states that a changing electric field, due to muscle contraction in this case, generates a respective magnetic field.

This speculation was validated with the following experiment; it was hypothesised that if such relationship exists between EMG, accelerometer and magnetometer data, then it should be possible to use one type of signal to estimate another, and vice-versa. Simple *linear regression* (LR) models were trained to reconstruct the envelopes (i.e. mean absolute value) of the EMG signals from accelerometer, gyroscope, and magnetometer measurements. This process was performed individually for each sensor, that is, the reconstruction of each EMG signal was achieved by using accelerometer, gyroscope, or magnetometer data from the same sensor only. The results of this analysis are shown in Figure 3.18. The accelerometer and magnetometer data were able to capture on average 25%-30% of the variance of the EMG envelopes. Conversely, it was not possible to decode EMG activity by using gyroscope data. Examples of EMG envelope reconstruction with accelerometer and magnetometer measurements are shown in the same graph, both for able-bodied and amputee subjects.

Certainly, there is no reason to expect that the relationship between EMG, accelerometer, and magnetometer data should be linear; therefore, one would expect to achieve higher decoding accuracies by using non-linear regression models. Nevertheless, the results from this experiment demonstrate that surface EMG and inertial signals are indeed closely related, which provides evidence that they might reflect different and perhaps complementary aspects and impacts of the same underlying phenomenon, that is, the muscular activity. Consequently, it should come as no surprise that the combined EMG-IMU decoder yielded more accurate hand gesture recognition (see Figures 3.8 and 3.13). The fact that gyroscope data alone failed to decode both hand gesture and EMG envelopes provides further support for this hypothesis. It is worth noting that the use of magnetometers has been previously proposed for measuring skeletal muscle contraction (Cohen and Givler, 1972; Egeraat, Friedman, and Wikswo, 1990; Garcia and Baffa, 2015); however, this is the first study to demonstrate that the measured magnetic field arising from muscle contraction can be used as a source signal for myoelectric control.

Taking everything into consideration, it seems likely that the added benefit of using inertial measurements can be attributed to their ability to both capture dynamic spatial information, as well as to increase the robustness of muscular activity estimation which is subsequently employed to decode movement intention.

3.4.6 *Limitations and future work*

Throughout this chapter, raw sensor values from IMUs were used, which correspond to proper acceleration for accelerometers, angular velocity for gyroscopes, and magnetic field for magnetometers, respectively (see Section 2.3.1). An alternative would have been to perform sensor fusion and work with a different representation, such as quaternions or Euler angles (Madgwick, Harrison, and Vaidyanathan, 2011); however, such representations are informative of the orientation of the sensors only, and as a result, any muscular activity-related information encoded in raw accelerometer and magnetometer readings (see Section 3.4.5) might get lost. On the other hand, accelerometers measure proper acceleration that is affected by gravity (Woodman, 2007), and which might negatively affect the performance of the proposed method. One possible solution would be to adopt a dual approach; that is, use a quaternion representation to subtract the gravitational component from raw accelerometer readings and subsequently make use of the transformed accelerometer and raw mangetometer readings for movement intent classification. Another promising future direction would be to optimally combine the different modalities using multiple time scales and a Bayesian approach (Bishop, 2006); in other words, exploit the temporal structure in inertial measurements (e.g. 3D acceleration) to encode prior information about grasping timings which can be then updated in the light of muscle activity information recorded with both EMG and inertial (i.e. instantaneous accelerometer and magnetometer) measurements.

With regards to training data collection, it was shown that efficient myoelectric control could by achieved by acquiring data with dynamic movements covering the regions of interest, as was previously proposed by Radmand, Scheme, and Englehart (2016) and Yang et al. (2017); however, the generalisation ability of the decoders under novel postures was not tested. One possible direction for future research would be to test the generalisation of EMG-IMU decoders while including arm postures and orientations not present in the training dataset.

Additionally, it was demonstrated that by using multi-modal prosthetic control it is possible to reduce the number of sensors required for accurate hand movement classification; however, the number of sensors identified by the proposed SFSS algorithm was on average five, which might still be regarded as a large number for clinical solutions. Finally, the effect of using different classification strategies on decoding performance was not investigated. The latter two issues are addressed in the following two chapters of the thesis.

4

DISCRIMINANT ANALYSIS FOR HAND MOVEMENT CLASSIFICATION

In the previous chapter, it was shown that the use of inertial measurements can offer a remarkable boost in decoding performance of myoelectric classifiers. To this end, a standard classification method was employed, namely *linear discriminant analysis* (LDA), and no further algorithmic comparisons were performed.

The LDA algorithm is perhaps the most commonly used classification method in myoelectric control (e.g Englehart and Hudgins, 2003; Hargrove, Englehart, and Hudgins, 2008; Al-Timemy et al., 2013) and there are good reasons for that; ease of implementation, short training times, and minimal computational/memory requirements at testing time. All of the above, in combination with a demonstrated high decoding performance, make LDA very attractive for use in this context. Nonetheless, in the heart of LDA lies a strong probabilistic modelling assumption that is almost always violated. Despite that, it has been demonstrated that it can achieve high *classification accuracy* (CA) which is often comparable to that of more sophisticated algorithms, such as *multi-layer perceptron*s (MLPs) and support vector machines (e.g Scheme and Englehart, 2011; Ortiz-Catalan, Brånemark, and Håkansson, 2013; Al-Timemy et al., 2013).

In this chapter, a thorough investigation of the performance of various *discriminant analysis* (DA) classifiers on hand movement recognition is performed. It is demonstrated that by using a DA variant that generalises a family of class-conditional Gaussian models, namely *regularised discriminant analysis* (RDA), it is possible to achieve significant improvement in decoding accuracy for hand movement classification. By performing an exhaustive analysis on datasets comprising recordings from 60 able-bodied and 12 transradial amputee subjects, it is shown that via careful tuning of the RDA hyper-parameters it is possible to achieve a median increase in CA of 13.5% as compared to LDA.

The findings of the study presented here are subsequently exploited in the following chapter, in which it is demonstrated that by employing RDA in conjunction with a confidence-based rejection strategy it is feasible to achieve robust *machine learning* (ML)-based prosthetic control with only two surface *electromyography* (EMG)-*inertial measurement unit* (IMU) sensors.

4.1 CLASSIFICATION ALGORITHMS FOR MYOELECTRIC CONTROL

A wide range of classifiers have been proposed for myoelectric decoding and control (see Section 2.2.4). Undoubtedly, among them the two most popular have been LDA and MLP classification (Peerdeman et al., 2011). The LDA method offers some advantages over MLPs, such as ease of implementation, existence of an analytical solution, fast training times, and computational efficiency. For all the above reasons, the LDA algorithm has been the preferred choice for myoelectric classification (e.g. Englehart and Hudgins, 2003; Hargrove, Englehart, and Hudgins, 2008; Hargrove et al., 2010; Simon et al., 2011; Smith et al., 2011; Young et al., 2013; Young, Kuiken, and Hargrove, 2014; Naik, Al-Timemy, and Nguyen, 2016; Vidovic et al., 2016).

Many studies have carried out comparisons of the decoding power of various classifiers, often with contradictory results. For example, a few studies have shown that LDA can achieve comparable or even higher performance than other methods (Huang et al., 2005; Hargrove, Englehart, and Hudgins, 2007; Scheme and Englehart, 2011; Kanitz et al., 2011; Phinyomark et al., 2013; Kamavuako et al., 2013; Ortiz-Catalan, Brånemark, and Håkansson, 2013; Al-Timemy et al., 2013; Ortiz-Catalan, Håkansson, and Brånemark, 2014b), while others have shown that LDA classifiers are outperformed by MLPs, support vector machines, *K-nearest neighbours* (k-NN), and convolutional neural networks (Atzori et al., 2014; Atzori et al., 2015; Atzori, Cognolato, and Müller, 2016; Geng et al., 2016; Du et al., 2017). Nevertheless, taking into consideration the diversity in behavioural tasks, pre-processing steps, feature engineering, and implementation differences such discrepancies should not be entirely surprising.

4.2 DISCRIMINANT ANALYSIS

DA is a family of supervised generative models that assumes class-conditional multivariate Gaussian densities (Friedman, Hastie, and Tibshirani, 2001). In the general case, the probability density function of a data point $\mathbf{x}$ generated by class c is given by:

$$p(\mathbf{x}|y = c) = \mathcal{N}(\mathbf{x}; \boldsymbol{\mu}_c, \boldsymbol{\Sigma}_c), \tag{4.1}$$

where $\mathcal{N}(\mathbf{x}; \boldsymbol{\mu}, \boldsymbol{\Sigma})$ denotes the multivariate normal distribution with mean vector $\boldsymbol{\mu}$ and covariance matrix $\boldsymbol{\Sigma}$. For classification, the posterior probability of a data point $\mathbf{x}_\star$ being assigned to class c is estimated by using the Bayes' rule:

$$\begin{aligned} p(y = c|\mathbf{x}_\star) &= \frac{p(\mathbf{x}_\star|y = c)\, p(y = c)}{p(\mathbf{x}_\star)} \\ &= \frac{\mathcal{N}(\mathbf{x}_\star; \boldsymbol{\mu}_c, \boldsymbol{\Sigma}_c)\, p(y = c)}{\sum_{c'=1}^{C} \mathcal{N}(\mathbf{x}_\star; \boldsymbol{\mu}_{c'}, \boldsymbol{\Sigma}_{c'})\, p(y = c')}, \end{aligned} \tag{4.2}$$

where $p(y = c)$ is the prior probability for class c, and C denotes the number of classes.

4.2.1 *Linear discriminant analysis*

LDA is a special case of the DA family that assumes a common covariance matrix shared across classes. This is usually referred to as the pooled covariance, or within-class scatter matrix. This assumption leads to linear decision boundaries (i.e. hyperplanes) (Friedman, Hastie, and Tibshirani, 2001). With LDA, a test data point $\mathbf{x}_\star$ is assigned to the class c for which the linear *discriminant function* $\delta_c(\mathbf{x}_\star)$ is maximised:

$$\delta_c(\mathbf{x}_\star) = \mathbf{x}_\star^\top \boldsymbol{\Sigma}^{-1} \boldsymbol{\mu}_c - \frac{1}{2} \boldsymbol{\mu}_c^\top \boldsymbol{\Sigma}^{-1} \boldsymbol{\mu}_c + \log \pi_c, \tag{4.3}$$

where π_c and $\boldsymbol{\mu}_c$, for $c = 1, \ldots, C$ are the class prior probabilities and means, respectively, and $\boldsymbol{\Sigma}$ is the pooled covariance matrix. The prior probabilities, mean vectors, and pooled covariance matrix can be estimated from the training data:

$$\hat{\pi}_c = \frac{N_c}{N}, \tag{4.4}$$

$$\hat{\boldsymbol{\mu}}_c = \frac{1}{N_c} \sum_{y_n = c} \mathbf{x}_n, \tag{4.5}$$

$$\hat{\boldsymbol{\Sigma}} = \frac{1}{N - C} \sum_{c=1}^{C} \sum_{y_n = c} (\mathbf{x}_n - \hat{\boldsymbol{\mu}}_c)(\mathbf{x}_n - \hat{\boldsymbol{\mu}}_c)^\top, \tag{4.6}$$

where N_c is the number of training instances in class c and N is the total number of training samples. The posterior probability for class c is then given by the softmax function:

$$p(y = c|\mathbf{x}_\star) = \frac{e^{\delta_c(\mathbf{x}_\star)}}{\sum_{c'=1}^{C} e^{\delta_{c'}(\mathbf{x}_\star)}}. \tag{4.7}$$

4.2.2 *Quadratic discriminant analysis*

Quadratic discriminant analysis (QDA) is a general-case class-conditional Gaussian model that does not make the LDA assumption (i.e. shared covariance matrix); therefore, a separate covariance matrix has to be estimated for each class. In this case, the decision boundaries are quadratic in feature space and the discriminant functions are given by:

$$\begin{aligned}\delta_c(\mathbf{x}_\star) = &-\frac{1}{2}\mathbf{x}_\star^\top \boldsymbol{\Sigma}_c^{-1}\mathbf{x}_\star + \boldsymbol{\mu}_c^\top \boldsymbol{\Sigma}_c^{-1}\mathbf{x}_\star \\ &-\frac{1}{2}\log|\boldsymbol{\Sigma}_c| + \log\pi_c - \frac{1}{2}\boldsymbol{\mu}_c^\top \boldsymbol{\Sigma}_c^{-1}\boldsymbol{\mu}_c,\end{aligned} \tag{4.8}$$

where $\boldsymbol{\Sigma}_c$ is the covariance matrix of class c, which can be estimated from the training data:

$$\hat{\boldsymbol{\Sigma}}_c = \frac{1}{N-1}\sum_{y_n=c}(\mathbf{x}_n - \hat{\boldsymbol{\mu}}_c)(\mathbf{x}_n - \hat{\boldsymbol{\mu}}_c)^\top. \tag{4.9}$$

4.2.3 *Gaussian naive Bayes*

The *Gaussian naive Bayes* (GNB) model is another special case of DA which assumes diagonal covariance matrices, that is, $\boldsymbol{\Sigma}_c$ takes the form:

$$\boldsymbol{\Sigma}_c = \begin{bmatrix} \sigma_{1,c}^2 & & & \\ & \sigma_{2,c}^2 & & \\ & & \ddots & \\ & & & \sigma_{D,c}^2 \end{bmatrix}, \tag{4.10}$$

where $\sigma_{i,c}^2$ denotes the variance of feature i for class c, and D is the dimensionality of the input space. The GNB model is more rarely referred to as *diagonal quadratic discriminant analysis* (DQDA).

4.2.4 *Diagonal linear discriminant analysis*

Diagonal linear discriminant analysis (DLDA) is an extreme case of DA which assumes that a common diagonal covariance matrix is shared across classes. In other words, it combines the LDA and GNB assumptions. In this case:

$$\boldsymbol{\Sigma}_c = \boldsymbol{\Sigma} = \begin{bmatrix} \sigma_1^2 & & & \\ & \sigma_2^2 & & \\ & & \ddots & \\ & & & \sigma_D^2 \end{bmatrix}. \tag{4.11}$$

4.2.5 *Regularised discriminant analysis*

RDA is a method that generalises LDA and QDA and provides a continuum of models between the two (Friedman, 1989). As with QDA, the class covariance matrices for this model are separate; however, they are regularised towards the pooled covariance matrix and, thus, take the form:

$$\hat{\boldsymbol{\Sigma}}_c(\alpha) = \alpha\hat{\boldsymbol{\Sigma}}_c + (1-\alpha)\,\hat{\boldsymbol{\Sigma}}, \qquad 0 \leqslant \alpha \leqslant 1. \tag{4.12}$$

The parameter α controls the amount of regularisation. A different form of regularisation occurs when the estimated covariance matrices are regularised towards diagonal matrices, that is:

$$\hat{\boldsymbol{\Sigma}}(\gamma) = (1-\gamma)\,\hat{\boldsymbol{\Sigma}} + \gamma\,\mathrm{diag}(\hat{\boldsymbol{\Sigma}}), \qquad 0 \leqslant \gamma \leqslant 1, \tag{4.13}$$

and

$$\hat{\boldsymbol{\Sigma}}_c(\gamma) = (1-\gamma)\,\hat{\boldsymbol{\Sigma}}_c + \gamma\,\mathrm{diag}(\hat{\boldsymbol{\Sigma}}_c), \qquad 0 \leqslant \gamma \leqslant 1. \tag{4.14}$$

The two regularisation approaches are orthogonal, so they can be combined into:

$$\begin{aligned} \hat{\boldsymbol{\Sigma}}_c(\alpha,\gamma) =& \alpha(1-\gamma)\,\hat{\boldsymbol{\Sigma}}_c + (1-\alpha)(1-\gamma)\,\hat{\boldsymbol{\Sigma}} \\ &+ \alpha\gamma\,\mathrm{diag}(\hat{\boldsymbol{\Sigma}}_c) + (1-\alpha)\,\mathrm{diag}(\hat{\boldsymbol{\Sigma}}). \end{aligned} \tag{4.15}$$

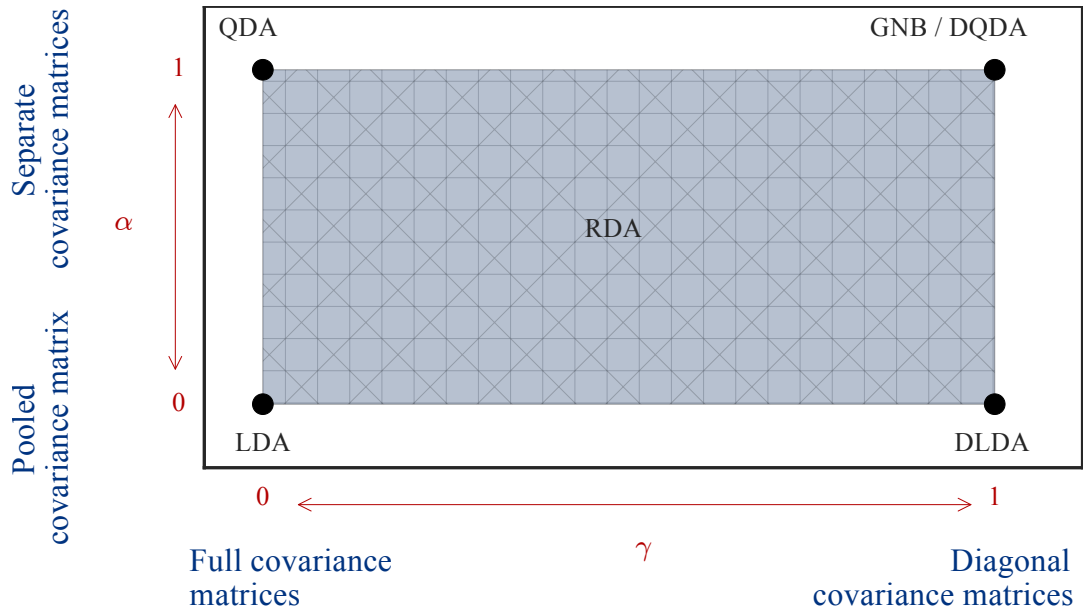

Figure 4.1: Sketch of DA family of classifiers. Classifiers such as LDA, QDA, DLDA, and GNB/DQDA can be recovered as special cases of RDA via appropriate selection of regularisation hyper-parameters α and γ.

The model described by Equation (4.15) leads to a general family of models which treats as special cases all the DA models introduced in the previous sections, that is, LDA, QDA, GNB, and DLDA. In other words, all these models can be recovered by RDA via appropriate selection of the model hyper-parameters α and γ. A schematic representation of this family of models is shown in Figure 4.1.

4.2.6 *Toy example*

In this section, we use a toy example to illustrate the differences between LDA, QDA, and RDA. A small artificial dataset is created consisting of two two-dimensional clusters, each one containing 50 samples generated from two normal distributions with two variables and the following parameters:

$$\mu_1 = \begin{bmatrix} 0.5 \\ -1 \end{bmatrix},$$

$$\mu_2 = \begin{bmatrix} -0.5 \\ 1 \end{bmatrix},$$

$$\boldsymbol{\Sigma}_1 = \begin{bmatrix} 1 & 0.2 \\ 0.2 & 1 \end{bmatrix}, \text{and}$$

$$\boldsymbol{\Sigma}_2 = \begin{bmatrix} 0.3 & -0.1 \\ -0.1 & 0.4 \end{bmatrix}.$$

Figure 4.2 shows the estimated class-specific marginal probability density functions of one of the variables, by using LDA, QDA, and RDA with $\alpha = 0.5$ and $\gamma = 0$. Because of the shared covariance matrix assumption, LDA estimates the same variance $\hat{\sigma}_1^2$ for both classes; with this model, the difference between the class density functions lies only in their means. The QDA model does not make this assumption, and as a result, the estimated probability distributions match more closely the true distributions that generated the data. The RDA estimates lie in the space between the ones provided by LDA and QDA; separate variances are estimated for each class, but they are regularised towards the respective elements of the pooled covariance matrix.

The decision boundaries of the three classifiers are shown in Figure 4.2. Because of the LDA assumption, the quadratic term $\mathbf{x}^\top \boldsymbol{\Sigma}^{-1} \mathbf{x}$ vanishes from the decision boundary solution, and as a result, the latter becomes linear in feature space (see Equation 4.3). Both RDA and QDA yield quadratic decision boundaries, but due to the regularisation applied in the case of RDA, the decision boundary is "pushed" towards the linear solution provided by LDA.

4.3 COMPARISON OF DISCRIMINANT ANALYSIS CLASSIFIERS

4.3.1 *Motivation*

This section features an investigation of the performance of various DA models on myoelectric data classification. It is hypothesised that the LDA assumption might be often violated in practice, since there is no reason to expect that different hand movements result in similar co-activations between muscle groups, and thereby, to a common covariance matrix. For this reason, estimating separate covariance matrices for each class might be more appropriate for this task.

As a first step towards validating this hypothesis, the dataset collected previously (see Section 3.2) was examined. The feature extraction described in Section 3.2.3 was used, hence the dimensionality of the input space was D=192 (12 sensors $\times$ 16 fea-

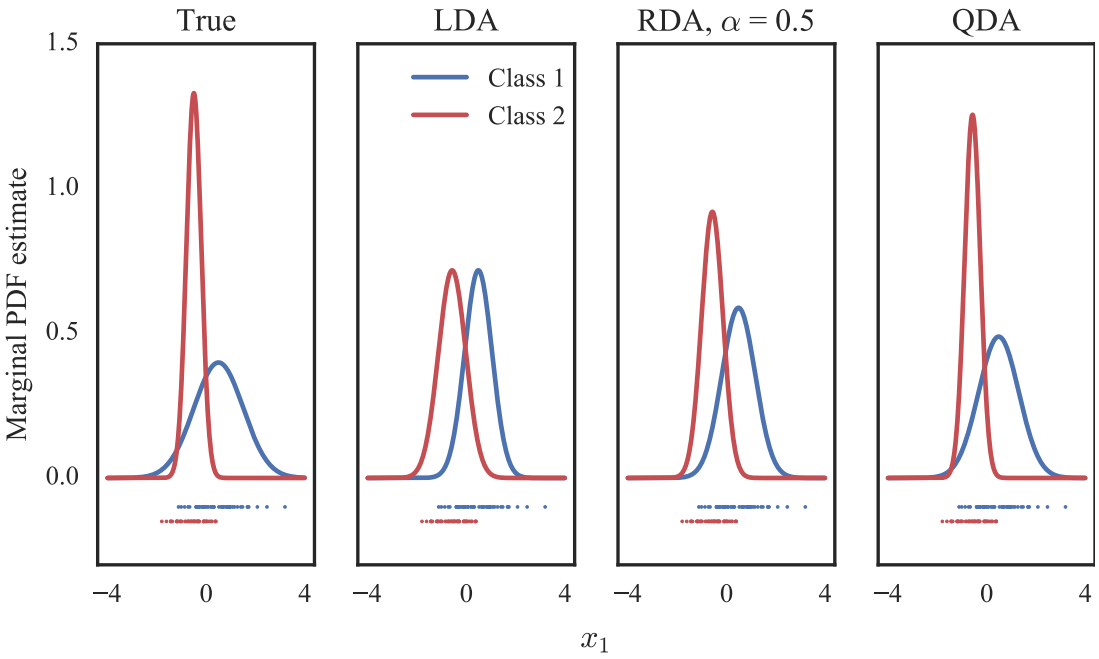

Figure 4.2: Toy example: density estimation with DA models. The marginal probability distribution of one of the variables (x_1) of a two-dimensional artificial dataset is estimated with various DA models, separately for each class. The true distributions that were used to generate the dataset are shown in the leftmost column. Due to the common covariance matrix assumption, LDA estimates the same variance $\hat{\sigma}_1^2$ for both classes. The variance estimate with RDA ($\alpha = 0.5$) is a compromise between the estimates obtained with LDA and QDA. Coloured points show the observations for the two classes.

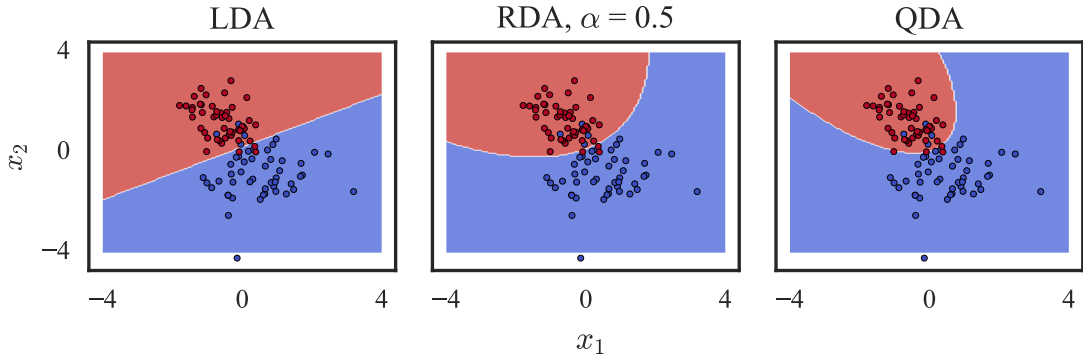

Figure 4.3: Toy example: decision boundaries for DA models. The common covariance matrix assumption leads to linear decision boundaries for LDA (left column), as opposed to quadratic solutions for QDA (right column). Although the decision boundary for RDA ($\alpha = 0.5$) is quadratic, regularisation "pushes" it towards the linear solution obtained with LDA (middle column).

tures/sensor). Data from all subjects were pooled together and both the shared (i.e. LDA) as well as class-specific (i.e. QDA) covariance matrices were estimated. Features were standardised to zero mean and unit standard deviation prior to covariance matrix estimation. Covariance matrix estimates for a subset of the classes are shown in Figure 4.4, along with the estimated pooled covariance matrix. As it was hypothe-

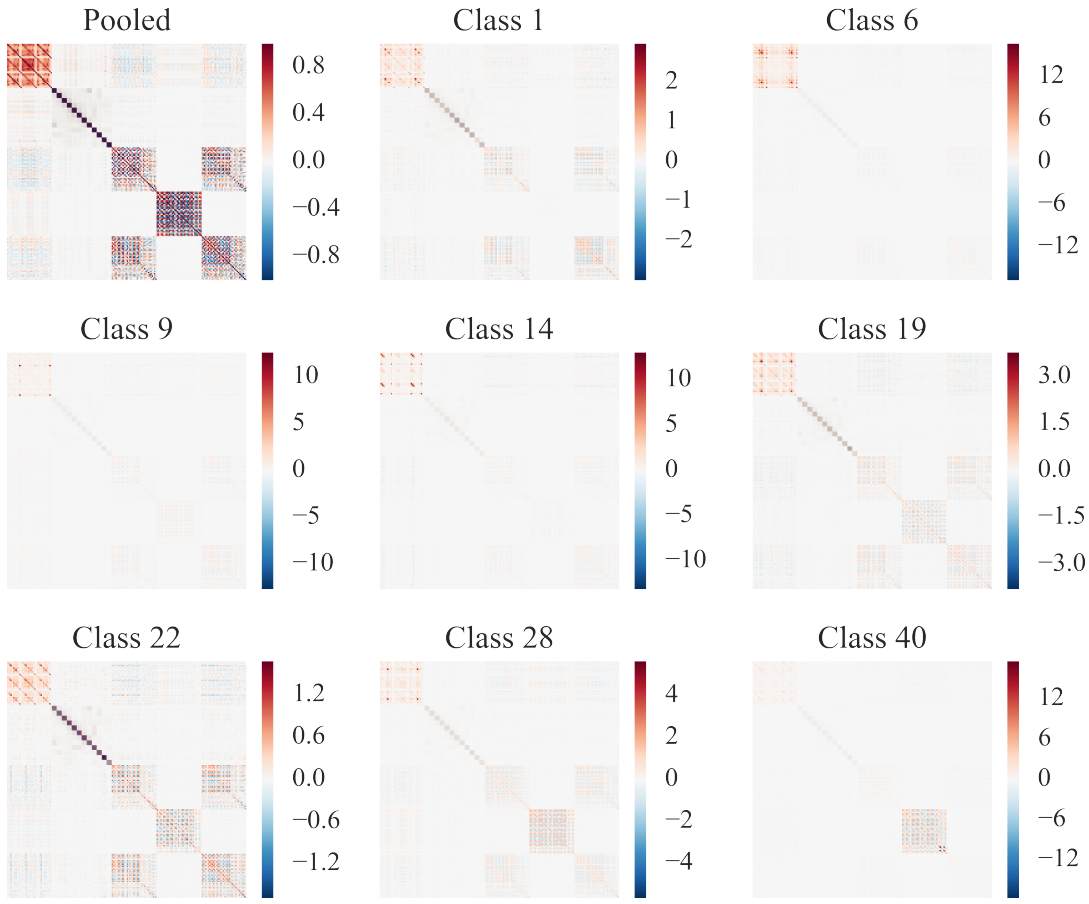

Figure 4.4: Heatmap visualisation of pooled and individual covariance matrices for myoelectric data. A subset of 8 out of 41 classes is shown. Covariance matrices were estimated by pooling data from 22 subjects (20 able-bodied, two amputees). The dimensionality of the shown covariance matrices is 192×192. Features were standardised to zero mean and unit standard deviation prior to covariance matrix estimation. Note different ranges of colour bars.

sised, it was found that class-specific covariance matrices were not identical to one another. Nevertheless, there were some distinct patterns shared across classes, which were also apparent in the pooled covariance matrix. This observation provides further motivation for considering DA models that do not make the LDA assumption (i.e. RDA, QDA) for the purposes of myoelectric control.

4.3.2 *Datasets and feature extraction*

In this study, four datasets were used to evaluate and compare the performance of the family of DA classifiers introduced in Section 4.2; namely, two publicly available released by Atzori et al. (2014), and the two datasets introduced in Section 3.2. The two pairs of datasets were identical in terms of behavioural protocols, signal acquisition, and data pre-processing. One difference was that for the first pair, the

Table 4.1: Experimental datasets used for algorithmic comparison. AB, able-bodied; Amp, amputee; EMG, electromyography; Acc, accelerometer; Gyro, gyroscope; Mag, magnetometer.

ID	Number of subjects	Medical condition	Sensing modalities	Input data dimensionality
1	40	AB	EMG, Acc	120
2	10	Amp	EMG, Acc	120
3	20	AB	EMG, Acc, Gyro, Mag	192
4	2	Amp	EMG, Acc, Gyro, Mag	192

standard Delsys® Trigno™ sensors were used, which incorporate EMG electrodes and accelerometers, whereas the Delsys® Trigno™ IM sensors were used for the latter, which also include gyroscopes and magnetometers (see Section A.1.1). The four features introduced in Section 3.2.3 were extracted from EMG signals. Inertial data were used in their raw format. For the first pair of datasets, the dimensionality of the input space was lower than for the second pair, due to the lack of gyroscope and magnetometer data. A summary of the four datasets, including information on numbers of participants, their medical condition, sensing modalities used, and input data dimensionality is provided in Table 4.1.

4.3.3 *Algorithms*

In the following sections, the decoding performance of the whole family of DA classifiers introduced in Section 4.2 is investigated. Furthermore, the k-NN classifier is considered (Fix and Hodges Jr., 1951), which is a non-parametric classification algorithm that has been extensively used in the context of myoelectric control (e.g. Nazarpour, Sharafat, and Firoozabadi, 2007; Scheme and Englehart, 2011; Kanitz et al., 2011; Boschmann and Platzner, 2013; Atzori et al., 2015; Atzori, Cognolato, and Müller, 2016; Du et al., 2017).

The k-NN algorithm belongs to the family of *instance-based*, also called *lazy* classifiers, which means that no training is required and all the computation is carried out at testing time. Given a test point $\mathbf{x}_\star$, we find the k training points $\mathbf{x}_1, \ldots, \mathbf{x}_k$ that are closest in distance to $\mathbf{x}_\star$ and then classify by using a majority vote among the k neighbours. The posterior probability of a class c can be estimated by using the fraction of neighbours labelled as c over the number of neighbours k. Ties are broken at random, although it is common to select k to be an odd number so that they are

avoided. To compute the distance between two data points, any valid distance metric can be used; some common choices include Euclidean, Manhattan, Chebyshev, and Minkowski distances.

4.3.4 *Cross-validation, hyper-parameter tuning, and performance assessment*

The 6-fold *cross-validation* (CV) procedure described in Section 3.2.5 was used; five repetitions of each movement were used to train classifiers, and the left-out repetition was used to assess classification performance (see Figure 3.6).

To tune the regularisation hyper-parameters α and γ of RDA, a grid search was performed in the range $[0, 1]$ with a step size of 0.05. In this case, inner-fold CV was used and the combination which yielded the highest average CA was selected. A similar linear search in the range $[0, 20]$ was used to select the k parameter for k-NN.

As in Section 3.2.5, the test dataset was balanced and classification performance was finally assessed by using the CA metric (see Section B.2).

4.3.5 *Statistical tests*

As in Section 3.2.7, the non-parametric Friedman test (Friedman, 1937) was used to compare the classification performance of the different algorithms. Post-hoc pair-wise comparisons were performed using the Wilcoxon signed-rank test (Wilcoxon, 1945) with Šidák correction for multiple comparisons (Šidák, 1967).

4.3.6 *Results*

A performance comparison of the five DA classifiers (LDA, QDA, GNB, DLDA, RDA) and k-NN is shown in Figure 4.5. For all four datasets, RDA consistently outperformed all other classifiers and it was followed by LDA, GNB, QDA, and DLDA. The average median difference in CA between RDA and LDA was 13.53%. All pairwise differences were statistically significant ($p < 0.001$), except for the QDA-GNB pair ($p > 0.05$).

Representative confusion matrices for one amputee subject (dataset 4) are shown in Figure 4.6. The colour code in the graph represents normalised CA scores. A one-to-one comparison between the performance of LDA and RDA is shown in Figure 4.7. For this graph, data from all datasets, subjects, and CV folds have been pooled together and each dot in the scatter plot corresponds to one testing fold (total number

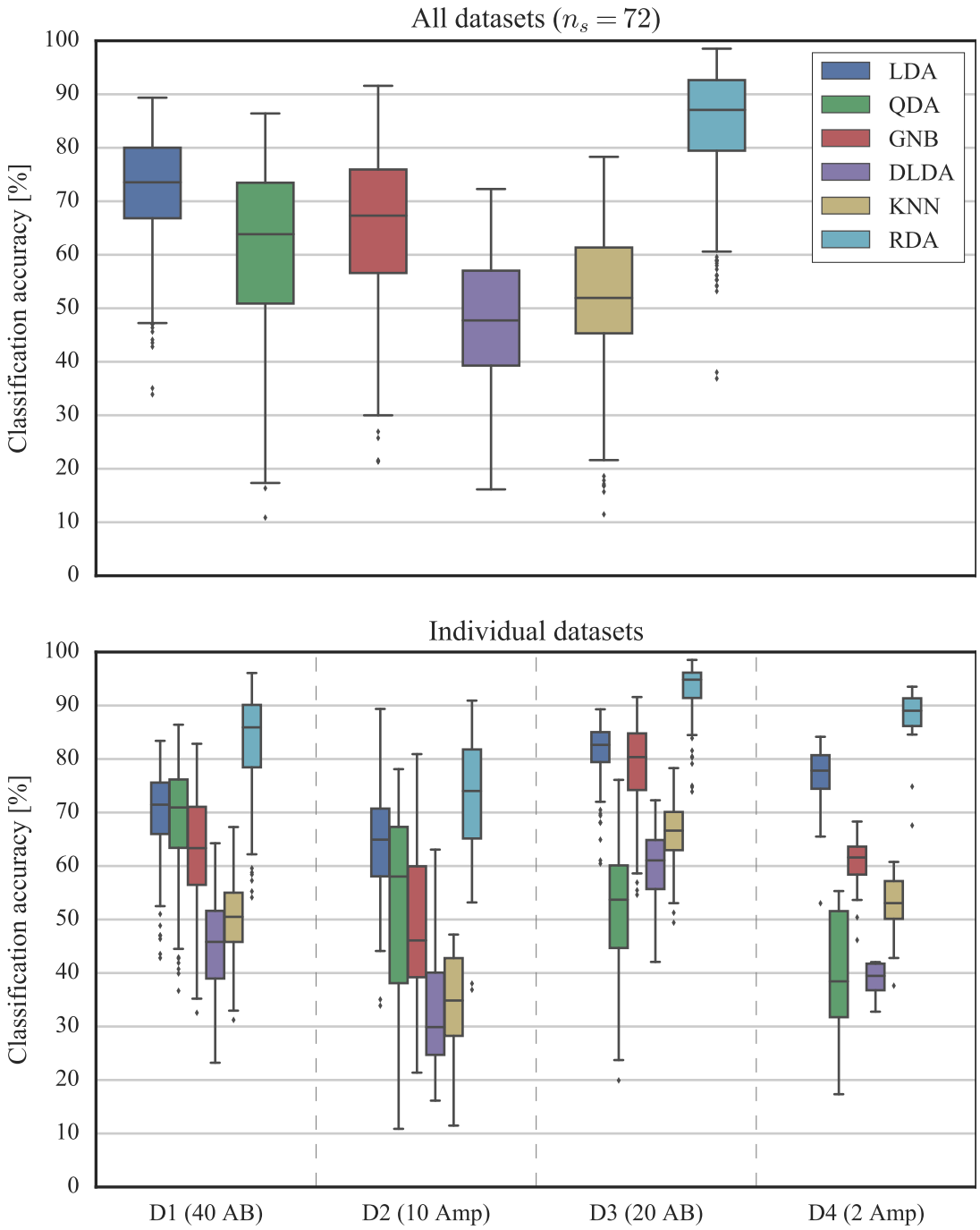

Figure 4.5: Algorithmic performance comparison. (Top panel) CA results for pooled subjects (n_s=72) and datasets (n_d=4); (bottom panel) results for individual datasets (see Table 4.1). Straight lines, medians; solid boxes, interquartile ranges; whiskers, overall ranges of non-outlier data (1.5 IQR); diamonds, outliers.

of folds n_f = 432). It is evident from this graph that RDA consistently outperformed LDA (98.8% of times).

The joint distribution of hyper-parameters α and γ for RDA as selected by inner-fold CV is shown in Figure 4.8. The optimal selection for γ was almost consistently

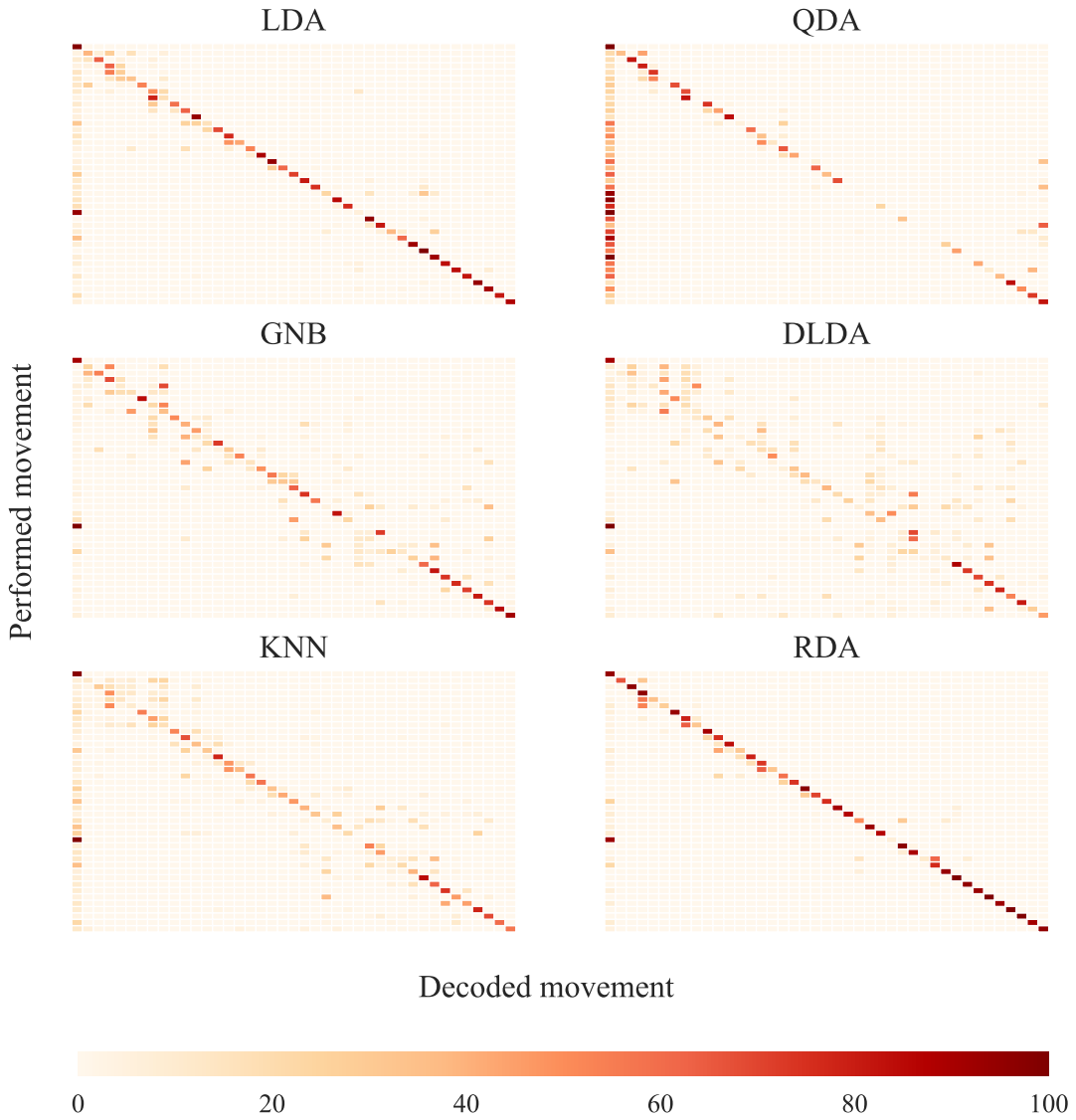

Figure 4.6: Representative confusion matrices for an amputee subject (dataset 4) with different classifiers. Colour map indicates normalised CA scores. Number of classes, $c = 41$.

0 (with very few exceptions where it was 0.05), whereas for α it varied in the range $[0.15, 1]$.

4.4 DISCUSSION

4.4.1 *Comparison of models, overfitting, and regularisation*

The RDA classifier consistently outperformed all other models. This was expected, since the RDA model is flexible and can treat all other models as special cases (see Equation 4.15 and Figure 4.1). The two hyper-parameters of the RDA classifier were

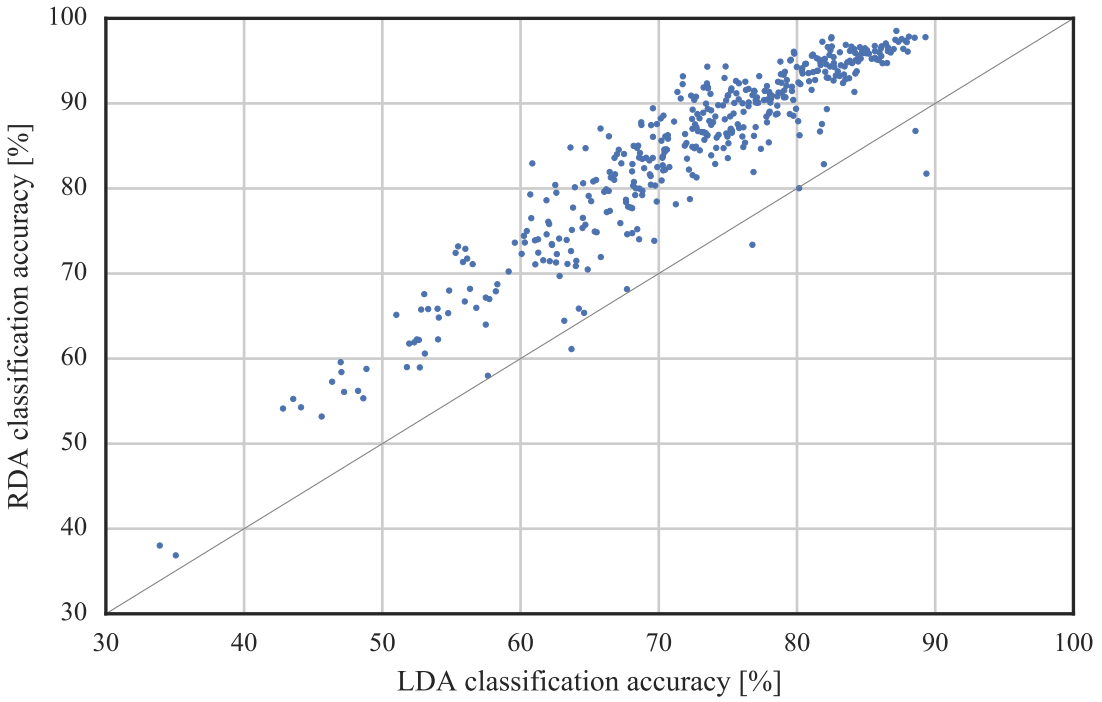

Figure 4.7: One-to-one comparison between LDA and RDA. Results shown for all datasets, subjects, and folds. Each dot in the scatter plot corresponds to one testing fold. Number of folds, n_f=432.

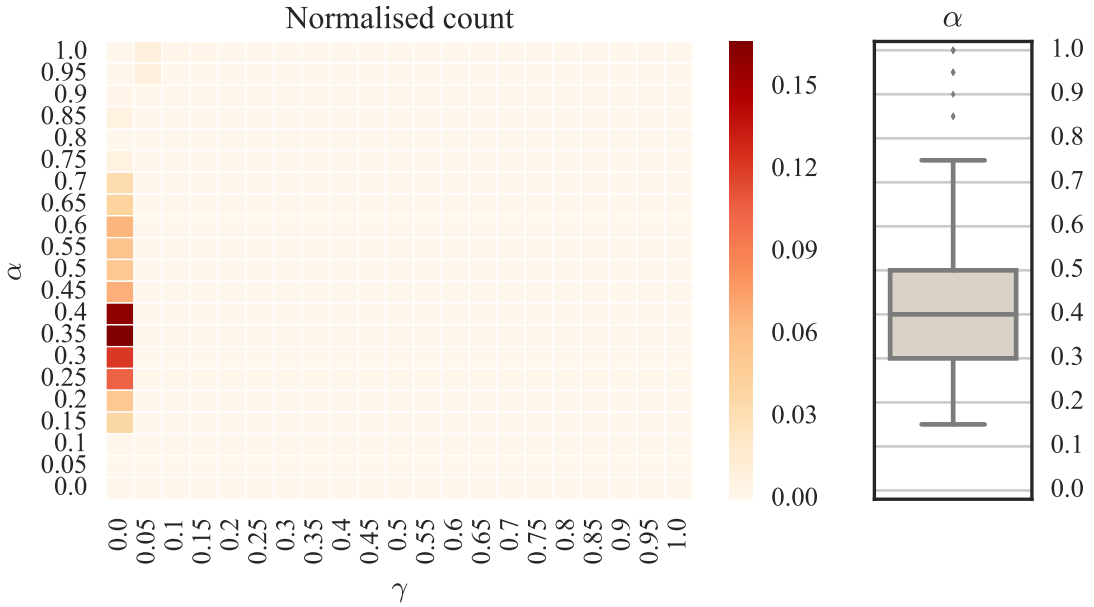

Figure 4.8: RDA hyper-parameter tuning. The colour map encodes the normalised count of selected pairs of values for RDA hyper-parameters α and γ. The marginal distribution of selected α values is shown separately on the right. Results shown for all datasets, subjects, and folds.

tuned such that the cross-validated CA was maximised; therefore, it was guaranteed that its performance would be at least as good as that of any other DA model.

The LDA model assumption, that is, classes share a common covariance matrix, is very strong and most often violated (see Figure 4.4). One would expect that QDA should outperform LDA as it is more flexible and does not make this assumption. The reason why this is not often the case is because QDA is heavily prone to overfitting. The number of free parameters that have to be estimated in the general class-conditional Gaussian model is $C\,(D+1)\,D/2$, where C is the number of classes and D is the dimensionality of the feature space. In our case, $C = 41$ and $D = 120$ (datasets 1 and 2), or $D = 192$ (datasets 3 and 4). Thus, the number of free parameters was approximately 2.86×10^5, and 7.6×10^5, respectively. Taking into consideration that a typical CV fold included on average 3.6×10^3 training samples, it is obvious that this method suffered profoundly from overfitting; the number of fitted parameters was orders of magnitude larger than the number of training samples. Consequently, it should come as no surprise that the classification performance of QDA for datasets 3 and 4 was inferior to that for datasets 1 and 2 (see Figure 4.5), since overfitting was exacerbated in the former case by the larger input dimensionality (see Table 4.1). As was to be expected, the performance of the other classifiers was improved when the additional sensing modalities (gyroscopes and magnetometers) were included in the set of features (see Chapter 3).

In the limit of infinite amount of data, one should expect that QDA would always outperform LDA. In practice, however, it is not feasible to collect vast quantities of training data, especially with amputees. The benefit of using RDA lies in that it can make use of the theoretical advantage of QDA over LDA without being susceptible to overfitting, as a result of regularising the class covariance matrices towards the pooled covariance matrix (α hyper-parameter).

The γ hyper-parameter is used in the RDA model to introduce a different form of regularisation, that is, it shrinks the estimated covariance matrices towards diagonal matrices. In the extreme case (i.e. $\gamma = 1$) the GNB model is recovered, which assumes class-conditional feature independence. Nevertheless, such behaviour should neither be desired nor expected, since many features originate from the same measurements (i.e. we extract multiple features from the same EMG signals). Input features which do not stem from the same measurements are still expected to exhibit strong correlations due to, for example, muscle crosstalk (Farina et al., 2014), or the relationship between surface EMG and inertial measurements (see Section 3.4.5). Thus, it should not be surprising that the optimal value for γ was almost consistently 0 (see Figure 4.8).

4.4.2 *Benchmarking*

The CA achieved with the RDA classifier was remarkably high, especially when taking into consideration the large number of classes ($C = 41$) included in the datasets. For a comparison, Atzori, Cognolato, and Müller (2016) reported an average CA of 75.27% ± 7.89% (mean ± standard error) with random forests, and 46.27% ± 7.89% with support vector machines, on datasets 1 and 2, respectively[1]. The same figures in the current study were 83.34% ± 8.97%, and 72.52% ± 12.05%, an average increase in performance of 8.07% and 26.25%, respectively, for able-bodied and amputee subjects. Furthermore, Geng et al. (2016) used only a subset of 8 classes from dataset 1 and reported a best CA of slightly less than 80% by using convolutional neural networks. This figure is still lower than the average CA achieved in the current study with RDA (83.34%) when the full set of 41 classes was considered. In agreement with previous studies (e.g. Li, Schultz, and Kuiken, 2010; Atzori et al., 2014), it was found that performance scores for amputees were moderately worse than for able-bodied participants (see Figure 4.5).

4.4.3 *Computational and memory requirement considerations*

One strong advantage of the LDA model is that decision boundaries are linear in feature space. As a result, the time complexity of assigning class probabilities to a test sample is $O(CD)$, that is, it scales linearly with the feature dimensionality. The space complexity for LDA is also $O(CD)$, since a weight vector of dimensionality D is only required to be stored in memory.

For general class-conditional Gaussian models like QDA and RDA, covariance matrix inverses have to be computed. Such operations require $O(CD^3)$ computational time during training. If these algorithms are implemented efficiently, that is, if inverse covariance matrices are precomputed and stored in memory, the computational complexity in testing time is $O(CD^2)$ and space complexity is $O(CD^3)$. As we shall see in the following chapter, for small to medium-sized feature spaces (i.e. orders of hundreds), this does not pose a problem for real-time implementations.

4.4.4 *Limitations and future work*

The purpose of the current study was to demonstrate that although LDA is the preferred classifier in the context of myoelectric control, the violation of its fundamental

1 Denoted as *datasets 2 and 3* in Atzori, Cognolato, and Müller (2016)

assumption about a shared covariance matrix may negatively affect decoding performance. For this reason, this study primarily focused on DA variants and did not investigate the performance of various other algorithms commonly used in this context, such as support vector machine and MLP classification. Moreover, although ensemble methods such as random forests (Breiman, 2001) and gradient boosting (Friedman, 2002) have been demonstrated to achieve high decoding performance on various tasks, they were not considered here due to their associated high computational complexity which would make them unsuitable for real-time implementations.

It is worth noting that there exist other DA variants which were not considered in this study. For example, penalised discriminant analysis (Hastie, Buja, and Tibshirani, 1995) applies a different form of regularisation that enforces coefficients to be smooth over the spatial (e.g. images) or temporal (e.g. time-series) domain. In our application, the temporal structure of the data is not taken into account when fitting classifiers, except that myoelectric data are smoothed as a result of using an overlapping sliding window approach. An interesting avenue to explore would be to use penalised discriminant analysis to account for the smoothness properties of data in conjunction with a much shorter time window. One potential benefit of this approach might be a significant decrease in the controller's delay without compromising performance. A different variant is mixture discriminant analysis (Hastie and Tibshirani, 1996) which, unlike QDA and RDA, allows classes to be modelled as mixtures of multiple Gaussian clusters. As with Gaussian mixture models, an expectation-maximisation algorithm can be used to train a mixture discriminant analysis model. The nature of this classifier allows it to model well multi-modal distributions. Whether its use could provide benefit in myoelectric data classification remains, however, to be investigated. Huang et al. (2005) reported promising results in this direction by using a similar approach to classify wrist and hand motions.

It is also worth mentioning that algorithmic comparisons were performed for a given feature representation. The mean absolute value, waveform length, 4^{th}-order auto-regressive coefficients, and log-variance features were extracted from EMG data, whereas for inertial data the mean value within the processing window was used (see Section 3.2.3). It has been previously reported that the choice of features is of particular significance for myoelectric classification performance (e.g. Zardoshti-Kermani et al., 1995; Englehart et al., 1999; Boostani and Moradi, 2003; Phinyomark, Limsakul, and Phukpattaranont, 2009; Phinyomark et al., 2013). Nevertheless, by taking into account that the benefit of using the RDA classifier lies in that it can treat other DA models as special cases (see Equation 4.15 and Figure 4.1), it is reasonable to expect that the findings presented here can generalise to arbitrary feature representations.

As a final note, the current study was limited to offline analyses. The following chapter addresses this limitation by deploying RDA classification for real-time prosthetic hand control.

5

REAL-TIME FAULT-TOLERANT PROSTHETIC HAND CONTROL WITH ONLY TWO SENSORS

The previous two chapters proposed ways of improving hand motion intent decoding and myoelectric control of prosthetic hands by using *inertial measurement unit*s (IMUs) (see Chapter 3) and a *regularised discriminant analysis* (RDA) classifier (see Chapter 4).

It has been already pointed out that in the myoelectric control field there is a remarkable gap between academic/research achievements and their commercial adoption (Jiang et al., 2012b; Farina et al., 2014). Among the reasons causing this discrepancy is the fact that *machine learning* (ML)-based algorithms require a relatively large number of *electromyography* (EMG) sensors to produce accurate and robust predictions. This requirement both increases the cost of the prosthesis and also reduces the practicality of the system (e.g. increased weight, additional burden for the user). As of today, most commercial prosthetic solutions incorporate a single pair of surface EMG sensors, usually targeting the forearm extensor and flexor muscle groups. Achieving classification-based myoelectric control with such minimal resources is a great challenge, which has not been previously tackled.

Drastically reducing the number of sensors used for myoelectric control may inevitably lead to a decrease in classification performance. Additionally, it has been reported that unintended prosthesis motions can lead to user frustration (Hargrove et al., 2010), which in turn may increase the risk of prosthesis rejection. Thus, to ensure user satisfaction, it is important to design fault-tolerant myoelectric controllers with the ability to reject classification predictions estimated with low confidence. This may come at the expense of increasing computational complexity (Hargrove et al., 2010; Scheme, Englehart, and Hudgins, 2011; Amsüss et al., 2014), introducing a response delay (Englehart and Hudgins, 2003), or even decreasing overall *classification accuracy* (CA) (Hargrove et al., 2010).

In this chapter, a framework for real-time, robust myoelectric control of hand prostheses is proposed by using a single pair of sensors, in a similar architecture to that of most commercial systems (see Section 2.4.1.1). Special attention is given to optimising the parameters of the system in order to minimise the amount of unintended performed motions. The efficacy of the proposed system is evaluated with experiments involving both able-bodied and transradial amputee participants.

5.1.1 *EMG channel reduction in myoelectric control*

The majority of studies investigating hand movement intent decoding have traditionally used a large number of surface EMG electrodes (e.g. Tenore et al., 2009; Al-Timemy et al., 2013) or high-density electrode arrays (e.g. Ison et al., 2016; Geng et al., 2016; Khushaba et al., 2017). Nevertheless, a large body of work has explored potential ways of reducing the number of recording electrodes and analysed the relationship between the amount of sensors used and classification performance. The current section provides a literature review of this topic.

Hargrove, Englehart, and Hudgins (2007) classified 10 forearm and hand motions in six normally-limbed subjects. The motions included wrist flexion/extension, forearm supination/pronation, and hand opening/closing. The authors selected a set of three optimal electrodes with respect to classification performance by using a brute-force method (i.e. exhaustive search) and reported a CA of 97% for those six classes.

Huang et al. (2008) recorded muscular activity from four patients having undergone targeted muscle reinnervation (see Section 2.4.2.5) by using high-density EMG arrays (116-128 monopolar electrodes). Their study included 16 classes comprising forearm, hand, and finger motions. It was found that only 12 electrodes selected via *sequential forward sensor selection* (SFSS) could achieve classification performance that was comparable to that of the whole set.

Li, Schultz, and Kuiken (2010) recruited five unilateral transradial amputees who were trained to control a virtual arm by modulating their muscular activity. Ten wrist and hand movements were tested and it was found that average CA scores reached a plateau after the inclusion of 4-6 EMG channels selected via exhaustive search.

Geng et al. (2014) used 56 EMG electrodes to record muscular activity of 12 mildly-impaired subjects with traumatic brain injury whilst they performed 21 forearm and hand movements. They proposed a method for channel selection based on common spatial pattern analysis (Müller-Gerking, Pfurtscheller, and Flyvbjerg, 1999) and compared their method to SFSS and a Fisher-Markov selector. The authors reported that their proposed algorithm achieved the highest performance out of the three methods. It was additionally observed that CA plateaued after the inclusion of 7-11 electrodes on average.

Muceli, Jiang, and Farina (2014) used high-density EMG recordings from forearm muscles of 10 able-bodied subjects to reconstruct 2-*degree of freedom* (DOF) wrist movement trajectories. Performance was validated with real-time myoelectric control of the position of an arrow on a screen. Interestingly, no significant differences were ob-

served in performance when the number of electrodes was reduced from 16 to either 8 or 6 by using a uniform selection approach.

In a related study, Hwang, Hahne, and Müller (2014) compared the performance of various EMG channel reduction techniques, namely least absolute shrinkage and selection operator, SFSS, and uniform selection on the task of reconstructing 2-DOF wrist kinematic trajectories. It was observed that SFSS outperformed the other two methods, while on average 12 electrodes selected via SFSS could achieve comparable performance to that obtained with the whole set of 64 electrodes.

Promising results in the same direction were also reported by Fougner, Stavdahl, and Kyberd (2014) who used only five EMG electrodes to achieve simultaneous and proportional control of two DOFs, namely wrist pronation/supination and hand opening/closing. The efficacy of the method was evaluated with the SHAP and clothespin tests (see Section 2.5.2).

Additionally, Naik, Al-Timemy, and Nguyen (2016) analysed myoelectric data recorded from five transradial amputees who performed 11 finger motions. They introduced a method for electrode selection which was based on a modified version of *independent component analysis* (ICA). The proposed method provided a slight improvement in CA as compared to the benchmark methods, and it was also shown that classification performance plateaued after the inclusion of 7-9 electrodes.

Adewuyi, Hargrove, and Kuiken (2016) investigated the potential benefit of combining EMG recordings from extrinsic and intrinsic hand muscles on the task of classifying 19 motion classes. The selected motions included various grasp types, individual finger movements, hand opening, and the rest pose. The authors used an SFSS algorithm for channel reduction and found that when using only extrinsic hand muscles, classification performance reached a plateau after the inclusion of 5-6 electrodes. Not surprisingly, the performance increased further when activity of intrinsic hand muscles was included in the decoders, thus suggesting that the latter can offer complementary information which cannot be extracted from extrinsic muscles.

More recently, Clancy et al. (2017) recorded and analysed myoelectric data from ten normally-limbed subjects and three transradial amputees whilst they performed a series of wrist movements. By using sequential backward sensor selection they demonstrated that it was feasible to accurately reconstruct wrist kinematic trajectories of a single DOF by using only two electrodes, while four electrodes were required to decode 2-DOF wrist kinematics.

Finally, Menon et al. (2017) investigated the interaction effect of processing window length, window overlap, and number of used electrodes on the classification of seven hand gestures. Able-bodied subjects, transradial, and partial-hand amputees were included in the study and their muscular activity was recorded with a pair of

64-channel high-density EMG arrays. Although no interaction effect was identified between the processing window length and number of electrodes, the authors found that the amount of sensors required to observe a plateau in performance differed across the three populations of participants; for the partial-hand amputee group the plateau occurred when 12 electrodes were included in the decoders, whereas eight sensors were only required in the case of transradial amputees.

5.1.2 *Fault-tolerant myoelectric control*

Pattern recognition-based prosthesis control cannot be seen as a mere ML problem. Once an estimate of a discrete (i.e. classification) or continuous (i.e. regression) target variable has been computed, there are several steps before it can be translated into a control action for the motors of a terminal device, such as a prosthetic hand.

During prosthetic control experiments, it has been reported that unintended prosthesis motions can cause increased frustration to the user (Hargrove et al., 2010). Furthermore, such errors require the user to perform compensatory motions and might also lead to dropped objects, collisions and/or accidents (Scheme, Hudgins, and Englehart, 2013). For all the above reasons, it is sensible to try to minimise the amount of unintended prosthesis activations, even at the cost of failing to execute a small proportion of correctly identified motions. The current section summarises the several attempts that have been made towards designing fault-tolerant myoelectric controllers. The reader is referred to Appendix B for an introduction to the various classification metrics and types of errors mentioned throughout this chapter.

Englehart and Hudgins (2003) decoded four wrist motions, namely flexion, extension, radial and ulnar deviation in 12 normally-limbed subjects. They suggested using a majority voting scheme as a post-processing step for classification predictions, whereby the control action at a given time step is affected by both previous and future predictions (i.e. non-causal filter). The proposed method was found to improve accuracy at the cost of introducing a response delay, in addition to that caused by using a window processing approach (see Section 2.2.4.3).

Hargrove et al. (2010) instructed 12 able-bodied subjects to perform seven forearm and hand motions in order to carry out a clothespin relocation task on a virtual environment (Lock, Englehart, and Hudgins, 2005). The authors trained multiple binary (i.e. one-vs.-all) *linear discriminant analysis* (LDA) classifiers and rejected classification predictions that were not shared across all classifiers. The proposed control strategy was compared to standard multi-class LDA classification without post-processing. The authors reported that their method led to an increase in classification error, however the *false positive rate* (FPR) was decreased. As a result, the total number of pin

drops was reduced when the rejection post-processing step was included in the control loop.

Scheme and Englehart (2011) extended the work of Hargrove et al. (2010) by training multiple one-vs.-one classifiers. In their proposed strategy, a class had to be unanimously selected by all classifiers it was part of, otherwise the algorithm would output the "rest" class (i.e. no motion) as its final decision. This method was validated in a follow-up study (Scheme and Englehart, 2013b) during real-time control by using a *three-dimensional* (3D) Fitts' Law test (see Section 2.5.4). The proposed control strategy improved the efficiency, overshoot, stopping distance, and *completion rate* (CR) as compared to standard multi-class LDA. However, the throughput, which implicitly represents the time taken to accomplish the task, was not improved. This led the authors to propose an alternative strategy based on multi-class LDA followed by confidence-based rejection (Scheme, Hudgins, and Englehart, 2013). In this paradigm, a prediction would be rejected if the respective posterior probability did not exceed a pre-defined threshold. This latter strategy outperformed LDA classification without post-processing on all metrics, including throughput. One disadvantage of this approach is that a single threshold is shared across classes and, additionally, it has to be set empirically.

Menon et al. (2015) tried to extend the work of Scheme, Hudgins, and Englehart (2013) by selecting class-specific thresholds in an automated fashion. They recruited eight transradial and five partial-hand amputees and used a pair of 64-channel high-density EMG arrays to record the subjects' forearm muscular activity whilst they performed a series of seven hand motions. The authors derived class-specific *receiving operating characteristic* (ROC) curves (see Section B.3) and suggested selecting the thresholds so as to maximise the distance of the obtained ROC curves from that of a random classifier (see Section B.3.2 and Figure B.1). They reported that their proposed strategy led to an increase in *true positive rate* (TPR), but also increased the classification error.

Amsüss et al. (2014) followed a slightly different approach. They trained a *multi-layer perceptron* (MLP) that mapped EMG features and decisions made by a base LDA classifier to a discrete binary target variable, encoding whether the prediction of the base classifier was accurate. Their method was evaluated on a dataset comprising recordings from seven normally-limbed and four transradial amputee subjects whilst they performed seven forearm and hand motions. The authors compared their proposed control strategy to standard multi-class LDA without post-processing, majority voting (Englehart and Hudgins, 2003), and confidence-based rejection (Scheme and Englehart, 2013b). It was reported that their proposed scheme achieved a higher CA,

and also increased the TPR. Comparisons on the FPR scores were, however, not reported.

Finally, Li et al. (2016) proposed to reduce the amount of unintended prosthesis activations by creating an additional class consisting of several movements not intended to be executed by the prosthesis. In this way, whenever the aforementioned class was predicted by the classifier, the prosthesis would not respond. This approach, however, requires collecting training data corresponding to an "*unwanted movements*" class, which may not be practical from a clinical point of view.

5.1.3 *Motivation*

Although a large body of work has reported various ways of reducing the number of EMG electrodes required for ML-based myoelectric control, the vast majority have suggested the use of 4-10 sensors, which can still be regarded as a high number. The purpose of the work presented in this chapter is to achieve robust pattern recognition-based upper-limb myoelectric control with only two sensors, which are usually available in commercial prosthetic systems (see Section 2.4.1.1). To address this challenging problem, this study will heavily rely on the advancements proposed in the previous two chapters of the thesis.

A significant reduction in the number of sensors would inevitably affect classification performance. To address this issue, it is sensible to design a fault-tolerant controller that does not allow for the execution of decoded motions unless they are estimated with high confidence. Such design will also allow to minimise the classification FPR that leads to unintended motions, which have been described as a primary cause of frustration for prosthesis users (Hargrove et al., 2010).

5.2 EXPERIMENTAL SETUP AND METHODOLOGY

The experimental paradigm followed in this study bears strong similarities to the one described in Section 3.3. The main aspects are summarised for completeness in the following sections.

5.2.1 *Participant recruitment*

Twelve able-bodied (10 male, two female; 10 right-hand, two left-hand dominant; median age 28 years) and two right-hand amputee subjects were recruited. Some of the able-bodied and both amputee participants had taken part in a previous myoelec-

tric control experiment (see Section 3.3). The medical records of the two amputee participants have been presented in Table 3.1.

5.2.2 *Signal acquisition and socket fitting*

For the able-bodied group, 16 EMG-IMU Delsys® Trigno™ IM sensors (see Section A.1.1 and Figure A.1) were placed on the participants' forearm arranged in two rows of eight equally spaced sensors each (see Figure 5.1, top row). For the two amputee participants, 13 and 12 sensors were used, respectively, due to limited space availability. The sensors were placed on the able-bodied participants' dominant hand, whereas for amputees they were placed on the subjects' phantom limb (right arm in both cases). Prior to sensor placement, the participants' skin was cleansed using 70% isopropyl alcohol. Elastic bandage was used to secure the sensor positions throughout the experimental sessions. Following sensor placement, the quality of all EMG channels was verified by visual inspection. The sampling frequency was set to 2 kHz for EMG signals and to 128 Hz for inertial data. Readings from IMUs were used in their raw format.

Custom built sockets were used to accommodate the robo-limb™ prosthetic hand (see Section A.2.1 and Figure A.2) that was used in this round of experiments. For the able-bodied group, the same socket was used for all participants and was adjusted for individual subjects using Velcro straps (see Figure 5.1, bottom left). Subject-specific sockets were used in the case of amputee participants, which were designed by taking into account the individuals' stump anatomy (see Figure 5.1, bottom right).

5.2.3 *Behavioural task*

The participants sat comfortably on an office chair and were asked to reproduce a series of motions instructed to them on a computer monitor. As in the real-time experiment described in Section 3.3.1, six motion classes were included: power grip, lateral grip, tripod grip, index pointer, hand opening, and rest pose (see Table 3.3).

As in the previous experiment, each session comprised a training and a testing phase. During the training phase, subjects were instructed to perform 20 reach-to-grasp repetitions of each of the five poses/grips. Two separate blocks of data were collected (*dataset A* and *dataset B*), each one comprising 10 repetitions for each grip.

During the testing phase, the participants were required to use the prosthetic hand to grasp, relocate, and release three objects and finally press down the "space" key on a computer keyboard (see Figure 5.1, bottom left). Trials were considered successful if all objects were relocated and the key was pressed within 75 s. In case an object was

dropped, the trial would be interrupted and considered as unsuccessful. The number of trials per subject was set to 10, and participants were given 45 s of rest in-between consecutive trials.

5.2.4 *Signal pre-processing*

For signal pre-processing, the same procedure as the one described in Section 3.2.3 was used, except that the length of the processing window was reduced to 128 ms with an increment of 50 ms (60% overlap). The total number of extracted features was 256 for able-bodied subjects (i.e. 16 sensors $\times$ 16 features/sensor), 208 for the first, and 192 for the second amputee participant, respectively (i.e. 13 or 12 sensors $\times$ 16 features/sensor).

5.2.5 *Sensor selection*

For each subject, two EMG-IMU sensors were selected out of the full set by using the SFSS method (Section 3.2.6). For sensor selection, LDA classifiers were trained by using dataset A (training set) and performance was assessed on dataset B (validation set). The objective function used for sensor selection was the *cross-entropy loss* (CEL). In contrast to CA which only considers the percentage of correct classifications, CEL also evaluates the accuracy of posterior probability estimates (see Section B.2.2 for details). As before, prior to performance evaluation, the distribution of the validation samples was balanced by removing a large proportion of the "rest" class (see Section 3.2.5).

5.2.6 *Classifier training and optimisation*

For hand movement intent decoding, the RDA classifier was chosen because of its superior performance to other *discriminant analysis* (DA) models (see Figure 4.5). It was shown in Section 4.3 that the optimal value for the γ hyper-parameter of RDA was almost consistently equal to 0. Taking this observation into consideration, this parameter was set *a priori* to 0 in an effort to reduce required training times; thus, only the α hyper-parameter was optimised. To achieve this, a line search was used in the range $[0, 1]$ with a step size of 0.025 and the parameter value that yielded the lowest CEL score on the validation set (i.e. dataset B) was selected. Following hyper-parameter optimisation, the training and validation datasets were merged and used

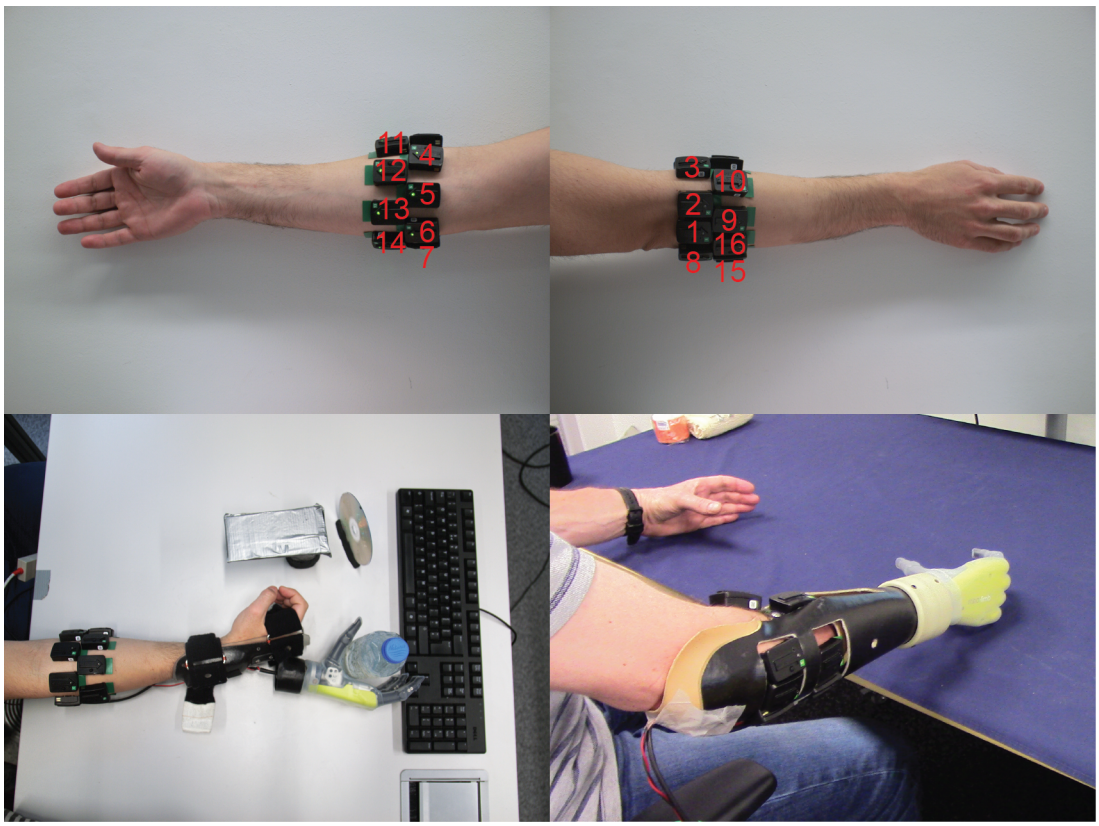

Figure 5.1: Experimental setup. Sixteen sensors were placed on the subjects' forearm below the elbow in two rows of eight equally-spaced sensors (top row). Custom built sockets were used to accommodate the robo-limb prosthetic hand for able-bodied (bottom left) and amputee (bottom right) subjects.

to train the final models. Model training and hyper-parameter optimisation were performed in a subject-specific fashion.

5.2.7 *Confidence-based rejection and threshold selection*

For real-time control, a confidence-based rejection strategy was used. In other words, classification decisions were discarded unless they were predicted with a posterior probability exceeding a pre-defined, class-specific threshold. The rejection thresholds were selected by using ROC curve analysis (see Section B.3) on the validation set (dataset B). To achieve this, multiple one-vs.-all RDA classifiers were trained and the corresponding FPR and TPR scores were computed for threshold values in the range $[0, 1]$ (see Section B.2).

The rejection threshold for each class was selected such that the TPR was maximised, while at the same time the respective FPR was constrained to be smaller than a cut-off value, set *a priori* to $5 \cdot 10^{-4}$. This was done in order to minimise the number of false positives that would translate into unintended hand motions. It was observed

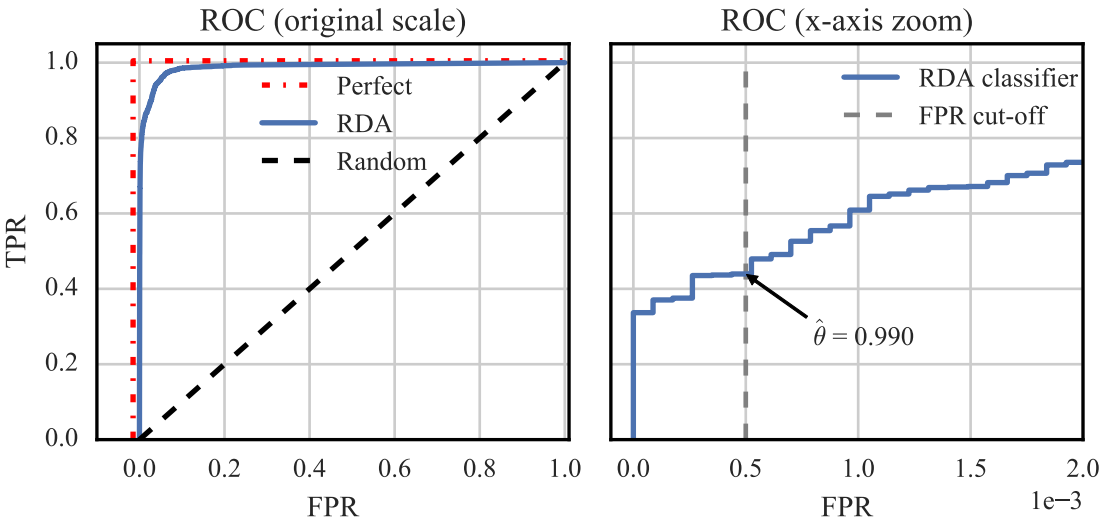

Figure 5.2: Example of rejection threshold selection using ROC curves. The procedure for selecting the rejection threshold for a single subject (able-bodied) and class (lateral grip) is shown. (Left column) ROC curves for three classifiers (perfect, random, RDA classifier); (right column) selection of the rejection threshold for the specific class and the RDA classifier. The threshold is selected such that the TPR is maximised while the FPR is smaller than $5 \cdot 10^{-4}$. For the specific threshold value, the corresponding TPR was 0.439. Note, the right column is a zoomed version of the the left column (x-axis).

during pilot trials that for well-separated classes this method would yield rejection thresholds extremely close to 1, which would then dramatically reduce the TPR for the same classes during real-time control. For that reason, an additional constraint was included that required rejection threshold values to not exceed 0.995. In mathematical terms, the strategy for rejection threshold selection for each class can be summarised as follows:

$$\hat{\theta}_c = \min \left\{ \max_{\theta_c} \mathrm{TPR}(\theta_c) : \mathrm{FPR}(\theta_c) < 5 \cdot 10^{-4}, 0.995 \right\}, \tag{5.1}$$

where $\hat{\theta}_c$ denotes the rejection threshold selection for class c. A typical example of this procedure performed for one class and a single subject is shown in Figure 5.2. For this example, the selected threshold value was 0.990, and the corresponding TPR was 0.439.

5.2.8 *Statistical tests*

Offline CA comparisons were performed using the non-parametric Friedman test (Friedman, 1937), followed by post-hoc pair-wise comparisons using the Wilcoxon

signed-rank test (Wilcoxon, 1945) with Šidák correction for multiple comparisons (Šidák, 1967).

To compare the performance between the able-bodied and amputee groups in the real-time experiment, two different statistical tests were used: the Fisher's exact test (Fisher, 1922) was chosen in the case of CR, because the observations were unpaired, the trials could take only two possible outcomes (i.e. success or fail), and the sample size was small; for *completion time*s (CTs), the non-parametric Wilcoxon rank-sum test, also known as the Mann-Whitney U test (Mann and Whitney, 1947), was used, again because observations were unpaired. The same test was additionally used to compare CTs between early and late trials.

5.3 RESULTS

5.3.1 *Offline analysis*

An offline analysis was performed to evaluate classification performance with a varying number of sensors and three DA classifiers, namely, LDA, RDA, and *quadratic discriminant analysis* (QDA) (see Section 4.2). To achieve this, 10-fold *cross-validation* (CV) was performed on dataset B, by using a 90%-10% split. In other words, the whole of dataset A was used to train models (*training set*), 9 out of 10 repetitions of each motion from dataset B were used as a *validation set* for sensor selection and RDA hyper-parameter optimisation, and the collection of left-out repetitions from dataset B were used as a *test set*. Note, this procedure was only followed for the purposes of offline analysis. During the experimental sessions, datasets A and B were used as the training and validation sets, respectively; a test set was not required in this case, as classification performance was subsequently evaluated during real-time prosthetic control.

The results of the offline analysis are presented in Figures 5.3 and 5.4. Performance was assessed by using both the CA and CEL metrics (see Section B.2). In general, performance improved as new sensors were added to the decoders and reached a plateau after the inclusion of 6-8 sensors. In terms of CEL (Figure 5.3, top row), RDA outperformed LDA for small numbers of sensors, but the two algorithms yielded comparable scores for more than five sensors. The performance of QDA was remarkably worse than that of LDA and RDA. Notably, the performance of QDA deteriorated when a large number of sensors was used, a clear sign of overfitting due to the large number of fitted covariance parameters and lack of regularisation (see Section 4.4.1). The results were consistent across the able-bodied and amputee populations.

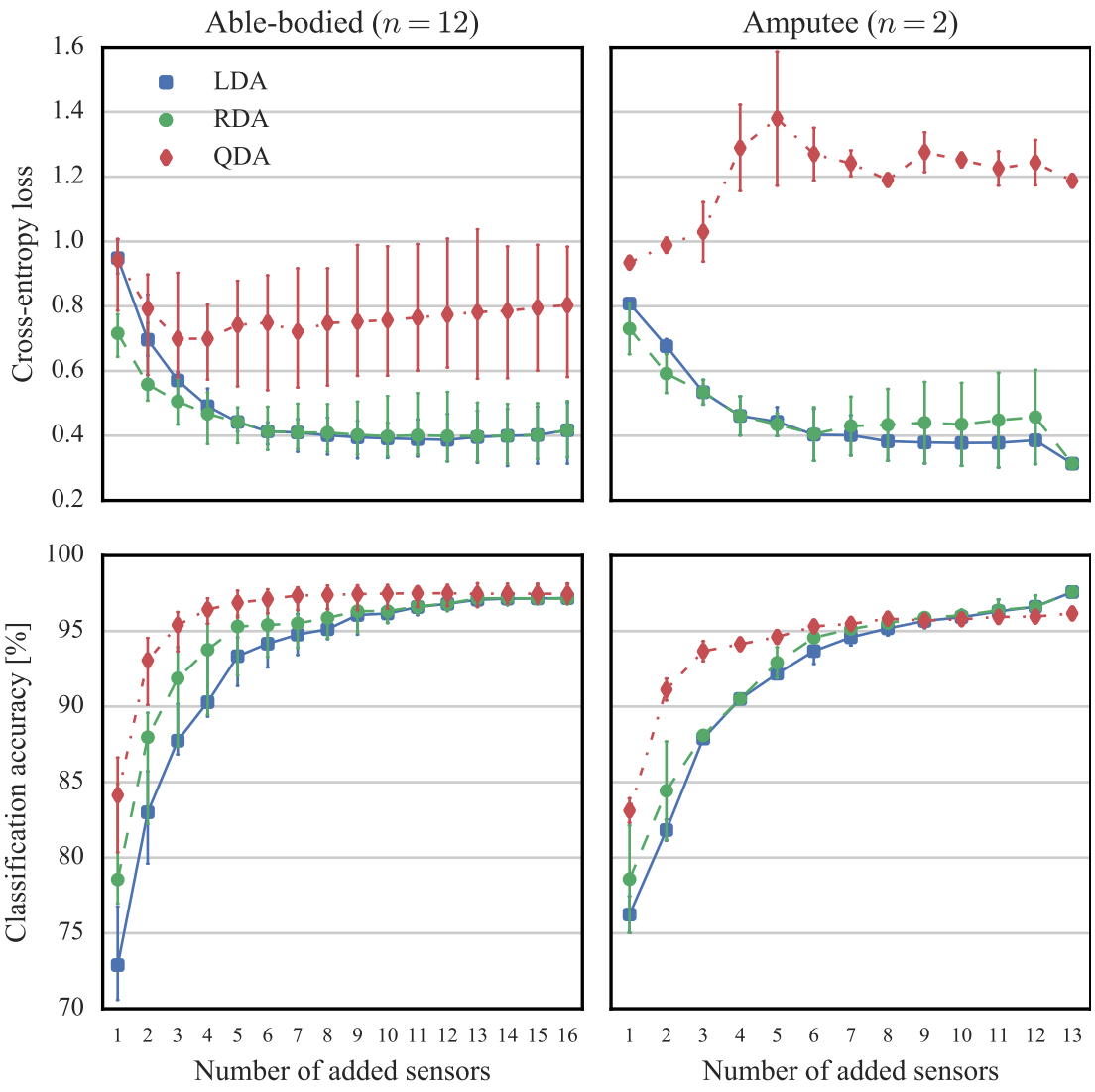

Figure 5.3: Offline comparison of DA classifiers for varying number of added EMG-IMU sensors. LDA, RDA, and QDA are compared with respect to CA and CEL metrics. The α parameter for RDA was optimised by using the CEL objective function. Results shown for 12 able-bodied (left column) and two amputee (right column) subjects. Points, medians; error bars, 95% confidence intervals estimated via bootstrapping (1000 iterations).

Interestingly, a different pattern was observed with respect to CA scores (see Figure 5.3, bottom row). The highest performance for this metric was achieved by QDA followed by RDA and then LDA. Differences in algorithmic performance were mostly noticeable when the number of used sensors was less than 10. Note, in this particular case, RDA was not guaranteed to achieve the best performance across the three algorithms, as a result of being able to treat LDA and QDA as special cases (see Section 4.4.1). This is because the objective function used for hyper-parameter optimisation was in this case not CA, but the CEL metric. On the contrary, it can be verified that

in terms of CEL, the performance achieved with RDA was at least as good as that of the other two methods (see Figure 5.3, top row).

The results from using the optimal subset of two EMG-IMU sensors are presented in more detail in Figure 5.4, separately for the able-bodied and amputee participants. In terms of CEL, RDA significantly outperformed LDA and QDA. LDA performed marginally better, although not significantly than QDA. On the other hand, the highest CA was achieved with QDA followed by RDA. For this metric, all pairwise differences were significant ($p < 0.01$).

Average confusion matrices for RDA classification with the two optimally selected EMG-IMU sensors are shown in Figure 5.5. It can be verified that despite using only two sensors, the six classes were highly separable.

Figure 5.6 shows the distribution of selected values for the RDA α hyper-parameter, as a function of the number of included sensors. Not surprisingly, as the input dimensionality grows larger due to more sensors being added to the pool, the median of this distribution is moved towards lower values, hence implying that stronger regularisation is required. When the number of included sensors exceeded 10, the median of this distribution was exactly 0, which corresponds to the LDA model (see Figure 4.1).

5.3.2 *Real-time prosthetic control experiment*

The working principle of the real-time prosthetic control paradigm is shown in Figure 5.7. For the shown trial, the sequence of objects to be relocated was "bottle", "CD", and "card". Therefore, the optimal sequence of hand motions was "power grip", "hand open", "tripod grip", "hand open", "lateral grip", "hand open", and "index pointer". It can be observed that there was a relatively large number of incorrectly classified instances (blue line, top panel) in this trial; however, the confidence-based rejection strategy discarded most of them, since the corresponding posterior probabilities (bottom panel) were below the respective rejection thresholds (see Section 5.2.7). Overall, there were two unintended hand motions (red ellipses, top panel), and the trial was successful with a completion time of 24.45 s. A video recording showing one trial of the experiment with an amputee participant is provided in the supplementary material (SV3, see Appendix E).

Performance results for the 12 able-bodied and two amputee participants are shown in Figure 5.8. Each subject performed 10 trials and the CR and CT metrics were used to evaluate prosthetic control performance (see Section 3.3.3). Summary scores across the two populations of participants are also shown on the right-hand side of the graph. The median CRs were 95% and 85% for the able-bodied and amputee groups,

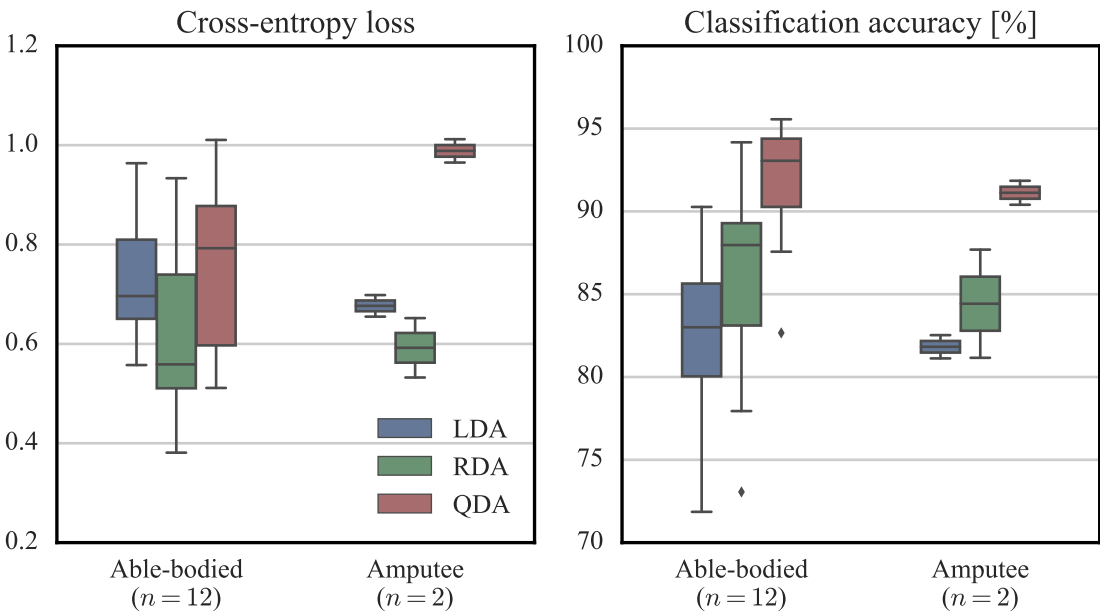

Figure 5.4: Offline comparison of DA classifiers for the optimal subset of two EMG-IMU sensors. LDA, RDA, and QDA are compared with respect to CEL (left column) and CA (right column) metrics. Data shown for all subjects (12 able-bodied, two amputees) and CV folds (k = 10). Straight lines, medians; solid boxes, interquartile ranges; whiskers, overall ranges of non-outlier data (1.5 IQR); diamonds, outliers.

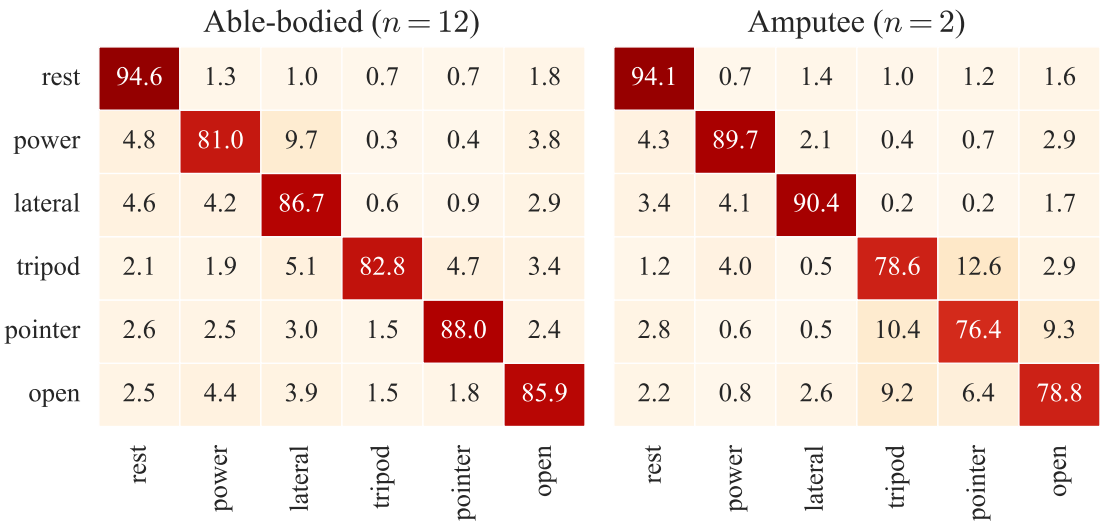

Figure 5.5: Average offline confusion matrices with RDA and selected subset of two EMG-IMU sensors. Data shown for all subjects (12 able-bodied, two amputees) and CV folds (k = 10). Annotated scores represent normalised CA scores.

respectively. Median CTs for successful trials were 37.43 and 44.28 s, respectively. Able-bodied subjects performed on average higher than amputees with respect to both metrics; however, differences in performance between the groups were not significant ($p > 0.05$).

The effect of user adaptation on prosthesis control was also investigated and the results of this analysis are presented in Figure 5.9. In this graph, average CTs across

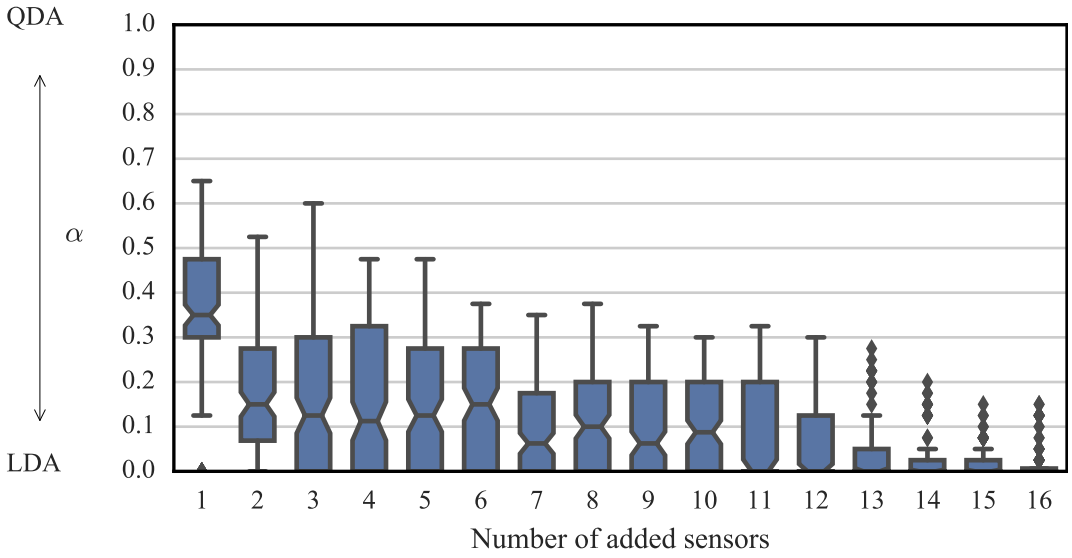

Figure 5.6: RDA hyper-parameter optimisation. Selections for the RDA α hyper-parameter are shown for an increasing number of EMG-IMU sensors. Data shown for all subjects (12 able-bodied, two amputees) and CV folds ($k = 10$).

subjects are plotted against trial numbers, separately for the two groups of participants. It was found that the median CT significantly decreased from the first two ("early") to the last two ("late") trials (median difference of 6.81 s, $p < 0.05$). The average time elapsed between the initiation of the early (i.e. first) and late (i.e. ninth) trials was 16.08 ± 1.39 min (mean $\pm$ standard error).

The optimally selected pairs of EMG-IMU sensors for all participants are presented in Figure 5.10 using a matrix representation. Average (across-subject) selections for individual sensors are shown in the rightmost column of the graph. As in Figure 3.17, no specific patterns of subset selection were identified, although some units were selected slightly more frequently than others (e.g. sensors, 2, 6, and 8).

Finally, a summary of the thresholds selected for the different classes is provided in Figure 5.11. While for three out of six classes (i.e. "power grip", "lateral grip", and "tripod grip") the threshold varied in the range [0.950, 0.995], the upper-bound (i.e. 0.995) was consistently selected for the remaining three classes.

5.4 DISCUSSION

5.4.1 *Impact*

The current study demonstrates the feasibility of using classification-based grip control for hand prostheses by using a single pair of surface EMG-IMU sensors. This achievement, which to the author's best knowledge has not been previously reported,

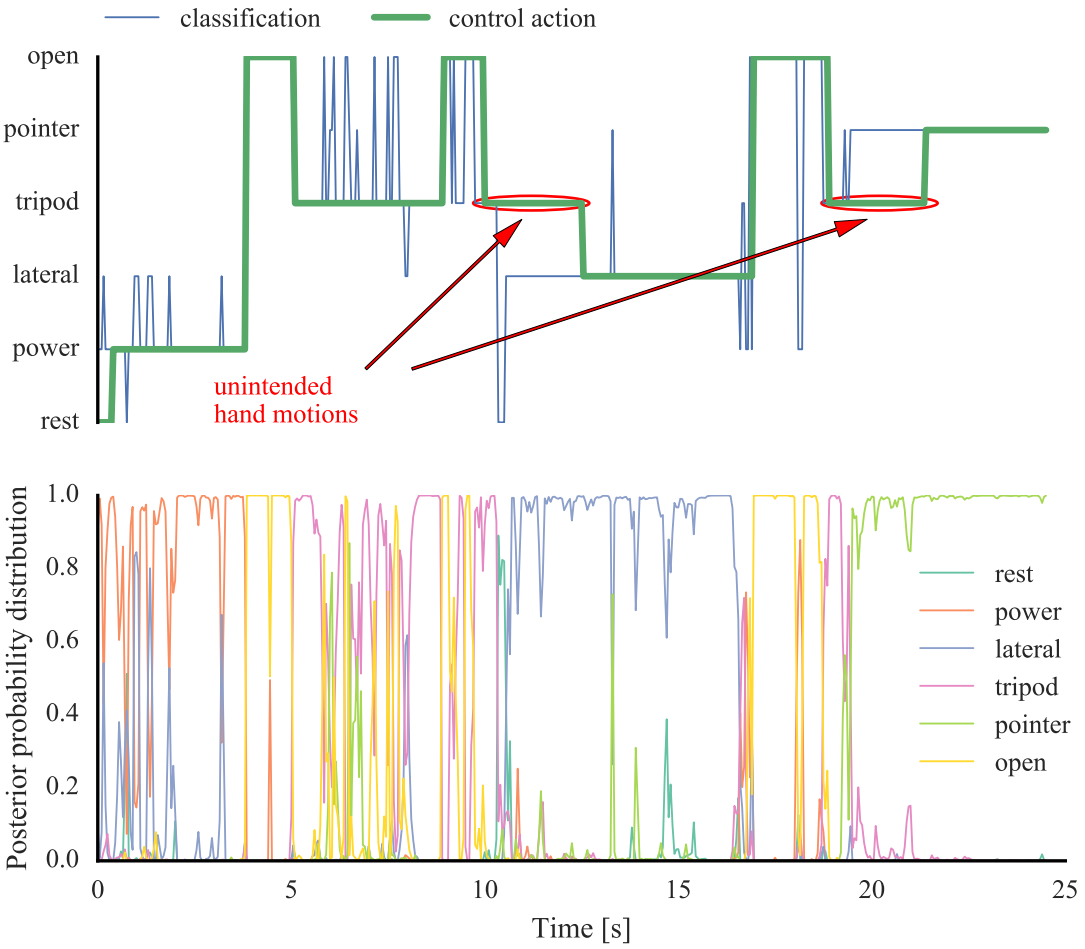

Figure 5.7: Real-time classification and control. The time-series of classification predictions and control actions are shown in blue and green, respectively (top panel). A new classification was translated into a control action only if the corresponding posterior probability (bottom panel) exceeded the respective class-specific threshold. Unintentionally performed hand motions are marked with red ellipses (top panel).

can have a substantial impact in the field of upper-limb control, since it demonstrates that ML-based prosthetic control can be potentially applied to currently available commercial solutions, subject to minimal modifications. Minimising the number of sensors used for myoelectric control is of significant importance for two reasons: firstly, a large number of used sensors is associated with high computational, and thus, power requirements; secondly, it is not practical from a user's point of view.

The achievement presented in this chapter has been made possible by combining a series of advancements introduced in the current and earlier chapters. First and foremost, it has been exploited that RDA classification can attain higher decoding performance than LDA (see Figure 4.5), especially when the number of used sensors is small (see Figure 5.4). Notwithstanding this improvement, reducing the number of sensors to only two inevitably leads to a higher classification error (see Figure 5.3).

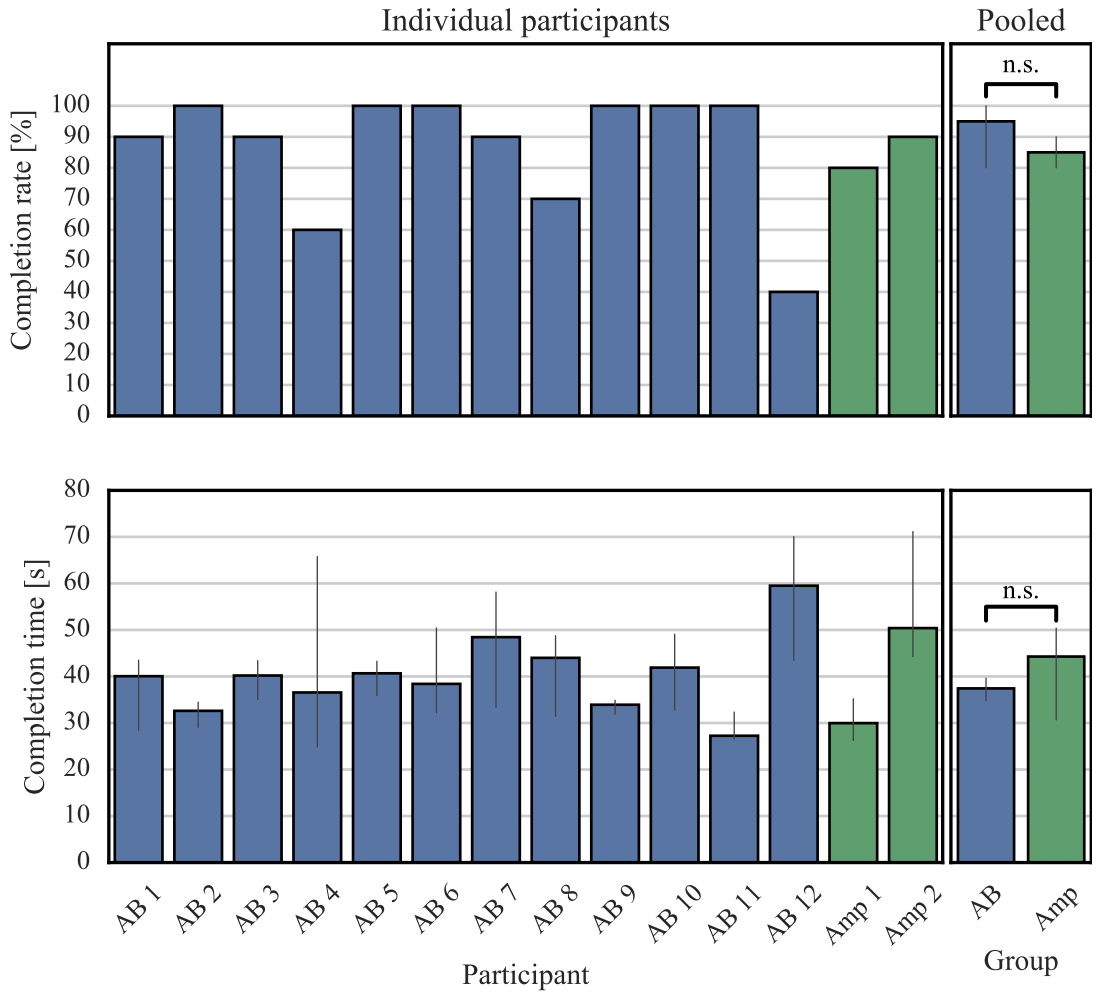

Figure 5.8: Real-time prosthetic control experiment results. CRs and CTs shown for 12 able-bodied and two amputee subjects. Data shown separately for individual participants (left column) and populations of able-bodied and amputee subjects (right column). Bars, medians; error bars, 95% confidence intervals estimated via bootstrapping (1000 iterations); n.s., non-significant difference.

To compensate for this increase in classification error, confidence-based rejection was deployed to discard predictions that were not made with high confidence.

5.4.2 *Technical considerations*

During offline analysis, it was found that the optimal number of sensors may actually be in the range of five to seven (see Figure 5.3). This is in agreement with the results obtained in the real-time control experiment presented in Chapter 3. The purpose of the current study, however, was to investigate whether ML-based control would be feasible with currently existing commercial architectures; therefore, it was decided to only include two sensors. Contrasting CTs in the current experiment with those corresponding to condition IV in Section 3.3.5, in which an optimal subset of EMG-

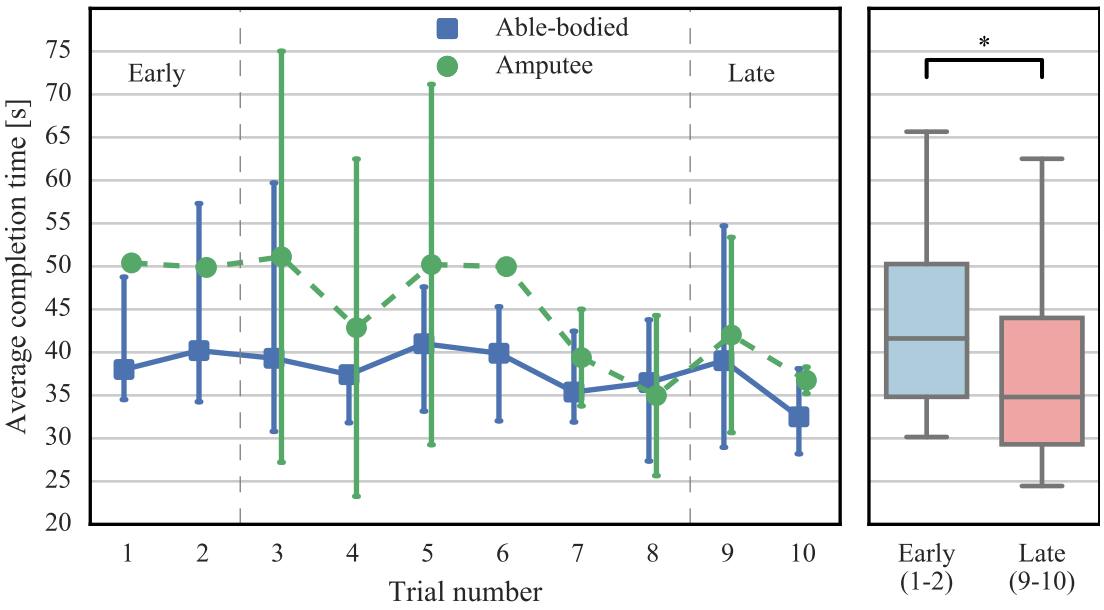

Figure 5.9: Real-time prosthesis control learning curves. (Left) average CTs are plotted against the trial number for able-bodied ($n = 12$) and amputee ($n = 2$) populations. (Right column) average CT comparison between early (i.e. 1-2) and late (i.e. 9-10) trials. Asterisk, $p < 0.05$.

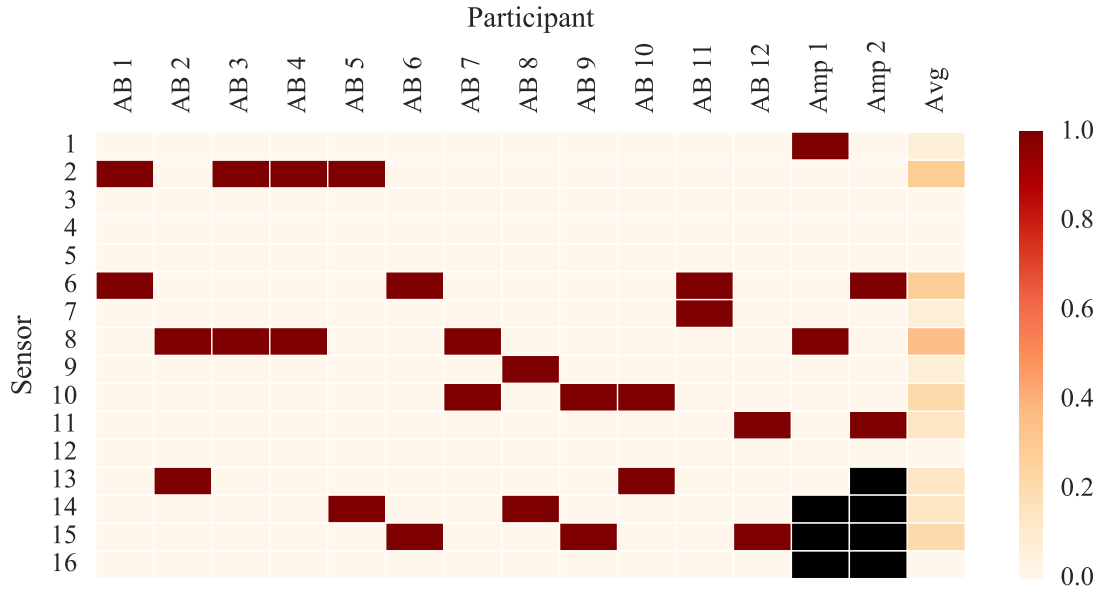

Figure 5.10: Sensor selection for individual participants. The selected EMG-IMU sensors are shown column-wise as red boxes for 12 able-bodied and two amputee subjects. The rightmost column represents the average selection frequency of individual sensors. Black boxes represent unavailable sensors due to limited space on amputee participants' forearm. The reader is referred to Figure 5.1 for details on sensor placement.

IMU sensors were used for a similar task, it can be noted that performance between the two conditions was comparable. Nevertheless, a direct comparison is not possible

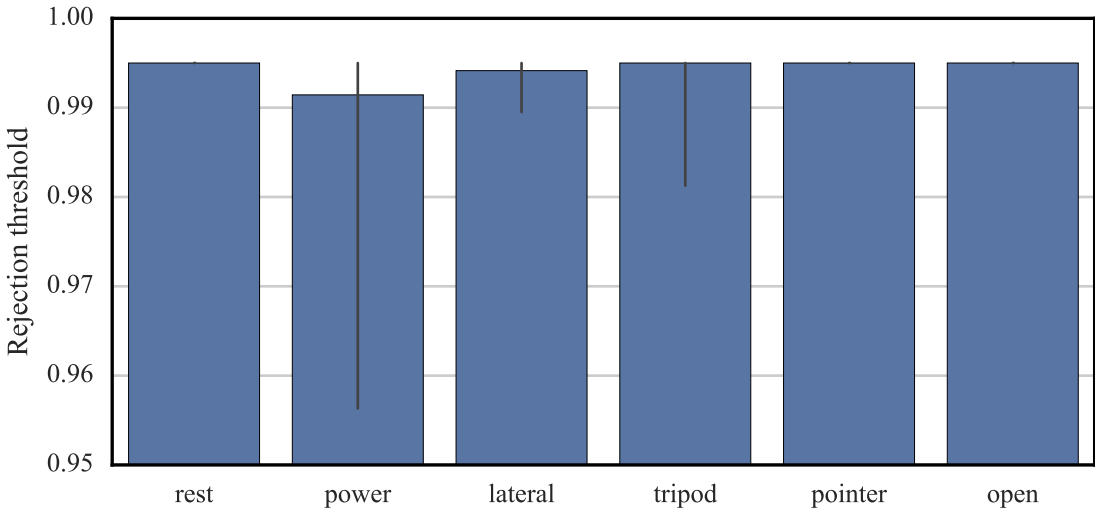

Figure 5.11: Rejection thresholds. Selected thresholds shown for all subjects (12 able-bodied, two amputees), separately for each class. Bars, medians; error bars, 95% confidence intervals estimated via bootstrapping (1000 iterations).

due to differences in experimental design (e.g. number of trials, length of processing window, confidence-based rejection strategy used).

Various algorithms have been proposed for optimal sensor selection (see Section 5.1.1). The standard SFSS method was used in this study, mainly because of its speed and efficiency during training. It has also been demonstrated that despite its simplicity, it can outperform more sophisticated methods, such as the least absolute shrinkage and selection operator (Hwang, Hahne, and Müller, 2014). An alternative would be to optimally select the pair of used sensors with a brute-force method (i.e. exhaustive search), but this approach can cause a substantial increase in training times.

5.4.3 *Clinical implications*

This study demonstrates the feasibility of using ML-based hand grip control with commercially available prosthetic hands, which are usually driven by a pair of surface EMG sensors (see Section 2.4.1.1). One difference between commercial prostheses and the setup used in this study is that in the latter case, the sensors incorporated IMUs that are typically not available in commercial systems. Nevertheless, IMUs are cheap units (average cost of £30) and their integration into an existing system should be rather straightforward. In fact, some commercial devices already comprise IMUs to monitor the orientation of the prosthesis, but these are usually embedded in the prosthetic hand and not placed on the forearm of the user, as was the case in the current study.

With regards to sensor subset selection, there were no shared patterns identified across the different participants (see Figure 5.10). From a clinical point of view, this finding suggests that it might not be straightforward to identify the optimal sensor placement locations for a specific patient *a priori*. One possible solution to this problem is to use the approach followed in the current study; that is, record muscular activity from many sites during an initial screening, and subsequently identify the optimal locations based on a sensor selection algorithm. This procedure should though precede the socket fabrication stage, which requires sensor positions to be established.

It has been previously demonstrated on numerous occasions that myoelectric control performance can increase over time because of user adaptation (e.g. Pistohl et al., 2013; Jiang et al., 2014b; Powell, Kaliki, and Thakor, 2014; He et al., 2015). In agreement with previous reports, a significant decrease was observed in CTs between early and late trials. Taking into consideration that the testing phase of the experiment lasted on average 20 minutes, it is reasonable to expect that performance can potentially further improve with daily use, provided that exogenous parameters such as sensor positions are controlled. It could also be argued that the observed increase in performance in such a short period of time validates the intuitiveness of the myoelectric control interface.

5.4.4 *Performance metrics*

One of the most important aspects of the control scheme proposed in this study is the decision-making element, which is based on confidence-based classification rejection. Without this component, a substantial number of incorrect classifications may be executed by the prosthetic hand leading to performance deterioration, user frustration, and potentially damage or injury during daily life use (Hargrove et al., 2010; Scheme, Hudgins, and Englehart, 2013). Taking into consideration that many parameters have to be optimised during training, such as sensor location, classification algorithm hyper-parameters, and rejection thresholds, a metric quantifying performance with respect to the quality of posterior probability estimates is deemed necessary. To this end, the CEL metric was chosen, which is typically used as loss function for training artificial neural networks (see Section B.2.2).

The choice of metric is crucial for hyper-parameter optimisation; different metrics may yield utterly different results. For instance, it was observed during offline analysis that QDA achieved higher CA scores than RDA, but the latter method performed better than the former with respect to the CEL metric (see Figure 5.3). This observation may be attributed to overfitting issues associated with QDA training (see Section

4.4.1); the large uncertainty in estimating the covariance parameters in the case of full Gaussian models (i.e. QDA) may yield inaccurate predictions of posterior probabilities (see Equation 4.8), even though the classes may still be well-separated in the projection plane which might explain the high CA scores. During pilot trials that included the confidence-based rejection component, it was observed that despite the high offline CA scores attained by QDA, the real-time performance of the algorithm was particularly low, and also involved a large number of false positive activations. This behaviour is a sign of the incapacity of the algorithm to produce accurate posterior probability estimates, which was also reflected in the high CEL scores.

The observation described above is in accordance with previous studies reporting a discrepancy between offline CA scores and real-time prosthetic control performance. For instance, Ortiz-Catalan et al. (2015) found no correlation between offline CA scores and real-time accuracy when using the motion test (see Section 2.5.5). Additionally, Vujaklija et al. (2017) found only a weak correlation between SHAP scores (see Section 2.5.1) and offline CA for the same subjects.

To investigate whether the CEL metric could provide a better estimate of real-time performance than CA, an analysis was performed on the relationship between these two measures and average CTs during the real-time experiment. The results of this analysis are shown in Figure 5.12, where each point in the graph corresponds to a single subject. Average CTs exhibited a marginally stronger (positive) correlation with CEL than with CA (negative correlation); however, neither of the two linear relationships were significant. In both cases, the points corresponding to the amputee participants lay quite far from the regression lines, hence suggesting that predicting prosthetic control performance from offline metrics might be even harder for amputee subjects.

Finally, it is worth stressing the importance of using a validation dataset for performing sensor selection, hyper-parameter tuning, and rejection threshold selection. All the aforementioned parameters can have a remarkable impact on final control performance and, as such, it is crucial to select them by evaluating performance on a different dataset to the one used to train the classifiers to avoid introducing biases (Domingos, 2012).

5.4.5 *Limitations and future work*

One limitation of the current study is that, due to experimental time constraints, it did not perform a comparison between the proposed methodology and the clinical state of the art (see Section 2.4.1). It shall be, therefore, valuable to compare in the future the proposed classification-based myoelectric control paradigm to clinical stan-

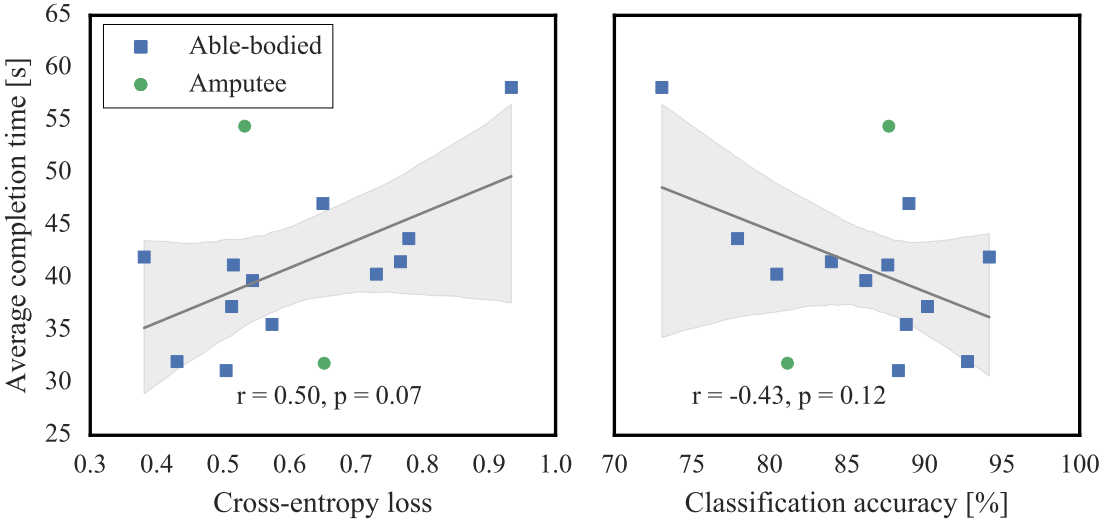

Figure 5.12: Relationship between mean CTs and offline metrics (i.e. CEL and CA). Points, individual observations (i.e. subjects); lines, linear regression fits; translucent bands, 95% confidence intervals estimated via bootstrapping (1000 iterations).

dards such as myoelectric mode switching and body-powered prostheses (e.g. hooks,) both quantitatively, that is, using performance scores such as CRs and CTs, and also qualitatively using, for example, questionnaires and user satisfaction metrics.

With regards to sensor selection, the LDA classifier was used to assess the predictive performance of the set of candidate sensors within each iteration. Once the SFSS algorithm was terminated, the RDA α hyper-parameter was optimised for the selected subset of sensors. This approach might have produced slightly suboptimal results, since the interaction effect of sensor selection and regularisation was not examined. Optimising for the two parameters at the same time would however incur prohibitive training times and, for that reason, was not considered as an option. One possible alternative could be to optimise for these two parameters simultaneously by using sophisticated optimisation strategies. For instance, Bayesian optimisation (Snoek, Larochelle, and Adams, 2012) is a probabilistic inference-based strategy for optimising black-box functions without the need for computing derivatives. It can prove very useful for optimising the hyper-parameters of ML models in arbitrary search spaces for both continuous and discrete-valued hyper-parameters. Bayesian optimisation has been successfully applied in a variety of tasks, including automatic ML and hyper-parameter tuning for neural networks (Shahriari et al., 2016). It would be, therefore, interesting to investigate whether it can be successfully applied to myoelectric classification for simultaneous subset selection and hyper-parameter tuning.

For rejection threshold selection using ROC curve analysis, the most commonly used strategies involve either maximising the vertical distance from a random classifier, or minimising the distance from an ideal classifier (see Section B.3.2). However,

neither of the two methods impose a constraint on the FPR. This was regarded as a high priority in the current task, given the high associated cost of false positive activations which, in turn, translate into unintended hand motions. To address this issue, thresholds were selected such that the TPR was maximised, while at the same time the FPR was kept below a cut-off threshold value (not to be confused with the actual rejection threshold). However, this FPR cut-off value was selected empirically during pilot trials. An interesting avenue for future research would be to attempt to systematically identify the optimal FPR cut-off value during real-time myoelectric control. One possible way to achieve this might be by giving the user control over this value, for example, via a knob switch, and asking them to select it according to their individual preference. It would be also interesting to assess whether a shared pattern of preference can be observed across different participants.

As a final note, the focus of the current and earlier chapters has been on decoding hand movement intent and driving prosthetic hands by using grip control, that is, by using a pre-defined set of motions. Although this control scheme can offer a tremendous benefit to the quality of life of an amputee, it still lacks the level of dexterity enjoyed by the human hand. This is mainly due to the discrete and sequential nature of the artificial hand motion. The following chapters attempt to address this limitation by investigating hand joint angle reconstruction for individual digit prosthetic control.

6

RECONSTRUCTION OF FINGER JOINT ANGLE TRAJECTORIES WITH SURFACE ELECTROMYOGRAPHY

This thesis has hitherto investigated grip-based myoelectric control of upper-limb prosthetic hands. In this approach, the most appropriate grip is selected via classification of *electromyographic* (EMG) and/or other input signals (e.g. inertial measurements), and subsequently transmitted to the prosthesis in the form of a discrete action. Although this control scheme can offer a remarkable boost to the end user's ability to perform activities of daily living, it suffers from two main limitations: 1) it results in severe under-actuation of the prosthesis which dramatically limits its functionality, since the user can only have access to a set of pre-determined modules; and 2) it is sequential in nature, that is, a single class of movement can be active at a time as opposed to the natural continuous and asynchronous finger movement exhibited by the human hand.

One way of enhancing the dexterity of powered myoelectric prostheses is via continuous and simultaneous control of multiple *degrees of freedom* (DOFs) (Fougner et al., 2011, see Section 2.4.2.2). The majority of previous work on proportional myoelectric control studied the decoding of wrist joint angle kinematics from surface EMG signals (e.g. Jiang, Englehart, and Parker, 2009; Muceli and Farina, 2012; Muceli, Jiang, and Farina, 2014; Jiang et al., 2014a). Additionally, a few research groups have addressed the challenge of using upper-limb muscular activity to decode finger joint angles (e.g. Smith et al., 2009; Hioki and Kawasaki, 2012; Ngeo, Tamei, and Shibata, 2012; Ngeo, Tamei, and Shibata, 2014a; Xiloyannis et al., 2015) as well as fingertip forces (e.g. Castellini et al., 2009; Nielsen et al., 2011; Gijsberts et al., 2014a), ultimately aiming to achieve individual digit continuous prosthetic control.

In this chapter, a thorough investigation is conducted on reconstructing multidimensional finger joint angle trajectories from surface EMG signals. Various decoding-related aspects are considered, including feature selection, filter length, and choice of regression algorithm. Special attention is given to ensure the feasibility of implementing the proposed methodology in real-time. The latter aspect forms the basis of Chapter 8, where a surface EMG-based, prosthetic digit position control scheme is implemented on a robotic hand and evaluated by carrying out experiments with able-bodied and amputee participants.

6.1.1 *Wrist kinematics decoding with surface electromyography*

Numerous studies have demonstrated the feasibility of reconstructing wrist joint angle trajectories from muscular activity signals. Jiang, Englehart, and Parker (2009) proposed a semi-supervised method based on *non-negative matrix factorisation* (NMF) to extract neural control information from surface EMG signals that was subsequently used to reconstruct 3-DOF wrist movement. Wrist flexion/extension and radial/ulnar deviation movements could be reconstructed with high accuracy; however, this was not the case with pronation/supination. This issue was later addressed by Jiang et al. (2012a) and Muceli and Farina (2012) who used *multi-layer perceptron*s (MLPs) to offline reconstruct 3-DOF wrist movement in both able-bodied and amputee subjects. The same authors later demonstrated that by using high-density EMG arrays and an NMF-based algorithm, the performance of the decoding method was robust against simulated electrode shifting (Muceli, Jiang, and Farina, 2014).

Ziai and Menon (2011) compared the offline decoding performance of various algorithms, including ridge regression, least absolute shrinkage and selection operator, support vector regression, artificial neural network regression, locally-weighted projection regression, and a physiological-based model. They found that all methods achieved high accuracy when trained and tested on data from the same sessions; however, the performance of all methods suffered when tested on datasets recorded one and 24 hours after the training sessions. Change of limb posture and electrode displacement were also found to negatively affect performance. Based on these observations, the authors concluded that in practice, frequent model retraining might be required to preserve decoding accuracy to an acceptable level.

Hahne et al. (2014) compared linear and non-linear methods (i.e. *linear regression* (LR), *kernel ridge regression* (KRR), MLPs, and mixture of linear experts) for reconstructing 2-DOF wrist joint angles. Interestingly, they found that while LR was outperformed by non-linear methods when the energy of the EMG signal was fed as input to the decoders, the performance of the four methods was comparable when the EMG signal energy was pre-processed through a log-transformation. The same group also performed a comparison of electrode selection algorithms on the task of decoding 2-DOF wrist movement (see Section 5.1.1).

More recently, a number of studies have demonstrated the feasibility of employing real-time simultaneous proportional wrist control of multiple DOFs (e.g. Jiang et al., 2014a; Ameri et al., 2014a; Ameri et al., 2014b; Smith, Kuiken, and Hargrove, 2014;

Smith, Kuiken, and Hargrove, 2015; Smith, Kuiken, and Hargrove, 2016). These are discussed in detail in Chapter 8 (see Section 8.1.1).

6.1.2 *Finger joint angle reconstruction with surface electromyography*

A small number of groups have addressed the problem of reconstructing individual finger joint angle trajectories from surface EMG signals. Promising results in this direction were first reported by Afshar and Matsuoka (2004) who used the activity recorded from seven muscles and a two-layer MLP to decode the index fingertip position in an able-bodied subject. The authors reported reconstruction accuracies of 0.6 - 0.8, as measured by the correlation coefficient between measured and reconstructed signals (see Section C.2.2). The first proof-of-principle demonstration on transradial amputees was reported in a study by Sebelius, Rosén, and Lundborg (2005), in which an artificial neural network based on locally-weighted regression was used to decode finger joint angles from eight EMG channels. Ground truth kinematic data were obtained from the participants' contralateral hand with a data glove.

Smith et al. (2008) also used an MLP to estimate the five *metacarpophalangeal* (MCP) joint angles in an able-bodied subject and reported an average correlation coefficient of 0.74. The same group later used this methodology to produce estimates of the end positions of five fingers that were used to control a virtual hand (Smith et al., 2009).

Ngeo, Tamei, and Shibata (2012) used an electromechanical delay model and an MLP to estimate 14 joint angles in an able-bodied subject, which were used in a follow-up study to control an exoskeleton (Ngeo et al., 2013). The same authors performed a comparison of Gaussian process and artificial neural network regression on data recorded from 10 healthy subjects by using a muscle activity model as the input feature to the decoders (Ngeo, Tamei, and Shibata, 2014a). The authors later explored the potential benefit of using a multi-output Gaussian process model, but no improvement in performance was observed (Ngeo, Tamei, and Shibata, 2014b).

Various other methods have been proposed for the reconstruction of finger movement kinematics, including recurrent neural networks (Hioki and Kawasaki, 2009; Hioki and Kawasaki, 2012), state-space models (Pan et al., 2013), and auto-regressive moving average models (Xiloyannis et al., 2015).

Alternative non-invasive recording methods have also been recently proposed for reconstruction of finger movement. For instance, Kadkhodayan, Jiang, and Menon (2016) used force myography to predict fingertip trajectories of the thumb, index, and middle fingers in 10 normally-limbed subjects whilst they performed three different grasps. The authors reported an impressive average squared correlation coefficient of 0.96. Finally, Nissler, Mouriki, and Castellini (2016) used visual fiducial markers to

track forearm skin deformation, which was subsequently mapped to finger positions by using ridge regression. Ten able-bodied subjects took part in the study and the authors reported average normalised root mean squared errors (see Section C.2.2) of 0.05-0.22.

6.1.3 *Force estimation*

In the last decade, a small number of studies have investigated continuous decoding of grasping and fingertip forces by using surface EMG signals. Grasp force estimation in amputees was first reported by Castellini et al. (2009) by using surface electrodes and support vector regression. Nielsen et al. (2011) used an MLP to reconstruct wrist force trajectories in 10 able-bodied participants and a subject with congenital amputation. In both cases, training data were collected by instructing participants to perform bilateral mirrored movements. Liu et al. (2011) used EMG electrode arrays to record muscle activity from the forearm of a normally-limbed subject which was subsequently mapped to fingertip forces of the four long fingers using LR. In the same direction, Castellini and Koiva (2012) used support vector regression to decode fingertip forces of the five fingers and the force exerted by the thumb during rotation. Li et al. (2015) combined finger motion classification and fingertip force prediction using MLP classifiers and polynomial regression, respectively. Recently, proportional fingertip force prosthetic control has been implemented and tested in real-time (Gijsberts et al., 2014b; Patel, Nowak, and Castellini, 2017; Gailey, Artemiadis, and Santello, 2017). A detailed review is provided in Section 8.1.3.

6.1.4 *Motivation*

The current study considers the problem of finger joint angle reconstruction with surface EMG signals for digit position prosthetic control. Although this topic has been previously investigated (see Section 6.1.2), a systematic analysis of various decoding aspects, such as feature selection and choice of algorithm is missing from the literature. The results obtained with the current analysis are taken into consideration for the design and implementation of a continuous digit position controller, which is presented and evaluated with real-time experiments in Chapter 8.

6.2.1 *Datasets*

Two datasets were used in the current study comprising recordings from a total of 60 able-bodied subjects (datasets 1 and 3 in Table 4.1). For both datasets, muscular activity and hand kinematics were recorded from the participants' right arm. A 22-DOF CyberGlove data glove was used for dataset 1, whereas an 18-DOF model was used for dataset 3 (see Section A.3.1). Amputee subjects were not included in the current analysis, due to hand kinematic data being unavailable.

Each dataset comprised recordings from two groups of movements (see Section 3.2.1 and Figure 3.3). For exercise B, wrist movements (i.e. B9-B17 in Figure 3.3) were discarded, as there was no finger motion associated with these exercises.

6.2.2 *Decoding algorithms*

To reconstruct finger joint angles from EMG signals, linear and non-linear regression methods were considered. For the former, a regularised version of a multiple-input-multiple-output linear system identification algorithm, namely the *Wiener filter*, was deployed. For the latter, the standard KRR algorithm was chosen, which is a powerful method for approximating non-linear functions by using the kernel trick.

6.2.2.1 *Linear regression (Wiener filter)*

Assume without loss of generality a zero-mean D-dimensional input variable $\mathbf{x} = [x_1, \ldots, x_D]^\top$ and a zero-mean scalar output variable (i.e. target) z, and let $z[n]$ denote the output activity at time n. If either of the variables has non-zero mean, then it is possible to estimate it from the training data and remove it (i.e. *data centering*). The Wiener filter model assumes that each system input (i.e. feature) x_d is convolved with its finite impulse response function:

$$z[n] = \sum_{d=1}^{D} \sum_{m=0}^{M-1} h_d[m]\, x_d[n-m], \tag{6.1}$$

where $h_d[m]$ accounts for the contribution of the input d at time instance m, $x_d[n-m]$ is the activation of the input d at time $n-m$, M is the filter length, and we also

assume a finite number of samples $n = 1, \ldots, N$. The linear system described by Equation 6.1 can be written in matrix form as follows:

$$\mathbf{z} = \mathbf{X}\mathbf{h}, \tag{6.2}$$

where $\mathbf{z}$ is the N-dimensional vector containing $z[n]$ for $n = 1, \ldots, N$, $\mathbf{h}$ is the DM-dimensional vector

$$\mathbf{h} = [\mathbf{h}_1, \mathbf{h}_2, \ldots, \mathbf{h}_D]^\top, \tag{6.3}$$

with

$$\mathbf{h}_d = [h_d[0], h_d[1], \ldots, h_d[M-1]]^\top, \tag{6.4}$$

and $\mathbf{X}$ is a block matrix

$$\mathbf{X} = [\mathbf{X}_1, \mathbf{X}_2, \ldots, \mathbf{X}_D], \tag{6.5}$$

where $\mathbf{X}_d$ are $N \times M$ matrices

$$\mathbf{X}_d = \begin{bmatrix} x_d[1] & 0 & \ldots & 0 \\ x_d[2] & x_d[1] & \ldots & 0 \\ \vdots & \vdots & \ddots & \vdots \\ x_d[N] & x_d[N-1] & \ldots & x_d[N-M+1] \end{bmatrix}. \tag{6.6}$$

Equation 6.2 can be solved analytically by using the normal equation:

$$\hat{\mathbf{h}} = \left(\mathbf{X}^\top \mathbf{X}\right)^{-1} \mathbf{X}^\top \mathbf{z}. \tag{6.7}$$

However, the inversion of the matrix $\mathbf{X}^\top\mathbf{X}$ can become computationally expensive for large number of inputs. An efficient solution to the multiple-input-single-output system identification problem described above can be achieved by considering the equivalent input-output relationship based on autocorrelation and cross-correlation matrices. Let $\mathbf{\Phi}_{XX}$ and $\boldsymbol{\phi}_{Xz}$ denote the $DM \times DM$ input autocorrelation matrix and the DM-dimensional input-output cross-correlation vector, respectively. Perreault, Kirsch, and Acosta (1999) showed that the solution of the problem described by Equation 6.2 is equivalent to the solution of the following system:

$$\boldsymbol{\phi}_{Xz} = \mathbf{\Phi}_{XX}\mathbf{h}. \tag{6.8}$$

The autocorrelation matrix $\mathbf{\Phi}_{XX}$ is symmetric and Toeplitz. If the input variable $\mathbf{x}$ is wide-sense stationary, that is, if its mean and autocovariance do not vary with respect to time, then $\mathbf{\Phi}_{XX}$ is also positive definite and, therefore, invertible. The solution of Equation 6.8 is achieved through inversion of the autocorrelation matrix $\mathbf{\Phi}_{XX}$:

$$\hat{\mathbf{h}} = \mathbf{\Phi}_{XX}^{-1}\mathbf{\phi}_{Xz}. \tag{6.9}$$

A regularised version (i.e. *ridge regression*) of the solution described by Equation 6.9 can be obtained as follows:

$$\hat{\mathbf{h}} = \left(\mathbf{\Phi}_{XX} + \lambda \mathbf{I}_{DM}\right)^{-1} \mathbf{\phi}_{Xz}, \tag{6.10}$$

where $\mathbf{I}_{DM}$ denotes the $DM \times DM$ identity matrix, and λ is a hyper-parameter controlling the strength of regularisation.

The solution described by Equation 6.10 can be extended to multiple-input-multiple-output systems with K-dimensional output variables by replacing vectors $\mathbf{z}$ and $\mathbf{h}$ by matrices $\mathbf{Z}$ and $\mathbf{H}$ of dimensionality $N \times K$ and $MD \times K$, respectively:

$$\hat{\mathbf{H}} = \left(\mathbf{\Phi}_{XX} + \lambda \mathbf{I}_{DM}\right)^{-1} \mathbf{\Phi}_{XZ}, \tag{6.11}$$

where $\mathbf{\Phi}_{XZ}$ is the $DM \times K$ input-output cross-correlation matrix.

6.2.2.2 *Kernel ridge regression*

Kernel ridge regression attempts to find the solution of the following system of equations:

$$\hat{\mathbf{A}} = \left(\mathbf{G} + \lambda \mathbf{I}\right)^{-1} \mathbf{Z}, \tag{6.12}$$

where $\mathbf{G}$ represents the Gram matrix, whose elements are inner products in the kernel feature space:

$$G\left(\mathbf{x}, \mathbf{x}'\right) = \langle \widetilde{\phi}\left(\mathbf{x}\right), \widetilde{\phi}\left(\mathbf{x}'\right) \rangle. \tag{6.13}$$

The squared exponential kernel (also known as radial basis function or Gaussian kernel) was chosen in the current study. This is defined as follows:

$$G\left(\mathbf{x}, \mathbf{x}'\right) = exp\left(-\frac{\|\mathbf{x} - \mathbf{x}'\|^2}{2\sigma^2}\right), \tag{6.14}$$

where σ is a hyper-parameter controlling the width of the kernel and $\|\mathbf{x} - \mathbf{x}'\|$ denotes the Euclidean distance between observations $\mathbf{x}$ and $\mathbf{x}'$.

6.2.2.3 *Cross-validation and hyper-parameter optimisation*

As in Section 3.2.5, 6-fold *cross-validation* (CV) was used to assess decoding performance. To optimise the hyper-parameters of the two methods, inner-fold CV was used; four repetitions of each movement within the training dataset were used to train models and accuracy was validated on the left-out repetition by using the *coefficient of determination* (R^2) score (see Section C.2.2.2). The hyper-parameter values that yielded the highest average accuracy were selected and used to train final models by making use of the entire training set. Performance was finally evaluated on the test set.

To optimise the λ hyper-parameter for LR, a search was performed in the log-space $\{10^{-6}, 10^{-5}, \ldots, 10^{7}\}$ using a factor (i.e. multiplication step) of 10. Similarly, a log-grid search was used to optimise the λ and σ hyper-parameters for KRR in the ranges $\{10^{-6}, 10^{-5}, \ldots, 10^{7}\}$ and $\{10^{0}, 10^{1}, \ldots, 10^{4}\}$, respectively, using the same factor as above for both parameters.

6.2.3 *Feature selection and comparisons*

As a first step, a feature comparison was performed on the task of reconstructing finger joint angle trajectories from surface EMG data by using LR. The following time-domain EMG features were considered (see Section 2.2.3.1): mean absolute value, Wilson amplitude (θ=50 mV), log-variance, waveform length, variance, root mean square, zero-crossing, slope sign change, 4^{th}-order auto-regressive coefficients, histogram (number of bins $k = 5$), and kurtosis. Frequency or time-frequency domain features were not considered, due to their associated increased computational complexity that might be prohibitive for real-time implementations (Boostani and Moradi, 2003).

In addition to performing one-to-one comparisons of individual features, *sequential forward feature selection* (SFFS) was used to identify an optimal set of features for the current task. The inclusion of a new feature in the subset was based on the overall decoding performance averaged across subjects, exercises, and CV folds. This ensured that the algorithm would identify a single subset of features for all subjects and exercises. Features that extract multiple attributes from a single EMG channel (i.e. auto-regressive coefficients and histogram) could only be included all together. The cost function used to assess the performance of a certain pool of features at each iteration was the multivariate R^2 (see Section C.2.2.2). The algorithm terminated execution

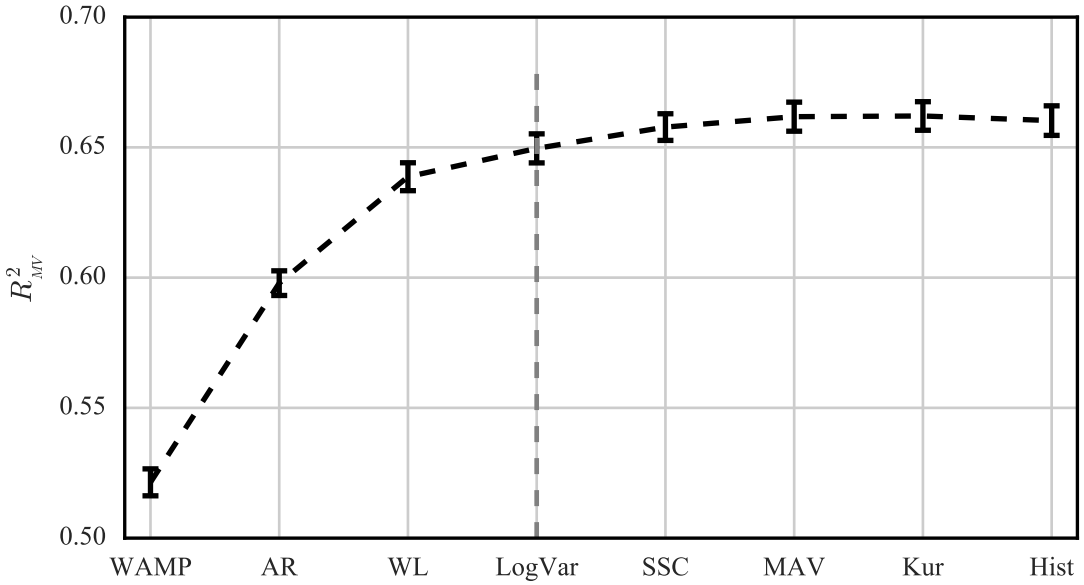

Figure 6.1: Sequential forward feature selection. The average reconstruction accuracy (multivariate R^2, see Section C.2.2.2) across all subjects (60 able-bodied) and CV folds ($k = 6$) using LR is shown as new features are added to the pool. The grey dashed line indicates the last feature to be included in the subset, as inclusion of further features does not yield an average increase in performance greater than 1%. Points, means; error bars, standard error. The reader is referred to Section 2.2.3.1 for feature definitions and abbreviations used.

when the inclusion of any additional feature resulted in a decrease in the overall decoding performance. However, the finally selected subset only included features that yielded an increase in overall performance greater than 1%.

The results of the SFFS analysis are shown in Figure 6.1. Four features were selected, namely Wilson amplitude, auto-regressive coefficients, waveform length, and log-variance. The performance of individual features is reported in Table 6.1 and additionally compared to that of the subset selected with SFFS. Accuracy scores (R^2) are not normally distributed due to being right-bounded only (see Section C.2.2.1); therefore, median accuracies and median absolute deviations are reported.

6.2.4 *Filter length*

Next, the effect of filter length M (see Section 6.2.2.1) on decoding accuracy was investigated. The size of the sliding window was kept fixed at 128 ms and the increment was set to 50 ms. The results of the analysis are shown in Figure 6.2, where the multivariate R^2 averaged across subjects and CV folds is plotted against the length of the linear filters used for decoding. In general, it can be observed that reconstruction accuracy improved as the length of the linear filters was increased and reached a plateau at approximately 800 ms. As with the precedent SFFS analysis, the filter

Table 6.1: Feature comparison. MAD, median absolute deviation.

	Median R^2_{MV}	MAD
MAV	0.501	0.119
WAMP (θ=50 mV)	0.532	0.112
LogVar	0.510	0.110
WL	0.506	0.117
VAR	0.336	9.681
RMS	0.496	0.126
ZC	0.269	0.089
AR (4^{th}-order)	0.451	0.100
Hist (k = 5)	0.259	0.082
Kur	0.157	0.065
SFFS selection (WAMP, WL, LogVar, AR)	0.663	0.103

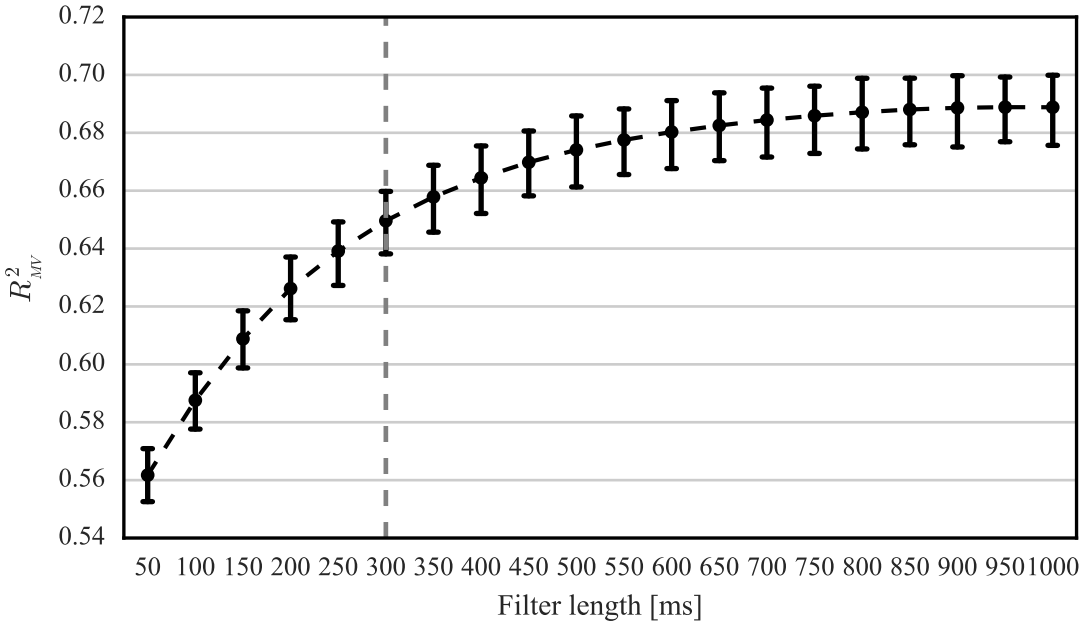

Figure 6.2: Effect of filter length on decoding performance. The average reconstruction accuracy across all subjects (60 able-bodied) and CV folds (k = 6) using LR is plotted against the length of the Wiener filter. The grey dashed line indicates the final selection, as further increase does not yield an average improvement in accuracy greater than 1%. The window increment was set to 50 ms, thus the selected filter length (i.e. 300 ms) corresponds to including M = 6 time lags. Points, means; error bars, 95% confidence intervals estimated via bootstrapping (1000 iterations).

length was chosen such that further increase did not yield an average performance improvement greater than 1%. This corresponded to using M = 6 time lags, which translates into filter lengths of 300 ms.

6.2.5 *Reconstruction accuracy and algorithmic performance comparison*

For the rest of the analyses, the features identified by the SFFS were used and the filter length was set to 300 ms (i.e. $M = 6$). The total number of features extracted from each EMG channel was seven, as the order for the auto-regressive coefficients was set to four. With these settings, the input dimensionality was $D \times M = 504$ (12 channels $\times$ 7 features/channel $\times$ 6 time lags). The output dimensionality was $K = 22$ and $K = 18$ for datasets 1 and 3, respectively, since different data glove models were used to collect the two datasets (see Section 6.2.1).

Typical predictions of joint angle trajectories for MCP and PIP joints with LR and KRR are shown in Figures 6.3 and 6.4, respectively. Overall decoding results for individual DOFs are presented in Table 6.2. A statistical comparison between the two methods was performed using the non-parametric Wilcoxon signed-rank test (Wilcoxon, 1945), which showed that KRR significantly outperformed LR ($p < 0.001$). A summary of the results is provided in Figure 6.5: the median performance difference between the two methods was 0.022 and 0.069, respectively, for exercises B and C; the highest performance achieved in a test fold was R^2=0.89 for LR, and R^2=0.91 for KRR; finally, in both cases the median accuracy for all DOFs was higher than 0.4 (see Table 6.2).

6.3 DISCUSSION

6.3.1 *Relation to previous work*

In this chapter, a systematic investigation was carried out on decoding 22 joint angles from surface EMG data in able-bodied subjects. In agreement with previous work (e.g. Smith et al., 2008; Ngeo, Tamei, and Shibata, 2014a; Xiloyannis et al., 2015), it was verified that it is feasible to reconstruct finger and wrist joint angle trajectories from EMG recordings with decent accuracy. To the best of the author's knowledge, the quality of decoding accuracy achieved for finger joint angles was higher than previously reported. For instance, Smith et al. (2008) decoded kinematics of the five MCP joint angles during unobstructed individuated finger movement and reported a mean correlation coefficient of 0.74 (see Section C.2.2). In the current study, the decoding accuracy of the same parameter for the first exercise was 0.83 and 0.84 for LR and KRR, respectively. Direct comparison to other studies is not straightforward due to differences in electrode placement. For example, many studies have reported high accuracy scores by recording from finger muscles located in the distal part of the forearm close to the wrist (Ngeo, Tamei, and Shibata, 2012; Ngeo et al., 2013; Ngeo,

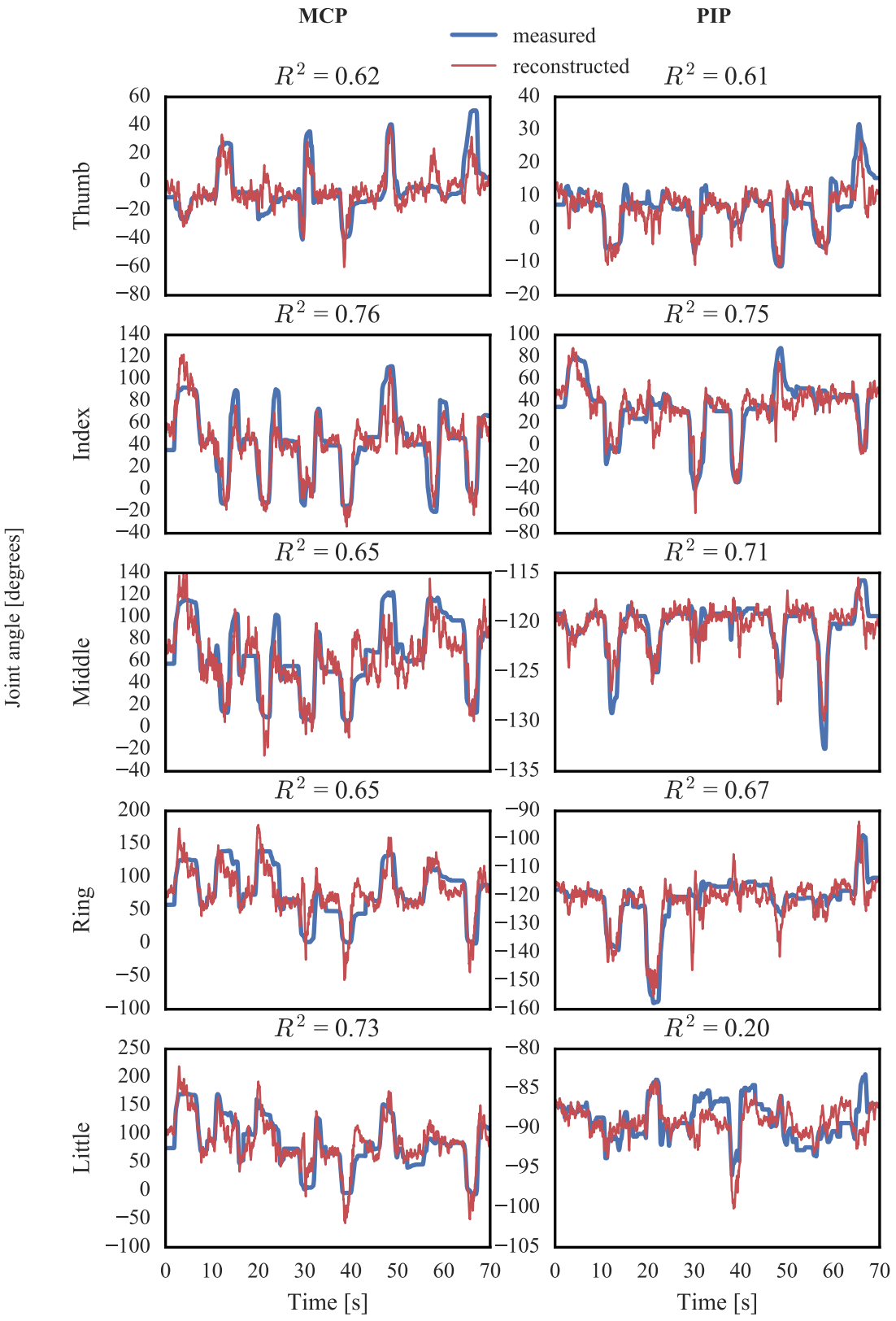

Figure 6.3: Finger joint angle reconstruction example with LR. Measured and reconstructed trajectories of the MCP and PIP joint angles are shown for a single subject. R^2, coefficient of determination (see Section C.2.2).

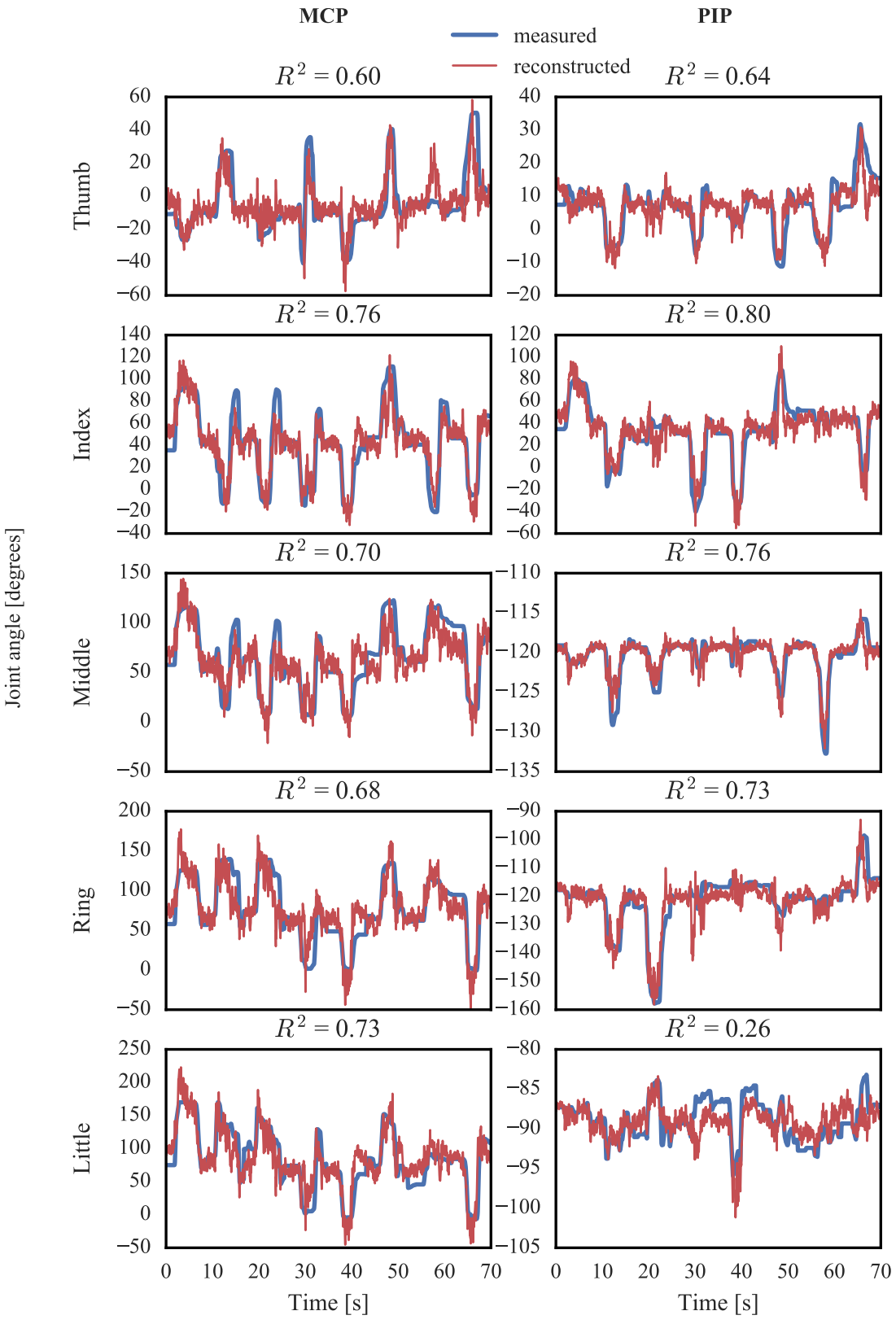

Figure 6.4: Finger joint angle reconstruction example with KRR. Measured and reconstructed trajectories of the MCP and PIP joint angles are shown for the same segment of activity as in Figure 6.3.

Table 6.2: Decoding algorithm performance comparison

	Linear regression		Kernel ridge regression	
	Median R^2	MAD	Median R^2	MAD
Thumb rotation	0.534	0.104	0.590	0.093
Thumb MCP joint	0.460	0.130	0.531	0.122
Thumb PIP joint	0.404	0.136	0.491	0.122
Thumb-index abbduction	0.541	0.105	0.605	0.093
Index MCP joint	0.608	0.152	0.671	0.113
Index PIP joint	0.555	0.149	0.626	0.122
Index DIP joint	0.444	0.169	0.498	0.182
Middle MCP joint	0.649	0.123	0.680	0.100
Middle PIP joint	0.623	0.133	0.662	0.114
Middle DIP joint	0.485	0.180	0.524	0.174
Index-middle abduction	0.697	0.103	0.751	0.082
Ring MCP joint	0.656	0.106	0.681	0.087
Ring PIP joint	0.639	0.129	0.666	0.113
Ring DIP joint	0.561	0.161	0.588	0.150
Middle-ring abduction	0.651	0.109	0.707	0.092
Little MCP joint	0.640	0.104	0.671	0.087
Little PIP joint	0.620	0.150	0.645	0.128
Little DIP joint	0.557	0.231	0.581	0.231
Ring-little abduction	0.587	0.112	0.645	0.101
Palm arch	0.490	0.133	0.559	0.116
Wrist flexion	0.614	0.110	0.660	0.104
Wrist abduction	0.680	0.158	0.708	0.149

Tamei, and Shibata, 2014a; Pan et al., 2013), but in the current study EMG data were not recorded from this area of the forearm, as it is not available in the majority of transradial amputations.

One limitation of previous work has been that joint angle decoding was only studied in the context of unobstructed, contact-free finger motion (e.g. Smith et al., 2008; Ngeo, Tamei, and Shibata, 2014a; Xiloyannis et al., 2015). In comparison, the current study included recordings during grasping of a variety of objects (exercise C, see Figure 3.1). It is worth noting, however, that decoding accuracy was worse in this case as compared to exercise B, which only involved contact-free finger motion (see Figure 6.5).

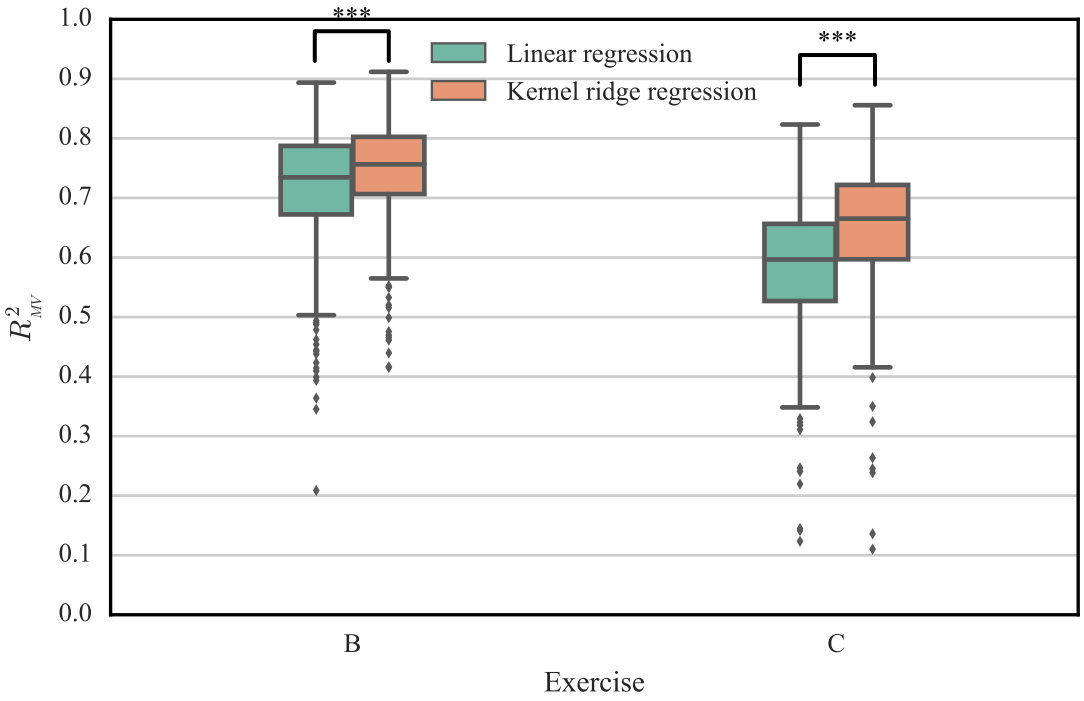

Figure 6.5: Decoding performance comparison of LR and KRR. Data shown for all subjects (60 able-bodied) and CV folds ($k = 6$), separately for the two groups of exercises (see Section 3.2.1 and Figure 3.1). Straight lines, medians; solid boxes, interquartile ranges; whiskers, overall ranges of non-outlier data (1.5 IQR); diamonds, outliers; triple asterisk, $p < 0.001$.

6.3.2 *Feature representation*

A few studies previously compared the decoding performance of EMG features with regards to *classification accuracy* (CA) (e.g. Zardoshti-Kermani et al., 1995; Boostani and Moradi, 2003). However, the selection of features for finger joint angle reconstruction has been either arbitrary or based on classification results. This issue was addressed in the current study in a systematic way by using an SFFS method. The algorithm was tweaked such that it yielded a single subset of features for the whole pool of 60 subjects, but this need not be restrictive; in practice, one could choose those EMG features that yield maximal performance for a specific subject, task, electrode configuration, or any other desired parameter.

6.3.3 *Filter length*

The length of the sliding window was set to 128 ms which is smaller than in previous studies, e.g. 200 ms in Smith et al. (2008) and Pan et al. (2013), and 256 ms in Hioki and Kawasaki (2009). It is well known, however, that a delay exists between the onset of EMG activity and finger tension (Cavanagh and Komi, 1979). To account for this

delay, embedding of muscle activity from previous time bins is required when a short processing window is used. This was verified in the current analysis, where it was found that decoding performance improved on average when the length of the linear filters was increased (see Figure 6.2). Although the average performance reached a plateau at approximately 800 ms, the rate of improvement slowed down for values higher than 300 ms. Taking this observation into account, and to avoid increasing the dimensionality of the input space further, it was decided to use 300 ms filters. This corresponds to including $M = 6$ time bins in the decoders.

6.3.4 *Linear vs. non-linear regression*

A performance comparison between LR and KRR was carried out and it was found that KRR significantly outperformed LR (see Figure 6.5). The median difference in accuracy between the two algorithms was 0.05. Nevertheless, one should keep in mind that the improvement in performance by using non-linear regression comes at the expense of increased computational complexity. The training and testing times for the two algorithms are shown in Figure 6.6. All analyses were performed using MATLAB R2015a (Mathworks, Inc.) on a SL7-operated machine with an eight-core Intel Xeon E5 processor@2.60 GHz and 128 GB of RAM. Both training and testing was significantly slower for KRR ($p < 0.001$, Wilcoxon signed-rank tests) by approximately an order of magnitude. The long testing times for KRR (average 450 ms per fold) could pose a significant challenge to real-time applications. Furthermore, in the context of wrist joint angle decoding, it has been shown that small differences in offline regression accuracy can be compensated by user adaptation during real-time continuous prosthetic control (Jiang et al., 2014b). For the above reasons, it was decided that LR would be a more appropriate algorithm to be used for real-time continuous digit control (see Chapter 8).

6.4 LIMITATIONS AND FUTURE WORK

There are two main limitations with the current study. Firstly, it was limited to able-bodied participants. One of the main challenges in achieving continuous digit control of hand prostheses with amputees is that they cannot provide ground truth kinematic data, a feature that is required for the supervised training of the decoders. One potential way of overcoming this problem is by acquiring training data from the subjects' contralateral hand whilst they perform bilateral mirrored movements. The second limitation is that the analysis presented in this chapter has been purely offline. The importance of validating proposed control schemes with real-time exper-

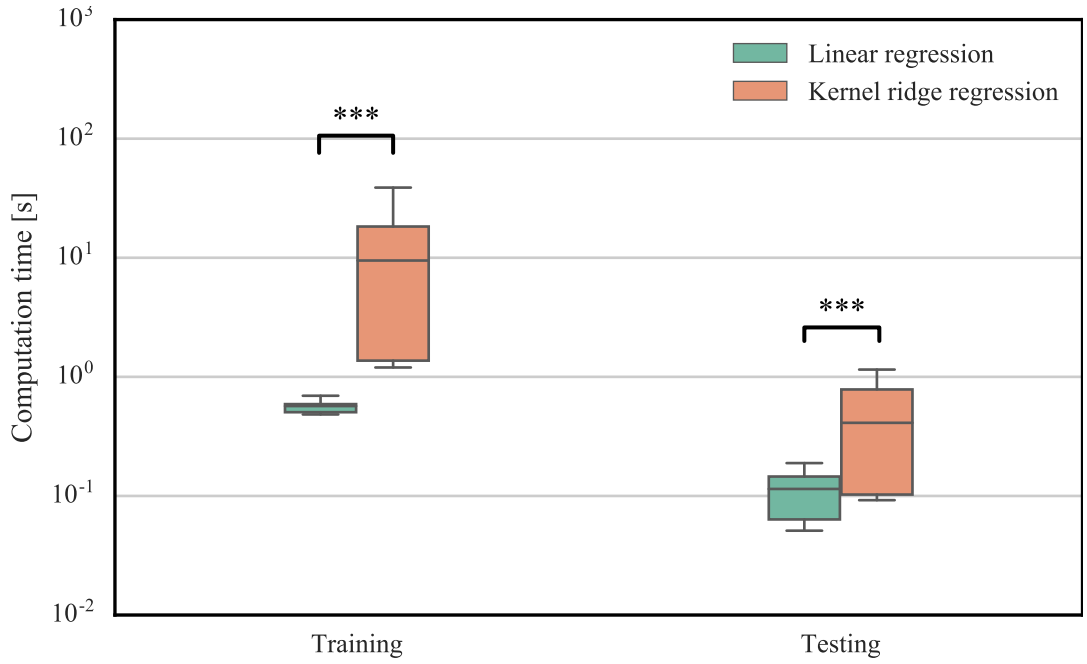

Figure 6.6: Computational complexity with LR and KRR. Training and testing times per CV iteration are shown for all subjects (6o able-bodied) and CV folds (k = 6). Note logarithmic scale on y-axis.

iments has been frequently advocated in the field of myoelectric control (Jiang et al., 2014b; Ortiz-Catalan et al., 2015; Vujaklija et al., 2017) and has been also emphasised throughout this thesis. The above two limitations are properly addressed in Chapter 8. The purpose of the current study was to provide insight into various decoding-related aspects before proceeding with implementing the proposed methodology in real-time and evaluating its potential by carrying out prosthetic control experiments with amputee participants.

As a final note, the decoding strategy proposed in this chapter treats each DOF as a multiple-input-single-output subsystem, that is to say, an independent estimate is produced for each joint. There has been evidence, however, that the activations of the human hand joints exhibit strong correlations (e.g. Santello, Flanders, and Soechting, 1998; Todorov and Ghahramani, 2004). In other words, the intrinsic dimensionality of finger movement might be smaller than the number of decoded DOFs. This issue is addressed in the following chapter, in which a simultaneous input-output dimensionality reduction method is proposed for synergistic joint angle decoding from EMG measurements.

7

SYNERGISTIC DECODING VIA SUPERVISED SIMULTANEOUS INPUT-OUTPUT DIMENSIONALITY REDUCTION

The previous chapter investigated the reconstruction of finger joint angles from surface *electromyographic* (EMG) measurements. In such applications, the dimensionality of the input space is typically large, e.g. in the order of hundreds. This may prove problematic when the amount of available training data is limited. At the same time, the number of accessible *degrees of freedom* (DOFs) in modern prosthetic/robotic hands is currently increasing. As an example, the Shadow Dexterous Hand™ (Shadow, 1998) has 20 actuated DOFs. From a user's perspective, it may not always be necessary to independently control each one of them. Therefore, in many regression-based myoelectric applications it may be desirable to reduce the dimensionality of input and output variables simultaneously.

To generate intentional movement, the human central nervous system has to coordinate a large number of DOFs. How this task is successfully accomplished from a neurological perspective has been a standing question in the field of motor neuroscience for several decades. Based on experimental evidence, it has been speculated that the central nervous system overcomes the complexity of motor control co-ordination by recruiting a specific number of predetermined modules in a synergistic approach. These modules are often called *muscle synergies* (Lee, 1984) and a plethora of computational methods (Tresch, Cheung, and D'Avella, 2006) have been used to extract them from muscular activity data both in humans (e.g. D'Avella et al., 2006; D'Avella et al., 2008) and other vertebrate species (e.g. Tresch, Saltiel, and Bizzi, 1999; D'Avella and Tresch, 2001; Brochier et al., 2004; Overduin et al., 2008).

With regards to grasping and manipulation, despite significant progress in the field of robotics, the human hand still remains the "*nature's most versatile and dexterous end-effector*" (Liarokapis et al., 2016). The great dexterity of the human hand is largely due to the high dimensionality of hand movement. A total of 31 muscles, 19 joints, and 18 tendons are involved, thus providing the human hand with at least 25 DOFs (Duinen and Gandevia, 2011). Similar to the muscle synergy hypothesis, it has been speculated that the activations of human hand joints exhibit strong correlation structure. In other words, there may exist low-dimensional manifolds that explain a large fraction of the hand movement variability observed in the high-dimensional joint space. Such patterns of co-activation have been called *postural synergies* (Santello, Flanders, and

Soechting, 1998) and their properties have been extensively investigated over the last two decades (e.g. Mason, Gomez, and Ebner, 2001; Todorov and Ghahramani, 2004; Todorov and Jordan, 2002; Weiss and Flanders, 2004; Vinjamuri et al., 2007; Vinjamuri et al., 2010).

Recently, there has been a considerable effort in exploiting the principles related to muscle and postural synergies for the purposes of myoelectric control (e.g. Jiang, Englehart, and Parker, 2009; Matrone et al., 2010; Segil and Weir, 2013; Kent, Karnati, and Engeberg, 2014; Konnaris, Thomik, and Faisal, 2016) and prosthetic/robotic hand design (Konnaris, Thomik, and Faisal, 2016; Catalano et al., 2014). However, the large majority of studies on synergy-based myoelectric control have used unsupervised methods for transforming muscular and/or hand kinematic data before supervised methods are deployed to decode a target variable. In supervised learning paradigms, such as proportional myoelectric applications, it might be more sensible to perform dimensionality reduction in a supervised fashion, that is, by ensuring that most of the output predictive power is retained under the transformation.

This chapter proposes a supervised method for simultaneous input-output linear dimensionality reduction with application to continuous decoding of finger joint angles from EMG data. It is shown that methods seeking to identify projections that minimise output reconstruction error are more efficient than unsupervised approaches, such as *principal component analysis* (PCA), when a small number of projection directions is used. The proposed methodology has the potential to be applied in proportional myoelectric control paradigms with high-dimensional input and output variables.

7.1 MUSCLE SYNERGY HYPOTHESIS AND EVIDENCE

7.1.1 *Muscle synergies in vertebrate species*

The idea of co-ordinated muscle activation for movement control dates back to 1947 (Sherrington, 1947), but it has only been quantitatively investigated in the last 30 years. The term "*neuromotor synergy*" was first used by Lee (1984) where it was defined as "*a set of muscles which act together to produce a desired effect*". Bizzi, Mussa-Ivaldi, and Giszter (1991) later proposed a model mechanism based on a coarse map of motor outputs from which vectorial combinations are derived, thereby generating motor behaviour.

Tresch, Saltiel, and Bizzi (1999) proposed the use of a non-negative linear decomposition method to extract synergies from muscle activation patterns in frogs during stimulation of the animals' hindlimbs. They found that these synergies could explain

some of the responses and, perhaps more interestingly, some of the synergies were shared across different animals of the same species.

D'Avella and Tresch (2001) developed an algorithm based on *non-negative matrix factorisation* (NMF) for extracting time-varying muscle synergies. The same algorithm was later used to expand previous work on studying muscle activation patterns in frogs (Tresch, Saltiel, and Bizzi, 1999). In a seminal follow-up study (D'Avella, Saltiel, and Bizzi, 2003), muscle synergies consisted of temporal patterns of co-ordinated muscle activation that could be combined to generate movement by amplitude scaling and time shifting. Only three muscle synergies were found to account for 80% of the variability of 13 recorded muscles, and it was also observed that some of the synergies were shared across different types of behaviour.

By following a slightly different approach based on PCA, Brochier et al. (2004) used EMG recordings from primates executing a grasping task in order to classify grasped objects. By recording EMG activity from 10 to 12 digit, hand, and arm muscles they showed that only three *principal component*s (PCs) could account for 81% of the variability of the entire dataset. Additionally, the authors used the same three PCs to classify the grasped objects and an average *classification accuracy* (CA) of 90% was reported.

D'Avella and Bizzi (2005) compared synchronous (i.e. time-invariant) and time-varying muscle synergies extracted from 13 hindlimb muscles of freely behaving frogs during different types of behaviour such as jump, walk, and swim. Their results provided evidence that three synergies were shared across all types of behaviour, but task-specific synergies were also identified.

Flanders and Herrmann (1992) suggested that the EMG signal might be decomposed into two basic components: the tonic waveform, which corresponds to the force element required to counteract gravity and hold the arm in a specific posture, and the phasic waveform, which corresponds to the component related to movement. D'Avella et al. (2006) recorded the activity of 19 shoulder and arm muscles in humans during fast-reaching movements. By removing the tonic component, they showed that time-varying synergies were able to reconstruct patterns of muscle activity, even when the experimental conditions, such as mechanical load and arm trajectory, were different to the ones present during the training period. Remarkably, high similarities between synergies from different subjects were observed. The same group later suggested a method for simultaneously extracting synchronous tonic and time-varying phasic synergies and found that the synergy coefficients were tuned to direction and speed of movement with a single or a double cosine function (D'Avella et al., 2008). Later, they provided evidence that phasic muscle synergies extracted during point-

to-point movements could generalise to target change movements induced by online target correction (D'Avella, Portone, and Lacquaniti, 2011).

Overduin et al. (2008) used intramuscular EMG electrodes to record the activity of 15 to 19 forelimb muscles of two rhesus macaques as the animals grasped and transported 25 objects of variable shape and size. It was shown that synergy coefficients were modulated by object shape and size, while synergies were found to be conserved between animals. Additionally, synergies extracted from a small subset of the objects could generalise to the entire dataset including all objects used in the experiments.

Ajiboye and Weir (2009) provided evidence that synchronous muscle synergies extracted from 11 hand muscles could form a predictive framework of EMG activity for American sign language gestures. Muscle synergies were extracted from a subset of postures and later used to reconstruct EMG activity for unseen gestures. It was observed that a subset of the extracted synergies were subject-specific while others were shared across subjects, although the latter were dominated by one muscle.

Muceli et al. (2010) studied whether a synergistic framework could account for the variability in muscle activity patterns during a multijoint reaching task. By recording EMG data from elbow and shoulder muscles of eight healthy subjects they provided evidence that a large set of multijoint movements can be generated by a synergy matrix of limited dimensionality, provided that the synergies are extracted from a large number of directions. In their study, a variation of the NMF algorithm was used, namely non-negative reconstruction, which estimates the activation matrix by keeping the component (i.e. synergy) matrix fixed.

Roh, Rymer, and Beer (2012) examined whether muscle synergies could account for the variability in human muscle activity during isometric force generation. They found that four time-invariant synergies could account for 95% of the variance of 8 elbow and shoulder muscles. Notably, these synergies were conserved across subjects, biomechanical task conditions, and experimental protocols, such as various load levels and hand positions in the *three-dimensional* (3D) workspace of the arm.

Finally, a study by Castellini and Smagt (2013) investigated the presence of muscle synergies during human grasping. Muscle activity was recorded with five surface EMG electrodes while six able-bodied subjects performed five different grasp types. Muscle synergies were extracted via PCA and it was shown that they could be used to classify grip types.

7.1.2 *Evidence for synergistic muscle encoding in the cortex*

A small number of studies have sought neural evidence of muscle synergistic encoding in the motor cortical areas. Holdefer and Miller (2002) found evidence that the

discharge of neurons in the primary motor cortex is more correlated with groups rather than with individual muscles, hence suggesting that movement might be encoded in motor cortical areas in a synergistic fashion.

Additionally, Yakovenko, Krouchev, and Drew (2011) simultaneously recorded the firing activity of pyramidal track neurons and muscle activity from contralateral forelimbs of three cats while the animals performed a reaching task. By extracting muscle synergies from the group of recorded muscles, they provided evidence that groups of pyramidal neurons were activated sequentially and coincidentally with each synergy. The authors suggested that the sequential activation of pyramidal neurons might be associated with the activation and modulation of synergistic modules.

Finally, Overduin et al. (2015) recorded forelimb muscular and primary motor cortex spiking activity in rhesus macaques during object reaching and grasping. The authors extracted spatio-temporal synergies using NMF and identified similarities in the characteristics of synergy recruitment in the two domains, including their dimensionality, timing, and amplitude modulation.

7.1.3 *Controversy over muscle synergy hypothesis*

The muscle synergy hypothesis has been somewhat controversial; indeed, a few studies have provided evidence against the hypothesis. Kutch et al. (2008) examined the characteristics of fingertip force generation and found evidence for independent recruitment of muscles. Similar findings were also independently reported by Valero-Cuevas, Venkadesan, and Todorov (2009).

Tresch and Jarc (2009) reviewed the relevant literature and proposed an alternative hypothesis suggesting that statistics of the musculoskeletal system and the external world may affect the structure and control strategy of motor systems; in other words, the observed structure in muscle co-activations may be task- and context-dependent. A direct implication of this hypothesis is that patterns of synergistic muscle recruitment may be flexible and adaptive to properties of the performed task and the environment.

7.1.4 *Algorithms for muscle synergy extraction*

Tresch, Cheung, and D'Avella (2006) performed a comparison of muscle synergy extraction methods on both simulated and real-world data. They compared the performance of algorithms such as factor analysis, PCA, *independent component analysis* (ICA), NMF, ICA on the PCA subspace, and probabilistic ICA with non-negativity constraints. For simulated data corrupted with noise, factor analysis and ICA on the

PCA subspace performed best; however, for real EMG data, all algorithms yielded very similar results. It is worth noting that only synchronous, that is, time-invariant synergies were examined in this study.

More recently, Steele, Tresch, and Perreault (2013) showed that the number and identity of recorded muscles can influence the extracted synergies. By using a musculoskeletal model to produce EMG data, they compared the similarity of extracted synergies by means of correlation coefficient for a varying number of included muscles. The authors concluded that the *variance accounted for* metric (see Section C.2.2), which is typically used in this context, might not be appropriate for evaluating muscle synergy decomposition performance for small numbers of included muscles. The authors supported their argument based on the evidence that when a small number of muscles were considered, this metric overestimated reconstruction performance.

Delis et al. (2014) proposed a sample-based non-negative matrix trifactorisation algorithm to develop a muscle synergy framework based on space-by-time decomposition. By extracting concurrent spatial and temporal modules, the algorithm can be seen as a generalisation of time-varying synergies which can also account for synchronous (i.e. time-invariant) synergies. The proposed algorithm was tested on an EMG dataset comprising recordings from 9 human upper-body and arm muscles during arm pointing movements. It was demonstrated that the proposed methodology could provide an accurate low-dimensional, albeit task-relevant, representation of muscle activity patterns.

7.1.5 *Use of muscle synergies for myoelectric control*

In the context of myoelectric control, several attempts have been made to exploit low-dimensional manifolds in the muscle domain to increase decoding performance and improve generalisation. An exhaustive review of this topic is given by Ison and Artemiadis (2014).

Yatsenko, McDonnall, and Guillory (2007) used a PCA variant to decompose muscle contraction activity corresponding to wrist flexion/extension and hand opening/closing during isometric and unconstrained movement. Although they did not use the extracted features to decode a target signal, the authors reported that component activations for the same movements were consistent across trials.

Hargrove et al. (2009) used a variant of supervised PCA to pre-process EMG data prior to feature extraction. By adopting this approach they reported a decrease in classification error for both able-bodied and amputee subjects. Interestingly, pre-processing the data by using standard (i.e. unsupervised) PCA was found to increase classification error.

Artemiadis and Kyriakopoulos (2010) used a framework based on low-dimensional embeddings to control a robotic arm with EMG signals recorded from muscles acting on the shoulder and elbow joints. The dimensionality of both spaces was reduced from three to two by using PCA. Motion decoding was performed on the two-dimensional space and predictions were subsequently projected onto the original 3D kinematic space of the robot.

Jiang, Englehart, and Parker (2009) proposed a generative model for surface EMG and an algorithm based on NMF to estimate joint force functions from EMG signals. The estimates were subsequently used as control signals for decoding the dynamic movement of the three DOFs of the wrist joint. The performance of the algorithm was also evaluated with simulated EMG data. The same group later deployed this algorithm in an online experiment with both amputees and able-bodied participants to achieve goal-directed simultaneous and proportional control of two DOFs of the wrist joint (Jiang et al., 2014a). In another study, the same algorithm was used to evaluate the robustness of the algorithm to the shifting of recorded electrodes (Muceli, Jiang, and Farina, 2014). By using high-density grids of EMG electrodes, synergies were firstly extracted offline during an initial experiment with 10 able-bodied subjects and the extracted synergies were later used for online control of two DOFs of the wrist joint. A similar study was performed by Choi and Kim (2011) who also achieved proportional control of 2-DOF wrist movement by using NMF applied to EMG data.

Berger and D'Avella (2014) derived 4-5 time-varying synergies (D'Avella and Tresch, 2001) from 13 arm muscles that were subsequently used to estimate intended force during a real-time bio-feedback experiment. It was found that to accomplish the task, participants could learn how to modulate the recruitment of these synergies in the same way that they learnt to modulate forces exerted by individual muscles.

Finally, it is worth noting that a few research groups have investigated the emergence of artificial muscle synergies during closed-loop myoelectric control. It has been demonstrated that users can "learn" task-specific muscle synergies (i.e. co-activations) in a variety of tasks, including *two-dimensional* (2D) cursor position control (Nazarpour, Barnard, and Jackson, 2012; Pistohl et al., 2013; Barnes, Dyson, and Nazarpour, 2016; Dyson, Barnes, and Nazarpour, 2017), prosthesis digit position (Pistohl et al., 2013), and high-dimensional robotic arm control (Ison and Artemiadis, 2015; Ison et al., 2016). Notably, it has been found that such synergistic patterns can be learnt even when they are not intuitive from a physiological perspective, for instance, due to requiring the co-activation of antagonist muscles (Nazarpour, Barnard, and Jackson, 2012). These observations are in line with the proposal made by Tresch and Jarc (2009) (see Section 7.1.3).

Research on muscle synergies has been inspired by the hypothesis that the central nervous system co-ordinates movement by recruiting groups of muscles with specific activation profiles and, as a result, muscle activation patterns span only a subspace of the multidimensional muscle space. Recently, a few research groups have addressed similar questions with regards to the postural properties of the human hand. These studies have mainly sought for evidence of low-dimensional representation in the shaping of the human hand. In other words, they have tried to answer the fundamental question of whether hand shaping is coordinated by recruiting groups of specific co-activations, often referred to as *postural synergies*.

Santello, Flanders, and Soechting (1998) used a data glove with 15 sensors to record hand kinematics from five subjects performing imaginary grasps of 57 objects and observed that not all joint angles were controlled independently. By using PCA, they extracted "*eigengrasps*" and found that three PCs could account for 90% of the total variance, while only two PCs could capture 84% of the variance. The first PC corresponded to flexion of the *metacarpophalangeal* (MCP) joints and adduction of the thumb, while the second PC described the extension of MCP joints, flexion of *proximal interphalangeal* (PIP) joints, and adduction of the thumb. These first two PCs were also found to be highly similar across subjects, as opposed to higher-order PCs that were subject-specific. The authors suggested that during grasping the hand shape might be controlled at two levels, with the first three PCs controlling coarse hand shape and the higher-order PCs being responsible for fine-tuning. Mason, Gomez, and Ebner (2001) later expanded this study by addressing the question of whether a small number of postural synergies could describe the whole act of reach-to-grasp. They used singular value decomposition to extract eigengrasps in five subjects performing five different types of grasps of 16 different objects of various sizes. Hand and wrist kinematics were reconstructed in 3D space by using a four-camera video system. The first eigenposture captured 97% of the total variance, while higher-order PCs contributed to the fine-tuning of the thumb and long fingers.

Todorov and Ghahramani (2004) recorded data from six subjects while they performed a range of complex everyday tasks and found that the number of observed postural synergies exceeded the ones previously reported during performance of simpler tasks. Furthermore, the synergies were consistent across subjects, but they were also task-dependent. The authors concluded that the biological origin of dimensionality reduction might be more associated with a task-optimal control policy employed by the central nervous system (Todorov and Jordan, 2002), rather than just emerging from a need for "simplification" of movement.

Weiss and Flanders (2004) recorded EMG activity from seven hand muscles as well as kinematics from 17 joint angles while subjects held their hands statically in 52 grasping and American sign language spelling shapes. By performing PCA in both the joint angle and EMG spaces, they found that three PCs accounted for 80% of the variance in both cases. They subsequently used *multiple linear regression* (MLR) to relate the EMG PCs to hand-shape PCs.

Vinjamuri et al. (2007) used time-varying synergies (D'Avella and Tresch, 2001) to decompose the velocity profiles of MCP and PIP joints of five fingers of the hand while five subjects reached and grasped for 28 different objects. The same group later used a 2-step synergy decomposition method based on singular value decomposition and gradient descent (Vinjamuri et al., 2010). In their implementation, one synergy could be recruited more than once in a single block. The velocity of 10 MCP and PIP joints from 10 subjects was reconstructed during grasp movements and American sign language finger-spelling, although the synergies had been extracted using data only from the first task. Performance in the latter task was decreased and, for that reason, the authors concluded that postural synergies might be task-dependent. On that note, there has been evidence that during highly-complex tasks such as for example, piano playing the movement of individual fingers is mostly independent from one another (Furuya, Flanders, and Soechting, 2011).

Finally, Thomik, Fenske, and Faisal (2015) proposed a method for learning low-dimensional finger kinematic manifolds based on sparse coding (Olshausen and Field, 1996). They recorded bilateral movement from both hands of able-bodied participants during daily life activities by using data gloves. They showed that by learning an over-complete dictionary with sparse coding in the joint velocity space, the same number of components could explain considerably more variance than PCA, which was used as a benchmark for comparison.

7.2.1 *Use of postural synergies in myoelectric control and robotics*

Matrone et al. (2010) used two PCs to control a 16-DOF under-actuated artificial hand that was used to grasp three different objects. The PCs were previously extracted from a dataset comprising joint angle measurements of the DOFs of the hand while it was used to grasp a series of objects of various shapes and sizes. The system was tested in a follow-up study during real-time experiments with twelve able-bodied subjects (Matrone et al., 2012). Participants controlled the activation of the two PCs using two-dimensional wrist movement (flexion/extension and abduction/adduction). Muscle activity was recorded with four EMG electrodes targeting the corresponding wrist muscles.

Segil and Weir (2013) adopted a slightly different approach to control a 15-DOF virtual hand by using only the first two PCs extracted from Santello, Flanders, and Soechting (1998). Four different linear maps were constructed from EMG signals to the PC domain and the joint angles of the virtual hand were subsequently controlled by an inverse PCA transformation. The authors reported promising results, with myoelectric control achieving similar performance to joystick control, which was used as a benchmark.

Kent, Karnati, and Engeberg (2014) used a sinusoidal synergy approach to control the human finger and thumb motions of an artificial hand during unscrewing and screwing of objects. The synergy controller was used to drive four DOFs of the hand and it was shown that it could achieve reduced *completion time*s (CTs) as compared to a range of commercial prosthetic hands.

Recently, postural synergies have been used for the design and control of robotic and prosthetic hands. For instance, Konnaris, Thomik, and Faisal (2016) used four eigenmotions derived by their proposed sparse coding-based approach (Thomik, Fenske, and Faisal, 2015) to control an under-actuated 24-DOF hand driven by only seven servo motors (Konnaris, Thomik, and Faisal, 2016). Catalano et al. (2014) developed a single-motor robotic hand and used the first PC identified in the original study of Santello, Flanders, and Soechting (1998) in combination with a variable stiffness actuation mechanism. The authors demonstrated that despite using a single motor, objects of various shapes and sizes could be grasped by the hand.

7.3 MOTIVATION

The algorithms used for muscle and postural synergy extraction are typically unsupervised (e.g. Santello, Flanders, and Soechting, 1998; Todorov and Ghahramani, 2004; Tresch, Cheung, and D'Avella, 2006). In other words, their objective is to learn a latent representation of the probability distribution of a variable of interest (i.e. muscle activity or hand kinematics). On the other hand, a typical *machine learning* (ML)-based myoelectric application is supervised, since the objective is to classify or decode a target variable (e.g. hand posture, wrist/hand joint angles). In this context, pre-processing the input and/or output data with unsupervised dimensionality reduction algorithms may yield suboptimal results, since the latter are driven by different optimisation criteria (e.g. maximisation of variance retained under linear transformation in the case of PCA).

In the context of myoelectric control, only one study has so far explored ways of identifying low-dimensional manifolds in the joint input-output space (Ngeo et al., 2015). The authors used a modified version of the Gaussian process latent variable

model (Lawrence, 2004; Lawrence, 2005) to learn a dynamical model of the input-output joint probability distribution in a shared latent space (Shon et al., 2006). The advantage of using such a probabilistic model lies in that it makes it possible to sample from the joint distribution and can thus be used to generate artificial hand kinematic data. In a different study, Hoffmann, Schaal, and Vijayakumar (2009) compared local linear dimensionality reduction methods within the context of using locally-weighted regression to reconstruct full human body kinematic data. The authors reported that the highest performance was achieved by methods that optimise the correlation between input projections and target variables, such as *reduced rank regression* (RRR) and *partial least squares* (PLS), as compared to methods that only model input or joint input-output data distribution, such as factor analysis and PCA.

The current chapter proposes a methodology for supervised, simultaneous input-output dimensionality reduction which is based on a generalised eigenvalue problem formulation of linear dimensionality reduction (Borga, Landelius, and Knutsson, 1992). The proposed methodology is presented in Section 7.4. A performance comparison of various linear dimensionality reductions is conducted in Section 7.5 on the task of reconstructing finger joint angle trajectories from EMG signals.

7.4 SUPERVISED INPUT-OUTPUT LINEAR DIMENSIONALITY REDUCTION

7.4.1 *The generalised eigenvalue problem*

Let A denote a Hermitian matrix. The *simple eigenvalue problem* considers finding all vectors $\boldsymbol{v}$ (called the *eigenvectors* of $\mathbf{A}$) and associated scalars λ (called the *eigenvalues* of $\mathbf{A}$), such that:

$$\mathbf{A}\boldsymbol{v} = \lambda\boldsymbol{v}. \tag{7.1}$$

Given two Hermitian matrices $\mathbf{A}$ and $\mathbf{B}$, the *generalised eigenvalue problem* is the problem of finding the vectors $\boldsymbol{v}$ and associated scalars λ, such that:

$$\mathbf{A}\boldsymbol{v} = \lambda\mathbf{B}\boldsymbol{v}. \tag{7.2}$$

The generalised eigenvalue problem described by Equation 7.2 can be transformed into a simple eigenvalue problem by making use of the *Cholesky decomposition* of $\mathbf{B}$:

$$\mathbf{B} = \mathbf{L}\mathbf{L}^*, \tag{7.3}$$

where $\mathbf{L}^*$ denotes the conjugate transpose of $\mathbf{L}$.

Note that the generalised eigenvalue problem of two Hermitian matrices $\mathbf{A}$ and $\mathbf{B}$ is closely related to the generalised Rayleigh quotient, which is defined as:

$$\mathbf{R}(\mathbf{A}, \mathbf{B}, \mathbf{x}) = \frac{\mathbf{x}^* \mathbf{A} \mathbf{x}}{\mathbf{x}^* \mathbf{B} \mathbf{x}}. \tag{7.4}$$

7.4.2 *A generalised eigenvalue problem formulation of dimensionality reduction*

Let $\mathbf{X} \in \mathbb{R}^{N \times D}$ denote a design (i.e. feature) matrix, where N and D are the number of observations and input variables, respectively, and $\mathbf{Y} \in \mathbb{R}^{N \times K}$ denote the target matrix, where K is the output dimensionality. We denote $\mathbf{C}_{xx}$ the input covariance matrix and $\mathbf{C}_{xy}$ the input-output covariance matrix. By definition, $\mathbf{C}_{xy} = \mathbf{C}_{yx}^\top$.

Borga, Landelius, and Knutsson (1992) introduced a unifying approach to the formulation of several linear dimensionality reduction methods, including PCA, PLS, MLR, and *canonical correlation analysis* (CCA) based on the generalised eigenvalue problem (see Equation 7.2). The square matrices $\mathbf{A}$ and $\mathbf{B}$ corresponding to the four cases can be derived from their respective objective functions (i.e. optimisation criteria) and are shown in Table 7.1. Given a single random variable $\mathbf{x}$, PCA aims to find directions of maximum variance. Given two random variables $\mathbf{x}$ and $\mathbf{y}$, PLS looks for directions of maximum data covariation, whereas CCA seeks directions of maximum correlation. Finally, given an input variable $\mathbf{x}$ and an output variable $\mathbf{y}$, MLR aims to find directions that minimise the reconstruction squared error of $\mathbf{y}$ given $\mathbf{x}$.

In all four cases, matrices $\mathbf{A}$ and $\mathbf{B}$ are symmetric, and $\mathbf{B}$ is also positive-definite, as a block diagonal matrix whose diagonal elements are all positive-definite matrices; therefore, all its eigenvalues are guaranteed to be positive. $\mathbf{A}$ is hollow symmetric, that is, a symmetric matrix with zero diagonal elements. A basic property of hollow symmetric matrices is that their eigenvalues are real and come in positive/negative pairs. In other words, the sum of the eigenvalues of a hollow symmetric matrix is equal to zero. Only in the case of PCA, $\mathbf{A}$ is also positive-definite, and as such, it has only positive eigenvalues.

By extending the work of Borga, Landelius, and Knutsson (1992), the following approach is proposed for simultaneous input-output dimensionality reduction with PLS, CCA or MLR; firstly, we solve the generalised eigenvalue problem described by Equation 7.2 by using the Cholesky decompositions of $\mathbf{C}_{xx}$ and $\mathbf{C}_{yy}$. Then, we order the eigenvalues in descending order and organise the normalised eigenvectors (i.e. unit vectors) in a matrix $\mathbf{W}$ column-wise:

$$\mathbf{W} = [\mathbf{w}_1, \ldots, \mathbf{w}_{D+K}] \in \mathbb{R}^{(D+K) \times (D+K)}. \tag{7.5}$$

Table 7.1: Dimensionality reduction via generalised eigenvalue problem (Borga, Landelius, and Knutsson, 1992)

	$\mathbf{A}$	$\mathbf{B}$
PCA	$\mathbf{C}_{xx}$	$\mathbf{I}$
PLS	$\begin{bmatrix} 0 & \mathbf{C}_{xy} \\ \mathbf{C}_{yx} & 0 \end{bmatrix}$	$\begin{bmatrix} \mathbf{I} & 0 \\ 0 & \mathbf{I} \end{bmatrix}$
CCA	$\begin{bmatrix} 0 & \mathbf{C}_{xy} \\ \mathbf{C}_{yx} & 0 \end{bmatrix}$	$\begin{bmatrix} \mathbf{C}_{xx} & 0 \\ 0 & \mathbf{C}_{yy} \end{bmatrix}$
MLR	$\begin{bmatrix} 0 & \mathbf{C}_{xy} \\ \mathbf{C}_{yx} & 0 \end{bmatrix}$	$\begin{bmatrix} \mathbf{C}_{xx} & 0 \\ 0 & \mathbf{I} \end{bmatrix}$

Note that in the general case, the columns of $\boldsymbol{W}$ are not orthogonal to each other.

The cumulative sum of the positive eigenvalues is computed and the largest L eigenvalues are chosen, such that:

$$\sum_{i=1}^{L} \lambda_i^+ \geqslant \alpha \sum_{i=1}^{(D+K)/2} \lambda_i^+, \tag{7.6}$$

where λ_i^+ are the positive eigenvalues of Equation 7.2, $D + K$ is the joint input-output dimensionality, and α is a threshold on the cumulative eigenvalue sum that it is wished to be retained by the low-rank approximation. The input is then transformed as follows:

$$\mathbf{X}' = \mathbf{X}\boldsymbol{W}_{1:D,1:L}, \tag{7.7}$$

where $\boldsymbol{W}_{1:D,1:L} \in \mathbb{R}^{D \times L}$ is the matrix consisting of the first D rows and L columns of $\boldsymbol{W}$. The output is accordingly transformed as:

$$\mathbf{Y}' = \mathbf{Y}\boldsymbol{W}_{D+1:D+K,1:L}, \tag{7.8}$$

where $\boldsymbol{W}_{D+1:D+K,1:L} \in \mathbb{R}^{K \times L}$. This procedure is summarised in Algorithm 1.

Algorithm 1 Supervised input-output linear dimensionality reduction (PLS, CCA, MLR) via generalised eigenvalue problem

Require: $\mathbf{A}$, $\mathbf{B}$ (see Table 7.1), α

1: Compute Cholesky decompositions of $\mathbf{C}_{xx}$ and $\mathbf{C}_{yy}$:
$\mathbf{L}_x \leftarrow \text{chol}(\mathbf{C}_{xx})$,
$\mathbf{L}_y \leftarrow \text{chol}(\mathbf{C}_{yy})$.
2: Use $\mathbf{L}_x$, $\mathbf{L}_y$ to solve Equation 7.2:
$\boldsymbol{A}\boldsymbol{v} = \lambda \boldsymbol{B}\boldsymbol{v}$.
3: Order eigenvalues and eigenvectors in eigenvalue descending order:
$\boldsymbol{\lambda}' = [\lambda_1, \lambda_2, \ldots, \lambda_{D+K}]$, $\lambda_1 > \lambda_2 > \ldots > \lambda_{D+K}$,
$\boldsymbol{W} \leftarrow [\boldsymbol{w}_1, \ldots, \boldsymbol{w}_{D+K}]$.
4: Normalize columns of $\boldsymbol{W}$.
5: Choose L, such that:
$\sum_{i=1}^{L} \lambda_i^+ \geqslant \alpha \sum_{i=1}^{(D+K)/2} \lambda_i^+$.
6: Project data:
$\mathbf{X}' \leftarrow \mathbf{X}\boldsymbol{W}_{1:D,1:L}$,
$\mathbf{Y}' \leftarrow \mathbf{Y}\boldsymbol{W}_{D+1:D+K,1:L}$.

Algorithm 2 Unsupervised input-output linear dimensionality reduction (PCA) via generalised eigenvalue problem

Require: $\mathbf{C}_{xx}$, $\mathbf{C}_{yy}$, α

1: Compute Cholesky decompositions of $\mathbf{C}_{xx}$ and $\mathbf{C}_{yy}$:
$\mathbf{L}_x \leftarrow \text{chol}(\mathbf{C}_{xx})$,
$\mathbf{L}_y \leftarrow \text{chol}(\mathbf{C}_{yy})$.
2: Use $\mathbf{L}_x$, $\mathbf{L}_y$ to solve Equation 7.2:
$\mathbf{C}_{xx}\boldsymbol{v}_x = \lambda_x \boldsymbol{v}_x$,
$\mathbf{C}_{yy}\boldsymbol{v}_y = \lambda_y \boldsymbol{v}_y$.
3: Order eigenvalues and eigenvectors in eigenvalue descending order:
$\boldsymbol{\lambda}'_x = \left[\lambda_1^{(x)}, \lambda_2^{(x)}, \ldots, \lambda_D^{(x)}\right]$, $\lambda_1^{(x)} > \lambda_2^{(x)} > \ldots > \lambda_D^{(x)}$,
$\boldsymbol{\lambda}'_y = \left[\lambda_1^{(y)}, \lambda_2^{(y)}, \ldots, \lambda_K^{(y)}\right]$, $\lambda_1^{(y)} > \lambda_2^{(y)} > \ldots > \lambda_K^{(y)}$,
$\boldsymbol{W}^{(x)} \leftarrow \left[\boldsymbol{w}_1^{(x)}, \ldots, \boldsymbol{w}_D^{(x)}\right]$,
$\boldsymbol{W}^{(y)} \leftarrow \left[\boldsymbol{w}_1^{(y)}, \ldots, \boldsymbol{w}_K^{(y)}\right]$.
4: Normalize columns of $\boldsymbol{W}^{(x)}$, $\boldsymbol{W}^{(y)}$.
5: Choose L_x, L_y, such that:
$\sum_{i=1}^{L_x} \lambda_i^{(x)} \geqslant \alpha \sum_{i=1}^{D} \lambda_i^{(x)}$,
$\sum_{i=1}^{L_y} \lambda_i^{(y)} \geqslant \alpha \sum_{i=1}^{K} \lambda_i^{(y)}$.
6: Project data:
$\mathbf{X}' \leftarrow \mathbf{X}\boldsymbol{W}^{(x)}_{:,1:L_x}$,
$\mathbf{X}' \leftarrow \mathbf{X}\boldsymbol{W}^{(y)}_{:,1:L_y}$.

In the case of simultaneous input-output dimensionality reduction with PCA, the procedure described above is followed for the input and output variables independently, except that Equation 7.6 now takes the form:

$$\sum_{i=1}^{L_x} \lambda_i^{(x)} \geqslant \alpha \sum_{i=1}^{D} \lambda_i, \tag{7.9}$$

and

$$\sum_{i=1}^{L_y} \lambda_i^{(y)} \geqslant \alpha \sum_{i=1}^{K} \lambda_i, \tag{7.10}$$

where $\left[\lambda_1^{(x)}, \lambda_2^{(x)}, \ldots, \lambda_D^{(x)}\right]$ and $\left[\lambda_1^{(y)}, \lambda_2^{(y)}, \ldots, \lambda_K^{(y)}\right]$ are the eigenvalues of $\mathbf{C}_{xx}$ and $\mathbf{C}_{yy}$, respectively, sorted in descending order. Input-output dimensionality reduction with PCA is summarised in Algorithm 2.

7.5 APPLICATION TO MYOELECTRIC DATA

In this section, an investigation on the performance of the four methods introduced in Section 7.4 is carried out. The comparison of the four dimensionality reduction algorithms is performed in the context of joint angle reconstruction from surface EMG signals (see Chapter 6). The linear regression method introduced in Section 6.2.2.1 without dimensionality reduction, which will be hereafter referred to as *full rank regression* (FRR), is used as a benchmark. The term RRR is used to describe the same algorithm after MLR-based dimensionality reduction has been applied (see Section 7.4).

7.5.1 *Datasets and methodology*

The same datasets that were used in Chapter 6 were considered (i.e. datasets 1 and 3 in Table 4.1). The features selected by the *sequential forward feature selection* (SFFS) procedure introduced in the previous chapter, namely Wilson amplitude, 4^{th}-order auto-regressive coefficients, waveform length, and log-variance were used (see Section 6.2.3 and Figure 6.1). For performance assessment, 6-fold *cross-validation* (CV) was used (see Section 3.2.5).

Following dimensionality reduction with any of the four methods introduced in the previous section (i.e. PCA, PLS, CCA, MLR), regression was performed by using LR (i.e. Wiener filter, see Section 6.2.2.1)) in the latent, that is, low-dimensional space. The regularisation parameter for the Wiener filter was set *a priori* to $\lambda = 10^{-5}$ and

the number of time lags used for decoding was set to $M = 6$ (see Section 6.2.4); thus, the input dimensionality was $DM = 504$ (12 channels $\times$ 7 features/channel $\times$ 6 time lags). The output dimensionality was $K = 22$ for dataset 1 (22-DOF data glove) and $K = 18$ for dataset 3 (18-DOF data glove).

7.5.2 *Statistical tests*

No prior assumptions were made about the distribution of *coefficient of determination* (R^2) scores; therefore, the non-parametric Friedman test (Friedman, 1937) was used to compare reconstruction accuracy scores between the different algorithms. Post-hoc pair-wise comparisons were performed using the Wilcoxon signed-rank test (Wilcoxon, 1945) with Šidák correction for multiple comparisons (Šidák, 1967).

7.5.3 *Results*

A systematic analysis on reconstructing finger joint angles from EMG data was performed by applying the four dimensionality reductions methods introduced in Section 7.4 followed by LR. The results of this analysis are presented in Figure 7.1. The highest performance scores were achieved by CCA and RRR, followed by input-output PCA. The worst performance was observed for PLS. Interestingly, the performance obtained with CCA and RRR was marginally higher than with FRR, that is, when no dimensionality reduction was applied. One-to-one comparisons between FRR-RRR and PCA-RRR are shown in Figure 7.2.

The bottom panel of Figure 7.1 shows the average intrinsic dimensionality estimated and used by each of the four dimensionality reduction methods. For PLS, CCA and RRR, the intrinsic dimensionality was estimated from Equation 7.6 by choosing $\alpha = 0.99$. For input-output PCA, the dimensionality was estimated independently for the input and output variables using Equations 7.9 and 7.10, respectively, and again setting $\alpha = 0.99$. Although the smallest number of components was used by PLS, its performance was significantly worse than that of the other methods ($p < 0.001$). Among the three methods that achieved comparable accuracy (i.e. CCA, RRR and FRR), RRR used the smallest number of components (average $L = 18$).

As a next step, the performance of the four linear dimensionality reduction methods was compared whilst the number of used projection directions was varied from 1 to 50. It was hypothesised that the RRR optimisation criterion, that is, minimisation of output reconstruction squared error given the input would allow the specific method to perform best when using a small number of components. The results of this analysis are presented in Figure 7.3. As was to be expected, the performance of RRR was

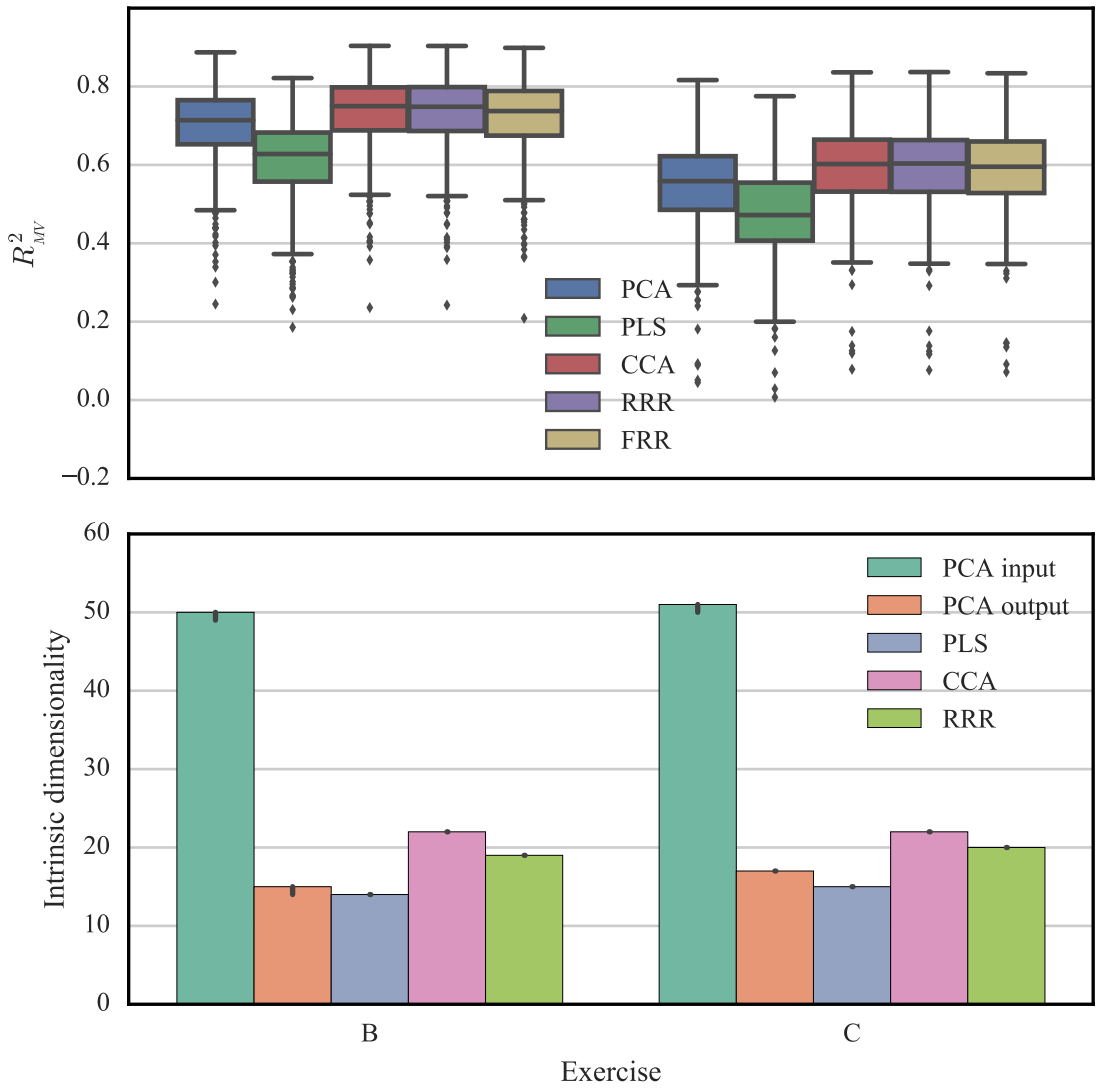

Figure 7.1: Comparison of input-output linear dimensionality reduction methods. (Top panel) reconstruction accuracy (multivariate R^2, see Section C.2.2.2) of different simultaneous input-output linear dimensionality reduction methods followed by LR. Results shown separately for two groups of exercises (see Section 3.2.1 and Figure 3.1). Straight lines, medians; solid boxes, interquartile ranges; whiskers, overall ranges of non-outlier data (1.5 IQR); diamonds, outliers. (Bottom panel) intrinsic dimensionality estimated and used by each dimensionality reduction method ($\alpha = 0.99$, see Equations 7.6, 7.9 and 7.10). For PCA, intrinsic dimensionality estimation was performed independently in the input and output domains. Original input dimensionality, $DM = 504$; output dimensionality, $K = 18$ for dataset 1, and $K = 22$ for dataset 3 (see main text). Bars, medians; error bars, 95% confidence intervals estimated via bootstrapping (1000 iterations).

superior to that of CCA, PLS, and input-output PCA by a large margin when only a few projections were used (i.e. less than 15). Remarkably, it was found that RRR could achieve benchmark accuracy, that is, similar to FRR by using only nine input and output projection directions. The same number was 22 for CA, whereas for PLS

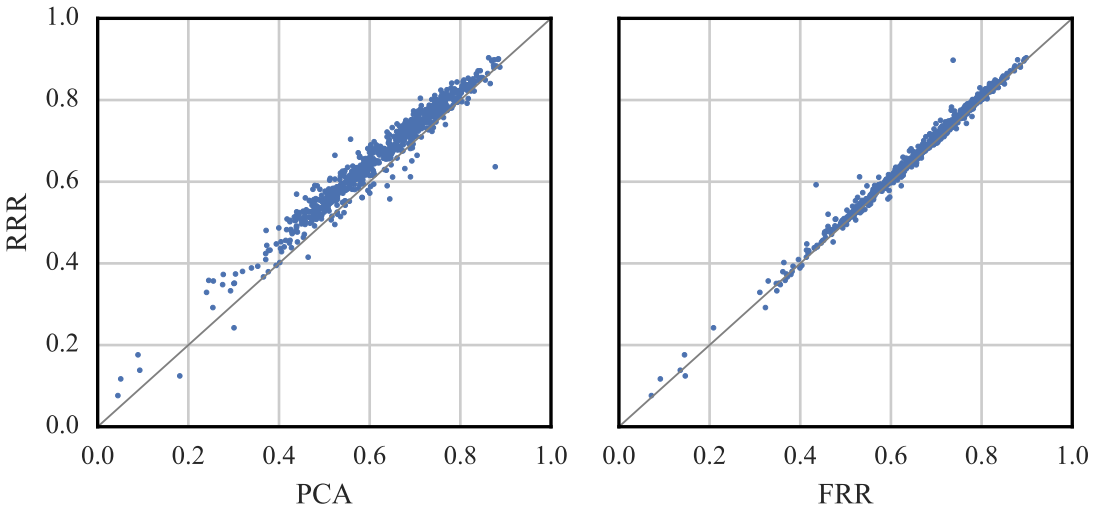

Figure 7.2: One-to-one comparisons of linear dimensionality reduction methods. Results shown for all datasets, subjects, and folds. Each dot in the scatter plots corresponds to one testing fold. Number of folds, $n_f = 720$.

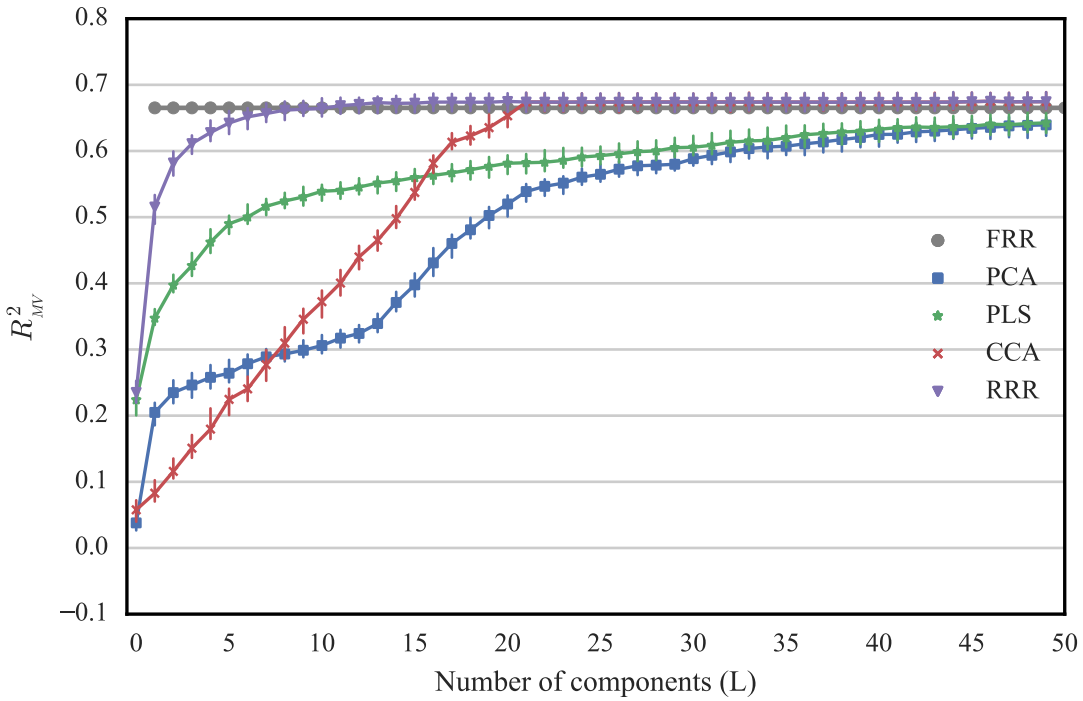

Figure 7.3: Comparison of input-output linear dimensionality reduction methods for a varying number of projection directions. Average performance of the four linear input-output dimensionality reduction methods is plotted against the number of used components. The average benchmark performance, that is, without dimensionality reduction is shown in grey (FRR). Points, medians; error bars, 95% confidence intervals estimated via bootstrapping (1000 iterations).

and input-output PCA, 50 projections were not sufficient to approximate benchmark accuracy.

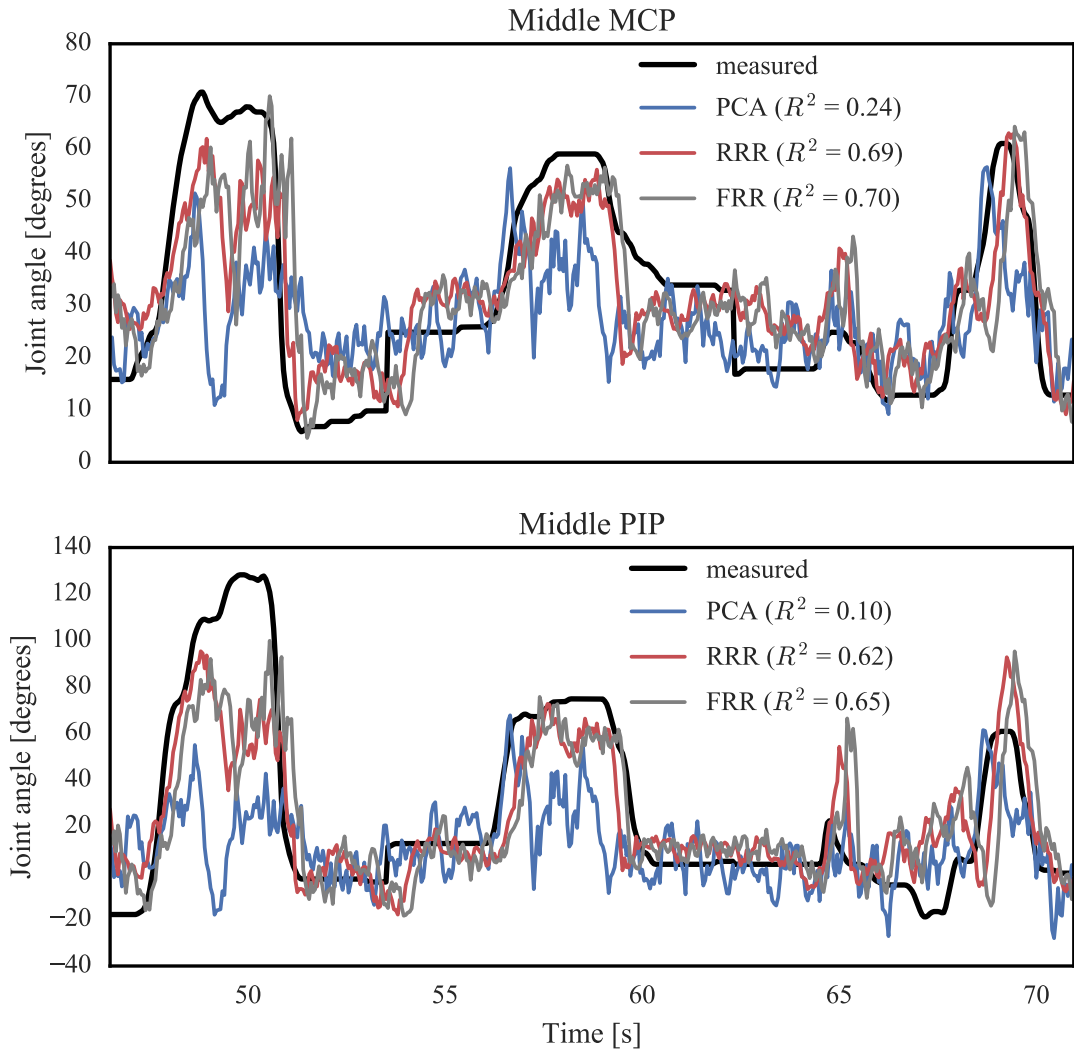

Figure 7.4: Joint angle reconstruction examples with dimensionality reduction. Predictions of the trajectories of the middle MCP and PIP joints are shown for one subject with input-output PCA, RRR, and FRR. For PCA and RRR, L = 10 projection directions (i.e. components) were used.

Typical predictions of middle MCP and PIP joint angle trajectories with FRR, RRR, and input-output PCA are shown in Figure 7.4. For this example, the number of components used by RRR and input-output PCA was set to L = 10. It can be observed from the graph that the accuracy achieved with RRR by using only 10 input and 10 output projections was comparable to the control case, that is, when no dimensionality reduction was applied. Conversely, when using input-output PCA with an equal number of components, the reconstruction accuracy for the same joint angle was considerably worse.

7.6 DISCUSSION

7.6.1 *Application*

The current study investigated and compared the performance of various linear dimensionality reduction methods within the context of finger joint angle reconstruction from surface EMG data. The proposed MLR-based methodology for supervised simultaneous input-output dimensionality reduction has the potential to be applied to continuous digit control of prosthetic hands with a large number of DOFs (e.g. Shadow Dexterous Hand™ (Shadow, 1998)). Depending upon the specifics of the desired application, independent activation of each DOF may not be necessary and could potentially increase the cognitive load for the user. It is likely that the control of multi-DOF hands may be facilitated by a synergistic approach, although this remains to be verified with psychophysical experiments.

7.6.2 *Supervised vs. unsupervised dimensionality reduction*

Previous attempts to capture synergistic activations in the muscle and finger kinematic domains almost exclusively used unsupervised methods (see Sections 7.1 and 7.2). The study presented in this chapter follows a different approach; rather than seeking physiological evidence for low-dimensional manifolds that capture a large fraction of movement variance in high-dimensional space, it looks for projection directions that are optimal with respect to a regression-based decoding task. Although little effort has been previously made to achieve simultaneous input-output dimensionality reduction, at least two studies have proposed reducing the dimensionality of the two domains independently in an unsupervised fashion (Weiss and Flanders, 2004; Artemiadis and Kyriakopoulos, 2010). This approach, however, can produce highly suboptimal results, since the output predictive power captured by the input variables may lie within non-maximal variance directions; thus, information relevant to the decoding of the target variable of interest may be discarded during the dimensionality reduction step.

In contrast, a supervised approach is proposed here for simultaneous input-output dimensionality reduction. The method is based on the general eigenvalue problem formulation of MLR and is closely related to RRR (Velu and Reinsel, 2013). Given that the MLR objective function (i.e. optimisation criterion) is to minimise the output reconstruction squared error given the input, this algorithm is guaranteed to find projection directions that retain as much of the output predictive power as possible. The theoretical advantage of RRR over input-output PCA was verified with offline exper-

iments. It was found that the performance attained by RRR with only nine input and output projection directions was comparable to that of FRR (see Figure 7.3). On some occasions, RRR even outperformed FRR (see Figure 7.2). This may be attributed to the extra level of regularisation applied by RRR due to the low rank of the regression model fitted. Conversely, input-output PCA performed worse than FRR, even when 50 input projection directions were used and no dimensionality reduction was applied to the output variable (see Figure 7.3). This finding provides further support to the argument that input variance discarded by PCA-based dimensionality reduction may convey useful information about the target variable.

The results of the current analysis are mostly in accordance with findings of a previous study (Hoffmann, Schaal, and Vijayakumar, 2009) that investigated local linear dimensionality reduction for non-parametric regression applied to full-body kinematic data. One notable difference is that it in the current study, PLS achieved inferior performance to RRR, as compared to the work of Hoffmann, Schaal, and Vijayakumar, in which the performance of the two methods was comparable. This discrepancy might be due to differences in implementation of the algorithm.

7.6.3 *On the origins of correlations*

The observed correlation structure in the input (i.e. muscle) domain might be only partially attributed to physiological synergistic muscle activation patterns. One should keep in mind that muscular activity is typically recorded from multiple neighbouring sites on the skin surface, which produces signal crosstalk (Farina et al., 2014). Moreover, multiple features are extracted from the same EMG sensors, a process that unavoidably introduces correlations between the input variables. The latter aspect is further intensified by the use of an overlapping sliding window approach (see Section 2.2.3) and inclusion of input features from previous time steps (i.e. time delay embedding, see Section 6.2.4). These factors do not, however, apply to the output domain, that is, hand kinematic signals recorded with data gloves; therefore, it may be argued that the observed correlation structure in the output domain may indeed be primarily attributed to synergistic finger motion (i.e. postural synergies).

7.6.4 *Limitations and future work*

In an effort to keep computational complexity to a low level, which is essential for real-time implementations, linear dimensionality reduction methods were only considered in the current study. Non-linear algorithms may, however, provide better decoding results, thanks to their potential to capture non-linear relationship between

the observed and latent spaces. As an example, non-linear dimensionality reduction could be achieved by using a neural network with a single hidden layer of size that is smaller than the dimensionality of the input and output variables. A different approach could be based on the use of autoencoders both in the input and output domains. An autoencoder is a specific type of neural network that reduces the dimensionality of an input variable via defining an objective function based on the reconstruction error of the variable itself from the latent space (i.e. hidden layers of the network). The reconstruction error is then minimised via standard backpropagation and gradient-based optimisation techniques (Hinton and Salakhutdinov, 2006).

For each of the algorithms used in the current analysis, the intrinsic dimensionality was estimated from Equations 7.6, 7.9 and 7.10 by selecting $\alpha = 0.99$. Although choosing to retain 99% of the cumulative sum of the positive eigenvalues may appear sensible, this threshold was set somewhat arbitrarily. To select the threshold in a principled way, knowledge about the noise variance in the system may be required which is usually unavailable. An alternative solution would be to select the number of projection directions in a data-driven fashion, for example, by validating performance on a held-out subset of the data or via cross-validation.

Finally, it is worth noting that previous studies have found evidence that muscle and postural synergies may be conserved across different subjects (e.g. Santello, Flanders, and Soechting, 1998; Todorov and Ghahramani, 2004; Ajiboye and Weir, 2009; Roh, Rymer, and Beer, 2012). Investigating the generalisation of low-dimensional input-output relationships across different subjects may provide further insight into the physiology of human hand movement and principles of motor control, and is thus regarded as a promising avenue for future research.

8

REAL-TIME FINGER POSITION PROPORTIONAL CONTROL WITH SURFACE ELECTROMYOGRAPHY

The previous two chapters demonstrated the feasibility of reconstructing finger joint angle trajectories from muscular activity data recorded on the skin surface of able-bodied subjects. However, all analyses presented so far have been purely offline. Previous work on proportional control of the wrist joint has found evidence that accuracy results obtained with offline analyses may not always correlate with metrics quantifying the performance of real-time, goal-oriented prosthetic control (Jiang et al., 2014b). Such discrepancies have been partially attributed to user adaptation mechanisms taking place in the latter case, as a result of placing the human in the control loop (Nazarpour, Barnard, and Jackson, 2012; Hahne, Markovic, and Farina, 2017). Thus, it is imperative to validate the efficacy of the finger position control scheme proposed in the previous chapters with real-time prosthetic control experiments.

A particular challenge related to deploying proportional finger control for amputee subjects is the need for collecting ground truth kinematic data, which is required for the supervised training of the decoders. One potential way of overcoming this issue is by instructing users to perform bilateral mirrored movements, although this strategy can only be used in the case of unilateral amputation. Moreover, this procedure introduces noise to the system due to potential inconsistencies between the movement performed by the healthy hand and the one imagined by the phantom limb, which might negatively affect decoding accuracy. The level of this influence has not been previously investigated and, therefore, is not yet clearly understood.

The main advantage of proportional over classification-based control is the potential to generalise to a continuous space of movement. Although a few previous studies have implemented and tested continuous finger position control in real-time, the same motions were used in most cases for training and testing the performance of the decoders; therefore, the generalisation ability of the control scheme has yet to be assessed. Furthermore, previous studies were limited to contact-free movements. In other words, the capability of using this approach to perform functional movements, such as object grasping, has not been previously demonstrated.

The current chapter addresses the challenges outlined above by assessing the efficacy of continuous finger position control during real-time experiments involving both able-bodied and amputee participants. Two different experimental protocols are

tested. In the first experiment, participants are presented with various target postures and are required to modulate their muscular activity to control five *degrees of actuation* (DOAs) of a prosthetic hand in order to match the desired postures as closely as possible. In the second experiment, participants are instructed to use their muscular activity to control the prosthetic hand to grasp, relocate, and release a series of objects, as in the classification-based experiments presented in Chapters 3 and 5. Analysing the outcomes of these two experiments provides insight into the learning mechanisms taking place during individual finger prosthetic control, as well as the feasibility of deploying the proposed paradigm in clinical applications.

8.1 INTRODUCTION

8.1.1 *Proportional wrist control*

Several research groups have achieved real-time proportional myoelectric control of multiple *degrees of freedom* (DOFs) of the wrist. Jiang et al. (2014a) used an algorithm based on *non-negative matrix factorisation* (NMF) (Jiang, Englehart, and Parker, 2009) to control a virtual target on a screen. The study included both able-bodied and upper-limb amputees and no significant differences in performance were observed between the two groups. Importantly, the proposed algorithm was semi-supervised, that is, it only required an initial calibration phase without the need for collecting labelled data. Of particular interest is another study from the same authors (Jiang et al., 2014b) that compared the offline and real-time performance of linear and non-linear algorithms (i.e. *linear regression* (LR), *multi-layer perceptron* (MLP), and NMF). It was shown that while there were significant differences in the offline decoding accuracy of the three algorithms, their real-time performance assessed with task-related metrics (i.e. *completion rate* (CR), *completion time* (CT), throughput, speed, overshoot, and efficiency) was comparable. Furthermore, no correlation was found between offline accuracy and real-time control metrics. It was thus concluded that user adaptation induced by the continuous provision of visual feedback can compensate for decoding inaccuracies during real-time proportional myoelectric control. In the same direction, Hahne, Markovic, and Farina (2017) compared the effect of introducing a varying level of white noise to *electromyographic* (EMG) recordings on both offline decoding accuracy and real-time proportional wrist control performance. It was found that the effect was significantly lower in the latter case, suggesting that subjects are able to modulate their control strategy to compensate for decoding errors. Furthermore, it was shown that the decline in performance due to the introduced disturbances was larger in the case of classification-based than with proportional control. Based on

this finding, the authors concluded that *"regression allows for a better user correction of control commands than classification"*.

Additionally, Ameri et al. (2014a) provided a proof of principle for using MLPs to reconstruct 3-DOF wrist movement (flexion/extension, abduction/adduction, and pronation/supination) in able-bodied subjects. Participants were instructed to perform bilateral mirrored movements during the training data collection phase. A follow-up study (Ameri et al., 2014b), which also included transradial amputee participants, compared the real-time performance of artificial neural network and support vector regression and reported significantly better results for the latter method. To evaluate performance, the two studies used the target achievement control and a Fitts' law test (see Section 2.5.4), respectively.

Finally, it is worth noting that intramuscular recordings with fine-wire EMG electrodes have also been used to decode 3-DOF movement of the wrist. Smith, Kuiken, and Hargrove (2014) demonstrated that regression-based decoding outperformed sequential classification-based control in a Fitts' law test. A follow-up study (Smith, Kuiken, and Hargrove, 2015) proposed to use the outputs of three-class motion classifiers, one per DOF (i.e. no movement, or movement in either direction), to weight the predictions of LR decoders. It was reported that this strategy resulted in a significant increase in performance both for able-bodied and amputee subjects. In these two studies, each DOF was controlled by a single pair of agonist/antagonist muscles (i.e. *one-to-one mapping*). More recently, it was proposed to train LR models receiving input from all pairs of recorded muscles (Smith, Kuiken, and Hargrove, 2016). It was found that this method achieved higher performance during simultaneous activation of multiple DOFs; however, for single-DOF motions, the former method based on a one-to-one mapping between muscle pairs and DOFs performed better.

8.1.2 *Proportional finger position control*

A smaller number of studies have attempted to address the challenge of achieving real-time continuous finger position control. Smith et al. (2009) recorded hand kinematics and surface EMG activity from the ipsilateral limb of two able-bodied subjects. A mapping between muscular activity and the position of four fingers (thumb, index, middle, and ring) was created by using an MLP. In the evaluation phase, the subjects modulated their muscle activity to control the flexion of individual fingers of a virtual hand in a target reaching task.

Ngeo et al. (2013) used a previously proposed method (Ngeo, Tamei, and Shibata, 2012) to control the flexion of the index finger of an exoskeleton. One able-bodied participant was recruited and training data (EMG and finger kinematics) were recorded

from the same limb. An MLP was used to decode the *metacarpophalangeal* (MCP), *proximal interphalangeal* (PIP), and *distal interphalangeal* (DIP) joint angles of the index finger and predictions were translated into control commands for the exoskeleton.

Cipriani et al. (2011) recruited five able-bodied and an equal number of transradial amputee subjects and instructed them to perform bilateral mirrored movements that included both individuated finger and synergistic motions. In the evaluation phase, in which participants were asked to repeat the same motions as the ones used during training, muscle activity was used to decode the joint angle of six DOFs (flexion of all fingers and thumb abduction) using *K-nearest neighbours* (k-NN) regression. The joint angle predictions were subsequently mapped into discrete classes of movement and performance was evaluated by means of *classification accuracy* (CA), CRs and CTs.

By using a slightly different approach, Pistohl et al. (2013) recorded the activity of intrinsic hand muscles and built non-intuitive one-to-one mappings between the normalised activation of each muscle and an associated DOA of a prosthetic hand. Despite the lack of intuitiveness of the deployed control scheme, it was shown that users can rather rapidly adapt their strategy and learn novel muscle control schemes to achieve dexterous prosthetic control.

As with proportional wrist control studies (Smith, Kuiken, and Hargrove, 2014; Smith, Kuiken, and Hargrove, 2015; Smith, Kuiken, and Hargrove, 2016), the use of intramuscular EMG recordings has been proposed as a potential means of achieving proportional finger position control. Intramuscular recordings offer the advantage of low level of muscle cross-talk (Birdwell et al., 2013). Hence, it is possible to create multiple one-to-one mappings between specific muscles and prostheses DOAs. This idea has been explored in the context of controlling both virtual (Birdwell et al., 2015) as well as prosthetic (Cipriani et al., 2014a) hands.

8.1.3 *Proportional finger force control*

Proportional finger force control has received much less attention than wrist and finger position control. Gijsberts et al. (2014b) proposed a non-linear incremental learning method based on ridge regression and random Fourier features to control the fingertip forces of the Touch Bionics i-Limb™ hand (Touch Bionics, Inc., 2003). In a follow-up study, Patel, Nowak, and Castellini (2017) trained multiple context-specific regression models to improve the performance of the algorithm. Celadon et al. (2016) compared the reconstruction accuracy of different regression methods during tasks that combined various force profiles and levels, as well as rates of change of force. More recently, Gailey, Artemiadis, and Santello (2017) combined real-time hand pos-

ture recognition and digit force control using support vector machine classification and random forest regression, respectively.

8.1.4 *Motivation*

Although a few previous studies have evaluated the efficacy of proportional finger position control from surface EMG recordings (see Section 8.1.2), several important aspects are yet to be investigated. For example, despite deploying a proportional finger control paradigm, Cipriani et al. (2011) used the exact same postures for training and testing; therefore, the generalisation ability of the control scheme to novel postures was not assessed. This aspect is of great significance, since it ranks among the main motivations for choosing proportional finger position control over classification-based methods. Moreover, the experimental design did not include any functional tasks, for example, using the prosthetic hand to grasp objects; therefore, it is not clear whether the proposed control scheme could enable users to perform activities of daily living.

Another important aspect related to the control of intuitive myoelectric interfaces is user adaptation and, as a consequence, performance improvement over time. Although Pistohl et al. (2013) investigated this feature, their interface was non-intuitive and not based on *machine learning* (ML). In other words, an arbitrary mapping was created from the muscle space to the DOAs of the prosthetic hand and the users had to learn that mapping from experience. For that reason, the learning curves reported in their study might not be representative of the case where a subject-specific, intuitive mapping is created by using initial training data from the same user.

The goal of the work presented in this chapter is twofold: 1) investigate and evaluate the efficacy of continuous finger position prosthetic control from surface EMG data, including generalisation to novel postures and functional tasks; and 2) investigate the effect of user adaptation during intuitive, multidimensional, proportional finger position control.

8.2 EXPERIMENTAL SETUP AND METHODOLOGY

8.2.1 *Participant recruitment*

Ten able-bodied (nine male, one female; all right-hand dominant; median age, 26.5 years) and two right-hand transradial amputee subjects were recruited. Some of the able-bodied and both amputee participants had taken part in previous myoelectric

control experiments (see Sections 3.3 and 5.2). The medical records of the two amputee participants have been previously reported in Table 3.1.

8.2.2 *Signal acquisition*

For the able-bodied group, 16 Delsys® Trigno™ sensors (see Section A.1.1 and Figure A.1) were placed on the participants' right forearm arranged in two rows of eight equally spaced sensors each (see Figure 5.1, top row). For the two amputee participants, 13 and 12 sensors were used, respectively, due to limited space availability on their phantom limb. Prior to sensor placement, the participants' skin was cleansed using 70% isopropyl alcohol. Elastic bandage was used to secure the sensor positions throughout the experimental sessions. Following sensor placement, the quality of all EMG channels was verified by visual inspection. The sampling frequency of EMG data was set to 2 kHz. Data from the *inertial measurement unit*s (IMUs) incorporated in the sensors were also recorded at 128 Hz sampling frequency, but were not used for model training or real-time control.

A 18-DOF CyberGlove II data glove (see Section A.3.1) was used to record hand kinematic data from the participants' left hand. For each participant, the glove was calibrated prior to data collection using dedicated software provided by the manufacturer. The sampling rate of glove data was set to 100 Hz.

8.2.3 *Training data collection*

The participants sat comfortably on an office chair and were asked to reproduce a series of motions instructed to them on a computer monitor. Nine exercises were selected for training data collection, which included both individuated-finger and full-hand motions (see Figure 8.1). The following nine motions were included: thumb flexion, thumb abduction, index flexion, middle flexion, ring/little flexion, index pointer, cylindrical grip, lateral grip, and tripod grip. Participants were asked to perform bilateral mirrored movements with both their arms resting on a table.

Three datasets (i.e. separate blocks of trials) were recorded for each participant: the first two (datasets *A* and *B*) comprised 10 repetitions of each motion, and the third one (dataset *C*), only two. The three datasets served, respectively, the following purposes: A, *training*; B, *validation*; C, *testing* (see Section 8.2.5).

Each motion execution lasted approximately 7 s and at the end of each trial subjects were instructed to go back to the rest pose which corresponded to muscle relaxation (shown in Figure 8.1(a)). Succeeding trials were interleaved with intervals of 3 s and participants were also given a 10 min break after the completion of each block.

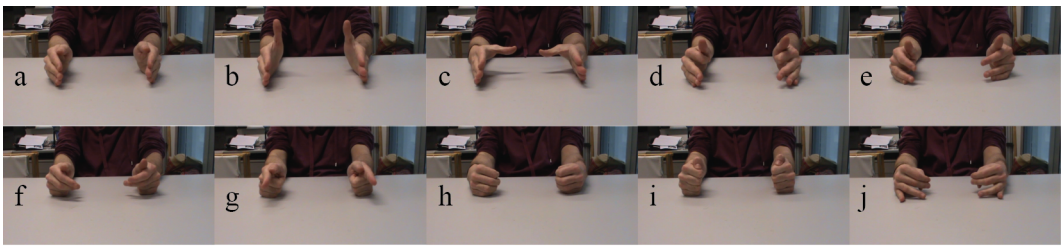

Figure 8.1: Training exercises. Subjects were instructed to perform bilateral mirrored movements. (a) rest; (b) thumb flexion; (c) thumb abduction; (d) index flexion; (e) middle flexion; (f) ring/little flexion; (g) index pointer; (h) cylindrical grip; (i) lateral grip; (j) tripod grip.

8.2.4 *Signal pre-processing*

As with previous experiments (e.g. see Section 5.2.4), a sliding window approach was used. The length of the window was set to 128 ms with an increment of 50 ms (60% overlap). Based on the results of the offline analysis presented in Chapter 6 (see Section 6.2.3 and Figure 6.1), the following features were extracted from the recorded EMG channels: Wilson amplitude, 4^{th}-order auto-regressive coefficients, waveform length, log-variance, and slope sign change. The columns of the design (i.e. feature) matrices were subsequently standardised by mean subtraction and unit variance scaling. Feature means and variances were estimated using training data only.

For hand kinematic data recorded with the data glove, the mean value within the processing window was computed for each DOF individually. The Prensilia IH2 Azzurra hand (see Section A.2.2) was used during the real-time control experiments. The calibrated glove measurements were converted into digit positions for the prosthetic hand using a linear mapping (see Section A.3.1.1). The columns of the target matrices were finally normalised in the range $[0, 1]$, where $y_j = 0$ corresponds to full extension and $y_j = 1$ to full flexion, respectively, of the j^{th} DOA.

8.2.5 *Model training, prediction post-processing, and hyper-parameter optimisation*

It was shown in Chapter 6 that *kernel ridge regression* (KRR) can slightly outperform LR in the task of reconstructing finger joint angles from EMG data (see Figure 6.5). However, this comes at the additional cost of increased computational complexity (see Figure 6.6). Given the small margin of performance improvement with non-linear regression and, at the same time, the considerable increase in computational requirements, it was decided that between the two considered methods LR was the most appropriate choice for real-time implementation. Thus, the regularised Wiener filter method (see Section 6.2.2.1) was used to decode finger positions from muscle activity.

The length of the linear filters was set to $M = 6$ (see Section 6.2.4). Given that the output dimensionality was in this case small (i.e. $K = 5$), no dimensionality reduction was performed.

To ensure smooth digit trajectories, predictions were post-processed using exponential smoothing. This is a form of infinite impulse response filtering, implemented in the time-domain as follows:

$$\tilde{y}_j[n] = \alpha \cdot y_j[n] + (1 - \alpha) \cdot \tilde{y}_j[n-1], \tag{8.1}$$

where $y_j[n]$ and $\tilde{y}_j[n]$ denote, respectively, the raw and smoothed predictions of the j^{th} DOA at time step n, and α is the *smoothing parameter*, which is constrained by $0 \leqslant \alpha \leqslant 1$. Smaller values of α result in "stronger" smoothing, but also increase the prediction response latency. An example of applying the post-processing smoothing step to the time-series prediction of a single DOA is illustrated in Figure 8.2 for two different settings of the smoothing parameter α.

Three types of model selection (i.e. hyper-parameter tuning) were performed for each participant during the training phase: sensor selection, regularisation, and smoothing parameter optimisation. Models were initially trained using data from the training set only. Model selection was carried out by means of maximising performance (i.e. multivariate R^2, see Section C.2.2.2) on the validation set. Following parameter optimisation, the training and validation sets were merged and used to train final models. The test set was only used to evaluate the offline performance of the final models.

For sensor selection, the standard *sequential forward sensor selection* (SFSS) method was used (see Section 3.2.6). The algorithm terminated execution when the inclusion of any remaining sensor caused a decrease in average performance. To optimise the regularisation parameter λ of the Wiener filter (see Equation 6.11), a search was performed in the log-space $\{10^{-6}, 10^{-5}, \ldots, 10^{1}\}$ using a factor (i.e. multiplicative step) of 10. The exponential smoothing parameter α (see Equation 8.1) was optimised via linear search in the range $[0, \ldots, 1]$ with a step size of 0.01. The three model selection steps were performed sequentially in the following order: sensor selection, λ optimisation, and α optimisation. In other words, the subset of sensors was firstly identified; using the selected subset, the regularisation parameter λ was tuned; finally, using the selected sensor subset and chosen value for λ, the smoothing parameter α was optimised. An example of the three sensor selection steps is illustrated in Figure 8.3 for an able-bodied participant.

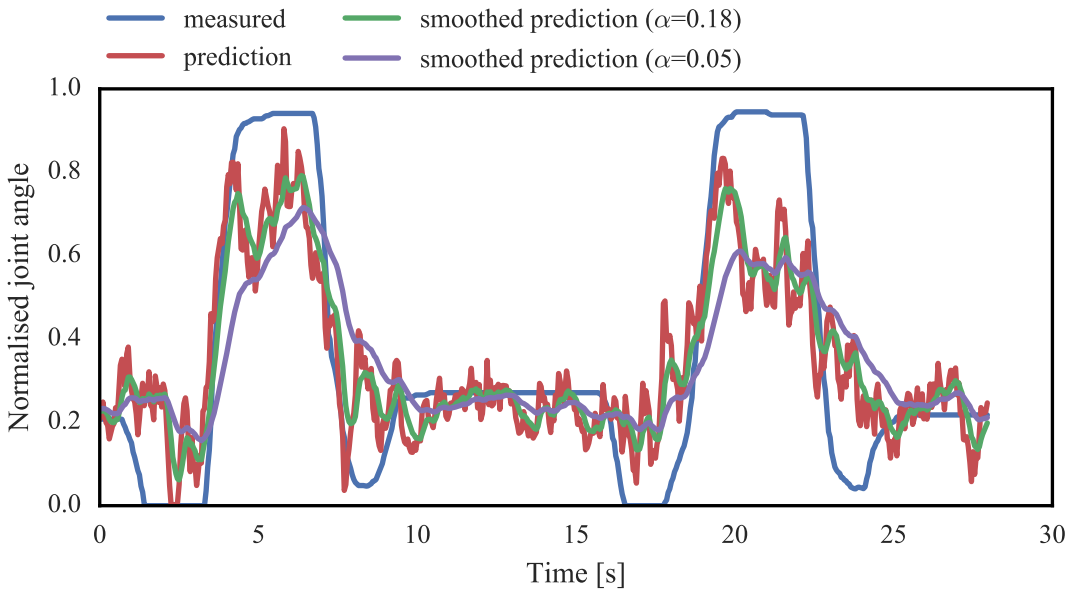

Figure 8.2: Exponential smoothing example. The post-processing exponential smoothing step is demonstrated on a segment of activity of the index finger for an able-bodied subject. The exponential smoothing parameter for the specific subject was set to $\alpha = 0.18$. The smoothed prediction time series is shown for an additional setting of $\alpha = 0.05$ (i.e. stronger smoothing effect).

8.2.6 *Behavioural tasks and evaluation*

Two experimental tasks were designed to evaluate the efficacy of real-time finger position control: a biofeedback *posture matching* task and a prosthetic control *pick and place* task, which was similar to the one previously described in Chapters 3 and 5. For both tasks, two modes of control were used: in *EMG control mode*, participants were required to modulate their muscle activity to control the prosthetic hand; in *glove control mode*, participants teleoperated the hand using the CyberGlove II data glove. The glove control mode was used in both tasks to provide an estimate of the upper-bound of prosthetic control performance (i.e. *benchmark*).

All subjects took part in the posture matching task. Upon completion, they were given a 10 min break. A screening trial was then carried out to assess whether participants were able to accomplish a full trial in the pick and place task with EMG control. When the screening trial was successful, participants moved on to performing the task. This was the case for only six out of ten able-bodied participants. The remaining four able-bodied and both amputee subjects did not accomplish the screening trial and, thus, did not perform the pick and place task.

The two experimental tasks are introduced in the following sections.

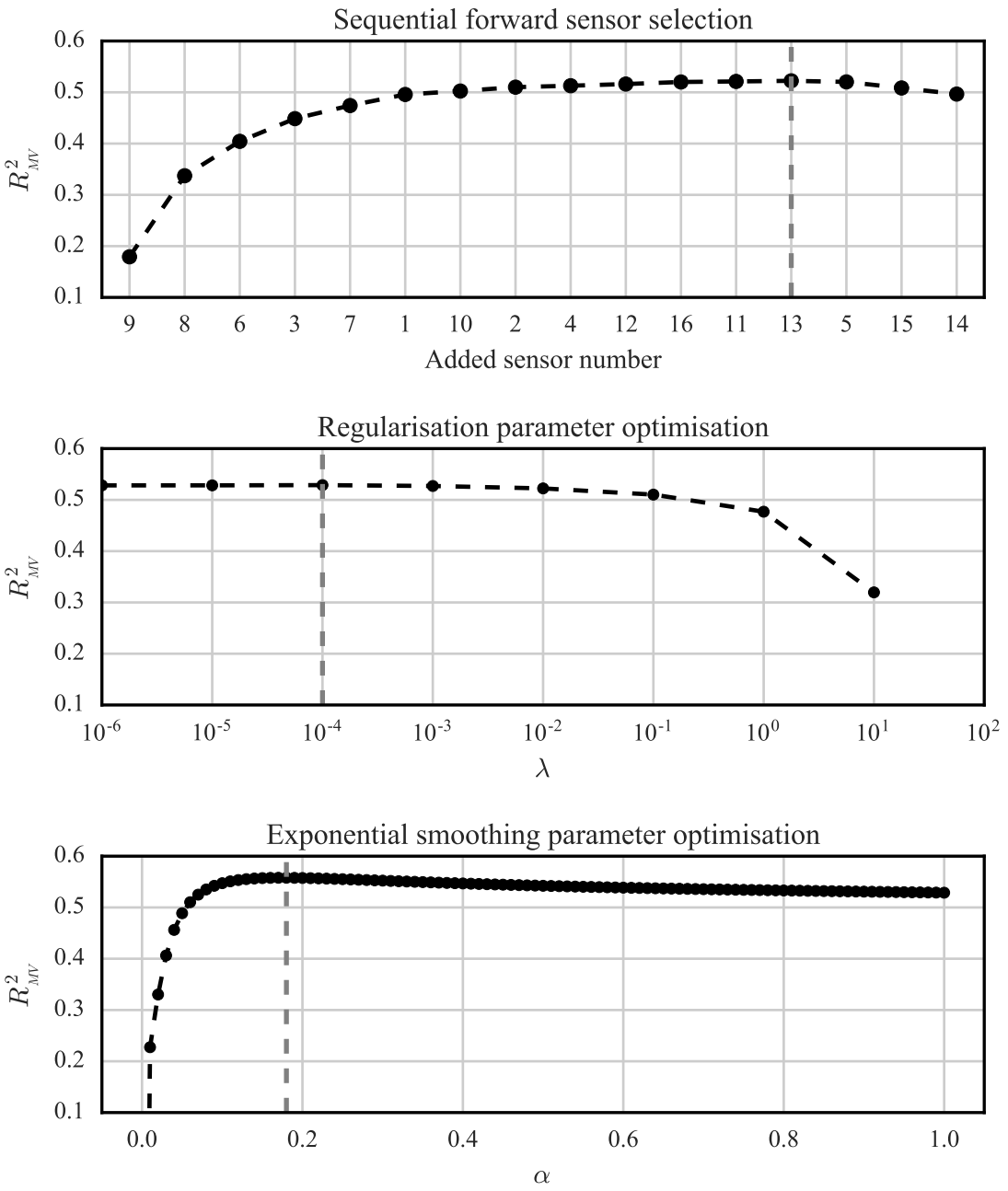

Figure 8.3: Model selection and hyper-parameter tuning. An example of the three sequential model selection steps (i.e. sensor subset selection, regularisation parameter optimisation, and exponential smoothing parameter optimisation) is shown for an able-bodied subject. R^2_{MV}, multivariate coefficient of determination score (see Section C.2.2.2) on the validation set. Dashed lines indicate final parameter selections.

8.2.6.1 *Task 1: posture matching*

During the posture matching task, participants were presented with a series of target postures on a computer screen and were instructed to control the prosthetic hand to match the desired postures as closely as possible. All participants performed the task in both EMG and glove control modes. The presentation order of the two modes was

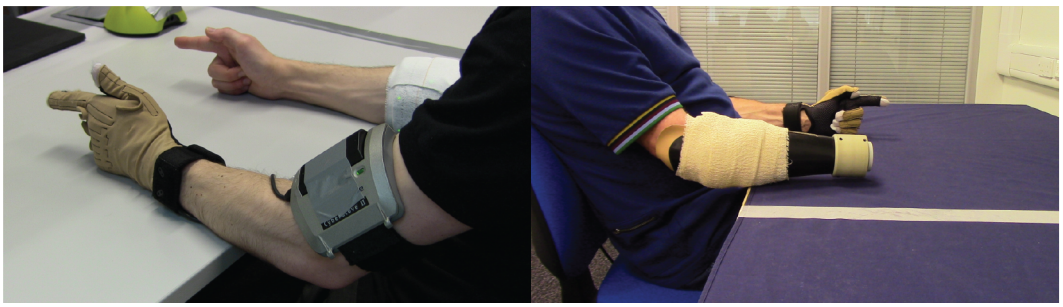

Figure 8.4: Bilateral mirrored movement training. Two participants, an able-bodied (left) and an amputee (right), shown during training data collection. Muscle activity was recorded from the participants' right forearm (i.e. the phantom limb for amputees), whereas hand kinematic data were recorded from the participants' left hand with an 18-DOF data glove.

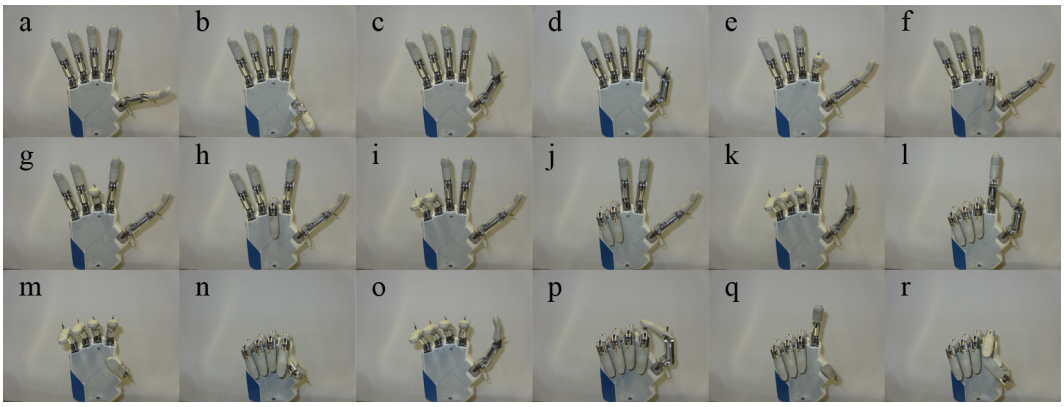

Figure 8.5: Target poses for posture matching task. (a) thumb abduction (half); (b) thumb abduction (full); (c) thumb flexion (half); (d) thumb flexion (full); (e) index flexion (half); (f) index flexion (full); (g) middle flexion (half); (h) middle flexion (full); (i) ring/little flexion (half); (j) ring/little flexion (full); (k) index pointer (half); (l) index pointer (full); (m) cylindrical grip (half); (n) cylindrical grip (full); (o) lateral grip (half); (p) lateral grip (full); (q) tripod grip (half); (r) tripod grip (full).

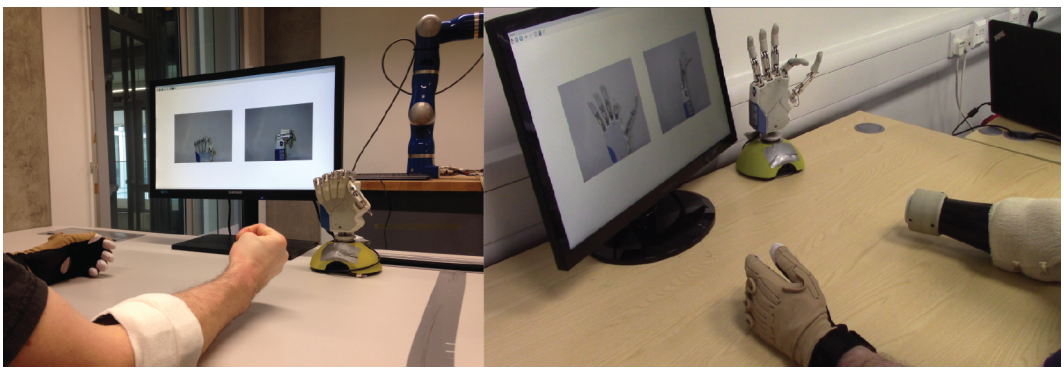

Figure 8.6: Posture matching task. An able-bodied (left) and an amputee participant (right) shown while they modulate their muscle activity to drive the robotic hand into the desired posture. The target postures for the shown trials were full cylindrical grip and half index flexion, respectively.

Table 8.1: Target positions for posture matching task. DOA 1, thumb opposition; DOA 2, thumb flexion; DOA 3, index flexion; DOA 4, middle flexion; DOA 5, ring/little flexion. ID column refers to posture labelling used in Figure 8.5.

ID	Posture	DOA 1	DOA 2	DOA 3	DOA 4	DOA 5
a	Thumb abduction (half)	0.5	0.0	0.2	0.2	0.2
b	Thumb abduction (full)	1.0	0.0	0.2	0.2	0.2
c	Thumb flexion (half)	0.0	0.5	0.2	0.2	0.2
d	Thumb flexion (full)	0.0	1.0	0.2	0.2	0.2
e	Index flexion (half)	0.0	0.2	0.5	0.2	0.2
f	Index flexion (full)	0.0	0.2	1.0	0.2	0.2
g	Middle flexion (half)	0.0	0.2	0.2	0.5	0.2
h	Middle flexion (full)	0.0	0.2	0.2	1.0	0.2
i	Ring/little flexion (half)	0.0	0.2	0.2	0.2	0.5
j	Ring/little flexion (full)	0.0	0.2	0.2	0.2	1.0
k	Index pointer (half)	0.0	0.5	0.0	0.5	0.5
l	Index pointer (full)	0.0	0.96	0.0	1.0	1.0
m	Cylindrical grip (half)	1.0	0.5	0.5	0.5	0.5
n	Cylindrical grip (full)	1.0	1.0	1.0	1.0	1.0
o	Lateral grip (half)	0.0	0.5	0.5	0.5	0.5
p	Lateral grip (full)	0.0	1.0	1.0	1.0	1.0
q	Tripod grip (half)	0.92	0.33	0.37	0.96	0.96
r	Tripod grip (full)	0.92	0.66	0.76	0.96	0.96

counter-balanced across participants (both for the able-bodied and amputee groups). During this task, the prosthetic hand was connected to a base stand placed on the surface of a table and sitting in front of the participant (see Figure 8.6).

Nine hand postures were included, each of them with two variations: half, and full motion; therefore, the total number of postures was 18. The included hand postures were: thumb abduction, thumb flexion, index flexion, middle flexion, ring/little flexion, index pointer, cylindrical grip, lateral grip, and tripod grip. The target postures are shown in Figure 8.5, and the associated target values for the DOAs of the prosthetic hand are given in Table 8.1.

At the beginning of each trial, participants were presented with a pair of pictures providing front and side views of the desired posture. An audio cue (waveform, sine wave; frequency, 400 Hz; duration, 500 ms) was used to signal the initiation of each trial. Participants were then given 3.5 s to drive the prosthetic hand into the desired posture. At the end of this period, a second audio cue (waveform, sine wave; frequency, 800 Hz; duration, 500 ms) was used to signal the initiation of the evaluation phase of the trial, which lasted 1.5 s. During the evaluation phase, participants were

instructed to hold the hand in the performed posture. At the end of the evaluation phase, the hand was reset to its initial posture (i.e. fully open) signalling the end of the trial. Pictures illustrating the posture matching task are shown in Figure 8.6 for two participants, one able-bodied and one amputee.

At the end of each trial, participants received a score characterising their performance. This score was based on the average L_1 *distance* between the target and performed postures during the evaluation phase (i.e. the last 1.5 s) of the trial.

Let $\mathbf{y}$ and $\hat{\mathbf{y}}$ denote K-dimensional vectors in a real vector space. In our case, the two vectors represent the target and performed postures, respectively, of the prosthetic hand at a given time step, and $K = 5$ is the number of DOAs of the hand. The L_1 distance is defined as follows:

$$d_1 = \|\mathbf{y} - \hat{\mathbf{y}}\|_1 = \sum_{j=1}^{K} \left| y_j - \hat{y}_j \right|, \tag{8.2}$$

where y_i and $\hat{y}_i$ denote, respectively, the target and true positions of the j^{th} DOA. The evaluation phase lasted for 1.5 s, and a finger position update was made every 50 ms, that is, the increment time of the sliding window. Thus, there were $N = 300$ distance samples associated with each trial. The average distance during the evaluation phase of a trial was estimated by computing the median across the samples of the population.

To provide the participants with an intuitive performance measure for each trial, L_1 distances were transformed into scores in the range of 0% to 100%. This transformation was achieved as follows: firstly, a baseline average L_1 distance between the target posture and random predictions was established by simulating 1 million random predictions uniformly sampled in the range $[0, 1]$; the normalised score was then computed as follows:

$$\text{normalised score} = \max\left\{0, \left(1 - \frac{\overline{L_1}}{\overline{L_{1,r}}}\right)\right\} \times 100\%, \tag{8.3}$$

where $\overline{L_1}$ denotes the average (i.e. median) L_1 distance during the evaluation phase, and $\overline{L_{1,r}}$ is the pre-computed, average random prediction distance for the specified posture. This transformation ensured that a perfect reproduction of the desired posture would correspond to a 100% score, whereas a randomly performed posture would yield a score close to 0%. Negative scores were not allowed by the max operation. The random seed was controlled during the experiments to ensure identical random prediction distances for all participants.

The posture matching task was split into several blocks. Within each block, all 18 postures were presented to the participants exactly once in a pseudo-randomised order. Each participant performed six blocks for each control mode, that is, EMG and data glove control. The execution of each block lasted approximately 3 min. The stimulus presentation sequence was the same for all participants.

8.2.6.2 *Task 2: object pick and place*

The pick and place task was similar to the one previously presented in Chapters 3 and 5. Briefly, participants were instructed to use the prosthetic hand to grasp, relocate, and release three objects, and finally press the "space" key on a computer keyboard. The included objects were: a plastic water bottle, capacity 500 ml, half-filled with water; a malleable foam ball (i.e. "stress" ball), 7 cm diameter; and a credit card simulator, made of cardboard. Participants were instructed to grasp the three objects using the cylindrical, tripod, and lateral grips, respectively. To accomplish a trial, subjects were required to firstly relocate the three objects and finally press the "space" button on a computer keyboard using an index pointer. A trial was considered successful if it was accomplished within 75 s. To assess prosthetic control performance during the pick and place task, two metrics introduced previously were used; namely, CR and CT (see Section 3.3.3).

One difference between the experiment presented here and that reported in previous chapters was that participants were not required to fully open the prosthetic hand between different grasps, as a result of using a continuous finger position control scheme. Moreover, during EMG control, subjects operated the hand with their contralateral limb. In other words, muscle activity was recorded from the participants' right forearm, whereas the prosthetic hand was attached to their left arm. This simplification was introduced to avoid potential issues arising from the increased weight of the Azzurra IH2 hand (approximately 800 g including the wrist connection unit), which was used in this experiment. Therefore, the participants' right forearm was kept still on the table surface throughout the experiments. Conversely, during glove control, the prosthetic hand was attached to the participants' right forearm, whereas finger kinematics were recorded from their left hand. The direction of object relocation was in each case adjusted according to the employed control mode, that is, right-to-left for EMG control, and left-to-right for data glove control. Pictures illustrating the pick and place task for EMG and data glove control are shown in Figure 8.7.

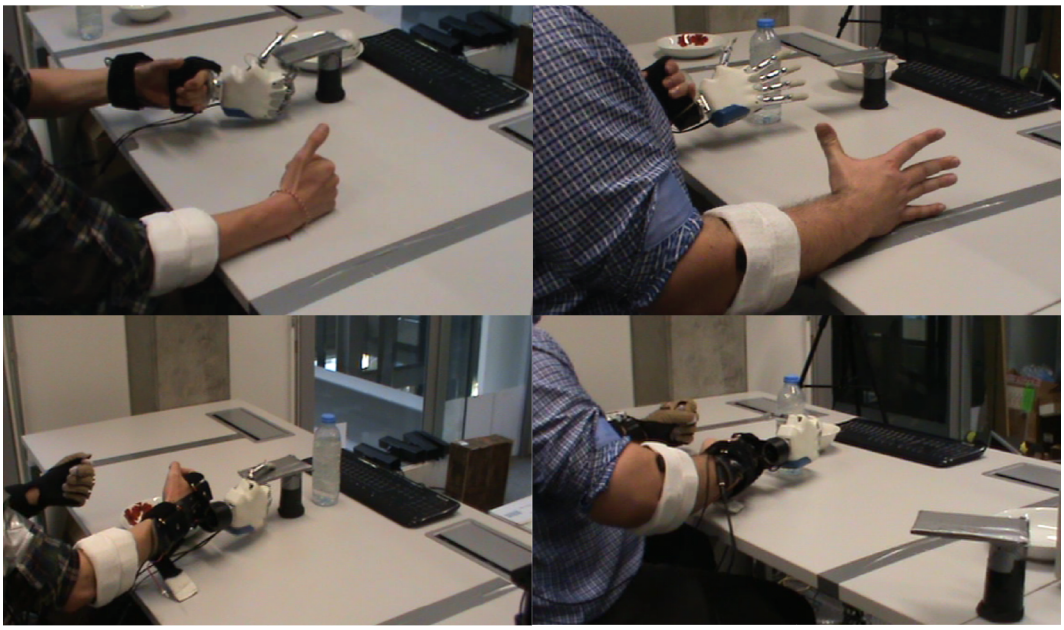

Figure 8.7: Pick and place task. Two able-bodied participants shown while they use the prosthetic hand to grasp, relocate, and release the objects used in the experiments. (Top row) EMG control mode; (bottom row) data glove control mode.

8.2.6.3 *Statistical tests*

No prior assumptions were made about the distributions of reconstruction accuracy scores (i.e. R^2, see Equation C.11), L_1 distances (see Equation 8.2), and performance scores (see Equation 8.3). Thus, the following non-parametric tests were used for statistical comparisons: the Wilcoxon signed-rank test (Wilcoxon, 1945) was used in the case of paired observations (e.g. offline analysis); conversely, for non-paired observations (e.g. CTs in the pick and place task), the Wilcoxon rank-sum test, also known as the Mann-Whitney U test (Mann and Whitney, 1947), was used.

8.3 RESULTS

8.3.1 *Offline analysis*

Typical predictions of the five DOAs of the prosthetic hand are shown in Figures 8.8 and 8.9 for an able-bodied and an amputee participant, respectively. Both graphs show finger kinematic activity in the test set, during which participants performed two repetitions (see Section 8.2.3) of each of the exercises shown in Figure 8.4.

Offline reconstruction accuracy results are summarised in Figure 8.10. The multivariate R^2 is shown in the top panel for all participants on the three different sets, that is, training, validation, and test sets. As was to be expected, performance on the vali-

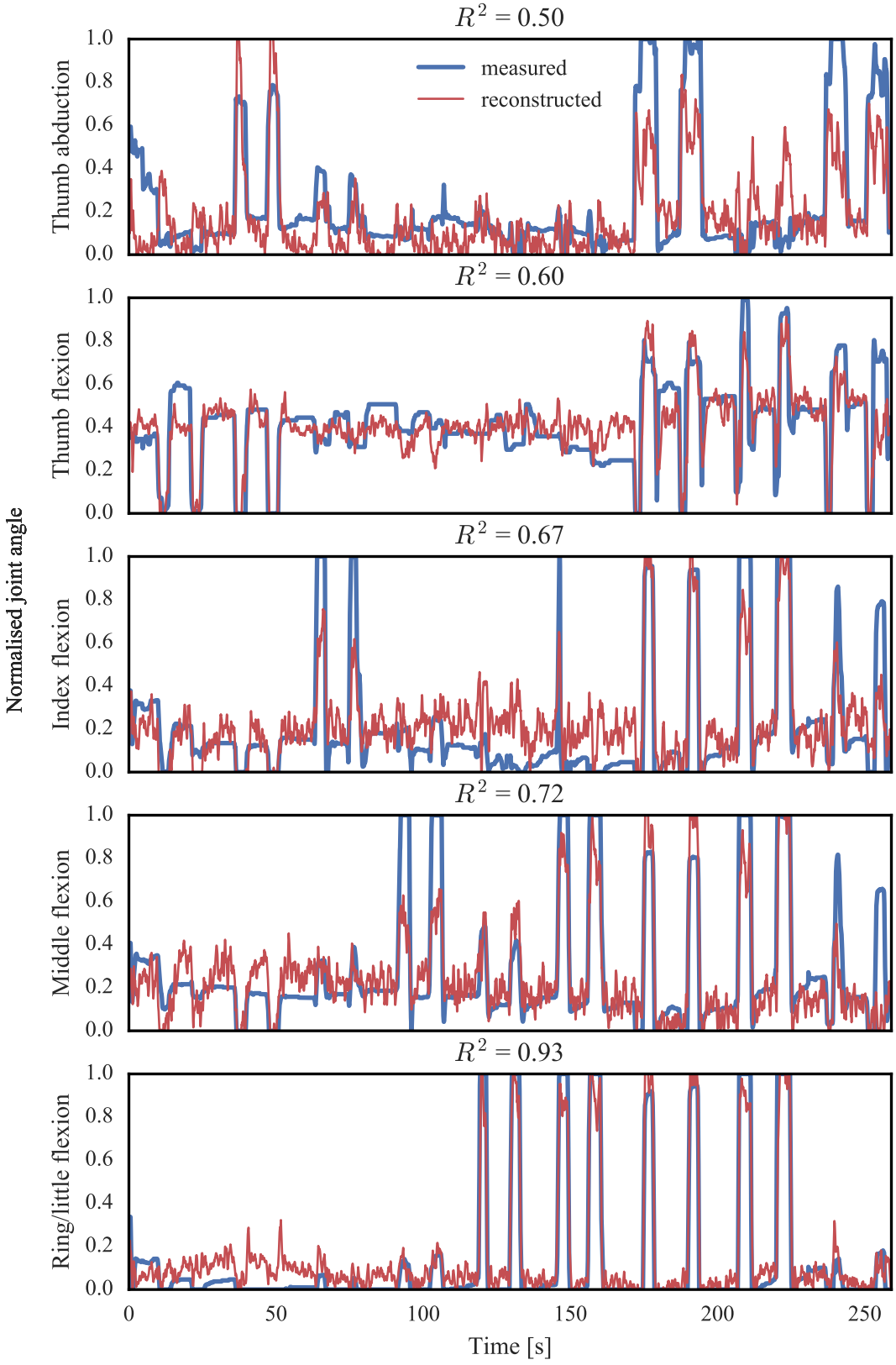

Figure 8.8: Offline joint angle reconstruction example for an able-bodied subject. Predictions shown for all five DOAs of the prosthetic hand on the test set.

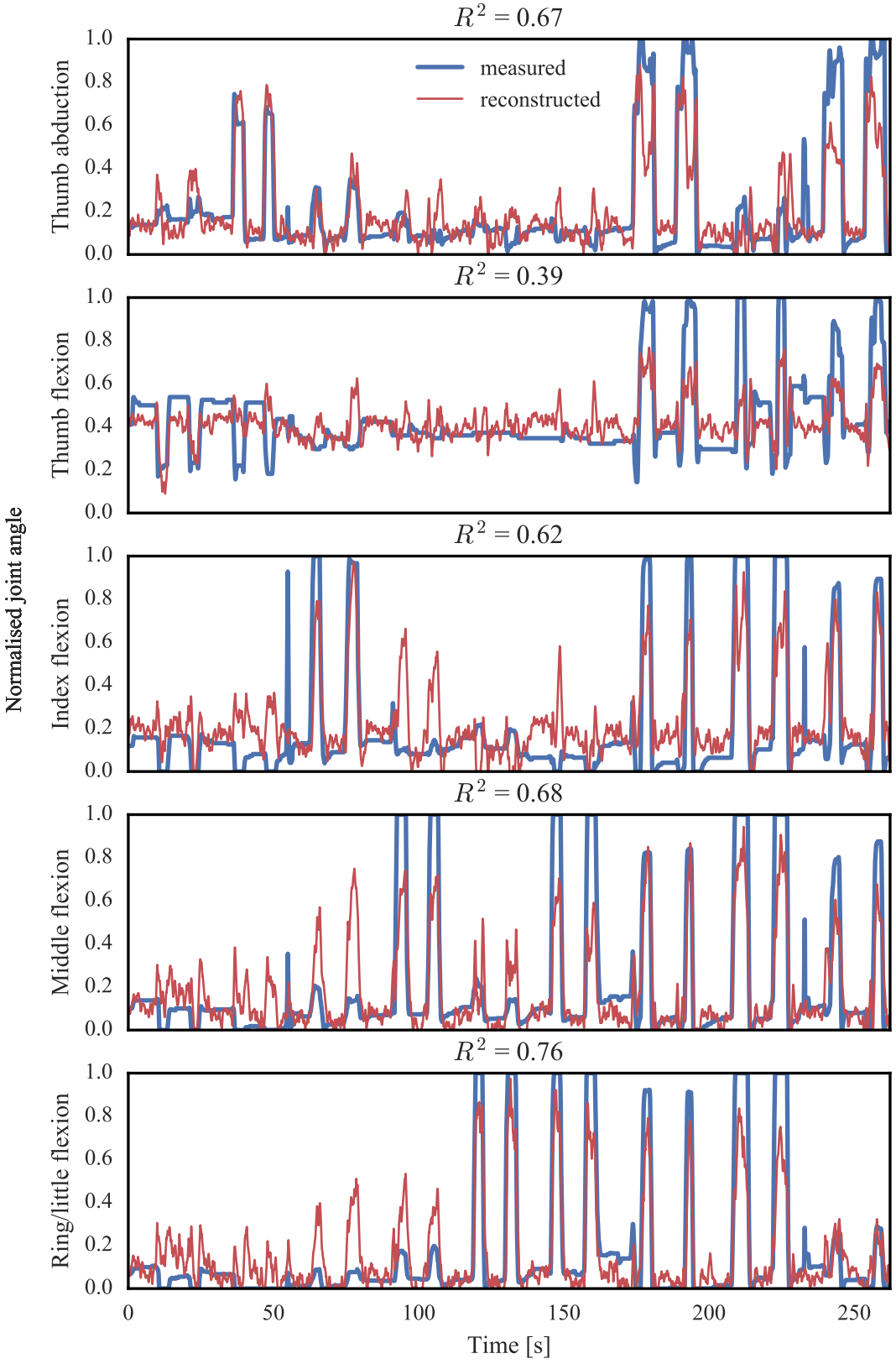

Figure 8.9: Offline joint angle reconstruction example for an amputee subject. Predictions shown for all five DOAs of the prosthetic hand on the test set.

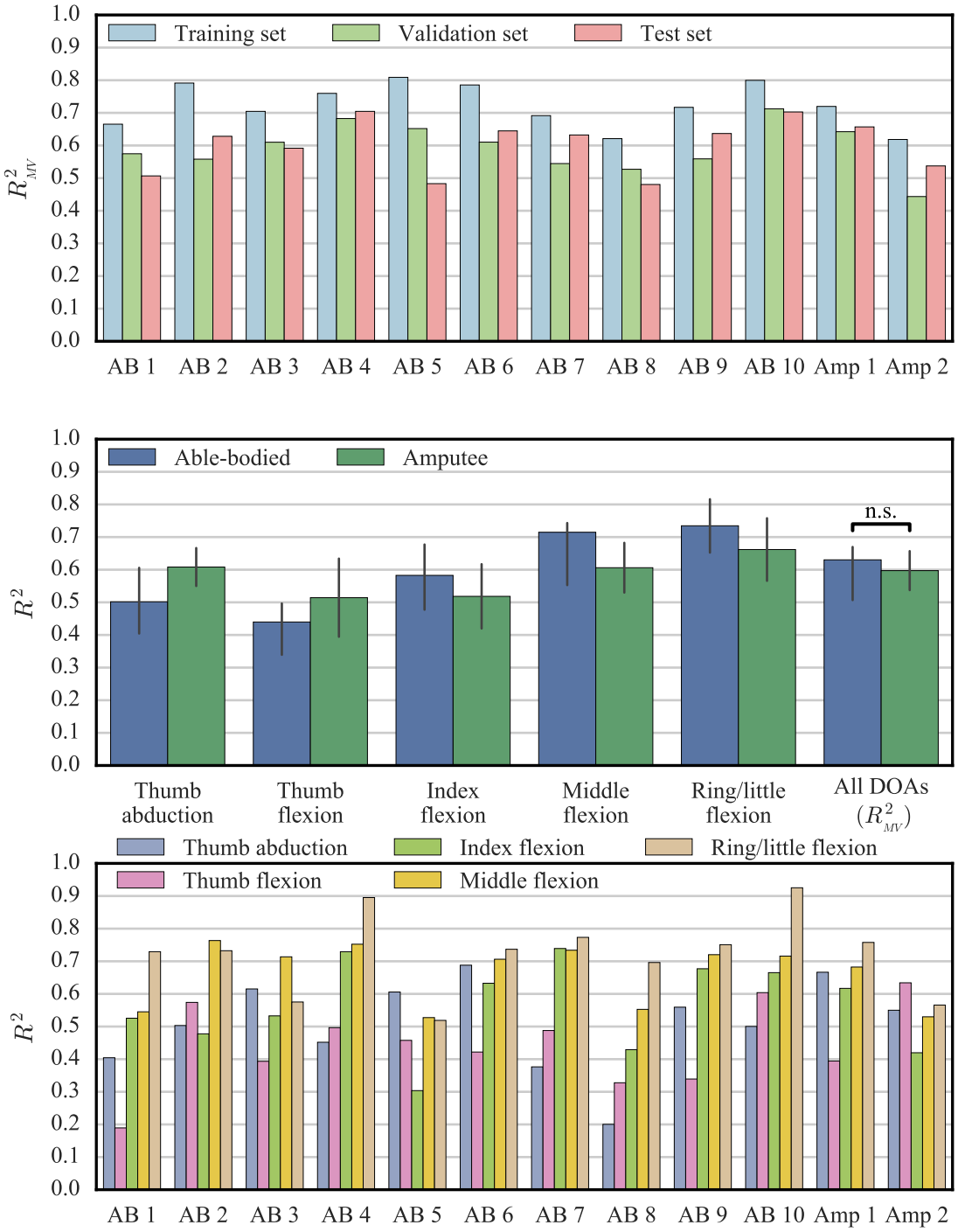

Figure 8.10: Offline reconstruction accuracy results. (Top panel) reconstruction accuracy on different datasets (training, validation, and test) for individual subjects; (middle panel) offline reconstruction accuracy of individual DOAs on test set for pooled subjects; (bottom panel) reconstruction accuracy results on test set for individual DOAs and participants. AB, able-bodied; Amp, amputee; R^2, coefficient of determination (see Section C.2.2); Bars, medians; error bars, 95% confidence intervals estimated via bootstrapping (1000 iterations); n.s., non-significant difference.

dation and test sets was slightly inferior to that on the training set. The middle panel of the same figure provides a summary of the offline accuracy achieved on the test

set for individual DOAs. The last column summarises the overall performance, separately for the able-bodied and amputee groups. Differences in performance between the two groups were not significant ($p > 0.05$, Wilcoxon rank-sum test). The highest offline decoding accuracy was achieved for the ring/little fingers DOA, followed by the middle finger DOA. The worst performance was observed for the thumb flexion DOA. This pattern was generally consistent across participants in both groups. This can be verified by inspection of the last row of the figure, where decoding results on the test set are presented separately for each DOA and participant.

The EMG sensor subset selection for individual subjects is illustrated in Figure 8.11 using a matrix representation. The rightmost column of the graph shows the average selection frequency of individual sensors. The number of used sensors varied from eight (subject "Amp 2") to 16 (subject "AB 9") and had a median value of 12. Finally, the tuning of the exponential smoothing and regularisation parameters for each participant is shown in Figure 8.12.

8.3.2 *Task 1: posture matching*

Ten able-bodied and two transradial amputee subjects took part in the real-time posture matching task. Performance results for this task are summarised in Figure 8.13. Two metrics are reported, namely the normalised score received by the participants at the end of each trial (see Equation 8.3) and the average L_1 distance between the target and executed postures during the evaluation phase of the trials. As was to be expected, glove control performance was significantly higher than that of EMG control for both performance metrics ($p < 0.001$, Wilcoxon signed-rank tests). The average normalised scores across all participants, blocks, and trials were 35.95% and 67.97%, respectively, for EMG and glove control. Able-bodied subjects performed significantly better than amputees in both control modes ($p < 0.01$, Wilcoxon signed-rank tests). The mean normalised scores with EMG control were 36.95% and 30.90%, respectively, for the able-bodied and amputee groups. For glove control, the same figures were 68.37% and 65.94%, respectively. A video recording showing an amputee participant performing six trials with EMG control is provided in the supplementary material (SV4, see Appendix E).

Learning curves during the posture matching task are depicted in Figure 8.14, in which average performance scores are plotted against the experimental block number (ranging from one to six). In all cases, an improvement in performance can be observed as the block number increases. A statistical comparison between early (i.e. 1-2) and late (i.e. 5-6) blocks is further provided in Figure 8.15. For EMG control, the normalised scores were on average higher in late as compared to early blocks,

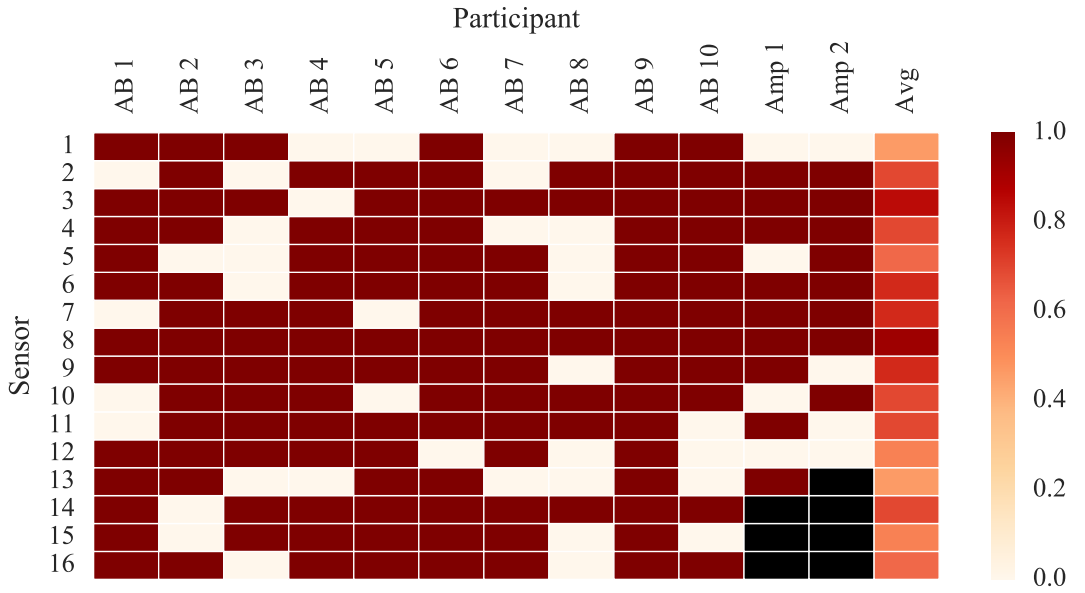

Figure 8.11: Sensor selection for individual subjects. The selected EMG sensors are shown column-wise as red boxes for 10 able-bodied and two amputee subjects. The rightmost column represents the average selection frequency of individual sensors. Black boxes represent unavailable sensors due to limited space on amputee participants' forearm. The reader is referred to Figure 5.1 (top row) for details on sensor placement.

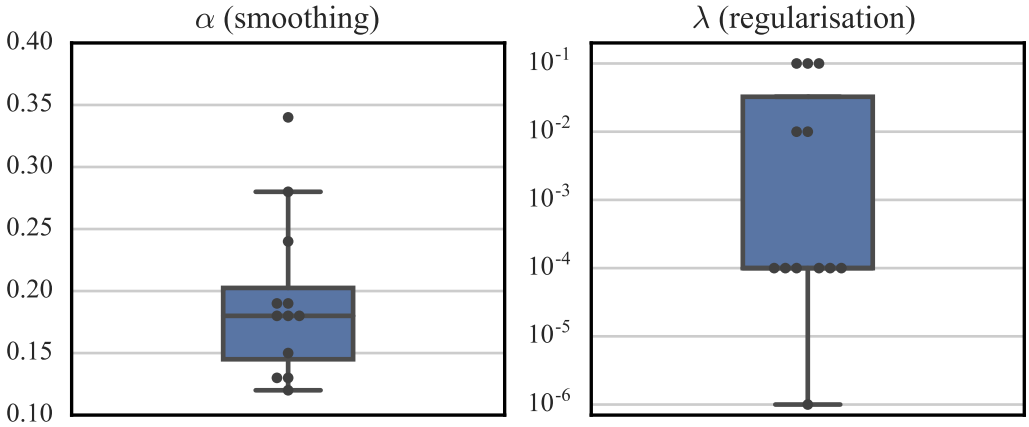

Figure 8.12: Hyper-parameter optimisation. The selection of the post-processing smoothing parameter α and regularisation parameter λ is shown for all subjects (10 able-bodied, two amputees). Points, individual samples; straight lines, medians; solid boxes, interquartile ranges; whiskers, overall ranges of non-outlier data (1.5 IQR).

although this difference was not significant ($p > 0.05$). Conversely, the decrease in average L_1 distance between target and executed postures from early to late blocks was significant ($p < 0.05$). For glove control, both metrics were significantly improved in late blocks ($p < 0.001$). All statistical comparisons were performed using Wilcoxon signed-rank tests (see Section 8.2.6.3).

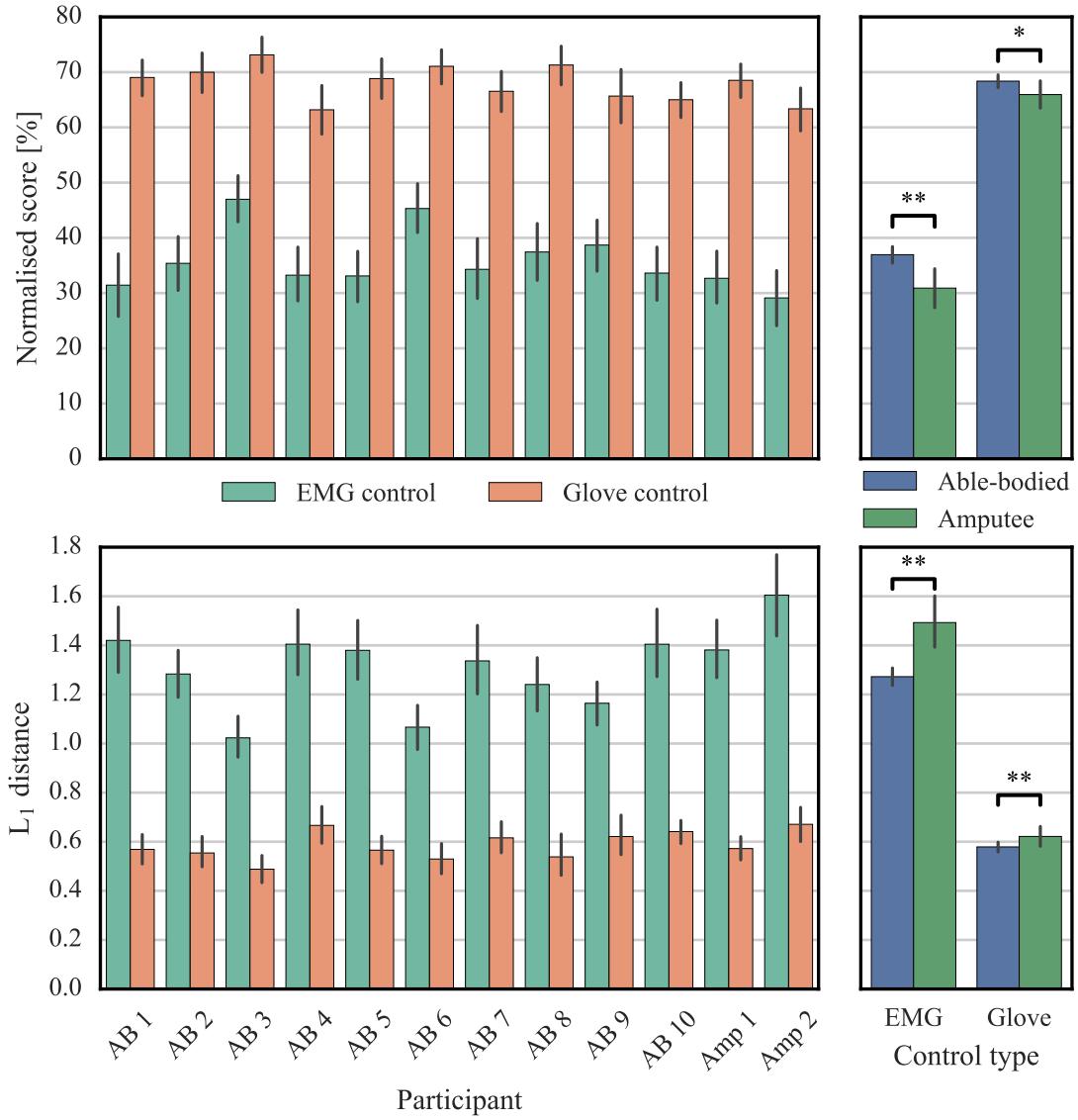

Figure 8.13: Posture matching task results. (Left column) performance scores shown for individual subjects by means of normalised scores (top row) and L_1 distances (bottom row); (right column) summary results for able-bodied and amputee subjects for EMG and glove control. Bars, means; error bars, 95% confidence intervals estimated via bootstrapping (1000 iterations); asterisk, $p < 0.05$; double asterisk, $p < 0.01$.

8.3.3 *Task 2: object pick and place*

Only six able-bodied subjects completed the pick and place task. The remaining four, as well as both amputee participants, did not perform this task as they did not succeed in the initial screening trial (see Section 8.2.6). One common cause of failing the screening trial was the inability to reliably execute one of the four required grips, for example, the cylindrical grip which was necessary for grasping the water bottle. Nevertheless, all participants were able to execute 2-3 grips. A video recording show-

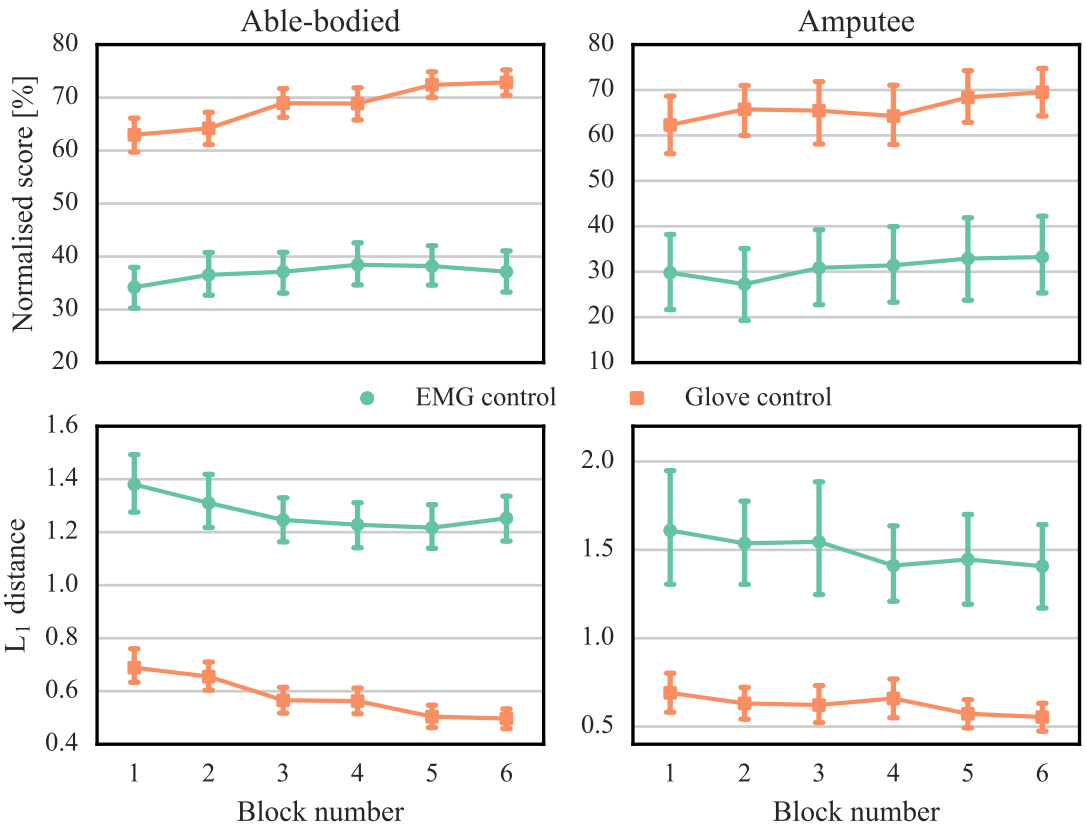

Figure 8.14: Posture matching task learning curves. Normalised scores received by participants (top row) and L_1 distances (bottom row) are plotted against the experimental block number. Results shown separately for able-bodied (left column) and amputee (right column) subjects during EMG and glove control. Points, means; error bars, 95% confidence intervals estimated via bootstrapping (1000 iterations).

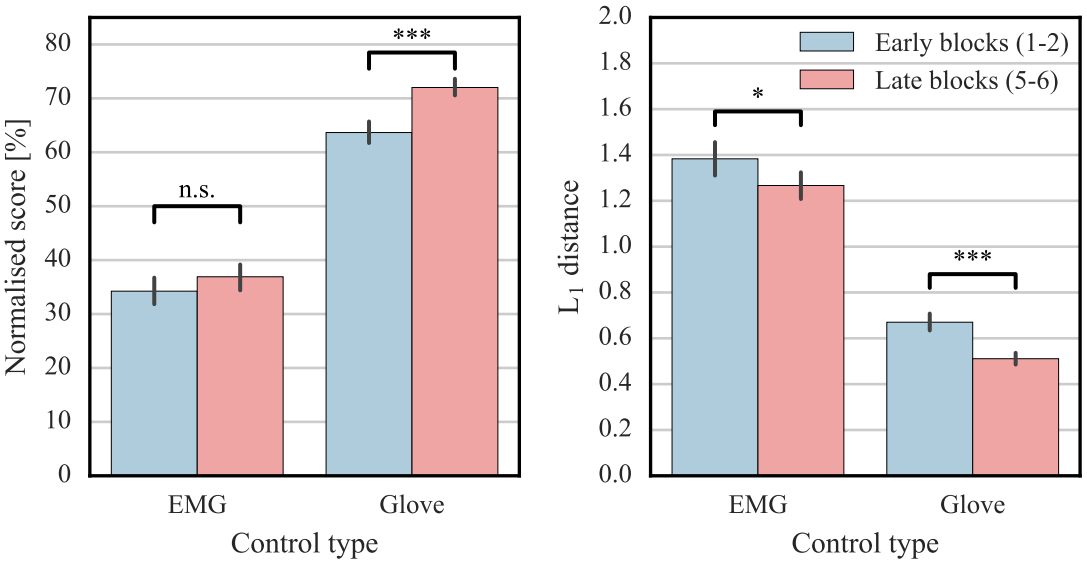

Figure 8.15: Comparison of early vs. late blocks for posture matching task. Bars, means; error bars, 95% confidence intervals estimated via bootstrapping (1000 iterations); n.s., non-significant difference; asterisk, $p < 0.05$; triple asterisk, $p < 0.001$.

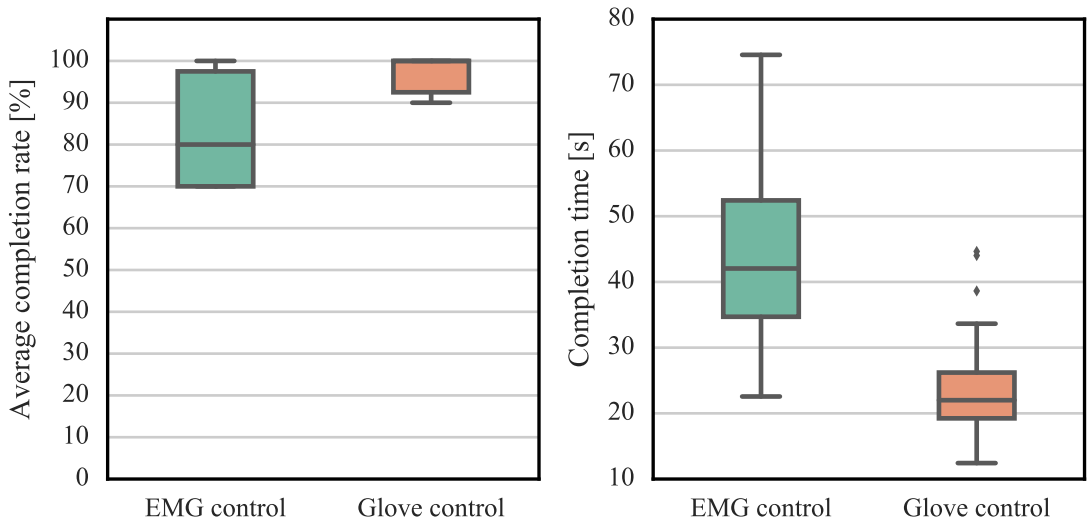

Figure 8.16: Pick and place task results. Average CRs and CTs shown for six able-bodied participants during EMG and glove control. Straight lines, medians; solid boxes, interquartile ranges; whiskers, overall ranges of non-outlier data (1.5 IQR); diamonds, outliers.

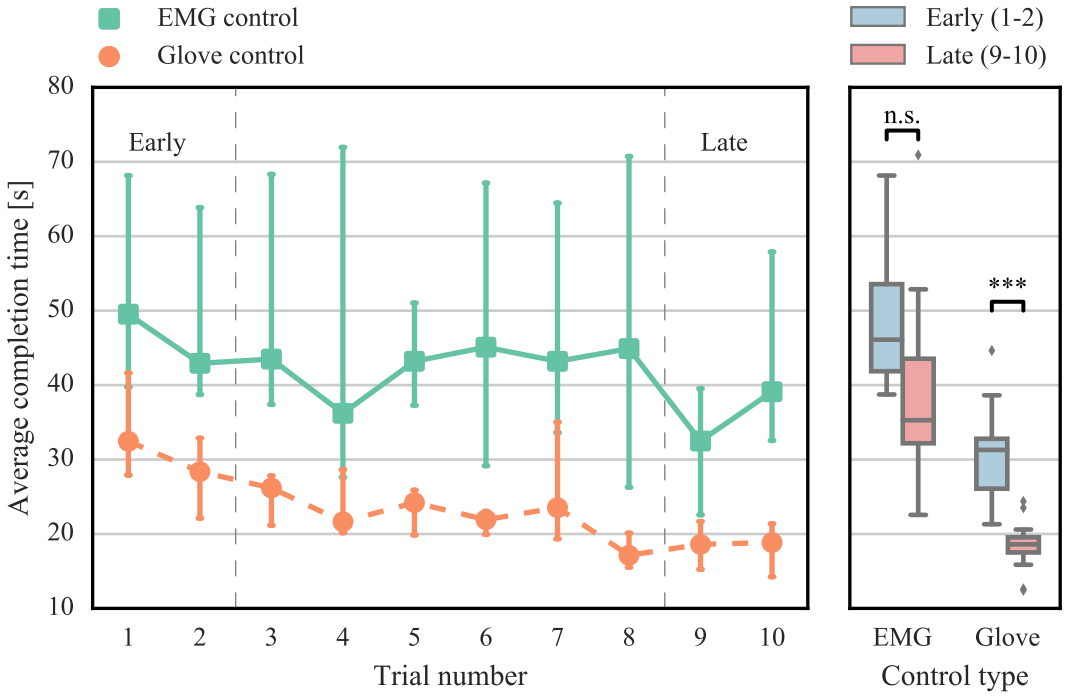

Figure 8.17: Pick and place task learning curves. (Left) average CTs are plotted against the trial number for EMG and glove control. Points, medians; error bars, 95% confidence intervals estimated via bootstrapping (1000 iterations). (Right) performance comparison of early vs. late trials. Straight lines, medians; solid boxes, interquartile ranges; whiskers, overall ranges of non-outlier data (1.5 IQR); diamonds, outliers; n.s., non-significant difference; triple asterisk, $p < 0.001$.

ing one trial of the experiment with an able-bodied participant is provided in the supplementary material (SV5, see Appendix E).

Performance results for the six able-bodied participants who completed the task are presented in Figure 8.16, by means of CRs and CTs (shown in the left and right columns of the graph, respectively). For EMG control, the median CR was 80%. The median CT for successful trials was 42.04 sec. For data glove teleoperation, the median CR was 100% with a median CT of 22.00 s.

The average CT is plotted against the trial number in Figure 8.17. For both EMG and glove control modes, the average CT decreased within the course of the experiment. A comparison between early (i.e. 1-2) and late (i.e. 9-10) trials is shown on the right-hand side of the graph. The difference in median CT between early and late trials was 10.41 s and 13.59 s, respectively, for EMG and glove control. Statistical analysis (Wilcoxon rank-sum tests) revealed that the decrease was significant in the case of glove control ($p < 0.001$); however, for EMG control, the average decrease was marginally above the significance level ($p > 0.05$), most likely due to the small sample size.

8.4 DISCUSSION

8.4.1 *Impact*

The study presented in this chapter investigated the feasibility of achieving continuous finger position prosthetic control by using muscle activity recorded on the surface of the forearm. In agreement with previous work (e.g. Smith et al., 2009; Cipriani et al., 2011; Ngeo et al., 2013), it was shown that it is feasible to use surface EMG measurements to decode finger position and subsequently use predictions to control individual digits of a prosthesis. The controlled DOAs included flexion of all fingers and thumb opposition. The ring and little fingers were controlled together because they are mechanically coupled in the prosthetic device.

During the posture matching task, participants were required to execute hand postures for which training data were not available (see Figures 8.1 and 8.5); therefore, this study provides a first proof-of-principle demonstrating the ability of the proposed scheme to attain prosthesis control in a continuous space of finger movement.

Furthermore, it is shown that the proposed approach can enable a prosthesis user to accomplish functional tasks; for example, grasping, relocating, and releasing objects. Only six able-bodied participants performed the pick and place task, since the remaining four able-bodied and both amputee subjects failed the initial screening trial. Nevertheless, all participants were able to execute at least two of the four grips included in the screening trial (i.e. index pointer, cylindrical, lateral, and tripod grips).

8.4.2 *Limitations and clinical implications*

A number of simplifications were made in this study: firstly, the participants' forearm was kept still throughout the experiment; secondly, during the pick and place task, the prosthetic hand was attached to the participants' contralateral arm, so as to avoid muscle fatigue due to the increased weight of the prosthesis used; thirdly, no wrist movement was involved in the study. These simplifications would not occur in a realistic scenario and, thus, it is expected that myoelectric performance would deteriorate given the non-stationarities that are likely to be induced by removing them (Amsüss, 2014). Even under ideal, lab-controlled conditions, only six out of twelve participants were able to complete the pick and place task. Importantly, both amputees failed the initial screening trial. Although offline analysis suggested that the performance of able-bodied and amputee participants was comparable (see Figure 8.10), a significant difference between the two groups was observed during real-time prosthetic control (see Figure 8.13). On the other hand, for participants who completed the pick and place task, performance was only slightly worse than that achieved with classification-based control (contrast Figures 5.8 and 8.16). This finding is encouraging, taking into account that once the intended motion has been predicted in the case of classification, the activation sequence of the fingers is hard-coded and, thus, optimal. Taking all the above into consideration, it can be argued that the efficacy of a proportional finger control scheme might depend on individual characteristics of the user, and thus, be subject-specific. Additional experiments with a larger number of amputee participants are required to validate the clinical viability of the proposed method.

8.4.3 *User adaptation*

In agreement with previous work (Pistohl et al., 2013; Powell, Kaliki, and Thakor, 2014; Pistohl et al., 2015), it was found that the provision of continuous feedback during real-time prosthetic control can result in performance improvement over time. In this study, two types of feedback were provided: visual, since the prosthetic hand was within the visual field of the participant and responded to their control input; and a performance score, which was presented to the participants at the end of each trial of the posture matching task. A learning effect was observed in both tasks (see Figures 8.14, 8.15, and 8.17).

Pistohl et al. (2013) made use of a similar performance measure to the one used in the current study and reported an increase from 0% to 40% after approximately 200 trials. In the present study, the average performance increased from 33.47% to 36.49%

after 108 trials (i.e. 6 blocks $\times$ 18 trials/block) with EMG control. This improvement is smaller than the one reported by Pistohl et al., but this should not be surprising; Pistohl et al. used a fixed and non-intuitive mapping from muscle activity to the DOAs of the prosthetic hand, and thus, participants had to learn the underlying control principle of the interface from scratch. Conversely, the current study employed a mapping that was based on a regression model trained with subject-specific data; therefore, this mapping was intuitive for the user from the beginning of the task. In the latter case, the improvement might be primarily attributed to participants getting used to the protocol and fine-tuning their control strategy to increase their performance. A similar improvement was also observed for the data glove control mode (see Figures 8.14 and 8.15).

8.4.4 *On the use of inertial measurements for finger position proportional control*

It was shown in Chapter 3 that the use of inertial data can improve classification-based myoelectric control. Although one might expect that the same could hold for the case of proportional finger control, preliminary offline analysis provided evidence for exactly the opposite; for that reason, only EMG recordings were considered in this study.

The offline reconstruction accuracy of models trained by combining EMG and inertial measurements is shown in Figure 8.18 and also compared to the case of EMG-based decoding. It can be observed that while the inclusion of inertial data can improve training accuracy, performance on the validation and test sets is severely deteriorated. One possible explanation for this finding is that the inclusion of inertial data may result in model overfitting with regards to arm posture. Although the same has been proposed for classification, it has also been shown that collecting training data with dynamic motions can help overcome this issue (Radmand, Scheme, and Englehart, 2014). For regression tasks, however, where the target signal is continuous, the posture overfitting effect may be considerably more profound than with classification. Another possible reason causing the lack of generalisation may be accelerometer and gyroscope drifting over time (see Section 2.3.2). By using the same rationale as before, it is likely that regression predictions are considerably more affected by such drifting issues as compared to classification tasks. Properly addressing these challenges might provide a means of achieving multi-modal finger proportional control, which could potentially largely improve decoding accuracy, and is therefore regarded as a promising direction for future research.

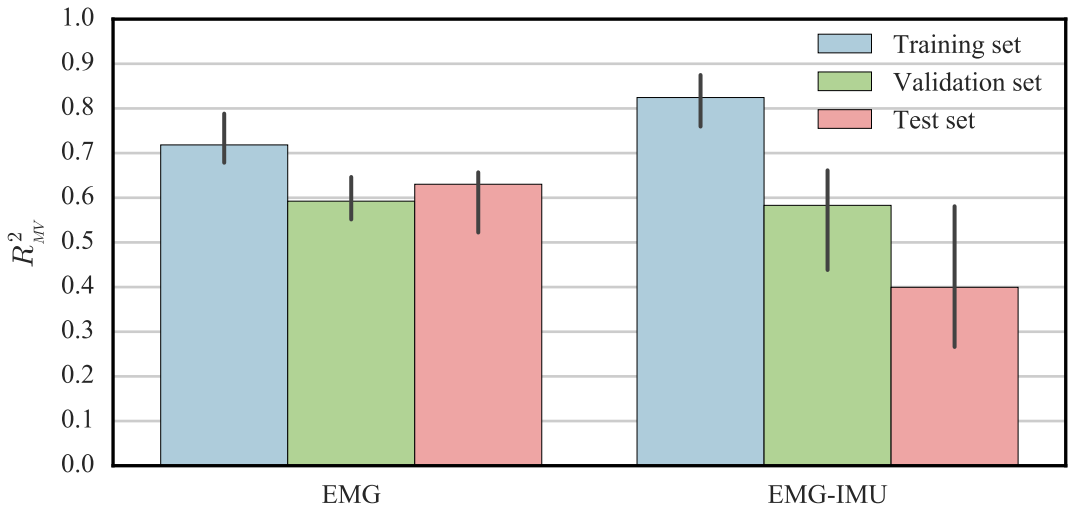

Figure 8.18: Offline reconstruction accuracy with EMG and EMG-IMU data. Results shown for all participants on training, validation, and test sets. Bars, medians; error bars, 95% confidence intervals estimated via bootstrapping (1000 iterations).

8.4.5 *On the relationship between offline and real-time performance metrics*

In the context of myoelectric classification, it has been shown that a discrepancy exists between offline accuracy and real-time control performance metrics (see Section 5.4.4). With regards to 2-DOF wrist proportional control, Jiang et al. (2014b) showed that only a weak correlation exists between offline R^2 and metrics characterising real-time prosthetic control performance, such as CR, CT, overshoots, throughput, speed, and efficiency coefficient (see Section 2.5.4).

To assess whether the same holds for proportional finger position control, offline reconstruction accuracy scores were compared to performance metrics during the posture matching task. The average L_1 distance and performance scores were computed for each subject across all trials and blocks and compared to the respective offline reconstruction accuracy score for the same subject on the test set. The results of this analysis are presented in Figure 8.19. In agreement with Jiang et al. (2014b), a very weak correlation was found between offline accuracy and real-time performance metrics. Contrasting the results of Figure 8.19 to those of Figure 5.12, in which a similar analysis was performed for classification-based prosthetic control, it can be deduced that for regression tasks it might be even more difficult to predict the quality of real-time prosthetic control purely based on offline analyses. This finding reiterates the need for testing ML-based prosthetic control methodologies in real-time by designing and making use of realistic experimental paradigms (Jiang et al., 2012b; Jiang et al., 2014b; Ortiz-Catalan et al., 2015; Vujaklija et al., 2017).

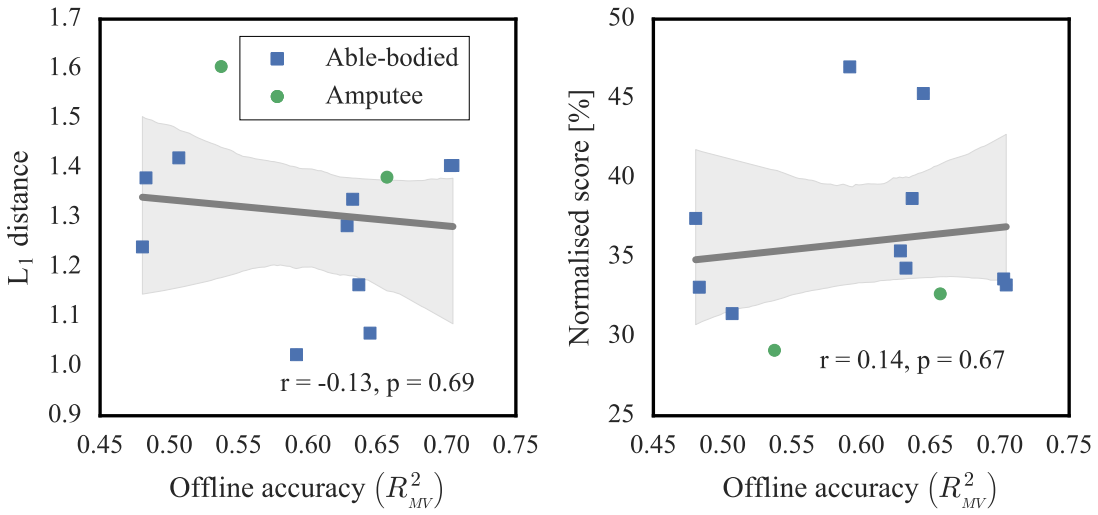

Figure 8.19: Relationship between offline reconstruction accuracy (i.e. multivariate R^2) and real-time performance metrics in the posture matching task (L_1 distance and normalised score). Points, individual observations (i.e. subjects); lines, linear regression fits; translucent bands, 95% confidence intervals estimated via bootstrapping (1000 iterations).

8.4.6 *Future work*

This chapter investigated and evaluated a non-invasive myoelectric scheme based on continuous position control of individual digits. The proposed controller has two main advantages: intuitiveness and dexterity. By training regression models using muscle signals and glove data the mapping from muscle to finger domain is natural and intuitive. In other words, the user does not need to learn a new mapping, unlike some previous studies where different wrist movements were mapped into specific digit functions (e.g. Matrone et al., 2012). Dexterity naturally arises from the fact that the user can control individual fingers in a continuous space. One particular advantage of this scheme over classification-based methods is the ability to move from one type of grip to another without the need for executing an intermediate hand opening action. The high level of dexterity, however, comes at a price; as it has become evident from the experimental results presented in this chapter, decoding individual finger positions is a much more challenging task than classifying EMG activity into hand postures. In its current form, the proposed scheme is unlikely to be suitable for adoption by amputees, as significant improvements are required to ensure its clinical viability. Nevertheless, given the potential of this method to achieve natural and truly dexterous prosthetic control, it is considered worthwhile to pursue further research in this direction.

One possible avenue for future research is to attempt improving the performance of the approach by using an alternative way of measuring muscle activity. It was

found in this study that, unlike hand posture classification where good performance can be achieved with a small number of sensors (see Chapter 5), a large number of electrodes was typically selected by the SFSS algorithm (see Figure 8.11). Therefore, it would be worthwhile exploring whether improved reconstruction accuracy can be achieved by recording muscle activity with high-density EMG arrays, which have been successfully used in hand posture classification (e.g. Geng et al., 2014), wrist kinematics decoding (e.g. Muceli and Farina, 2012; Muceli, Jiang, and Farina, 2014; Hahne et al., 2014), proportional finger force control (Celadon et al., 2016), and real-time, high-dimensional robot control (Ison et al., 2016). Moreover, force myography is a technique developed recently which uses force-sensing resistors to estimate muscle activity. This technique has already been used for hand/wrist motion (Radmand, Scheme, and Englehart, 2016) and hand grip classification (Cho et al., 2016; Ghataurah et al., 2017), as well as for finger movement trajectory reconstruction (Kadkhodayan, Jiang, and Menon, 2016) with promising results. Thus, it shall be interesting to investigate whether it can be also used to enhance the performance of proportional finger position control.

Finally, it is worth stressing that an invasive approach might indeed be required to achieve robust finger position control. Intramuscular EMG recordings have been previously used for proportional finger control of both virtual (Birdwell et al., 2015) and robotic (Cipriani et al., 2014a) hands. Both of these studies, however, had the following two limitations: firstly, they used a one-to-one mapping from individual pairs of muscles to DOAs of the hand; secondly, they were limited to able-bodied participants. An interesting avenue for future research would be to investigate the potential benefit of using regression models to map the activity of multiple muscles into the activation of the prosthesis DOAs, as opposed to the previously proposed one-to-one mapping scheme. Another compelling possibility would be to test the performance of proportional finger control in patients having undergone targeted muscle reinnervation (see Section 2.4.2.5). Kuiken et al. (2009) demonstrated that hand/wrist movements can be classified in targeted muscle reinnervation patients with high accuracy. Nevertheless, whether robust individual finger position control can be achieved using a similar approach remains to be investigated.

9

CONCLUSION

This thesis presented several proposals aimed at advancing the state-of-the-art in *machine learning* (ML)-based myoelectric control of upper-extremity prostheses. The main body of work was centred around the two objectives established in Section 1.2:

1. Improve the performance of classification-based myoelectric grip control.
2. Develop and evaluate a framework for continuous finger position control of multiple joints.

The following section provides an overview of the work addressing these two objectives (Chapters 3-5 and 6-8, respectively), and points out the contributions of the thesis.

9.1 OVERVIEW AND CONTRIBUTIONS

9.1.1 *Classification-based myoelectric grip control*

The concurrent use of surface *electromyography* (EMG) and *inertial measurement unit*s (IMUs) was proposed in Chapter 3 for improving the performance of myoelectric grip classification. Although accelerometers had been previously used in offline decoding of hand/wrist motions (e.g. Fougner et al., 2011; Geng, Zhou, and Li, 2012; Radmand, Scheme, and Englehart, 2014), this was the first work exploiting additional intertial sensors, such as gyroscopes and magnetometers. More importantly, it was demonstrated for the first time, that the concurrent use of EMG and inertial signals can significantly improve classification performance during real-time prosthetic hand control. The relationship between the different sensing modalities was investigated and it was suggested that they partially encode complementary information of the same underlying phenomenon, that is, the muscular activity.

In the field of myoelectric control, the *linear discriminant analysis* (LDA) model is regarded as the "gold standard" for classification, and with good reason; it is easy to implement, extremely efficient in computational terms during both training and testing, and can achieve top-level accuracy that is often comparable to that of more sophisticated algorithms. Nevertheless, in its core lies a fundamental assumption that is most often violated in practice. The work presented in Chapter 4 demonstrated that

relaxing this assumption and adopting the *regularised discriminant analysis* (RDA) classifier can lead to significant improvement in *classification accuracy* (CA) of myoelectric decoders. The offline CA achieved with RDA on a benchmark dataset (Atzori et al., 2014) was superior to that reported previously (Atzori, Cognolato, and Müller, 2016; Geng et al., 2016).

One factor limiting the clinical adoption of ML-based myoelectric systems is the requirement for a large number of EMG electrodes. The work presented in Chapter 5 was the first to demonstrate that it is feasible to decode in real-time five hand grips with high accuracy by using a single pair of surface EMG-IMU sensors. A novel framework for hyper-parameter optimisation and confidence-based prediction rejection was also introduced. The proposed strategy aims to minimise the rate of unintended hand motions via controlling the *false positive rate* (FPR) of the decoder in a class-specific fashion. The clinical implications of the specific study are of particular importance, since it was demonstrated that ML-based grip control can be adopted in existing commercial solutions subject to minimal hardware modifications.

9.1.2 *Continuous finger position control*

Although classification-based myoelectric control can offer a radical improvement in the quality of life of upper-extremity amputees, the use of regression methods has been suggested as a potential means of achieving more intuitive and dexterous myoelectric control (Fougner et al., 2012). Earlier work in this direction primarily focused on wrist movement, while finger position control has received less attention. In Chapter 6, a rigorous analysis was carried out on reconstructing finger joint angles from surface EMG measurements with the aim of controlling individual *degrees of actuation* (DOAs) of a prosthetic hand, including thumb opposition and flexion of individual fingers. An exhaustive EMG feature comparison was also performed, which had not been previously reported for this particular task.

The concepts of muscle and postural synergies have been recently used in the context of myoelectric control as a means of improving the generalisation of decoding algorithms. However, the methods used in previous work have been almost exclusively unsupervised which may lead to suboptimal results. A supervised, simultaneous input-output linear dimensionality reduction method was proposed in Chapter 7, which is optimal with respect to the task at hand, that is, joint angle reconstruction from EMG measurements. The proposed methodology, which is novel in this context, can be applied to regression problems with multidimensional inputs and outputs, including, but not limited to, EMG control of multi-articulated prosthetic hands.

A proof-of-principle of the proposed continuous finger control scheme was demonstrated in Chapter 8 and the efficacy of the approach was evaluated with real-time control experiments including both able-bodied and amputee participants. It was shown for the first time that this scheme can allow users to execute postures not present in the training dataset, as well as complete functional tasks, such as grasping and releasing objects.

9.2 LIMITATIONS AND FUTURE PERSPECTIVES

This section outlines the limitations of the thesis, proposes potential ways of addressing them, and finally presents general reflections on future research directions.

9.2.1 *Prosthetic wrist control*

Wrist control was not considered in this work. Wrist dexterity is of great significance for efficient prosthetic control and has been a long-standing requirement of prosthesis users (Atkins, Heard, and Donovan, 1996). Montagnani, Controzzi, and Cipriani (2015) showed that a combination of a 2-*degree of freedom* (DOF) wrist (pronation/supination and flexion/extension) with a single-DOF hand allows for overall limb function comparable to that of a single-DOF wrist (pronation/supination only) with a multi-DOF hand. Their study also demonstrated that the lack of dexterity in wrist movement leads to additional, compensatory movements of other parts of the body (e.g. arm, shoulder). Prosthetic wrist control has been extensively investigated in the research community with promising results; many studies have demonstrated the feasibility of accurately reconstructing 2-3 wrist DOFs in real-time (e.g. Jiang et al., 2014a; Ameri et al., 2014b; Smith, Kuiken, and Hargrove, 2016; Hahne, Markovic, and Farina, 2017, see Section 8.1.1 for a detailed review).

Although wrist movement was not considered here, it would be rather straightforward to integrate it into both frameworks investigated. The proposed scheme for grip classification adopted a natural control approach. In other words, to select a desired grip the user has to activate their muscles in the same way that they would naturally do with an intact limb. It is worth noting that this is fundamentally different to remapping wrist movements into grip types, which had been previously proposed by some studies (e.g. Shenoy et al., 2008). Similarly, simultaneous control of wrist and finger DOFs could be combined into a unified proportional control architecture. If successful, this approach is expected to lead to a great level of dexterity and, thus, is regarded as an avenue well worth exploring in the future.

9.2.2 *Decoder adaptation*

One important limitation of this work was the lack of decoder adaptation over time. In other words, all ML models considered here were initially fitted using a training dataset and subsequently kept fixed throughout the experimental sessions. This strategy can prove problematic as it is well known, and has also been experimentally verified, that the performance of ML-based myoelectric decoders degrades monotonically with time (Kaufmann, Englehart, and Platzner, 2010; Amsuss et al., 2013). This is attributed to various sources of non-stationarity present in EMG signals which can be due to, among other things, the limb position effect (e.g. Fougner et al., 2011, see also 3.1.1), electrode shift (Hargrove, Englehart, and Hudgins, 2008; Young, Hargrove, and Kuiken, 2011), differences in contraction levels (Scheme and Englehart, 2013a), and muscle fatigue (Kumar, Pah, and Bradley, 2003).

A significant amount of work has been carried out towards designing adaptive myoelectric classifiers (e.g. Sensinger, Lock, and Kuiken, 2009; Chen, Zhang, and Zhu, 2013; Zhang and Huang, 2015; Liu et al., 2016a; Liu et al., 2016b; Vidovic et al., 2016; Zhu et al., 2017; Zhai et al., 2017). In their majority, the proposed algorithms are unsupervised; in other words, decoder adaptation takes place by using unlabelled data made available at test time. Such algorithms could be seamlessly integrated into the classification-based grip control scheme proposed in Chapter 5. One possibility of extending this work would be to start with a small training dataset and an LDA model, that is, assume a pooled covariance matrix so as to avoid overfitting issues due to the small size of the initial dataset. Then at test time, use classifier predictions made with high confidence (Sensinger, Lock, and Kuiken, 2009) to update mean vectors and covariance matrices in a class-specific fashion, thus shifting towards the general case of the class-conditional Gaussian models (i.e. RDA/*quadratic discriminant analysis* (QDA)).

For regression-based applications, such as wrist and/or finger proportional control, decoder adaptation is more challenging, since in this case updating model parameters requires access to ground truth (i.e. labelled) data. In other words, for every model update, novel training data have to be collected in the form of a short recalibration phase which can prove cumbersome for the user. Some initial work has been done in this direction for proportional finger force (Gijsberts et al., 2014b) and wrist position (Hahne et al., 2015), but not for finger position control.

9.2.3 *Towards minimal calibration for prosthesis use*

Minimising calibration times for prosthesis users is one of the main challenges that researchers in the myoelectric control community will need to address in the future. For the real-time experiments presented in Chapters 5 and 8, training data collection lasted 40 min and 45 min, respectively. This amount of training time may prove discouraging, or even worse, prohibitive for many users, especially if the system needs to be recalibrated frequently. Some previous work has attempted to tackle this issue by proposing various methods for training classifiers capable of generalising to novel subjects, including, but not limited to, bilinear models (Matsubara and Morimoto, 2013), decision trees (Gibson, Ison, and Artemiadis, 2013), adaptive support vector machines (Tommasi et al., 2013), and *canonical correlation analysis* (CCA) (Khushaba, 2014). A promising research direction for addressing this challenge in the future might be via using techniques from the fields of domain adaptation, which concerns dealing with problems in which data distributions are different in the training and test sets (Daumé III and Marcu, 2006). To this end, Du et al. (2017) proposed a convolutional neural network-based domain adaptation framework and demonstrated promising results in achieving classification generalisation to novel users.

9.2.4 *Sensory feedback*

The use of artificial sensory feedback during prosthetic control was not considered in this work. A great amount of previous research has proposed various means of providing sensory feedback to prosthesis users including both non-invasive (e.g. Saunders and Vijayakumar, 2011; Cipriani et al., 2014b; Ninu et al., 2014; Pistohl et al., 2015; Markovic et al., 2017) and invasive methods based on nerve stimulation (Rossini et al., 2010; Marasco et al., 2011; Raspopovic et al., 2014; Tan et al., 2014; Ortiz-Catalan, Håkansson, and Brånemark, 2014a; Schiefer et al., 2016).

There has been experimental evidence that provision of artificial sensory feedback can enhance prosthetic control when visual information is not available (Ninu et al., 2014; Pistohl et al., 2015; Schiefer et al., 2016), under uncertainty (Saunders and Vijayakumar, 2011), or when executing complex tasks (Markovic et al., 2017). Moreover, transradial body-powered prosthesis users have expressed a desire for artificial limbs that "*require less visual attention to perform certain functions*" (Atkins, Heard, and Donovan, 1996). Although the functional benefit of artificial sensory feedback has been debated (Farina and Aszmann, 2014), it is generally accepted that it can increase the sense of ownership and embodiment of a prosthetic limb (Schiefer et al., 2016;

Marasco et al., 2011) and can also reduce the level of phantom limb pain experienced by amputees (Dietrich et al., 2012).

With regards to the work presented in this thesis, an intriguing direction for future investigation shall be the provision of multi-channel feedback conveying information about individual digit forces during proportional finger control. To this end, Raspopovic et al. (2014) inserted thin polyimide electrodes into the median and ulnar nerves of an amputee's residual limb. These two stimulation sites were used to provide feedback about the tension of the thumb/index fingers and little finger, respectively, of a robotic hand that was controlled in real-time by the participant using his EMG activity. The technique proposed by Raspopovic et al. is promising for future use in proportional finger control paradigms, since it allows for selective, multi-channel nerve stimulation. Whether providing force feedback for all available digits can be beneficial for myoelectric control remains, however, to be investigated.

9.2.5 *On bridging the gap between academia and industry*

At the time of writing, the gap between academic research in myoelectric control and industrial adoption, first pointed out by Jiang et al. (2012b), still remains. With the only exception being the Coapt Complete Control™ system (Coapt Engineering, LLC, 2013, see Section 2.4.1.3), two-site EMG control with mode switching (see Section 2.4.1.1) remains the preferred choice of the majority of upper-limb prostheses manufacturers. Thus, the question that naturally arises is: "what can researchers do to bridge this gap?" The answer to this question is rather simple; ensure that their proposed algorithms are *reliable* and *robust* under *realistic environmental conditions* (Jiang et al., 2012b).

The first step in a researcher's pipeline when proposing a novel ML-based method for myoelectric control typically concerns experimenting with datasets offline and evaluating performance based on standard metrics from the fields of statistics and ML. However, it has been demonstrated that currently used offline metrics do not correlate and, therefore, fail to predict myoelectric performance during real-time control (Jiang et al., 2014b; Ortiz-Catalan et al., 2015; Vujaklija et al., 2017). With this discrepancy being established, researchers need to seriously reconsider their current evaluation approaches and make significant progress towards developing appropriate *metrics* that could bridge the gap between offline analyses and real-time control experiments. One notable example was discussed in Section 5.4.4, where it was pointed out that although the majority of real-time classifiers are implemented using some sort of confidence-based rejection, little effort has been made in selecting algorithms or tuning hyper-parameters such that the quality of estimated posterior probabili-

ties is optimised. To this end, it was found that the *cross-entropy loss* (CEL), which is closely related to the Kullback–Leibler divergence between a target and an estimated probability distribution (see Section B.2.2), exhibited stronger correlation with a real-time performance measure, in this case *completion time* (CT), as compared to the typically used CA score. Note that these two metrics, that is, CA and CEL may often yield contradictory results in the context of algorithmic comparisons (an example is shown in Figure 5.4); therefore, it is evident that the choice of metric is crucial for algorithm/model selection and/or hyper-parameter tuning.

In the case of regression, this problem may be even more challenging. It was shown in Figure 8.19 that offline reconstruction accuracy and prosthetic control performance metrics exhibit very weak correlation, if any at all. The problem of linking the two types of measures is in this case exacerbated by the curse of dimensionality; the quality of predictions in a multidimensional space is characterised by a single scalar (e.g. multivariate *coefficient of determination* (R^2)), without taking into account the relative effect of individual target variables (i.e. joint angles or forces) on prosthetic control performance. To illustrate how this approach may prove problematic, consider an imaginary scenario where one has to choose between two regression models for deployment in a finger proportional controller. Suppose that both decoders achieve very similar accuracy scores, with the only difference being that the former yields poor predictions for the thumb opposition DOF and accurate estimates otherwise, whereas the latter yields poor predictions for the little finger DOF, but achieves high performance for decoding thumb opposition movement. These two models may be characterised by almost identical offline accuracy scores, but it is evident that from a functional perspective the latter model is clearly preferable given the importance of thumb opposition in human grasping. A potential solution to this problem might be weighting individual DOFs (i.e. dimensions) differently when calculating the overall accuracy score; however, choosing the weights in an appropriate manner may not always be straightforward.

On the other hand, despite the fact that real-time control experiments are to be trusted more and prioritised over offline analyses, they often suffer from their own limitations. Laboratory experiments typically take place under extremely controlled conditions which do not reflect the challenges present in the real world. Moreover, they often last only for a few hours —-although some studies do consider sessions over a few consecutive days—, and as a result, it is impossible to assess the long-term durability and robustness of the tested interface/controller. Ideally, prosthetic control experiments should take place outside the lab, in the wild. Modern wireless technologies allow for signal acquisition, processing, and robotic hand control using just a laptop computer and without the need for implementing prototype ap-

plications into embedded systems. Furthermore, portable computing devices, such as single-board microcontollers and computers (e.g. Arduinos and Raspberry Pis), are nowadays available at a low cost. These could be used for prototyping myoelectric control interfaces which could be then taken home by patients and used/tested over extended periods of time.

9.3 EPILOGUE

This thesis proposed computational methods for improving the control and functionality of hand prostheses. While some aspects of this work are already applicable to existing prosthetic solutions, others require further investigation and evaluation. However, they all have the following in common; they, hopefully, make an infinitesimal contribution towards the collective goal of developing dexterous and intuitively-controlled prosthetic hands, which have the power to improve the quality of life of a large number of upper-extremity amputees worldwide.

APPENDIX

A

HARDWARE

This appendix introduces the hardware used in all experiments carried out in the thesis. Section A.1 describes the system used for recording *electromyographic* (EMG) and inertial data; Section A.2 provides details about the prosthetic and robotic hands used in the experiments; finally, Section A.3 provides a description of the data glove used to record hand kinematic data.

A.1 SURFACE ELECTROMYOGRAPHY AND INERTIAL MEASUREMENT UNITS

A.1.1 *Delsys Trigno IM Wireless EMG system*

The Delsys® Trigno™ IM Wireless EMG System is a platform for recording, digitising, and transmitting EMG and inertial data. The system comprises a base station and 16 wireless sensors which are shown in Figure A.1. Each sensor incorporates an EMG electrode and a 9-*degree of freedom* (DOF) *inertial measurement unit* (IMU), that is, a tri-axial accelerometer, gyroscope, and magnetometer measuring *three-dimensional* (3D) acceleration, angular velocity, and magnetic field, respectively; therefore, the number of raw signals associated with each EMG-IMU sensor is 10 (e.g. see Figure 3.3).

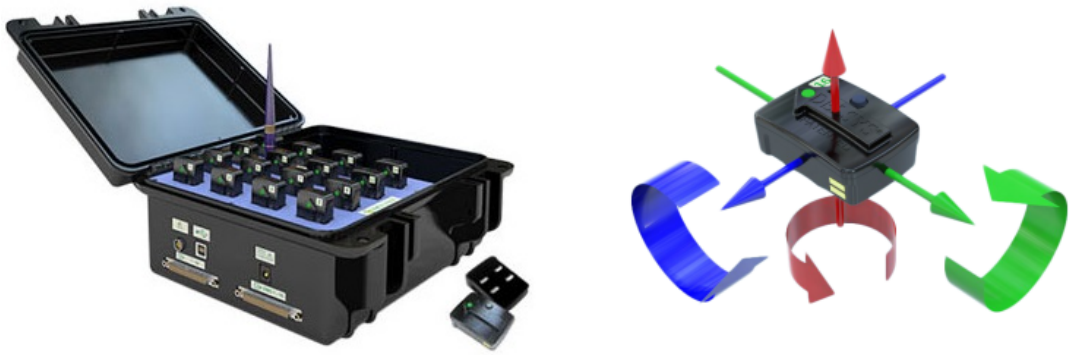

Figure A.1: Delsys® Trigno™ IM system. (Left) the full platform including the base station and sensors; (right) a single Trigno IM sensor incorporating an EMG electrode and an IMU. The IMU comprises three tri-axial components, that is, an accelerometer, a gyroscope, and a magnetometer providing 3D measurements of acceleration, angular velocity, and magnetic field, respectively. Photographs provided by and used with permission from Delsys, Inc. (Delsys, Inc., 1993).

The EMG electrodes have an input range of 11 mV, 16 bit resolution, and a bandwidth of 20-450 Hz. The electrodes use parallel bar technology comprising a total of four contacts with a fixed 1 cm spacing. The EMG hardware sampling rate is 1111 Hz. The IMUs also use 16 bit resolution and have hardware sampling rates of 148 Hz for the accelerometers and gyroscopes and 74 Hz for the magnetometers. Access to the raw data is obtained via dedicated software provided by the manufacturer that implements a TCP/IP server (i.e. *"Trigno Control Utility"*). The Wi-Fi transmission range of the sensors is 40 m (Delsys, Inc., 1993).

A.2 PROSTHETIC AND ROBOTIC HANDS

A.2.1 *Touch Bionics robo-limb*

The Touch Bionics robo-limb™ is an externally-powered, underactuated (11 DOFs, 6 *degrees of actuation* (DOAs)) anthropomorphic hand. It comprises 5 motors controlling the flexion/extension of the digits and an additional motor controlling the rotation of the thumb (see Figure A.2).

The hand operates under 7.4 V nominal voltage with a maximum current consumption of 7 A. The robo-limb weighs 507 g and has a maximum load limit of 90 kg. It can be powered by either a rechargeable set of batteries or an external power supply unit. During all experiments, the hand was externally powered with a doubly-insulated power supply unit which had been previously certified for medical experiments.

The robo-limb can be controlled by a computer via a CAN bus interface in an open-loop fashion. The control commands take the following form:

```
ID - Action - PWM,
```

where `ID` specifies the desired DOA to be activated (0-6), `Action` indicates the desired motion (open-close-stop), and `PWM` corresponds to the desired pulse width modulation level to be applied to the specified motor (in the range $[10, 127]$) and controls the velocity of movement. Whenever a motor current exceeds a pre-defined threshold set by the manufacturer, the respective digit motion is suspended. This protects the motors from overheating and also prevents the hand from crushing objects it may come in contact with (Touch Bionics, Inc., 2003).

A.2.2 *Prensilia IH2 Azzurra hand*

The Prensilia IH2 Azzurra hand is an externally-powered underactuated (11 DOFs, 5 DOAs) anthropomorphic hand. It comprises 4 intrinsic motors controlling the flexion

Figure A.2: Touch Bionics robo-limb™ prosthetic hand (right-hand model). Photograph provided by and used with permission from Touch Bionics Inc. (Touch Bionics, Inc., 2003).

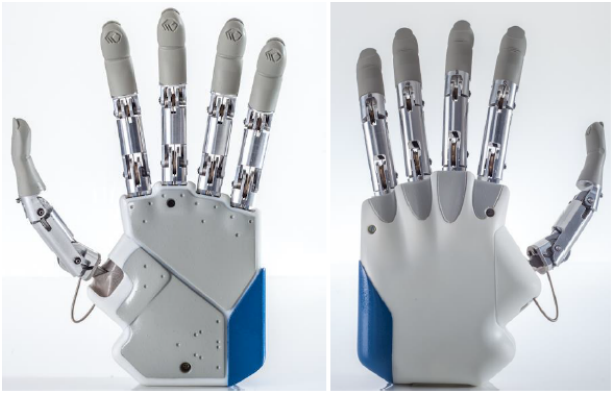

Figure A.3: Prensilia IH2 Azzurra hand (left-hand model). Palmar and dorsal views of the hand are shown. Photographs provided by and used with permission from Prensilia S.R.L. (Prensilia, S.R.L., 2009).

and extension of five digits (the ring and little fingers are mechanically coupled) and an additional motor controlling the rotation of the thumb.

Each finger has two phalanxes and is actuated by a tendon running inside them (see Figure A.3). The hand includes various sensors and encoders measuring finger positions, motor currents, and tendon tensions.

The hand weighs 640 g and operates under 9 V nominal voltage with a maximum current consumption of 5 A. It can be powered by a standard power supply unit.

The communication between the IH2 Azzurra hand and a PC is achieved via an RS232 serial protocol. The hand supports various control modes, including individual finger joint angle control, tension control, motor current control, and whole hand posture control. For the latter mode, several grasps are pre-programmed in the hardware, including cylindrical, tripod, bi-digit, lateral, and "thumb up" grasps (Prensilia, S.R.L., 2009).

A.3.1 *CyberGlove Systems CyberGlove II*

The CyberGlove Systems CyberGlove II is a motion capture system that uses resistive bend-sensing technology to measure joint angles in the human hand. It comprises a data glove and a wireless Bluetooth transmitter (see Figure A.4).

Two models are available comprising 18 and 22 sensors, respectively. The measured angles include *metacarpophalangeal* (MCP), *proximal interphalangeal* (PIP), and *distal interphalangeal* (DIP) (only for the 22-sensor model) joints, abduction between fingers, palm arch, wrist flexion, and wrist abduction (see Table A.1). The data glove sensor resolution is 1 degree and the hardware sampling rate is 90 Hz.

The CyberGlove II system operates under 8.4 V nominal voltage and is powered by a rechargeable battery. The glove and interface unit weigh 70 g and 470 g, respectively. The Wi-Fi transmission range of the system is 9.1 m (CyberGlove Systems, LLC, 1990).

A.3.1.1 *Mapping data glove measurements to degrees of actuation of the IH2 Azzurra hand*

A linear mapping between the measurements of the 18-DOF CyberGlove II and the DOAs of the IH2 Azzurra hand was created for the purposes of the finger position control experiment presented in Chapter 8. Due to cross-coupling between the data glove sensors (Wang and Neff, 2013), the mapping was identified in a heuristic fashion and its validity was subsequently verified with a test involving tele-operating the robotic hand in real-time using the data glove.

Let $\mathbf{x} \in \mathbb{R}^{18}$ denote the calibrated measurements returned by the data glove (see Table A.1) and $\mathbf{y} \in \mathbb{R}^{5}$ the digit position vector of the DOAs of the hand. The elements in $\mathbf{y}$ are ordered as follows: y_1, thumb rotation; y_2, thumb flexion; y_3, index flexion;

Figure A.4: CyberGlove Systems CyberGlove II data glove (right-hand model). The data glove and interface unit are shown. Photograph provided by and used with permission from CyberGlove Systems LLC (CyberGlove Systems, LLC, 1990).

Table A.1: CyberGlove II sensors

	18-sensor model	22-sensor model
Thumb rotation	1	1
Thumb MCP joint	2	2
Thumb PIP joint	3	3
Thumb-index abbduction	4	4
Index MCP joint	5	5
Index PIP joint	6	6
Index DIP joint	-	7
Middle MCP joint	7	8
Middle PIP joint	8	9
Middle DIP joint	-	10
Index-middle abduction	9	11
Ring MCP joint	10	12
Ring PIP joint	11	13
Ring DIP joint	-	14
Middle-ring abduction	12	15
Little MCP joint	13	16
Little PIP joint	14	17
Little DIP joint	-	18
Ring-little abduction	15	19
Palm arch	16	20
Wrist flexion	17	21
Wrist abduction	18	22

y_4, middle flexion; y_5, ring/little flexion. The calibrated data glove measurements are then mapped into robotic digit positions via a linear mapping:

$$\mathbf{y} = \mathbf{A}\mathbf{x}. \tag{A.1}$$

The transformation matrix $\mathbf{A}$ was selected as follows:

$$\mathbf{A}^\top = \begin{bmatrix} 0.639 & 0 & 0 & 0 & 0 \\ 0.383 & 0 & 0 & 0 & 0 \\ 0 & 1 & 0 & 0 & 0 \\ -0.639 & 0 & 0 & 0 & 0 \\ 0 & 0 & 0.4 & 0 & 0 \\ 0 & 0 & 0.6 & 0 & 0 \\ 0 & 0 & 0 & 0.4 & 0 \\ 0 & 0 & 0 & 0.6 & 0 \\ 0 & 0 & 0 & 0 & 0 \\ 0 & 0 & 0 & 0 & 0.1667 \\ 0 & 0 & 0 & 0 & 0.3333 \\ 0 & 0 & 0 & 0 & 0 \\ 0 & 0 & 0 & 0 & 0.1667 \\ 0 & 0 & 0 & 0 & 0.3333 \\ 0 & 0 & 0 & 0 & 0 \\ 0 & 0 & 0 & 0 & 0 \\ -0.19 & 0 & 0 & 0 & 0 \\ 0 & 0 & 0 & 0 & 0 \\ 0 & 0 & 0 & 0 & 0 \end{bmatrix} \tag{A.2}$$

B

CLASSIFICATION METRICS

B.1 TERMINOLOGY

In statistics and *machine learning* (ML) *classification* is the process of assigning an observation represented by an input vector $\mathbf{x}$ to a category (i.e. class) c which is part of a larger set of categories. In ML and pattern recognition, classification is a special case of *supervised learning*. Usually, a *training set* containing examples whose class membership is known is required, which can be used to *train* a classification model before the latter can be employed to generate predictions on a *test set*, which is a collection of examples with unknown class membership. *Binary classification* is a special case where there are only two possible classes. In the general case, the cardinality of the class set can be an arbitrary natural number C (*multi-class classification*).

Assume a binary classification problem with a positive and a negative class. The following terminology is introduced (Fawcett, 2006):

- **Condition positive** (P) is the number of real positive instances in the data.
- **Condition negative** (N) is the number of real negative instances in the data.
- **True positive** or **hit** (TP) is the number of real positive instances in the data classified as positive.
- **True negative** or **correct rejection** (TN) is the number of real negative instances in the data classified as negative.
- **False positive**, **false alarm**, or **Type I error** (FP) is the number of real negative instances in the data classified as positive.
- **False negative**, **miss**, or **Type II error** (FN) is the number of real positive instances in the data classified as negative.

B.2 METRICS

In this section, some of the most common metrics used to characterise the performance of a binary classifier are introduced:

- **True positive rate**, **sensitivity**, **recall**, or **hit rate**:

$$\mathrm{TPR} = \frac{\mathrm{TP}}{\mathrm{P}} = \frac{\mathrm{TP}}{\mathrm{TP} + \mathrm{FN}} \tag{B.1}$$

- **True negative rate** or **specificity**:

$$\mathrm{TNR} = \frac{\mathrm{TN}}{\mathrm{N}} = \frac{\mathrm{TN}}{\mathrm{TN} + \mathrm{FP}} \tag{B.2}$$

- **Positive predictive value** or **precision**:

$$\mathrm{PPV} = \frac{\mathrm{TP}}{\mathrm{TP} + \mathrm{FP}} \tag{B.3}$$

- **Negative predictive value**:

$$\mathrm{NPV} = \frac{\mathrm{TN}}{\mathrm{TN} + \mathrm{FN}} \tag{B.4}$$

- **False positive rate** or **fallout**:

$$\mathrm{FPR} = \frac{\mathrm{FP}}{\mathrm{N}} = \frac{\mathrm{FP}}{\mathrm{FP} + \mathrm{TN}} = 1 - \mathrm{TNR} \tag{B.5}$$

- **False negative rate** or **miss rate**:

$$\mathrm{FNR} = \frac{\mathrm{FN}}{\mathrm{P}} = \frac{\mathrm{FN}}{\mathrm{FN} + \mathrm{TP}} = 1 - \mathrm{TPR} \tag{B.6}$$

- **False discovery rate**:

$$\mathrm{FDR} = \frac{\mathrm{FP}}{\mathrm{FP} + \mathrm{TP}} = 1 - \mathrm{PPV} \tag{B.7}$$

- **False omission rate**:

$$\mathrm{FOR} = \frac{\mathrm{FN}}{\mathrm{FN} + \mathrm{TN}} = 1 - \mathrm{NPV} \tag{B.8}$$

- **Classification accuracy**:

$$\mathrm{CA} = \frac{\mathrm{TP} + \mathrm{TN}}{\mathrm{P} + \mathrm{N}} = \frac{\mathrm{TP} + \mathrm{TN}}{\mathrm{TP} + \mathrm{TN} + \mathrm{FP} + \mathrm{FN}} \tag{B.9}$$

- **F1-score**:

$$\mathrm{F1} - \mathrm{score} = 2 \cdot \frac{\mathrm{PPV} \cdot \mathrm{TPR}}{\mathrm{PPV} + \mathrm{TPR}} = \frac{2\mathrm{TP}}{2\mathrm{TP} + \mathrm{FP} + \mathrm{FN}} \tag{B.10}$$

B.2.1 *Confusion matrix*

A confusion matrix is a table which can be used to visualise the performance of a classifier. Columns and rows in the confusion matrix represent predicted and true classes, respectively. The $\{i, j\}$ cell of the matrix represents the number of instances in class j predicted as class i. The structure of a confusion matrix for a binary classifier is shown in Table B.1.

B.2.2 *Cross-entropy loss*

Most binary classifiers do not simply yield a classification prediction for a test example (i.e. positive vs. negative class), but rather compute class posterior probabilities. A typical example of *probabilistic classification* is logistic regression, wherein the probability of a test example being assigned to the positive class is modelled as follows:

$$p_+(\mathbf{x}_*) = \sigma\left(\boldsymbol{w}^\top \mathbf{x}_* + b\right), \tag{B.11}$$

where $\boldsymbol{w}$ and b are the model parameters, and $\sigma(\cdot)$ denotes the logistic function.

The *cross-entropy loss* (CEL), also called logistic loss, is used to evaluate the probability outputs of a classifier. It is closely related to the *Kullback-Leibler divergence* between the empirical and estimated distributions of the examples in the test set. Let $y \in \{0, 1\}$ denote a binary target variable with a probability estimate for the i^{th} example $\hat{p}_i = \Pr(y_i = 1)$. The CEL for a set containing N test examples is computed as:

$$\text{CEL} = -\frac{1}{N}\sum_{i=1}^{N} (y_i \log(\hat{p}_i)) + (1 - y_i)\log(1 - \hat{p}_i) \tag{B.12}$$

In the ideal case, that is, when all examples in a dataset are correctly classified and the corresponding posterior probabilities are equal to 1, the CEL will be equal to 0. On the other hand, there is no lower bound for CEL. That is, poor probability predictions can yield arbitrarily low (i.e. large negative) scores.

B.2.3 *Extension to multi-class problems*

The extension of most classification metrics introduced in this section to the multi-class case is not always trivial. Usually, the multi-class problem needs to be converted

Table B.1: Confusion matrix for binary classification task

		Predicted class	
		Positive	Negative
True class	Positive	TP	FN
	Negative	FP	TN

into multiple one-vs.-all binary problems, so that average metrics can be computed across the set of binary classifiers.

Nevertheless, extensions of the CA and CEL metrics are rather straightforward. Let $y \in \{1, \ldots, C\}$ denote a discrete target variable which is encoded as a "one-of-K" binary indicator matrix Y of dimensionality $N \times C$, such that:

$$y_{i,c} = \begin{cases} 1, & \text{if sample } i \text{ has label } c, \\ 0, & \text{otherwise.} \end{cases} \tag{B.13}$$

The multi-class CA and CEL metrics are defined as follows:

$$CA = \frac{1}{N} \sum_{i=1}^{N} \sum_{c=1}^{C} y_{i,c} \hat{y}_{i,c}, \tag{B.14}$$

and

$$CEL = -\frac{1}{N} \sum_{i=1}^{N} \sum_{c=1}^{C} y_{i,c} \log \left(\hat{p}_{i,c} \right), \tag{B.15}$$

where $\hat{y}_{i,c}$ and $\hat{p}_{i,c}$ denote the elements of the predicted indicator matrix $\hat{Y}$ and their respective posterior probabilities.

B.3 RECEIVING OPERATING CHARACTERISTICS ANALYSIS

B.3.1 *The rejection option*

In some applications it might be appropriate to avoid making classification decisions unless they are predicted with high confidence. This can be achieved by setting a rejection threshold θ for the class posterior probabilities such that a decision can only be made if there is a class c whose posterior probability $\hat{p}_c$ exceeds θ, i.e. $\hat{p}_c > \theta$.

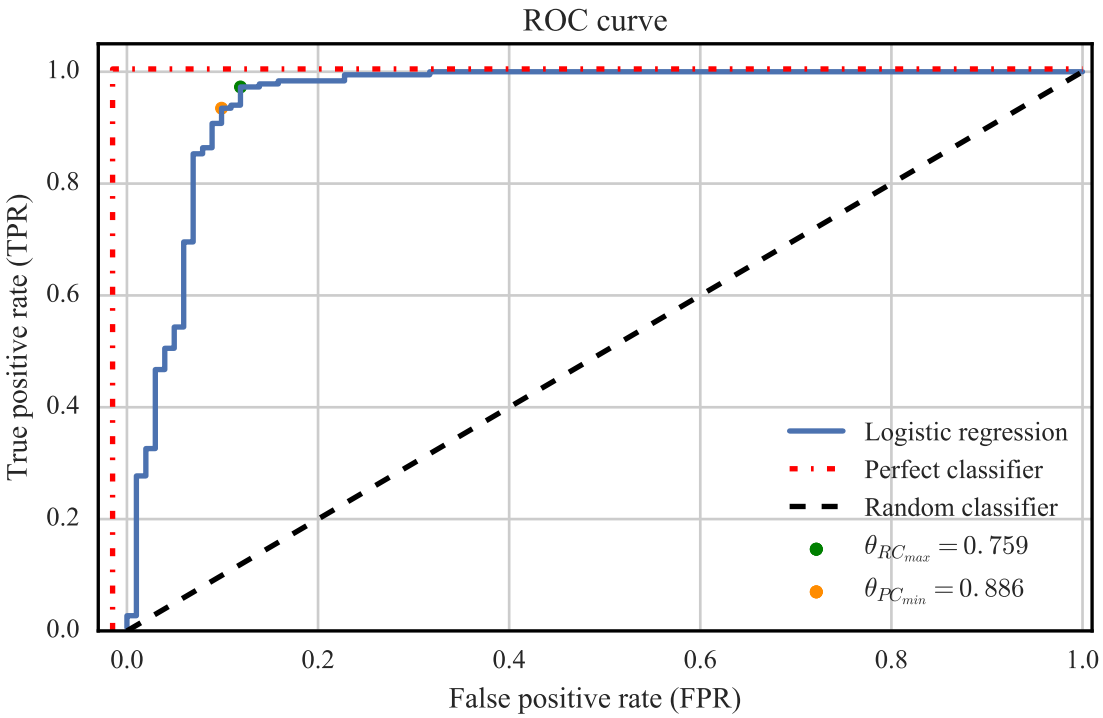

Figure B.1: ROC curve example. ROC curves shown for three classifiers on the breast cancer dataset (Street, Wolberg, and Mangasarian, 1993); logistic regression (blue), perfect classifier (red), and random classifier (black). The optimal thresholds selected with maximum distance from random classifier and minimum distance from perfect classifier strategies are shown with a green and orange dot, respectively.

B.3.2 *Receiving operating characteristic curves*

The *receiving operating characteristic* (ROC) curve is a graphical plot that allows evaluating the trade-off between the TPR and FPR of a binary classifier as its rejection threshold θ is varied. It is created by plotting the TPR against the FPR of the classifier at various threshold settings. The area under the ROC curve is a classification metric commonly used to summarise the curve information.

There exist various techniques for rejection threshold selection based on ROC analysis. Two common strategies are:

- *Distance minimisation from perfect classifier* selects the threshold with minimal distance from the point (0,1), which corresponds to a perfect classifier.
- *Distance maximisation from random classifier* selects the threshold with maximal vertical distance from the line $x = y$, which corresponds to a random binary classifier.

An example of a typical ROC curve for a binary classification task is shown in Figure B.1. Rejection thresholds selected with the two criteria introduced above are also shown in the same plot.

B.3.3 *Extension to multi-class problems*

Extension of ROC analysis to multi-class problems is not straightforward. Again, a common strategy is to break down the multi-class problem into multiple one-vs.-all binary classification tasks and perform separate ROC analyses within each of the binary tasks (Landgrebe and Duin, 2007).

C

REGRESSION METRICS

C.1 TERMINOLOGY

In statistics and *machine learning* (ML) regression is a process of estimating the relationship between a set of independent variables $\{x_1, x_2, \ldots, x_D\}$ and a dependent variable y, usually through a set of parameters $\theta = \{\theta_1, \theta_2, \ldots, \theta_Q\}$:

$$y \approx f(\mathbf{x}, \theta). \tag{C.1}$$

Linear regression (LR) is the simplest case where a linear relationship is assumed between the independent and dependent variables. The model also assumes an error variable ϵ that is unobservable and adds noise to the linear relationship:

$$y = \theta_0 1 + \theta_1 x_1 + \ldots + \theta_D x_D + \epsilon = \theta^\top \mathbf{x} + \epsilon, \tag{C.2}$$

where $\mathbf{x} = [1, x_1, x_2, \ldots, x_D]$ and $\theta = [\theta_0, \theta_1, \theta_2, \ldots, \theta_D]$. The special case where there is a signal independent variable x is called *simple linear regression*, as compared to the general case where $\mathbf{x}$ is d-dimensional and which is called *multiple linear regression* (MLR) or *multivariable linear regression*. The target variable may be either single-dimensional (i.e. scalar) or multidimensional (i.e. vector). The latter case is called *multivariate linear regression*.

Nonlinear regression methods model the relationship between the independent and dependent variables with nonlinear functions. Some examples of nonlinear regression include *kernel ridge regression* (KRR), Gaussian process regression, and support vector regression with non-linear kernels.

C.2.1 *Sample mean and variance*

Let x denote a single random variable and $\mathcal{D} = \{x_1, x_2, \ldots, x_N\}$ be a collection of measurements of the variable (i.e. *dataset*). The sample mean and variance of x can be estimated from the dataset as follows:

$$\bar{x} = \frac{1}{N} \sum_{n=1}^{N} x_n, \tag{C.3}$$

and

$$\sigma_x^2 = \frac{1}{N-1} \sum_{n=1}^{N} (x_n - \bar{x})^2 . \tag{C.4}$$

C.2.2 *Metrics*

Assume a scalar target variable y and a dataset comprising N instances of the variable with values $y_1, y_2, \ldots y_N$ each associated with a predicted value by a regression model $\hat{y}_1, \hat{y}_2, \ldots, \hat{y}_N$. The following regression performance metrics are defined:

- **Mean absolute error**:

$$\text{MAE} = \frac{1}{N} \sum_{n=1}^{N} |y_n - \hat{y}_n| \tag{C.5}$$

- **Median absolute error**:

$$\text{MedAE} = \text{median}\left(|y_1 - \hat{y}_1|, |y_2 - \hat{y}_2|, \ldots, |y_N - \hat{y}_N|\right) \tag{C.6}$$

- **Mean squared error**:

$$\text{MSE} = \frac{1}{N} \sum_{n=1}^{N} (y_n - \hat{y}_n)^2 \tag{C.7}$$

- **Root mean squared error**:

$$\text{RMSE} = \sqrt{\frac{\sum_{n=1}^{N} (y_n - \hat{y}_n)^2}{N}} \tag{C.8}$$

- **Normalised root mean squared error**:

$$\text{NRMSE} = \frac{\text{RMSE}}{y_{max} - y_{min}} = \frac{\sqrt{\frac{\sum_{n=1}^{N}(y_n - \hat{y}_n)^2}{N}}}{y_{max} - y_{min}} \tag{C.9}$$

- **Variance accounted for**, or **explained variance score**:

$$\text{VAF} = 1 - \frac{\sigma^2_{y-\hat{y}}}{\sigma^2_y} \tag{C.10}$$

- **Coefficient of determination**, or **R^2-score**:

$$R^2 = 1 - \frac{\sum_{n=1}^{N}(y_n - \hat{y}_n)^2}{\sum_{n=1}^{N}(y_n - \bar{y})^2}, \tag{C.11}$$

- **Correlation coefficient**:

$$\text{CC} = \frac{\sum_{n=1}^{N}(y_n - \bar{y})(\hat{y}_n - \bar{\hat{y}})}{\sqrt{\sum_{n=1}^{N}(y_n - \bar{y})^2}\sqrt{\sum_{n=1}^{N}(\hat{y}_n - \bar{\hat{y}})^2}} \tag{C.12}$$

C.2.2.1 *Properties*

The following metrics are non-negative by definition: MAE, MedAE, MSE, RMSE, NRMSE, and CC. The CC metric is additionally right-bounded at 1. The metrics VAF and R^2 are right-bounded at 1, but can take arbitrarily large negative values.

The CC is scale and offset invariant. For that reason, its use as a regression performance metric should be generally avoided.

C.2.2.2 *Multivariate extensions*

Various extensions exist for multivariate target variables. Some commonly used choices include uniform or weighted averages across the target variable dimensions. In this thesis, a multivariate version of R^2 is extensively used, which is defined as follows:

$$R^2_{MV} = 1 - \frac{\sum_{k=1}^{K}\sum_{n=1}^{N}(y_{k,n} - \hat{y}_{k,n})^2}{\sum_{k=1}^{K}\sum_{n=1}^{N}(y_{k,n} - \bar{y}_k)^2}, \tag{C.13}$$

where K denotes the dimensionality of the target variable, $y_{k,n}$ and $\hat{y}_{k,n}$ are the n^{th} observed and predicted values, respectively, of the k^{th} output variable, and $\bar{y}_k$ denotes the sample mean of the k^{th} output variable.

D

ETHICS PROCEDURES AND EXPERIMENTAL FORMS

All experiments involving human participants were approved by the local Ethics Committees of the School of Informatics, University of Edinburgh and School of Electrical and Electronic Engineering, Newcastle University.

Prior to the experiments, all subjects read a participant information sheet and signed an informed consent participation form. The forms used for one of the experiments (Chapter 5) are attached in this appendix.

THE UNIVERSITY of EDINBURGH
informatics

Participant Information Sheet

Study title: Prosthetic hand control with electromyography

1. Aim of the study

This study aims to analyse the different parameters of muscle activity and cognitive skills that allow a person to use their hands for daily life activities. The results of the study aim to enable amputees to learn how to control a prosthetic hand for functional movements.

2. Execution of the study

The data collection sessions will be conducted by researchers trained for this purpose. During the first part of the experiment, you will be instructed to perform a series of movements with your hand, while a set of electrodes (attached to your forearm with adhesive tape) will record muscular activity data and transmit them to a computer. During the second part of the experiment, a prosthetic hand will be attached to your forearm and you will be instructed to use it to perform the same series of movements as in the first part. Task completion rates and times will be monitored and stored in electronic format. In addition, you will be asked to fill in a consent form, a clinical and experimental data form and a payment receipt confirmation.

3. Your participation

The data acquisition session will last for approximately 150 minutes and will take place in room 1.30 of the Informatics Forum, University of Edinburgh. Participation in this study is entirely voluntary. You can refuse to take part or withdraw from the study at any time without having to give a reason. Such a decision has no adverse implications for you.

4. Risk assessment

Your participation to this study does not involve any risk. The electrodes attached to your forearm do not send any current. Slight discomfort might be caused by the socket hosting the prosthetic hand.

5. Privacy

All data acquired will be treated confidentially. The data might be disclosed anonymously to third parties for the purposes of the study. Your personal information will be stored separately to ensure data protection.

6. Contact

If you have any questions or require further information please do not hesitate to contact Mr. Agamemnon Krasoulis (a.krasoulis@sms.ed.ac.uk).

School of Informatics, 10 Crichton Street, Edinburgh, (City of) Edinburgh, EH8 9AB

THE UNIVERSITY of EDINBURGH
informatics

Informed Consent Form

Study title: Prosthetic hand control with electromyography

1. I confirm that I have read and understood the Participant Information Sheet for the above study and there is no reason I should not take part. I have had the opportunity to consider the information and ask questions, and have had these answered satisfactorily.

2. I understand that my participation is entirely voluntary and I am free to withdraw at any time without giving a reason.

3. I certify that I have been informed that the data collected during the study will be shared with the scientific community in respect of anonymity, Only researchers directly involved with the data acquisition and storage will have direct knowledge of my identity, and they will be bound by professional secrecy.

4. I understand that there are no risks involved in the participation of this study.

5. I agree to take part in this study.

….....	….....	….....
Name of participant	Date	Signature
….....	….....	….....
Name of researcher	Date	Signature

Clinical and Experimental Form

Study title: Prosthetic hand control with electromyography

To be completed by the researcher:

Subject Number	
Forearm circumference (cm)	
Location	
Date	
Time	
Dash score	

To be completed by the participant:

Personal information	
First name	
Family name	
Phone number	
E-mail address	

Clinical information	
Age	
Gender	
Weight	
Height	
Laterality (left or right handed)	
Job	
Hobbies related to use of hands	

THE UNIVERSITY of EDINBURGH
informatics

Payment receipt confirmation

Study title: Prosthetic hand control with electromyography

I certify that I was paid £ .... by Agamemnon Krasoulis for participating in this experiment.

….....	….....	….....
Name of participant	Date	Signature

E

SUPPLEMENTARY MATERIAL

Five video recordings are included in the provided supplementary material.

- **SV1**: Video recording from the real-time experiment presented in Chapter 3 corresponding to condition I (EMG). One trial shown for an amputee participant. Format, MP4; size, 71.6 MB.
- **SV2**: Video recording from the real-time experiment presented in Chapter 3 corresponding to condition IV (EMG-IMU (subset)). One trial shown for the same amputee participant as in SV1. Format, MP4; size, 37.6 MB.
- **SV3**: Video recording from the real-time experiment presented in Chapter 5. One trial shown for an amputee participant. Format, MP4; size, 12.7 MB.
- **SV4**: Video recording from the real-time experiment presented in Chapter 8 (posture matching task). Six trials shown from one block for an amputee participant. Format, MP4; size, 31.7 MB.
- **SV5**: Video recording from the real-time experiment presented in Chapter 8 (pick and place task). One trial shown for an able-bodied participant. Format, MP4; size, 25.1 MB.

BIBLIOGRAPHY

Adewuyi, A. A., L. J. Hargrove, and T. A. Kuiken (2016). "An analysis of intrinsic and extrinsic hand muscle EMG for improved pattern recognition control." In: *IEEE Transactions on Neural Systems and Rehabilitation Engineering* 24.4, pp. 485–494.

Afshar, P. and Y. Matsuoka (2004). "Neural-based control of a robotic hand: evidence for distinct muscle strategies." In: *2004 IEEE International Conference on Robotics and Automation (ICRA)*. Vol. 5. IEEE, pp. 4633–4638.

Ajiboye, A. B. and R. F. ff Weir (2009). "Muscle synergies as a predictive framework for the EMG patterns of new hand postures." In: *Journal of Neural Engineering* 6.3, p. 036004.

Al-Timemy, A. H., G. Bugmann, J. Escudero, and N. Outram (2013). "Classification of finger movements for the dexterous hand prosthesis control with surface electromyography." In: *IEEE Journal of Biomedical and Health Informatics* 17.3, pp. 608–618.

Al-Timemy, A. H., R. N. Khushaba, G. Bugmann, and J. Escudero (2016). "Improving the performance against force variation of EMG controlled multifunctional upper-limb prostheses for transradial amputees." In: *IEEE Transactions on Neural Systems and Rehabilitation Engineering* 24.6, pp. 650–661.

Allen, D. P. (2009). "A frequency domain Hampel filter for blind rejection of sinusoidal interference from electromyograms." In: *Journal of Neuroscience Methods* 177.2, pp. 303–310.

Ameri, A., E. J. Scheme, E. N. Kamavuako, K. B. Englehart, and P. A. Parker (2014a). "Real-time, simultaneous myoelectric control using force and position-based training paradigms." In: *IEEE Transactions on Biomedical Engineering* 61.2, pp. 279–287.

Ameri, A., E. N. Kamavuako, E. J. Scheme, K. B. Englehart, and P. A. Parker (2014b). "Support vector regression for improved real-time, simultaneous myoelectric control." In: *IEEE Transactions on Neural Systems and Rehabilitation Engineering* 22.6, pp. 1198–1209.

Amsüss, S. (2014). "Robust electromyography based control of multifunctional prostheses of the upper extremity." PhD thesis. University of Göttingen.

Amsuss, S., L. P. Paredes, N. Rudigkeit, B. Graimann, M. J. Herrmann, and D. Farina (2013). "Long term stability of surface EMG pattern classification for prosthetic control." In: *2013 35th Annual International Conference of the IEEE Engineering in Medicine and Biology Society (EMBC)*. IEEE, pp. 3622–3625.

Amsüss, S., P. M. Goebel, N. Jiang, B. Graimann, L. Paredes, and D. Farina (2014). "Self-correcting pattern recognition system of surface EMG signals for upper limb prosthesis control." In: *IEEE Transactions on Biomedical Engineering* 61.4, pp. 1167–1176.

Antonelli, M. G., P. Beomonte Zobel, and J. Giacomin (2009). "Use of MMG signals for the control of powered orthotic devices: development of a rectus femoris measurement protocol." In: *Assistive Technology* 21.1, pp. 1–12.

Artemiadis, P. and K. Kyriakopoulos (2010). "EMG-based control of a robot arm using low-dimensional embeddings." In: *IEEE Transactions on Robotics* 26.2, pp. 393–398.

Atkins, D. J., D. C. Heard, and W. H. Donovan (1996). "Epidemiologic overview of individuals with upper-limb loss and their reported research priorities." In: *JPO Journal of Prosthetics and Orthotics* 8.1, pp. 2–11.

Atzori, M., M. Cognolato, and H. Müller (2016). "Deep learning with convolutional neural networks applied to electromyography data: a resource for the classification of movements for prosthetic hands." In: *Frontiers in Neurorobotics* 10.

Atzori, M. and H. Müller (2015). "Control capabilities of myoelectric robotic prostheses by hand amputees: a scientific research and market overview." In: *Frontiers in Systems Neuroscience* 9.

Atzori, M., A. Gijsberts, S. Heynen, A.-G. M. Hager, O. Deriaz, P. van der Smagt, C. Castellini, B. Caputo, and H. Müller (2012). "Building the Ninapro database: a resource for the biorobotics community." In: *2012 4th IEEE RAS & EMBS International Conference on Biomedical Robotics and Biomechatronics (BioRob)*. IEEE, pp. 1258–1265.

Atzori, M., A. Gijsberts, C. Castellini, B. Caputo, A.-G. M. Hager, S. Elsig, G. Giatsidis, F. Bassetto, and H. Müller (2014). "Electromyography data for non-invasive naturally-controlled robotic hand prostheses." In: *Scientific Data* 1, p. 140053.

Atzori, M., A. Gijsberts, I. Kuzborskij, S. Elsig, A.-G. Mittaz Hager, O. Deriaz, C. Castellini, H. Müller, and B. Caputo (2015). "Characterization of a benchmark database for myoelectric movement classification." In: *IEEE Transactions on Neural Systems and Rehabilitation Engineering* 23.1, pp. 73–83.

Barnes, J., M. Dyson, and K. Nazarpour (2016). "Comparison of hand and forearm muscle pairs in controlling of a novel myoelectric interface." In: *2016 IEEE International Conference on Systems, Man, and Cybernetics (SMC)*. IEEE, pp. 2846–2849.

Battye, C. K., A. Nightingale, and J. Whillis (1955). "The use of myo-electric currents in the operation of prostheses." In: *Bone & Joint Journal* 37.3, pp. 506–510.

Batzianoulis, I., S. El-Khoury, E. Pirondini, M. Coscia, S. Micera, and A. Billard (2017). "EMG-based decoding of grasp gestures in reaching-to-grasping motions." In: *Robotics and Autonomous Systems* 91, pp. 59–70.

Berger, D. J. and A. D'Avella (2014). "Effective force control by muscle synergies." In: *Frontiers in Computational Neuroscience* 8.

Betthauser, J. L., C. L. Hunt, L. E. Osborn, M. R. Masters, G. Levay, R. R. Kaliki, and N. V. Thakor (2017). "Limb position tolerant pattern recognition for myoelectric prosthesis control with adaptive sparse representations from extreme learning." In: *IEEE Transactions on Biomedical Engineering* (In press).

Biddiss, E. A. and T. T. Chau (2007). "Upper limb prosthesis use and abandonment: a survey of the last 25 years." In: *Prosthetics and Orthotics International* 31.3, pp. 236–257.

Biddiss, E., D. Beaton, and T. Chau (2007). "Consumer design priorities for upper limb prosthetics." In: *Disability and Rehabilitation: Assistive Technology* 2.6, pp. 346–357.

Birdwell, J. A., L. J. Hargrove, T. A. Kuiken, and R. F. ff Weir (2013). "Activation of individual extrinsic thumb muscles and compartments of extrinsic finger muscles." In: *Journal of Neurophysiology* 110.6, pp. 1385–1392.

Birdwell, J. A., L. J. Hargrove, R. F. ff Weir, and T. A. Kuiken (2015). "Extrinsic finger and thumb muscles command a virtual hand to allow individual finger and grasp control." In: *IEEE Transactions on Biomedical Engineering* 62.1, pp. 218–226.

Bishop, C. M. (2006). *Pattern recognition and machine learning*. Springer.

Bizzi, E., F. A. Mussa-Ivaldi, and S. Giszter (1991). "Computations underlying the execution of movement: a biological perspective." In: *Science* 253.5017, pp. 287–291.

Blana, D., E. K. Chadwick, A. J. van den Bogert, and W. M. Murray (2017). "Real-time simulation of hand motion for prosthesis control." In: *Computer Methods in Biomechanics and Biomedical Engineering* 20.5, pp. 540–549.

Boostani, R. and M. H. Moradi (2003). "Evaluation of the forearm EMG signal features for the control of a prosthetic hand." In: *Physiological Measurement* 24.2, pp. 309–319.

Borga, M., T. Landelius, and H. Knutsson (1992). *A unified approach to pca, pls, mlr and cca*. Tech. rep. LiTH–ISY–R–1992. Linköping University, Department of Electrical Engineering.

Boschmann, A. and M. Platzner (2013). "Reducing the limb position effect in pattern recognition based myoelectric control using a high density electrode array." In: *2013 ISSNIP Biosignals and Biorobotics Conference: Biosignals and Robotics for Better and Safer Living (BRC)*. IEEE, pp. 1–5.

Breiman, L. (2001). "Random forests." In: *Machine learning* 45.1, pp. 5–32.

Brochier, T, R. L. Spinks, M. A. Umilta, and R. N. Lemon (2004). "Patterns of muscle activity underlying object-specific grasp by the macaque monkey." In: *Journal of Neurophysiology* 92.3, pp. 1770–1782.

Buchthal, F. and H. Schmalbruch (1980). "Motor unit of mammalian muscle." In: *Physiological Reviews* 60.1, pp. 90–142.

Castellini, C. and R. Koiva (2012). "Using surface electromyography to predict single finger forces." In: *2012 4th IEEE RAS & EMBS International Conference on Biomedical Robotics and Biomechatronics (BioRob)*. IEEE, pp. 1266–1272.

Castellini, C. and P. van der Smagt (2009). "Surface EMG in advanced hand prosthetics." In: *Biological Cybernetics* 100.1, pp. 35–47.

Castellini, C. and P. van der Smagt (2013). "Evidence of muscle synergies during human grasping." In: *Biological Cybernetics* 107.2, pp. 233–245.

Castellini, C., E. Gruppioni, A. Davalli, and G. Sandini (2009). "Fine detection of grasp force and posture by amputees via surface electromyography." In: *Journal of Physiology-Paris* 103.3-5, pp. 255–262.

Catalano, M., G. Grioli, E. Farnioli, A. Serio, C. Piazza, and A. Bicchi (2014). "Adaptive synergies for the design and control of the Pisa/IIT SoftHand." In: *The International Journal of Robotics Research* 33.5, pp. 768–782.

Cavanagh, P. R. and P. V. Komi (1979). "Electromechanical delay in human skeletal muscle under concentric and eccentric contractions." In: *European Journal of Applied Physiology and Occupational Physiology* 42.3, pp. 159–163.

Celadon, N., S. Došen, I. Binder, P. Ariano, and D. Farina (2016). "Proportional estimation of finger movements from high-density surface electromyography." In: *Journal of NeuroEngineering and Rehabilitation* 13.1, p. 73.

Chan, A. D. C. and K. B. Englehart (2005). "Continuous myoelectric control for powered prostheses using hidden Markov models." In: *IEEE Transactions on Biomedical Engineering* 52.1, pp. 121–124.

Chan, F., Y.-S. Yang, F. Lam, Y.-T. Zhang, and P. A. Parker (2000). "Fuzzy EMG classification for prosthesis control." In: *IEEE Transactions on Rehabilitation Engineering* 8.3, pp. 305–311.

Chen, X., D. Zhang, and X. Zhu (2013). "Application of a self-enhancing classification method to electromyography pattern recognition for multifunctional prosthesis control." In: *Journal of NeuroEngineering and Rehabilitation* 10.1, p. 44.
Chianura, A. and M. E. Giardini (2010). "An electrooptical muscle contraction sensor." In: *Medical & Biological Engineering & Computing* 48.7, pp. 731–734.
Cho, E., R. Chen, L.-K. Merhi, Z. Xiao, B. Pousett, and C. Menon (2016). "Force myography to control robotic upper extremity prostheses: a feasibility study." In: *Frontiers in Bioengineering and Biotechnology* 4.
Choi, C. and J. Kim (2011). "Synergy matrices to estimate fluid wrist movements by surface electromyography." In: *Medical Engineering & Physics* 33.8, pp. 916–923.
Cipriani, C., C. Antfolk, M. Controzzi, G. Lundborg, B. Rosen, M. C. Carrozza, and F. Sebelius (2011). "Online myoelectric control of a dexterous hand prosthesis by transradial amputees." In: *IEEE Transactions on Neural Systems and Rehabilitation Engineering* 19.3, pp. 260–270.
Cipriani, C., M. Controzzi, G. Kanitz, and R. Sassu (2012). "The effects of weight and inertia of the prosthesis on the sensitivity of electromyographic pattern recognition in relax state." In: *JPO Journal of Prosthetics and Orthotics* 24.2, pp. 86–92.
Cipriani, C., J. L. Segil, J. A. Birdwell, and R. F. ff Weir (2014a). "Dexterous control of a prosthetic hand using fine-wire intramuscular electrodes in targeted extrinsic muscles." In: *IEEE Transactions on Neural Systems and Rehabilitation Engineering* 22.4, pp. 828–836.
Cipriani, C., J. L. Segil, F. Clemente, R. F. ff Weir, and B. Edin (2014b). "Humans can integrate feedback of discrete events in their sensorimotor control of a robotic hand." In: *Experimental Brain Research* 232.11, pp. 3421–3429.
Clancy, E. A., C. Martinez-Luna, M. Wartenberg, C. Dai, and T. R. Farrell (2017). "Two degrees of freedom quasi-static EMG-force at the wrist using a minimum number of electrodes." In: *Journal of Electromyography and Kinesiology* 34, pp. 24–36.
Coapt Engineering, LLC (2013). URL: http://www.coaptengineering.com/ (visited on Aug. 1, 2017).
Cochran, W. G. (1950). "The comparison of percentages in matched samples." In: *Biometrika* 37.3/4, pp. 256–266.
Cohen, D. and E. Givler (1972). "Magnetomyography: magnetic fields around the human body produced by skeletal muscles." In: *Applied Physics Letters* 21.3, pp. 114–116.
Cromwell, F. S. (1960). *Occupational Therapist's Manual for Basic Skills Assessment Or Primary Pre-vocational Evaluation*. Fair Oaks Print. Company.
CyberGlove Systems, LLC (1990). URL: http://www.cyberglovesystems.com/ (visited on Aug. 1, 2017).
D'Avella, A. and M. C. Tresch (2001). "Modularity in the motor system: decomposition of muscle patterns as combinations of time-varying synergies." In: *Advances in Neural Information Processing Systems*. MIT Press, pp. 141–148.
D'Avella, A. and E. Bizzi (2005). "Shared and specific muscle synergies in natural motor behaviors." In: *Proceedings of the National Academy of Sciences of the United States of America* 102.8, pp. 3076–3081.
D'Avella, A., A. Portone, and F. Lacquaniti (2011). "Superposition and modulation of muscle synergies for reaching in response to a change in target location." In: *Journal of Neurophysiology* 106.6, pp. 2796–2812.

D'Avella, A., P. Saltiel, and E. Bizzi (2003). "Combinations of muscle synergies in the construction of a natural motor behavior." In: *Nature Neuroscience* 6.3, pp. 300–308.

D'Avella, A., A. Portone, L. Fernandez, and F. Lacquaniti (2006). "Control of fast-reaching movements by muscle synergy combinations." In: *The Journal of Neuroscience* 26.30, pp. 7791–7810.

D'Avella, A., L. Fernandez, A. Portone, and F. Lacquaniti (2008). "Modulation of phasic and tonic muscle synergies with reaching direction and speed." In: *Journal of Neurophysiology* 100.3, pp. 1433–1454.

Datta, D., J. Kingston, and J. Ronald (1989). "Myoelectric prostheses for below-elbow amputees: the Trent experience." In: *International Disability Studies* 11.4, pp. 167–170.

Daumé III, H. and D. Marcu (2006). "Domain adaptation for statistical classifiers." In: *Journal of Artificial Intelligence Research* 26, pp. 101–126.

De Luca, C. J. (1979). "Physiology and mathematics of myoelectric signals." In: *IEEE Transactions on Biomedical Engineering* 6, pp. 313–325.

De Luca, C. J. (1997). "The use of surface electromyography in biomechanics." In: *Journal of Applied Biomechanics* 13.2, pp. 135–163.

De Luca, C. J., L. Donald Gilmore, M. Kuznetsov, and S. H. Roy (2010). "Filtering the surface EMG signal: movement artifact and baseline noise contamination." In: *Journal of Biomechanics* 43.8, pp. 1573–1579.

Delis, I., S. Panzeri, T. Pozzo, and B. Berret (2014). "A unifying model of concurrent spatial and temporal modularity in muscle activity." In: *Journal of Neurophysiology* 111.3, pp. 675–93.

Delsys, Inc. (1993). URL: http://www.delsys.com/ (visited on Aug. 1, 2017).

Dietrich, C., K. Walter-Walsh, S. Preißler, G. O. Hofmann, O. W. Witte, W. H. Miltner, and T. Weiss (2012). "Sensory feedback prosthesis reduces phantom limb pain: proof of a principle." In: *Neuroscience Letters* 507.2, pp. 97–100.

Domingos, P. (2012). "A few useful things to know about machine learning." In: *Communications of the ACM* 55.10, p. 78.

Dosen, S., C. Cipriani, M. Kostic, M. Controzzi, M. C. Carrozza, and D. B. Popovic (2010). "Cognitive vision system for control of dexterous prosthetic hands: experimental evaluation." In: *Journal of NeuroEngineering and Rehabilitation* 7.1, p. 42.

Du, Y., W. Jin, W. Wei, Y. Hu, and W. Geng (2017). "Surface EMG-based inter-session gesture recognition enhanced by deep domain adaptation." In: *Sensors* 17.3, p. 458.

Duinen, H. van and S. C. Gandevia (2011). "Constraints for control of the human hand." In: *The Journal of Physiology* 589.23, pp. 5583–5593.

Dunnett, C. W. (1955). "A multiple comparison procedure for comparing several treatments with a control." In: *Journal of the American Statistical Association* 50.272, pp. 1096–1121.

Dyson, M., J. Barnes, and K. Nazarpour (2017). "Abstract myoelectric control with EMG drive estimated using linear, kurtosis and Bayesian filtering." In: *2017 8th International IEEE/EMBS Conference on Neural Engineering (NER)*. IEEE, pp. 54–57.

Egeraat, J. van, R. Friedman, and J. Wikswo (1990). "Magnetic field of a single muscle fiber. First measurements and a core conductor model." In: *Biophysical Journal* 57.3, pp. 663–667.

Englehart, K. B., B. S. Hudgins, and P. A. Parker (2001). "A wavelet-based continuous classification scheme for multifunction myoelectric control." In: *IEEE Transactions on Biomedical Engineering* 48.3, pp. 302–311.

Englehart, K. B., B. S. Hudgins, P. A. Parker, and M. Stevenson (1999). "Classification of the myoelectric signal using time-frequency based representations." In: *Medical Engineering & Physics* 21.6-7, pp. 431–438.

Englehart, K. B. and B. S. Hudgins (2003). "A robust, real-time control scheme for multifunction myoelectric control." In: *IEEE Transactions on Biomedical Engineering* 50.7, pp. 848–854.

Farina, D. and O. C. Aszmann (2014). "Bionic limbs: clinical reality and academic promises." In: *Science Translational Medicine* 6.257, 257ps12.

Farina, D., N. Jiang, H. Rehbaum, A. Holobar, B. Graimann, H. Dietl, and O. C. Aszmann (2014). "The extraction of neural information from the surface EMG for the control of upper-limb prostheses: emerging avenues and challenges." In: *IEEE Transactions on Neural Systems and Rehabilitation Engineering* 22.4, pp. 797–809.

Farrell, T. R. (2011). "Determining delay created by multifunctional prosthesis controllers." In: *The Journal of Rehabilitation Research and Development* 48.6, p. xxi.

Farrell, T. R. and R. F. ff Weir (2007). "The optimal controller delay for myoelectric prostheses." In: *IEEE Transactions on Neural Systems and Rehabilitation Engineering* 15.1, pp. 111–118.

Fawcett, T. (2006). "An introduction to ROC analysis." In: *Pattern Recognition Letters* 27.8, pp. 861–874.

Feinstein, B., B. Lindegård, E. Nyman, and G. Wohlfart (1955). "Morphologic studies of motor units in normal human muscles." In: *Cells Tissues Organs* 23.2, pp. 127–142.

Finch, J. (2011). "The ancient origins of prosthetic medicine." In: *The Lancet* 377.9765, pp. 548–549.

Fisher, R. A. (1922). "On the interpretation of χ 2 from contingency tables, and the calculation of P." In: *Journal of the Royal Statistical Society* 85.1, pp. 87–94.

Fitts, P. M. (1954). "The information capacity of the human motor system in controlling the amplitude of movement." In: *Journal of Experimental Psychology* 47.6, p. 381.

Fix, E. and J. L. Hodges Jr. (1951). *Discriminatory analysis-nonparametric discrimination: consistency properties*. Tech. rep. DTIC Document.

Flanders, M. and U. Herrmann (1992). "Two components of muscle activation: scaling with the speed of arm movement." In: *Journal of Neurophysiology* 67.4, pp. 931–943.

Fligge, N., H. Urbanek, and P. van der Smagt (2013). "Relation between object properties and EMG during reaching to grasp." In: *Journal of Electromyography and Kinesiology* 23.2, pp. 402–410.

Fougner, A. L., Ø. Stavdahl, and P. J. Kyberd (2014). "System training and assessment in simultaneous proportional myoelectric prosthesis control." In: *Journal of NeuroEngineering and Rehabilitation* 11.1, p. 75.

Fougner, A., E. J. Scheme, A. D. C. Chan, K. B. Englehart, and Ø. Stavdahl (2011). "Resolving the limb position effect in myoelectric pattern recognition." In: *IEEE Transactions on Neural Systems and Rehabilitation Engineering* 19.6, pp. 644–651.

Fougner, A., Ø. Stavdahl, P. J. Kyberd, Y. G. Losier, and P. A. Parker (2012). "Control of upper limb prostheses: terminology and proportional myoelectric control–A review." In: *IEEE Transactions on Neural Systems and Rehabilitation Engineering* 20.5, pp. 663–677.

Friedman, J. H. (1989). "Regularized discriminant analysis." In: *Journal of the American Statistical Association* 84.405, pp. 165–175.

Friedman, J. H. (2002). "Stochastic gradient boosting." In: *Computational Statistics & Data Analysis* 38.4, pp. 367–378.
Friedman, J., T. Hastie, and R. Tibshirani (2001). *The elements of statistical learning*. Vol. 1. Springer series in statistics New York.
Friedman, M. (1937). "The use of ranks to avoid the assumption of normality implicit in the analysis of variance." In: *Journal of the American Statistical Association* 32.200, pp. 675–701.
Furuya, S., M. Flanders, and J. F. Soechting (2011). "Hand kinematics of piano playing." In: *Journal of Neurophysiology* 106.6, pp. 2849–2864.
Gailey, A., P. Artemiadis, and M. Santello (2017). "Proof of concept of an online EMG-based decoding of hand postures and individual digit forces for prosthetic hand control." In: *Frontiers in Neurology* 8.
Garcia, M. A. C. and O. Baffa (2015). "Magnetic fields from skeletal muscles: a valuable physiological measurement?" In: *Frontiers in Physiology* 6.
Geng, W., Y. Du, W. Jin, W. Wei, Y. Hu, and J. Li (2016). "Gesture recognition by instantaneous surface EMG images." In: *Scientific Reports* 6.1, p. 36571.
Geng, Y., P. Zhou, and G. Li (2012). "Toward attenuating the impact of arm positions on electromyography pattern-recognition based motion classification in transradial amputees." In: *Journal of NeuroEngineering and Rehabilitation* 9.1, p. 74.
Geng, Y., X. Zhang, Y.-T. Zhang, and G. Li (2014). "A novel channel selection method for multiple motion classification using high-density electromyography." In: *Biomedical Engineering Online* 13.1, p. 102.
Gesslbauer, B., L. A. Hruby, A. D. Roche, D. Farina, R. Blumer, and O. C. Aszmann (2017). "Axonal components of nerves innervating the human arm." In: *Annals of Neurology* 82.3, pp. 396–408.
Ghataurah, J., D. Ferigo, L.-K. Merhi, B. Pousett, and C. Menon (2017). "A multisensor approach for biomimetic control of a robotic prosthetic hand." In: *International Conference on Bioinformatics and Biomedical Engineering*. Springer, pp. 74–84.
Ghazaei, G., A. Alameer, P. Degenaar, G. Morgan, and K. Nazarpour (2017). "Deep learning-based artificial vision for grasp classification in myoelectric hands." In: *Journal of Neural Engineering* 14.3, p. 036025.
Gibson, A. E., M. R. Ison, and P. Artemiadis (2013). "User-independent hand motion classification with electromyography." In: *Proceedings of the ASME 2013 Dynamic Systems and Control Conference*. ASME, pp. 21–23.
Gijsberts, A., M. Atzori, C. Castellini, H. Müller, and B. Caputo (2014a). "Movement error rate for evaluation of machine learning methods for sEMG-based hand movement classification." In: *IEEE Transactions on Neural Systems and Rehabilitation Engineering* 22.4, pp. 735–744.
Gijsberts, A., R. Bohra, D. S. Sierra González, A. Werner, M. Nowak, B. Caputo, M. A. Roa, and C. Castellini (2014b). "Stable myoelectric control of a hand prosthesis using non-linear incremental learning." In: *Frontiers in Neurorobotics* 8.
Glynn, M. K., H. R. Galway, G. Hunter, and W. F. Sauter (1986). "Management of the upper-limb-deficient child with a powered prosthetic device." In: *Clinical Orthopaedics and Related Research* 209, pp. 202–205.
Hahne, J. M., F. Biebmann, N. Jiang, H. Rehbaum, D. Farina, F. C. Meinecke, K.-R. Müller, and L. C. Parra (2014). "Linear and nonlinear regression techniques for simultaneous and proportional myoelectric control." In: *IEEE Transactions on Neural Systems and Rehabilitation Engineering* 22.2, pp. 269–279.

Hahne, J. M., M. Markovic, and D. Farina (2017). "User adaptation in myoelectric man-machine interfaces." In: *Scientific Reports* 7.1, p. 4437.

Hahne, J. M., S. Dahne, H.-J. Hwang, K.-R. Muller, and L. C. Parra (2015). "Concurrent adaptation of human and machine improves simultaneous and proportional myoelectric control." In: *IEEE Transactions on Neural Systems and Rehabilitation Engineering* 23.4, pp. 618–627.

Hargrove, L. J., G. Li, K. B. Englehart, and B. S. Hudgins (2009). "Principal components analysis preprocessing for improved classification accuracies in pattern-recognition-based myoelectric control." In: *IEEE Transactions on Biomedical Engineering* 56.5, pp. 1407–1414.

Hargrove, L. J., E. J. Scheme, K. B. Englehart, and B. S. Hudgins (2010). "Multiple binary classifications via linear discriminant analysis for improved controllability of a powered prosthesis." In: *IEEE Transactions on Neural Systems and Rehabilitation Engineering* 18.1, pp. 49–57.

Hargrove, L., K. B. Englehart, and B. S. Hudgins (2007). "A comparison of surface and intramuscular myoelectric signal classification." In: *IEEE Transactions on Biomedical Engineering* 54.5, pp. 847–853.

Hargrove, L. J., K. B. Englehart, and B. S. Hudgins (2008). "A training strategy to reduce classification degradation due to electrode displacements in pattern recognition based myoelectric control." In: *Biomedical Signal Processing and Control* 3.2, pp. 175–180.

Hastie, T., A. Buja, and R. Tibshirani (1995). "Penalized discriminant analysis." In: *The Annals of Statistics*, pp. 73–102.

Hastie, T. and R. Tibshirani (1996). "Discriminant analysis by Gaussian mixtures." In: *Journal of the Royal Statistical Society. Series B (Methodological)*, pp. 155–176.

He, J., D. Zhang, N. Jiang, X. Sheng, D. Farina, and X. Zhu (2015). "User adaptation in long-term, open-loop myoelectric training: implications for EMG pattern recognition in prosthesis control." In: *Journal of Neural Engineering* 12.4, p. 046005.

Hinton, G. E. and R. R. Salakhutdinov (2006). "Reducing the dimensionality of data with neural networks." In: *Science* 313.5786, pp. 504–7.

Hioki, M. and H. Kawasaki (2009). "Estimation of finger joint angles from sEMG using a recurrent neural network with time-delayed input vectors." In: *2009 IEEE International Conference on Rehabilitation Robotics*. IEEE, pp. 289–294.

Hioki, M. and H. Kawasaki (2012). "Estimation of finger joint angles from sEMG using a neural network including time delay factor and recurrent structure." In: *ISRN Rehabilitation* 2012, pp. 1–13.

Hoffmann, H., S. Schaal, and S. Vijayakumar (2009). "Local dimensionality reduction for non-parametric regression." In: *Neural Processing Letters* 29.2, pp. 109–131.

Holdefer, R. N. and L. E. Miller (2002). "Primary motor cortical neurons encode functional muscle synergies." In: *Experimental Brain Research* 146.2, pp. 233–243.

Huang, H., P. Zhou, G. Li, and T. A. Kuiken (2008). "An analysis of EMG electrode configuration for targeted muscle reinnervation based neural machine interface." In: *IEEE Transactions on Neural Systems and Rehabilitation Engineering* 16.1, pp. 37–45.

Huang, Y., K. B. Englehart, B. S. Hudgins, and A. D. C. Chan (2005). "A Gaussian mixture model based classification scheme for myoelectric control of powered upper limb prostheses." In: *IEEE Transactions on Biomedical Engineering* 52.11, pp. 1801–1811.

Hudgins, B. S., P. A. Parker, and R. N. Scott (1993). "A new strategy for multifunction myoelectric control." In: *IEEE Transactions on Biomedical Engineering* 40.1, pp. 82–94.

Hwang, H.-J., J. M. Hahne, and K.-R. Müller (2014). "Channel selection for simultaneous and proportional myoelectric prosthesis control of multiple degrees-of-freedom." In: *Journal of Neural Engineering* 11.5, p. 056008.

Ison, M. and P. Artemiadis (2014). "The role of muscle synergies in myoelectric control: trends and challenges for simultaneous multifunction control." In: *Journal of Neural Engineering* 11.5, p. 051001.

Ison, M. and P. Artemiadis (2015). "Proportional myoelectric control of robots: muscle synergy development drives performance enhancement, retainment, and generalization." In: *IEEE Transactions on Robotics* 31.2, pp. 259–268.

Ison, M., I. Vujaklija, B. Whitsell, D. Farina, and P. Artemiadis (2016). "High-density electromyography and motor skill learning for robust long-term control of a 7-DoF robot arm." In: *IEEE Transactions on Neural Systems and Rehabilitation Engineering* 24.4, pp. 424–433.

Jiang, N., K. B. Englehart, and P. A. Parker (2009). "Extracting simultaneous and proportional neural control information for multiple-DOF prostheses from the surface electromyographic signal." In: *IEEE Transactions on Biomedical Engineering* 56.4, pp. 1070–1080.

Jiang, N., J. L. Vest-Nielsen, S. Muceli, and D. Farina (2012a). "EMG-based simultaneous and proportional estimation of wrist/hand kinematics in uni-lateral transradial amputees." In: *Journal of NeuroEngineering and Rehabilitation* 9.1, p. 42.

Jiang, N., S. Dosen, K.-R. Müller, and D. Farina (2012b). "Myoelectric control of artificial limbs –is there a need to change focus? [In the spotlight]." In: *IEEE Signal Processing Magazine* 29.5, pp. 152–150.

Jiang, N., S. Muceli, B. Graimann, and D. Farina (2013). "Effect of arm position on the prediction of kinematics from EMG in amputees." In: *Medical & Biological Engineering & Computing* 51.1-2, pp. 143–51.

Jiang, N., H. Rehbaum, I. Vujaklija, B. Graimann, and D. Farina (2014a). "Intuitive, online, simultaneous, and proportional myoelectric control over two degrees-of-freedom in upper limb amputees." In: *IEEE Transactions on Neural Systems and Rehabilitation Engineering* 22.3, pp. 501–510.

Jiang, N., I. Vujaklija, H. Rehbaum, B. Graimann, and D. Farina (2014b). "Is accurate mapping of EMG signals on kinematics needed for precise online myoelectric control?" In: *IEEE Transactions on Neural Systems and Rehabilitation Engineering* 22.3, pp. 549–558.

Ju, Z., G. Ouyang, M. Wilamowska-Korsak, and H. Liu (2013). "Surface EMG based hand manipulation identification via nonlinear feature extraction and classification." In: *IEEE Sensors Journal* 13.9, pp. 3302–3311.

Kadkhodayan, A., X. Jiang, and C. Menon (2016). "Continuous prediction of finger movements using force myography." In: *Journal of Medical and Biological Engineering* 36.4, pp. 594–604.

Kamavuako, E. N., E. J. Scheme, and K. B. Englehart (2014a). "Combined surface and intramuscular EMG for improved real-time myoelectric control performance." In: *Biomedical Signal Processing and Control* 10.1, pp. 102–107.

Kamavuako, E. N., E. J. Scheme, and K. B. Englehart (2014b). "On the usability of intramuscular EMG for prosthetic control: a Fitts' law approach." In: *Journal of Electromyography and Kinesiology* 24.5, pp. 770–777.

Kamavuako, E. N., J. C. Rosenvang, R. Horup, W. Jensen, D. Farina, and K. B. Englehart (2013). "Surface versus untargeted intramuscular EMG based classification of simultaneous and dynamically changing movements." In: *IEEE Transactions on Neural Systems and Rehabilitation Engineering* 21.6, pp. 992–998.

Kanitz, G. R., C. Antfolk, C. Cipriani, F. Sebelius, and M. C. Carrozza (2011). "Decoding of individuated finger movements using surface EMG and input optimization applying a genetic algorithm." In: *2011 Annual International Conference of the IEEE Engineering in Medicine and Biology Society (EMBC)*. IEEE, pp. 1608–1611.

Kaufmann, P., K. B. Englehart, and M. Platzner (2010). "Fluctuating EMG signals: investigating long-term effects of pattern matching algorithms." In: *2010 Annual International Conference of the IEEE Engineering in Medicine and Biology*. IEEE, pp. 6357–6360.

Kelly, M., P. A. Parker, and R. N. Scott (1990). "The application of neural networks to myoelectric signal analysis: a preliminary study." In: *IEEE Transactions on Biomedical Engineering* 37.3, pp. 221–230.

Kent, B. A., N. Karnati, and E. D. Engeberg (2014). "Electromyogram synergy control of a dexterous artificial hand to unscrew and screw objects." In: *Journal of NeuroEngineering and Rehabilitation* 11.1, p. 41.

Khushaba, R. N. (2014). "Correlation analysis of electromyogram signals for multiuser myoelectric interfaces." In: *IEEE Transactions on Neural Systems and Rehabilitation Engineering* 22.4, pp. 745–755.

Khushaba, R. N., A. Al-Timemy, S. Kodagoda, and K. Nazarpour (2016). "Combined influence of forearm orientation and muscular contraction on EMG pattern recognition." In: *Expert Systems with Applications* 61, pp. 154–161.

Khushaba, R. N., A. H. Al-Timemy, A. Al-Ani, and A. Al-Jumaily (2017). "A framework of temporal-spatial descriptors based feature extraction for improved myoelectric pattern recognition." In: *IEEE Transactions on Neural Systems and Rehabilitation Engineering* 25.10, pp. 1821–1831.

Konnaris, C., A. A. C. Thomik, and A. A. Faisal (2016). "Sparse eigenmotions derived from daily life kinematics implemented on a dextrous robotic hand." In: *2016 6th IEEE International Conference on Biomedical Robotics and Biomechatronics (BioRob)*. IEEE, pp. 1358–1363.

Kruskal, W. H. and W. A. Wallis (1952). "Use of ranks in one-criterion variance analysis." In: *Journal of the American statistical Association* 47.260, pp. 583–621.

Kuiken, T. A., G. A. Dumanian, R. D. Lipschutz, L. A. Miller, and K. A. Stubblefield (2004). "The use of targeted muscle reinnervation for improved myoelectric prosthesis control in a bilateral shoulder disarticulation amputee." In: *Prosthetics and Orthotics International* 28.3, pp. 245–53.

Kuiken, T. A., G. Li, B. A. Lock, R. D. Lipschutz, L. A. Miller, K. A. Stubblefield, and K. B. Englehart (2009). "Targeted muscle reinnervation for real-time myoelectric control of multifunction artificial arms." In: *JAMA* 301.6, pp. 619–628.

Kumar, D. K., N. D. Pah, and A. Bradley (2003). "Wavelet analysis of surface electromyography to determine muscle fatigue." In: *IEEE Transactions on Neural Systems and Rehabilitation Engineering* 11.4, pp. 400–406.

Kutch, J. J., A. D. Kuo, A. M. Bloch, and W. Z. Rymer (2008). "Endpoint force fluctuations reveal flexible rather than synergistic patterns of muscle cooperation." In: *Journal of Neurophysiology* 100.5, pp. 2455–2471.

Kuzborskij, I., A. Gijsberts, and B. Caputo (2012). "On the challenge of classifying 52 hand movements from surface electromyography." In: *2012 Annual International*

Conference of the IEEE Engineering in Medicine and Biology Society (EMBC). IEEE, pp. 4931–4937.

Landgrebe, T. C. and R. P. Duin (2007). "Approximating the multiclass ROC by pairwise analysis." In: *Pattern Recognition Letters* 28.13, pp. 1747–1758.

Lawrence, N. D. (2004). "Gaussian process latent variable models for visualisation of high dimensional data." In: *Advances in Neural Information Processing Systems*. MIT Press, pp. 329–336.

Lawrence, N. D. (2005). "Probabilistic non-linear principal component analysis with Gaussian process latent variable models." In: *Journal of Machine Learning Research* 6, pp. 1783–1816.

Lee, W. A. (1984). "Neuromotor synergies as a basis for coordinated intentional action." In: *Journal of Motor Behavior* 16.2, pp. 135–170.

Li, G., A. E. Schultz, and T. A. Kuiken (2010). "Quantifying pattern recognition-based myoelectric control of multifunctional transradial prostheses." In: *IEEE Transactions on Neural Systems and Rehabilitation Engineering* 18.2, pp. 185–192.

Li, X., S. Chen, H. Zhang, O. W. Samuel, H. Wang, P. Fang, X. Zhang, and G. Li (2016). "Towards reducing the impacts of unwanted movements on identification of motion intentions." In: *Journal of Electromyography and Kinesiology* 28, pp. 90–98.

Li, X., J. Fu, L. Xiong, Y. Shi, R. Davoodi, and Y. Li (2015). "Identification of finger force and motion from forearm surface electromyography." In: *2015 IEEE International Conference on Multisensor Fusion and Integration for Intelligent Systems (MFI)*. IEEE, pp. 316–321.

Li, Z., B. Wang, C. Yang, Q. Xie, and C.-Y. Su (2013). "Boosting-based EMG patterns classification scheme for robustness enhancement." In: *IEEE Journal of Biomedical and Health Informatics* 17.3, pp. 545–552.

Liarokapis, M. V., C. P. Bechlioulis, G. I. Boutselis, and K. J. Kyriakopoulos (2016). "A learn by demonstration approach for closed-loop, robust, anthropomorphic grasp planning." In: *Human and Robot Hands*. Springer, pp. 127–149.

Light, C. M., P. H. Chappell, and P. J. Kyberd (2002). "Establishing a standardized clinical assessment tool of pathologic and prosthetic hand function: normative data, reliability, and validity." In: *Archives of Physical Medicine and Rehabilitation* 83.6, pp. 776–783.

Lipschutz, R. D., T. A. Kuiken, L. A. Miller, G. A. Dumanian, and K. A. Stubblefield (2006). "Shoulder disarticulation externally powered prosthetic fitting following targeted muscle reinnervation for improved myoelectric control." In: *JPO Journal of Prosthetics and Orthotics* 18.2, pp. 28–34.

Liu, J., X. Sheng, D. Zhang, J. He, and X. Zhu (2016a). "Reduced daily recalibration of myoelectric prosthesis classifiers based on domain adaptation." In: *IEEE Journal of Biomedical and Health Informatics* 20.1, pp. 166–176.

Liu, J., X. Sheng, D. Zhang, N. Jiang, and X. Zhu (2016b). "Towards zero retraining for myoelectric control based on common model component analysis." In: *IEEE Transactions on Neural Systems and Rehabilitation Engineering* 24.4, pp. 444–454.

Liu, J., X. Li, G. Li, and P. Zhou (2014). "EMG feature assessment for myoelectric pattern recognition and channel selection: a study with incomplete spinal cord injury." In: *Medical Engineering & Physics* 36.7, pp. 975–980.

Liu, L., P. Liu, E. A. Clancy, E. J. Scheme, and K. B. Englehart (2013). "Electromyogram whitening for improved classification accuracy in upper limb prosthesis control." In: *IEEE Transactions on Neural Systems and Rehabilitation Engineering* 21.5, pp. 767–774.

Liu, P., D. R. Brown, F. Martel, D. Rancourt, and E. A. Clancy (2011). "EMG-to-force modeling for multiple fingers." In: *2011 IEEE 37th Annual Northeast Bioengineering Conference (NEBEC)*. IEEE, pp. 1–2.

Lobo-Prat, J., P. N. Kooren, A. H. Stienen, J. L. Herder, B. F. Koopman, and P. H. Veltink (2014). "Non-invasive control interfaces for intention detection in active movement-assistive devices." In: *Journal of NeuroEngineering and Rehabilitation* 11.1, p. 168.

Lock, B. A., K. B. Englehart, and B. S. Hudgins (2005). "Real-time myoelectric control in a virtual environment to relate usability vs. accuracy." In: *Proceedings of the 2005 Myoelectric Controls Symposium (MEC)*, pp. 17–20.

Luff, R, J Forrest, and J Huntley (2009). "The amputee statistical database for the United Kingdom." In: *Edinburgh: NASDAB*.

MacKenzie, I. S. (1992). "Fitts' law as a research and design tool in human-computer interaction." In: *Human-Computer Interaction* 7.1, pp. 91–139.

Madgwick, S. O. H., A. J. L. Harrison, and R. Vaidyanathan (2011). "Estimation of IMU and MARG orientation using a gradient descent algorithm." In: *2011 IEEE International Conference on Rehabilitation Robotics*. IEEE, pp. 1–7.

Mann, H. B. and D. R. Whitney (1947). "On a test of whether one of two random variables is stochastically larger than the other." In: *The Annals of Mathematical Statistics*, pp. 50–60.

Marasco, P. D., K. Kim, J. E. Colgate, M. A. Peshkin, and T. A. Kuiken (2011). "Robotic touch shifts perception of embodiment to a prosthesis in targeted reinnervation amputees." In: *Brain* 134.3, pp. 747–758.

Markovic, M., S. Dosen, C. Cipriani, D. Popovic, and D. Farina (2014). "Stereovision and augmented reality for closed-loop control of grasping in hand prostheses." In: *Journal of Neural Engineering* 11.4, p. 046001.

Markovic, M., H. Karnal, B. Graimann, D. Farina, and S. Dosen (2017). "GLIMPSE: Google Glass interface for sensory feedback in myoelectric hand prostheses." In: *Journal of Neural Engineering* 14.3, p. 036007.

Mason, C. R., J. E. Gomez, and T. J. Ebner (2001). "Hand synergies during reach-to-grasp." In: *Journal of Neurophysiology* 86.6, pp. 2896–2910.

Mathiowetz, V., G. Volland, N. Kashman, and K. Weber (1985). "Adult norms for the box and block test of manual dexterity." In: *American Journal of Occupational Therapy* 39.6, pp. 386–391.

Matrone, G. C., C. Cipriani, E. L. Secco, G. Magenes, and M. C. Carrozza (2010). "Principal components analysis based control of a multi-DoF underactuated prosthetic hand." In: *Journal of NeuroEngineering and Rehabilitation* 7, p. 16.

Matrone, G. C., C. Cipriani, M. C. Carrozza, and G. Magenes (2012). "Real-time myoelectric control of a multi-fingered hand prosthesis using principal components analysis." In: *Journal of NeuroEngineering and Rehabilitation* 9.1, p. 40.

Matsubara, T. and J. Morimoto (2013). "Bilinear modeling of EMG signals to extract user-independent features for multiuser myoelectric interface." In: *IEEE Transactions on Biomedical Engineering* 60.8, pp. 2205–2213.

McCool, P., G. D. Fraser, A. D. C. Chan, L. Petropoulakis, and J. J. Soraghan (2014). "Identification of contaminant type in surface electromyography (EMG) signals." In: *IEEE Transactions on Neural Systems and Rehabilitation Engineering* 22.4, pp. 774–783.

Menon, R., G. Di Caterina, H. Lakany, L. Petropoulakis, B. A. Conway, and J. J. Soraghan (2015). "Automatic misclassification rejection for LDA classifier using ROC

curves." In: *2015 37th Annual International Conference of the IEEE Engineering in Medicine and Biology Society (EMBC)*. IEEE, pp. 482–485.
Menon, R., G. Di Caterina, H. Lakany, L. Petropoulakis, B. Conway, and J. Soraghan (2017). "Study on interaction between temporal and spatial information in classification of EMG signals in myoelectric prostheses." In: *IEEE Transactions on Neural Systems and Rehabilitation Engineering* 25.10, pp. 1832–1842.
Montagnani, F., M. Controzzi, and C. Cipriani (2015). "Is it finger or wrist dexterity that is missing in current hand prostheses?" In: *IEEE Transactions on Neural Systems and Rehabilitation Engineering* 23.4, pp. 600–609.
Mourikis, A. I. and S. I. Roumeliotis (2007). "A multi-state constraint Kalman filter for vision-aided inertial navigation." In: *2007 IEEE International Conference on Robotics and Automation (ICRA)*. IEEE, pp. 3565–3572.
Muceli, S. and D. Farina (2012). "Simultaneous and proportional estimation of hand kinematics from EMG during mirrored movements at multiple degrees-of-freedom." In: *IEEE Transactions on Neural Systems and Rehabilitation Engineering* 20.3, pp. 371–378.
Muceli, S., N. Jiang, and D. Farina (2014). "Extracting signals robust to electrode number and shift for online simultaneous and proportional myoelectric control by factorization algorithms." In: *IEEE Transactions on Neural Systems and Rehabilitation Engineering* 22.3, pp. 623–633.
Muceli, S., A. T. Boye, A. D'Avella, and D. Farina (2010). "Identifying representative synergy matrices for describing muscular activation patterns during multidirectional reaching in the horizontal plane." In: *Journal of Neurophysiology* 103.3, pp. 1532–1542.
Müller-Gerking, J., G. Pfurtscheller, and H. Flyvbjerg (1999). "Designing optimal spatial filters for single-trial EEG classification in a movement task." In: *Clinical Neurophysiology* 110.5, pp. 787–798.
NHS Scotland (2014). *Number of upper and lower limb amputations performed each year by the NHS in Scotland from 1981 to 2013*. URL: http://nhsnss.org/media/1397/limb_amputations_and_limb_absence.pdf (visited on Aug. 1, 2017).
Naik, G. R., A. H. Al-Timemy, and H. T. Nguyen (2016). "Transradial amputee gesture classification using an optimal number of sEMG sensors: an approach using ICA clustering." In: *IEEE Transactions on Neural Systems and Rehabilitation Engineering* 24.8, pp. 837–846.
Nazarpour, K., A. Barnard, and A. Jackson (2012). "Flexible cortical control of task-specific muscle synergies." In: *Journal of Neuroscience* 32.36, pp. 12349–12360.
Nazarpour, K., A. R. Sharafat, and S. M. P. Firoozabadi (2007). "Application of higher order statistics to surface electromyogram signal classification." In: *IEEE Transactions on Biomedical Engineering* 54.10, pp. 1762–1769.
Ngeo, J. G., T. Tamei, and T. Shibata (2012). "Continuous estimation of finger joint angles using muscle activation inputs from surface EMG signals." In: *2012 Annual International Conference of the IEEE Engineering in Medicine and Biology Society (EMBC)*. IEEE, pp. 2756–2759.
Ngeo, J. G., T. Tamei, and T. Shibata (2014a). "Continuous and simultaneous estimation of finger kinematics using inputs from an EMG-to-muscle activation model." In: *Journal of NeuroEngineering and Rehabilitation* 11.1, p. 122.
Ngeo, J. G., T. Tamei, and T. Shibata (2014b). "Estimation of continuous multi-DOF finger joint kinematics from surface EMG using a multi-output Gaussian process."

In: *2014 36th Annual International Conference of the IEEE Engineering in Medicine and Biology Society (EMBC)*. IEEE, pp. 3537–3540.
Ngeo, J. G., T. Tamei, T. Shibata, M. F. F. Orlando, L. Behera, A. Saxena, and A. Dutta (2013). "Control of an optimal finger exoskeleton based on continuous joint angle estimation from EMG signals." In: *2013 35th Annual International Conference of the IEEE Engineering in Medicine and Biology Society (EMBC)*. IEEE, pp. 338–341.
Ngeo, J. G., T. Tamei, K. Ikeda, and T. Shibata (2015). "Modeling dynamic high-DOF finger postures from surface EMG using nonlinear synergies in latent space representation." In: *2015 37th Annual International Conference of the IEEE Engineering in Medicine and Biology Society (EMBC)*. IEEE, pp. 2095–2098.
Nielsen, J. L. G., S. Holmgaard, N. Jiang, K. B. Englehart, D. Farina, and P. A. Parker (2011). "Simultaneous and proportional force estimation for multifunction myoelectric prostheses using mirrored bilateral training." In: *IEEE Transactions on Biomedical Engineering* 58.3, pp. 681–688.
Ninu, A., S. Dosen, S. Muceli, F. Rattay, H. Dietl, and D. Farina (2014). "Closed-loop control of grasping with a myoelectric hand prosthesis: which are the relevant feedback variables for force control?" In: *IEEE Transactions on Neural Systems and Rehabilitation Engineering* 22.5, pp. 1041–1052.
Nissler, C., N. Mouriki, and C. Castellini (2016). "Optical myography: detecting finger movements by looking at the forearm." In: *Frontiers in Neurorobotics* 10.
Olshausen, B. A. and D. J. Field (1996). "Emergence of simple-cell receptive field properties by learning a sparse code for natural images." In: *Nature* 381.6583, p. 607.
Ortiz-Catalan, M., B. Håkansson, and R. Brånemark (2014a). "An osseointegrated human-machine gateway for long-term sensory feedback and motor control of artificial limbs." In: *Science Translational Medicine* 6.257, 257re6.
Ortiz-Catalan, M., R. Brånemark, and B. Håkansson (2013). "BioPatRec: a modular research platform for the control of artificial limbs based on pattern recognition algorithms." In: *Source Code for Biology and Medicine* 8.1, p. 11.
Ortiz-Catalan, M., B. Håkansson, and R. Brånemark (2014b). "Real-time and simultaneous control of artificial limbs based on pattern recognition algorithms." In: *IEEE Transactions on Neural Systems and Rehabilitation Engineering* 22.4, pp. 756–764.
Ortiz-Catalan, M., F. Rouhani, R. Brånemark, and B. Håkansson (2015). "Offline accuracy: a potentially misleading metric in myoelectric pattern recognition for prosthetic control." In: *2015 37th Annual International Conference of the IEEE Engineering in Medicine and Biology Society (EMBC)*, pp. 1140–1143.
Oskoei, M. A. and H. Hu (2008). "Support vector machine-based classification scheme for myoelectric control applied to upper limb." In: *IEEE Transactions on Biomedical Engineering* 55.8, pp. 1956–1965.
Ottobock, Inc. (1919). URL: http://www.ottobock.com/ (visited on Aug. 1, 2017).
Overduin, S. A., A. D'Avella, J. Roh, J. M. Carmena, and E. Bizzi (2015). "Representation of muscle synergies in the primate brain." In: *Journal of Neuroscience* 35.37, pp. 12615–12624.
Overduin, S. A., A. D'Avella, J. Roh, and E. Bizzi (2008). "Modulation of muscle synergy recruitment in primate grasping." In: *The Journal of Neuroscience* 28.4, pp. 880–892.
Pan, L., X. Sheng, D. Zhang, and X. Zhu (2013). "Simultaneous and proportional estimation of finger joint angles from surface EMG signals during mirrored bilat-

eral movements." In: *International Conference on Intelligent Robotics and Applications*. Springer, pp. 493–499.
Parker, P. A., K. B. Englehart, and B. S. Hudgins (2006). "Myoelectric signal processing for control of powered limb prostheses." In: *Journal of Electromyography and Kinesiology* 16.6, pp. 541–548.
Patel, G., M. Nowak, and C. Castellini (2017). "Exploiting knowledge composition to improve real-life hand prosthetic control." In: *IEEE Transactions on Neural Systems and Rehabilitation Engineering* 25.7, pp. 967–975.
Peerdeman, B., D. Boere, H. Witteveen, R. Huis in 't Veld, H. Hermens, S. Stramigioli, H. Rietman, P. Veltink, and S. Misra (2011). "Myoelectric forearm prostheses: state of the art from a user-centered perspective." In: *The Journal of Rehabilitation Research and Development* 48.6, p. 719.
Perreault, E. J., R. F. Kirsch, and A. M. Acosta (1999). "Multiple-input, multiple-output system identification for characterization of limb stiffness dynamics." In: *Biological Cybernetics* 80.5, pp. 327–337.
Phinyomark, A., C. Limsakul, and P. Phukpattaranont (2009). "A novel feature extraction for robust EMG pattern recognition." In: *Journal of Computing* 1, pp. 71–80.
Phinyomark, A., P. Phukpattaranont, and C. Limsakul (2012). "Feature reduction and selection for EMG signal classification." In: *Expert Systems with Applications* 39.8, pp. 7420–7431.
Phinyomark, A., F. Quaine, S. Charbonnier, C. Serviere, F. Tarpin-Bernard, and Y. Laurillau (2013). "EMG feature evaluation for improving myoelectric pattern recognition robustness." In: *Expert Systems with Applications* 40.12, pp. 4832–4840.
Pistohl, T., C. Cipriani, A. Jackson, and K. Nazarpour (2013). "Abstract and proportional myoelectric control for multi-fingered hand prostheses." In: *Annals of Biomedical Engineering* 41.12, pp. 2687–2698.
Pistohl, T., D. Joshi, G. Ganesh, A. Jackson, and K. Nazarpour (2015). "Artificial Proprioceptive Feedback for Myoelectric Control." In: *IEEE Transactions on Neural Systems and Rehabilitation Engineering* 23.3, pp. 498–507.
Powell, M. A., R. R. Kaliki, and N. V. Thakor (2014). "User training for pattern recognition-based myoelectric prostheses: improving phantom limb movement consistency and distinguishability." In: *IEEE Transactions on Neural Systems and Rehabilitation Engineering* 22.3, pp. 522–532.
Prensilia, S.R.L. (2009). URL: http://www.prensilia.com/ (visited on Aug. 1, 2017).
Purves, D. (2012). *Neuroscience*. Oxford University Press.
Quigley, M., K. Conley, B. Gerkey, J. Faust, T. Foote, J. Leibs, R. Wheeler, and A. Y. Ng (2009). "ROS: an open-source Robot Operating System." In: *ICRA workshop on open source software*, p. 5.
Radmand, A., E. J. Scheme, and K. B. Englehart (2014). "On the suitability of integrating accelerometry data with electromyography signals for resolving the effect of changes in limb position during dynamic limb movement." In: *Journal of Prosthetics and Orthotics* 26.4, pp. 185–193.
Radmand, A., E. J. Scheme, and K. B. Englehart (2016). "High-density force myography: a possible alternative for upper-limb prosthetic control." In: *Journal of Rehabilitation Research and Development* 53.4, pp. 443–456.
Radomski, M. V. and C. A. T. Latham (2008). *Occupational therapy for physical dysfunction*. Lippincott Williams & Wilkins.

Rasool, G., K. Iqbal, N. Bouaynaya, and G. White (2016). "Real-time task discrimination for myoelectric control employing task-specific muscle synergies." In: *IEEE Transactions on Neural Systems and Rehabilitation Engineering* 24.1, pp. 98–108.

Raspopovic, S. et al. (2014). "Restoring natural sensory feedback in real-time bidirectional hand prostheses." In: *Science Translational Medicine* 6.222, 222ra19.

Reaz, M., M. Hussain, and F. Mohd-Yasin (2006). "Techniques of EMG signal analysis: detection, processing, classification and applications." In: *Biological Procedures Online* 8.1, pp. 11–35.

Reiter, R. (1948). "Eine neue Ekectrokunsthand." In: *Grenzgebiete der Medizin* 1.4, pp. 133–135.

Roh, J., W. Z. Rymer, and R. F. Beer (2012). "Robustness of muscle synergies underlying three-dimensional force generation at the hand in healthy humans." In: *Journal of Neurophysiology* 107.8, pp. 2123–2142.

Romm, S. (1989). "Arms by design: from antiquity to the Renaissance." In: *Plastic and Reconstructive Surgery* 84.1, pp. 158–163.

Rossini, P. M. et al. (2010). "Double nerve intraneural interface implant on a human amputee for robotic hand control." In: *Clinical Neurophysiology* 121.5, pp. 777–783.

Routhier, F., C. Vincent, M. J. Morissette, and L. Desaulniers (2001). "Clinical results of an investigation of paediatric upper limb myoelectric prosthesis fitting at the Quebec Rehabilitation Institute." In: *Prosthetics and Orthotics International* 25.2, pp. 119–131.

Santello, M., M. Flanders, and J. F. Soechting (1998). "Postural hand synergies for tool use." In: *The Journal of Neuroscience* 18.23, pp. 10105–10115.

Sartori, M., D. G. Llyod, and D. Farina (2016). "Neural data-driven musculoskeletal modeling for personalized neurorehabilitation technologies." In: *IEEE Transactions on Biomedical Engineering* 63.5, pp. 879–893.

Saunders, I. and S. Vijayakumar (2011). "The role of feed-forward and feedback processes for closed-loop prosthesis control." In: *Journal of NeuroEngineering and Rehabilitation* 8.1, p. 60.

Scheme, E. J. and K. B. Englehart (2011). "Electromyogram pattern recognition for control of powered upper-limb prostheses: state of the art and challenges for clinical use." In: *The Journal of Rehabilitation Research and Development* 48.6, p. 643.

Scheme, E. J. and K. B. Englehart (2013a). "Training strategies for mitigating the effect of proportional control on classification in pattern recognition–based myoelectric control." In: *JPO Journal of Prosthetics and Orthotics* 25.2, pp. 76–83.

Scheme, E. J. and K. B. Englehart (2013b). "Validation of a selective ensemble-based classification scheme for myoelectric control using a three-dimensional fitts' law test." In: *IEEE Transactions on Neural Systems and Rehabilitation Engineering* 21.4, pp. 616–623.

Scheme, E. J., K. B. Englehart, and B. S. Hudgins (2011). "Selective classification for improved robustness of myoelectric control under nonideal conditions." In: *IEEE Transactions on Biomedical Engineering* 58.6, pp. 1698–1705.

Scheme, E. J., B. S. Hudgins, and K. B. Englehart (2013). "Confidence-based rejection for improved pattern recognition myoelectric control." In: *IEEE Transactions on Biomedical Engineering* 60.6, pp. 1563–1570.

Scheme, E. J., B. A. Lock, L. J. Hargrove, W. Hill, U. Kuruganti, and K. B. Englehart (2014). "Motion normalized proportional control for improved pattern recognition-based myoelectric control." In: *IEEE Transactions on Neural Systems and Rehabilitation Engineering* 22.1, pp. 149–157.

Schiefer, M., D. Tan, S. M. Sidek, and D. J. Tyler (2016). "Sensory feedback by peripheral nerve stimulation improves task performance in individuals with upper limb loss using a myoelectric prosthesis." In: *Journal of Neural Engineering* 13.1, p. 016001.

Sebelius, F. C., B. N. Rosén, and G. N. Lundborg (2005). "Refined myoelectric control in below-elbow amputees using artificial neural networks and a data glove." In: *The Journal of Hand Surgery* 30.4, pp. 780–789.

Segil, J. and R. F. ff Weir (2013). "Design and validation of a morphing myoelectric hand posture controller based on principal component analysis of human grasping." In: *IEEE Transactions on Neural Systems and Rehabilitation Engineering* 22.2, pp. 249–257.

Sensinger, J. W., B. A. Lock, and T. A. Kuiken (2009). "Adaptive pattern recognition of myoelectric signals: exploration of conceptual framework and practical algorithms." In: *IEEE Transactions on Neural Systems and Rehabilitation Engineering* 17.3, pp. 270–278.

Shadow (1998). URL: http://www.shadowrobot.com// (visited on Aug. 1, 2017).

Shahriari, B., K. Swersky, Z. Wang, R. P. Adams, and N. de Freitas (2016). "Taking the human out of the loop: a review of Bayesian optimization." In: *Proceedings of the IEEE* 104.1, pp. 148–175.

Shannon, C. E. (1948). "A mathematical theory of communication." In: *Bell Systems Technical Journal* 27, pp. 623–656.

Shenoy, P., K. Miller, B. Crawford, and R. Rao (2008). "Online electromyographic control of a robotic prosthesis." In: *IEEE Transactions on Biomedical Engineering* 55.3, pp. 1128–1135.

Sherrington, C. S. (1947). *The integrative action of the nervous system*. The University Press.

Shon, A., K. Grochow, A. Hertzmann, and R. P. Rao (2006). "Learning shared latent structure for image synthesis and robotic imitation." In: *Advances in Neural Information Processing Systems*. MIT Press, pp. 1233–1240.

Šidák, Z. (1967). "Rectangular confidence regions for the means of multivariate normal distributions." In: *Journal of the American Statistical Association* 62.318, pp. 626–633.

Silva, J., W. Heim, and T. Chau (2005). "A self-contained, mechanomyography-driven externally powered prosthesis." In: *Archives of Physical Medicine and Rehabilitation* 86.10, pp. 2066–2070.

Simon, A. M., L. J. Hargrove, B. A. Lock, and T. A. Kuiken (2011). "Target achievement control test: evaluating real-time myoelectric pattern-recognition control of multifunctional upper-limb prostheses." In: *The Journal of Rehabilitation Research and Development* 48.6, p. 619.

Smith, L. H., T. A. Kuiken, and L. J. Hargrove (2014). "Real-time simultaneous and proportional myoelectric control using intramuscular EMG." In: *Journal of Neural Engineering* 11.6, p. 066013.

Smith, L. H., T. A. Kuiken, and L. J. Hargrove (2015). "Use of probabilistic weights to enhance linear regression myoelectric control." In: *Journal of Neural Engineering* 12.6, p. 066030.

Smith, L. H., T. A. Kuiken, and L. J. Hargrove (2016). "Evaluation of linear regression simultaneous myoelectric control using intramuscular EMG." In: *IEEE Transactions on Biomedical Engineering* 63.4, pp. 737–746.

Smith, L. H., L. J. Hargrove, B. A. Lock, and T. A. Kuiken (2011). "Determining the optimal window length for pattern recognition-based myoelectric control: balancing the competing effects of classification error and controller delay." In: *IEEE Transactions on Neural Systems and Rehabilitation Engineering* 19.2, pp. 186–192.

Smith, R., D. Huberdeau, F. Tenore, and N. Thakor (2009). "Real-time myoelectric decoding of individual finger movements for a virtual target task." In: *2009 Annual International Conference of the IEEE Engineering in Medicine and Biology Society (EMBC)*. IEEE, pp. 2376–2379.

Smith, R. J., F. Tenore, D. Huberdeau, R. Etienne-Cummings, and N. V. Thakor (2008). "Continuous decoding of finger position from surface EMG signals for the control of powered prostheses." In: *2008 30th Annual International Conference of the IEEE Engineering in Medicine and Biology Society (EMBC)*. IEEE, pp. 197–200.

Snoek, J., H. Larochelle, and R. P. Adams (2012). "Practical Bayesian optimization of machine learning algorithms." In: *Advances in Neural Information Processing Systems*, pp. 2951–2959.

Spanias, J. A., A. M. Simon, K. A. Ingraham, and L. J. Hargrove (2015). "Effect of additional mechanical sensor data on an EMG-based pattern recognition system for a powered leg prosthesis." In: *2015 7th International IEEE/EMBS Conference on Neural Engineering (NER)*. IEEE, pp. 639–642.

Staude, G. and W. Wolf (1999). "Objective motor response onset detection in surface myoelectric signals." In: *Medical Engineering & Physics* 21.6, pp. 449–467.

Steele, K. M., M. C. Tresch, and E. J. Perreault (2013). "The number and choice of muscles impact the results of muscle synergy analyses." In: *Frontiers in Computational Neuroscience* 7.

Street, W. N., W. H. Wolberg, and O. L. Mangasarian (1993). "Nuclear feature extraction for breast tumor diagnosis." In: *IS&T/SPIE Symposium on Electronic Imaging: Science and Technology*, pp. 861–870.

Tan, D. W., M. A. Schiefer, M. W. Keith, J. R. Anderson, J. Tyler, and D. J. Tyler (2014). "A neural interface provides long-term stable natural touch perception." In: *Science Translational Medicine* 6.257, 257ra138.

Tenore, F., A. Ramos, A. Fahmy, S. Acharya, R. Etienne-Cummings, and N. Thakor (2009). "Decoding of individuated finger movements using surface electromyography." In: *IEEE Transactions on Biomedical Engineering* 56.5, pp. 1427–1434.

Thomik, A. A. C., S. Fenske, and A. A. Faisal (2015). "Towards sparse coding of natural movements for neuroprosthetics and brain-machine interfaces." In: *2015 7th International IEEE/EMBS Conference on Neural Engineering (NER)*. IEEE, pp. 938–941.

Thurston, A. J. (2007). "Paré and prosthetics: the early history of artificial limbs." In: *ANZ Journal of Surgery* 77.12, pp. 1114–1119.

Tkach, D. C., A. J. Young, L. H. Smith, E. J. Rouse, and L. J. Hargrove (2014). "Real-time and offline performance of pattern recognition myoelectric control using a generic electrode grid with targeted muscle reinnervation patients." In: *IEEE Transactions on Neural Systems and Rehabilitation Engineering* 22.4, pp. 727–734.

Todorov, E. and Z. Ghahramani (2004). "Analysis of the synergies underlying complex hand manipulation." In: *2004 26th Annual International Conference of the IEEE Engineering in Medicine and Biology Society (EMBC)*. IEEE, pp. 4637–4640.

Todorov, E. and M. I. Jordan (2002). "Optimal feedback control as a theory of motor coordination." In: *Nature Neuroscience* 5.11, pp. 1226–1235.

Tommasi, T., F. Orabona, C. Castellini, and B. Caputo (2013). "Improving control of dexterous hand prostheses using adaptive learning." In: *IEEE Transactions on Robotics* 29.1, pp. 207–219.

Touch Bionics, Inc. (2003). URL: http://www.touchbionics.com/ (visited on Aug. 1, 2017).

Tresch, M. C., P. Saltiel, and E. Bizzi (1999). "The construction of movement by the spinal cord." In: *Nature Neuroscience* 2.2, pp. 162–167.

Tresch, M. C., V. C. K. Cheung, and A. D'Avella (2006). "Matrix factorization algorithms for the identification of muscle synergies: evaluation on simulated and experimental data sets." In: *Journal of Neurophysiology* 95.4, pp. 2199–212.

Tresch, M. C. and A. Jarc (2009). "The case for and against muscle synergies." In: *Current Opinion in Neurobiology* 19.6, pp. 601–607.

Valero-Cuevas, F. J., M. Venkadesan, and E. Todorov (2009). "Structured variability of muscle activations supports the minimal intervention principle of motor control." In: *Journal of Neurophysiology* 102.1, pp. 59–68.

Velu, R. and G. C. Reinsel (2013). *Multivariate reduced-rank regression: theory and applications*. Springer Science & Business Media.

Vidovic, M. M.-C., H.-J. Hwang, S. Amsüss, J. M. Hahne, D. Farina, and K.-R. Müller (2016). "Improving the robustness of myoelectric pattern recognition for upper limb prostheses by covariate shift adaptation." In: *IEEE Transactions on Neural Systems and Rehabilitation Engineering* 24.9, pp. 961–970.

Vincent Systems, GmbH (2013). URL: http://vincentsystems.de/en/ (visited on Aug. 1, 2017).

Vinjamuri, R., Z. H. Mao, R. Sclabassi, and M. Sun (2007). "Time-varying synergies in velocity profiles of finger joints of the hand during reach and grasp." In: *2007 29th Annual International Conference of the IEEE Engineering in Medicine and Biology Society (EMBC)*, pp. 4846–4849.

Vinjamuri, R., M. Sun, C. C. Chang, H. N. Lee, R. J. Sclabassi, and Z. H. Mao (2010). "Dimensionality reduction in control and coordination of the human hand." In: *IEEE Transactions on Biomedical Engineering* 57.2, pp. 284–295.

Vujaklija, I., A. D. Roche, T. Hasenoehrl, A. Sturma, S. Amsüss, D. Farina, and O. C. Aszmann (2017). "Translating research on myoelectric control into clinics—Are the performance assessment methods adequate?" In: *Frontiers in Neurorobotics* 11.

Wang, Y. and M. Neff (2013). "Data-driven glove calibration for hand motion capture." In: *Proceedings of the 12th ACM SIGGRAPH/Eurographics Symposium on Computer Animation (SCA)*. ACM Press, p. 15.

Weiss, E. J. and M. Flanders (2004). "Muscular and postural synergies of the human hand." In: *Journal of Neurophysiology* 92.1, pp. 523–535.

Wilcoxon, F. (1945). "Individual comparisons by ranking methods." In: *Biometrics Bulletin* 1.6, pp. 80–83.

Woodman, O. J. (2007). *An introduction to inertial navigation*. Tech. rep. University of Cambridge, Computer Laboratory.

Wurth, S. M. and L. J. Hargrove (2014). "A real-time comparison between direct control, sequential pattern recognition control and simultaneous pattern recognition control using a Fitts' law style assessment procedure." In: *Journal of NeuroEngineering and Rehabilitation* 11.1, p. 91.

Xiloyannis, M., C. Gavriel, A. A. C. Thomik, and A. A. Faisal (2015). "Dynamic forward prediction for prosthetic hand control by integration of EMG, MMG and

kinematic signals." In: *2015 7th International IEEE/EMBS Conference on Neural Engineering (NER)*. IEEE, pp. 611–614.

Yakovenko, S., N. Krouchev, and T. Drew (2011). "Sequential activation of motor cortical neurons contributes to intralimb coordination during reaching in the cat by modulating muscle synergies." In: *Journal of Neurophysiology* 105.1, pp. 388–409.

Yang, D., Y. Gu, L. Jiang, L. Osborn, and H. Liu (2017). "Dynamic training protocol improves the robustness of PR-based myoelectric control." In: *Biomedical Signal Processing and Control* 31, pp. 249–256.

Yatsenko, D., D. McDonnall, and K. S. Guillory (2007). "Simultaneous, proportional, multi-axis prosthesis control using multichannel surface EMG." In: *2007 29th Annual International Conference of the IEEE Engineering in Medicine and Biology Society (EMBC)*. IEEE, pp. 6133–6136.

Young, A. J., L. J. Hargrove, and T. A. Kuiken (2011). "The effects of electrode size and orientation on the sensitivity of myoelectric pattern recognition systems to electrode shift." In: *IEEE Transactions on Biomedical Engineering* 58.9, pp. 2537–2544.

Young, A. J., T. A. Kuiken, and L. J. Hargrove (2014). "Analysis of using EMG and mechanical sensors to enhance intent recognition in powered lower limb prostheses." In: *Journal of Neural Engineering* 11.5, p. 056021.

Young, A. J., L. H. Smith, E. J. Rouse, and L. J. Hargrove (2013). "Classification of simultaneous movements using surface EMG pattern recognition." In: *IEEE Transactions on Biomedical Engineering* 60.5, pp. 1250–1258.

Young, A. J., L. H. Smith, E. J. Rouse, and L. J. Hargrove (2014). "A comparison of the real-time controllability of pattern recognition to conventional myoelectric control for discrete and simultaneous movements." In: *Journal of NeuroEngineering and Rehabilitation* 11.1, p. 5.

Zardoshti-Kermani, M., B. Wheeler, K. Badie, and R. Hashemi (1995). "EMG feature evaluation for movement control of upper extremity prostheses." In: *IEEE Transactions on Rehabilitation Engineering* 3.4, pp. 324–333.

Zhai, X., B. Jelfs, R. H. M. Chan, and C. Tin (2017). "Self-recalibrating surface EMG pattern recognition for neuroprosthesis control based on convolutional neural network." In: *Frontiers in Neuroscience* 11.

Zhang, X. and H. Huang (2015). "A real-time, practical sensor fault-tolerant module for robust EMG pattern recognition." In: *Journal of NeuroEngineering and Rehabilitation* 12.1, p. 18.

Zhu, X., J. Liu, D. Zhang, X. Sheng, and N. Jiang (2017). "Cascaded adaptation framework for fast calibration of myoelectric control." In: *IEEE Transactions on Neural Systems and Rehabilitation Engineering* 25.3, pp. 254–264.

Ziai, A. and C. Menon (2011). "Comparison of regression models for estimation of isometric wrist joint torques using surface electromyography." In: *Journal of NeuroEngineering and Rehabilitation* 8.1, p. 56.

Ziegler-Graham, K., E. J. MacKenzie, P. L. Ephraim, T. G. Travison, and R. Brookmeyer (2008). "Estimating the prevalence of limb loss in the United States: 2005 to 2050." In: *Archives of Physical Medicine and Rehabilitation* 89.3, pp. 422–429.